Summer 9-1-2014

Yeast Prion Variants as Models of the Phenotypic and Pathological Consequences of Amyloid Polymorphism

Kevin Stein
Washington University in St. Louis

WASHINGTON UNIVERSITY IN ST. LOUIS

Division of Biology & Biomedical Sciences

Molecular Cell Biology

Dissertation Examination Committee:

Heather True, Chairperson
Kendall Blumer
Marc Diamond
Justin Fay
Jin-Moo Lee
Conrad Weihl

Yeast Prion Variants as Models of the Phenotypic and Pathological Consequences of Amyloid Polymorphism

By

Kevin Christopher Stein

A dissertation presented to the
Graduate School of Arts and Sciences
of Washington University in
partial fulfillment of the
requirements for the degree
of Doctor of Philosophy

August 2014

Saint Louis, Missouri

TABLE OF CONTENTS

LIST OF FIGURES

Chapter 1: Background and Significance

Chapter 2: Extensive Diversity of Prion Strains is Defined by Differential Chaperone Interactions and Distinct Amyloidogenic Regions

Chapter 3: Comparative Analysis of Yeast Prion Variants Reveals Conformation-Specific Requirements for Chaperone Machinery

Chapter 4: Myopathy-Causing Mutations in an Hsp40 Chaperone Disrupt Processing of Specific Client Conformers

Chapter 5: DNAJB6 Mutations that Cause Limb-Girdle Muscular Dystrophy Alter Select Hsp40 Functions

ACKNOWLEDGMENTS

First and foremost, I'm grateful to the Boss. She provided the kind of learning environment and mentoring that I needed as a grad student. She knew when to push me, when to give me flexibility, and was always willing to provide a second opinion when I needed, even on some pretty trivial details. Her balanced approach epitomized what it meant to be a good mentor, and gave me the confidence that is needed to move forward in my scientific career.

I thank my thesis committee for always pushing me to think about and explain the bigger picture and wider implications of my data. In particular, thanks to Chris for helping foster a productive and rewarding collaboration.

I thank all the members of the True lab over the years that tolerated my borderline OCD tendencies to keep the lab organized and running smoothly. I especially want to acknowledge A-Lin, for helping get my feet on the ground when I joined the lab; J-Lizzy, for spicing up the lab; LW, for almost always being on the same page as me; Vinny, for being the best wingman, always dedicated to performing to the best of his abilities (oh, and of course, for all the conversations about ultimate frisbee); and KWilt, for getting me another publication in the future.

I am grateful to my parents, Liz and Ben, who showed me what it meant to simultaneously work hard and work smart.

Lastly, I must thank my wife, Liana, who had to put up with all my venting, late-night time points, and incessant dabbling. She was a never-ending source of understanding and support throughout our time in graduate school, thus making said time points more tolerable (at least a little bit).

DEDICATION

This dissertation is dedicated to the shoulders of giants - the great minds of scientists and philosophers and the everyday tinkerers who have come before me. They empowered the scientific method and cemented its place in shaping society. Their passion demonstrated the wonder that can be found in revealing nature's secrets. It is through their efforts that the foundation for all modern-day scientists was established. It is their shoulders on which we stand.

ABSTRACT OF THE DISSERTATION

Yeast Prion Variants as Models of the Phenotypic and Pathological

Consequences of Amyloid Polymorphism

By

Kevin Christopher Stein

Doctor of Philosophy in Biology and Biomedical Sciences

Molecular Cell Biology

Washington University in St. Louis, 2014

Dr. Heather True, Chairperson

Protein aggregation is the hallmark of protein conformational disorders such as Alzheimer's disease and prion diseases. Prions are infectious proteins that propagate a self-templating amyloid structure, and have become a model for studying these diseases. Interestingly, a single protein can form a variety of distinct amyloid structures, a phenomenon referred to as amyloid polymorphism. In prion diseases, these different structures, called prion strains, dictate variation in pathology. However, the underlying basis for how structural variation modulates pathology remains unclear.

Yeast prions have been a valuable model for studying protein conformational disorders. Prion proteins endogenous to yeast similarly misfold and form different self-propagating prion strains (called variants) that modulate cellular phenotypes. Additionally, in both humans and yeast, molecular chaperones act to process misfolded substrates. Here, I explore the interplay

between molecular chaperones and prion variants and reveal novel determinants for how distinct aggregate structures can dictate phenotype.

Studies of the [*PSI*+] prion have served as the foundation for the biophysical analysis of prion strains for several years. I applied this knowledge to prion variants of another prion, [*RNQ*+]. I found a surprising diversity in the sequence elements that are required to maintain different [*RNQ*+] variants. Interestingly, I also found evidence to suggest that the prion conformation dictates the availability of interaction sites for chaperones. Moreover, different domains of the Hsp40 Sis1 are important for maintaining particular prion variants. In fact, Sis1 and its human homolog have distinct prion conformer selectivity, suggesting that the selectivity of Hsp40s has changed throughout evolution.

I also apply the concept of amyloid polymorphism to examine mutations in the human Hsp40 DNAJB6 that cause limb-girdle muscular dystrophy type 1D (LGMD1D). Using a chimeric protein of DNAJB6 and Sis1, I found that LGMD1D mutations impaired the propagation of prion conformers in a manner that depended on both the conformation and mutation. Additionally, while other functions of Sis1 were unaffected, over-expression of these mutants caused Hsp70-dependent cellular toxicity. These data show that impairing chaperone-mediated processing of particular substrate conformers may be one mechanism involved in the development of chaperonopathies.

Taken together, this dissertation highlights the complexity underlying the impact of amyloid polymorphism on dictating phenotypic diversity, and shows how amyloid conformation is an important variable when studying the pathogenesis of protein conformational disorders.

Chapter 1: Background and Significance

1.1 Protein Conformational Disorders and Amyloid Formation

The ability of a cell to synthesize, fold, and properly maintain its proteome is crucial for cell viability. Impairing this essential process has devastating consequences, often leading to the development of diseases called protein conformational disorders. Protein misfolding and the formation of insoluble protein aggregates characterize these diseases. This aggregation disrupts cellular and tissue functions, and for many of these diseases, is ultimately fatal.

There is a wide range of protein conformational disorders, which are generally divided into three broad categories [1,2]. Neurodegenerative diseases, such as Alzheimer's disease and Parkinson's disease, involve the accumulation of aggregates in the brain. Non-neuropathic or organ-limited diseases, such as type II diabetes, have aggregates present in one tissue other than the brain. Lastly, systemic disorders, like hemodialysis-related amyloidosis and AA amyloidosis, present with protein aggregates in multiple tissues.

A number of these diseases are familial, arising through the inheritance of a specific mutation [2]. Oftentimes, this mutation is present in the protein that forms the primary constituent of the aggregate deposits, thereby giving strong evidence that protein misfolding and aggregation is the major contributor to disease pathogenesis [3]. Some protein conformational disorders only occur as familial cases, such as Huntington's disease that is caused by a polyglutamine expansion [4]. However, several disorders predominantly arise sporadically, with a small percentage of familial cases. The same protein will aggregate in both sporadic and familial cases of the same disease, and these cases are symptomatically similar, suggesting that similar pathological mechanisms are involved. In addition to sporadic and familial cases, a subset of neurodegenerative diseases called prion diseases, or transmissible spongiform encephalopathies, can arise through infection [5]. In fact, under experimental conditions, some

evidence suggests that other protein conformational disorders might also be transmissible [4,6]. However, under natural conditions, it remains unclear to what degree other protein conformational disorders are infectious.

There are a wide variety of unrelated proteins that aggregate in protein conformational disorders, from proteins with no defined function (e.g. PrP in prion diseases) to a number of RNA-binding proteins (e.g. TDP-43 and FUS in amyotrophic lateral sclerosis (ALS)) [7,8]. Nevertheless, the deposits are often described as forming a common structure called amyloid that is characterized by a fibrillar morphology comprised of cross-β sheets [9]. This suggests that there might be shared pathogenic mechanisms for protein conformational disorders.

Interestingly, while the formation of amyloid is often studied in the context of protein conformational disorders, this structure transcends its association with disease. An increasing number of proteins from *Escherichia coli* to humans have been identified in which amyloid formation is proposed to be part of the protein's physiological function [10,11]. Some of the best-described examples of this phenomenon are the existence of prion proteins in the budding yeast *Saccharomyces cerevisiae* [12,13]. These proteins, many of which are involved in transcriptional regulation, can confer beneficial phenotypes, in certain conditions, when present in their prion state [14,15]. Moreover, it has been suggested that any polypeptide, independent of sequence, can form amyloid given the right conditions [16]. Hence, amyloid formation is a generic phenomenon, the study of which can have implications on several biological processes.

1.2 The Influence of Prion Strains and Amyloid Polymorphism on Pathological and Phenotypic Variation

Stein KC and True HL. Under review in the journal

1.2.1 Introduction

The deposition of protein aggregates is a unifying feature of a large class of diseases known as protein conformational disorders, which includes Alzheimer's disease and prion diseases. One of the most fascinating and puzzling aspects of such diseases is the phenomenon of amyloid polymorphism, whereby a single disease-associated protein forms different types of aggregate structures. This is best exemplified in prion diseases, where these different structures, called prion strains, are responsible for much of the variation in pathology and disease transmission. Here, we review the current knowledge of prion strains and amyloid polymorphism, highlighting how diversity in amyloid structure relates to phenotypic differences.

1.2.2 Mammalian Prion Strains Dictate Differential Pathological Consequences

Like other fatal human neurodegenerative diseases, transmissible spongiform encephalopathies (TSEs), or prion diseases, have cases that arise sporadically (Creutzfeldt-Jakob disease (CJD)) or are inherited (fatal familial insomnia, Gerstmann-Sträussler-Scheinker syndrome) [5]. Remarkably, prion diseases can also be acquired by infection (e.g. kuru in humans). TSEs afflict a wide variety of mammalian species (e.g. scrapie in sheep, chronic wasting disease in cervids, and bovine spongiform encephalopathy (BSE) in cattle). These disorders are caused by conversion of the protein PrP^{C} to an abnormal infectious conformation called PrP^{Sc} that generally adopts an amyloid structure. The widely accepted prion hypothesis suggests that PrP^{Sc} is the sole transmissible agent of prion diseases, thus making it distinct from conventional pathogens having a nucleic acid component. However, it was long unclear how a protein-based infectious agent could explain the existence of prion strains.

Even early observations of prion diseases describe considerable diversity in disease symptoms with different PrP^{Sc} isolates [17]. This typically presents as variation in incubation period (the time from infection to the onset of symptoms), or the distribution patterns of PrP^{Sc} or spongiform pathology in the brain. In addition, certain prion isolates show different degrees of transmissibility between species, a phenomenon called the "species barrier", whereby transmission between different species is generally less efficient than transmission within the same species. This was brought to the public's attention in the mid-1990s with the outbreak of BSE ("mad cow disease") and subsequent cross-species transmission to humans, causing a novel phenotype called variant CJD [17]. Some argued that this variation in pathology and transmissibility indicated that the infectious agent of prion strains must have a nucleic acid component, or be encoded by changes in the PrP sequence, in an analogous fashion as genetic polymorphisms that distinguish different strains of viral or bacterial infections. However, distinct prion strains were isolated having an identical primary structure, suggesting that the physical basis of prion strains was not simply determined by sequence variation. Indeed, these early studies demonstrated that two different strains of transmissible mink encephalopathy showed different resistance to proteases, suggesting that prion strains represent distinct conformations of the same protein [18].

1.2.3 PrP^{Sc} Strains Encode Variation in Structural Properties of Amyloid

In order to form distinct strains of PrP^{Sc}, PrP^{C} undergoes a dramatic conformational change. PrP^{C} consists of an unstructured N-terminal domain and a C-terminal domain comprised of three α helices and two short β strands, making this structure ~40% α helix and ~5% β sheet [19]. However, formation of PrP^{Sc} involves the conversion of the C-terminal domain into a β

sheet-rich amyloid structure (~20% α helix, ~43% β sheet), without any of the native α helices remaining [19].

While PrP^{Sc} strains exhibit amyloid polymorphism, and many other disease-related proteins also form amyloid structures, there are a number of properties that are common to amyloid. Amyloid fibrils are generally unbranched structures that are 5-15nm in diameter and often comprised of multiple entwined protofilaments [20]. There are two generic amyloid folds. The most common is a cross-β sheet structure with β sheets that run parallel to the fibril axis, and individual β strands that form the β sheets are oriented perpendicular to the fibril axis [9]. The β strands can run in the same (parallel) or opposite (anti-parallel) direction, and are generally in-register, whereby each strand aligns with the identical residue in the neighboring monomer of the β sheet [9]. The common motif formed by the β sheets is called a steric zipper, in which the side chains of opposing β sheets interdigitate using hydrogen bonds or van der Waals interactions to form a complementary interface that is free from exposure to solvent [21]. Such a strong underlying hydrophobic effect helps make amyloid a very stable structure [9].

By contrast, PrP^{Sc} is proposed to form the second generic amyloid fold called a β solenoid [19]. Here, a single monomer will form three β strands that loop around each other in a helix-like structure [20]. While it remains technically challenging to decipher many additional details about the structure of PrP^{Sc}, a number of observations indicate certain variables that can contribute to the structural differences of prion strains: 1) the length of the region protected in β sheets, as well as what sequence is protected [22]; 2) whether the protein is truncated, as the C-terminally truncated Y145Stop construct of human PrP has a very different region of the primary structure that forms the amyloid core as compared to longer versions of the protein [21] (and different truncated versions of PrP^{Sc} have been isolated from brains [5]); and 3) sensitivity to

protease digestion, with both protease-resistant and sensitive forms of PrP^{Sc} existing [23]. However, while these factors reveal the presence of amyloid polymorphism, their connection to pathological variation remains elusive.

1.2.4 Biophysical Parameters Define Strains of the Yeast Prion [*PSI*+]

Significant insight into how prion strains can mediate phenotypic differences has come from studying the endogenous prion proteins that exist in the budding yeast, *Saccharomyces cerevisiae* [14]. The [*PSI*+] prion is formed from the translation termination factor Sup35, which can form self-propagating aggregates. Sequestration of Sup35 into the prion state impairs translation termination, causing ribosomes to read through stop codons (nonsense suppression). Strains of [*PSI*+] (called variants in yeast, but for simplicity, we will use the term strains) are characterized by the degree of nonsense suppression: cells propagating a strong [*PSI*+] strain exhibit greater nonsense suppression as compared to weak [*PSI*+] cells [24].

A model describing the structural basis of these strain-dependent phenotypes has served as the foundation for understanding prion strains [25]. This model suggests that a set of biophysical parameters defines the nature of the prion strain that propagates. Structurally, these parameters are dictated by the length of the amyloid core, that is, the number of amino acid residues that are protected in β sheets [26]. An expansion of the core, by incorporating more residues into hydrogen-bonded β sheets, as in the case of weak [*PSI*+], correlated with an increase in aggregate stability [25,26]. It was reasoned that higher stability decreased how readily the amyloid could be fragmented, thus resulting in seeds that were fewer in number and had a larger average size. Consequently, fewer surfaces are available to recruit monomeric Sup35 in cells harboring weak [*PSI*+]. This leads to a larger pool of soluble Sup35 to function in

translation termination (i.e. less nonsense suppression) as compared to strong [*PSI*+] cells that have aggregates that sequester more Sup35 monomer. Hence, aggregate stability and amyloid core length were suggested to be the major determinants of strain-dependent phenotypes [25,26].

This same correlation was found to fit with synthetic prion strains of PrP^{Sc}: decreased aggregate stability correlated with a shorter incubation period of disease [27]. However, several recent examples of other PrP^{Sc} strains cannot be explained by the biophysical parameters established by the model of [*PSI*+] strains: 1) strains with different stability had a similar core length [28]; 2) decreased stability of other PrP^{Sc} strains correlated with a longer disease incubation time [29]; and 3) strains that are biochemically indistinguishable can confer distinct pathological consequences [30]. This exemplifies the wide variety of different aggregate structures that a single polypeptide can form, leaving it unclear how other factors might influence strain-mediated phenotypic variation.

1.2.5 Differential Chaperone Interactions and Amyloidogenic Regions Influence the Complex Nature of [*RNQ*+] *Strains*

Another yeast prion called [*RNQ*+], which is formed from the Rnq1 protein, manifests phenotypically by promoting the formation of [*PSI*+] [31]. Different prion strains of [*RNQ*+] are characterized by how readily [*PSI*+] forms. The Rnq1 protein was found to form a remarkable variety of structural variants that exhibit tremendous variation in the ability to promote [*PSI*+] induction [31,32]. As with Sup35 in [*PSI*+] cells, aggregate stability was shown to be a defining factor in the propagation of particular [*RNQ*+] strains [33]. However, it was recently found that aggregate stability, along with several other biophysical properties that distinguish strains of [*PSI*+], were unable to distinguish other [*RNQ*+] strains [34,35].

Mutation analysis of the Rnq1 protein with five different [*RNQ*+] strains revealed additional factors that can contribute to amyloid polymorphism and phenotypic differences. Multiple regions predicted to be amyloidogenic were identified throughout the Rnq1 protein [34]. These regions are postulated to influence the formation of amyloid [36]. It was found that the propagation and phenotypic variation (i.e. [*PSI*+] induction) of each [*RNQ*+] strain relied on a distinct set of non-adjacent amyloidogenic regions (Figure 1A,B) [34], in stark contrast to [*PSI*+] strains that have a contiguous region of Sup35 protected in the amyloid core [26]. Moreover, both Sup35 and Rnq1 have prion-forming domains (PFD) that are rich in glutamine and asparagine (Q/N) residues and are necessary for prion propagation [11]. However, it was shown that the region outside of the Rnq1-PFD played a major, but strain-dependent, role in prion propagation by facilitating sequestration of monomer into aggregates, thereby highlighting the influence of non-canonical regions on prion strains.

In addition to the differential influence of primary structure, it was found that [*RNQ*+] strains likely have diverse interactions with molecular chaperones [34]. From yeast to humans, molecular chaperones are involved in processing misfolded and aggregated proteins. Such processing, in the case of yeast prions, is required for the continued maintenance of the prion state [14]. A peptide-binding array identified one of the Rnq1 amyloidogenic regions as important for Sis1 binding, which is a required component of prion propagation [37]. However, in another study, it was shown that Sis1 could bind other regions of Rnq1 [34]. Indeed, a distinct amyloidogenic region was particularly important for the propagation of one [*RNQ*+] strain and might serve as a second Sis1 binding site. This suggests that conformation could dictate the exposure of different binding sites and/or the affinity of chaperones for the same site (Figure 1C). Moreover, chaperone binding to a specific site at an early stage of folding may influence the

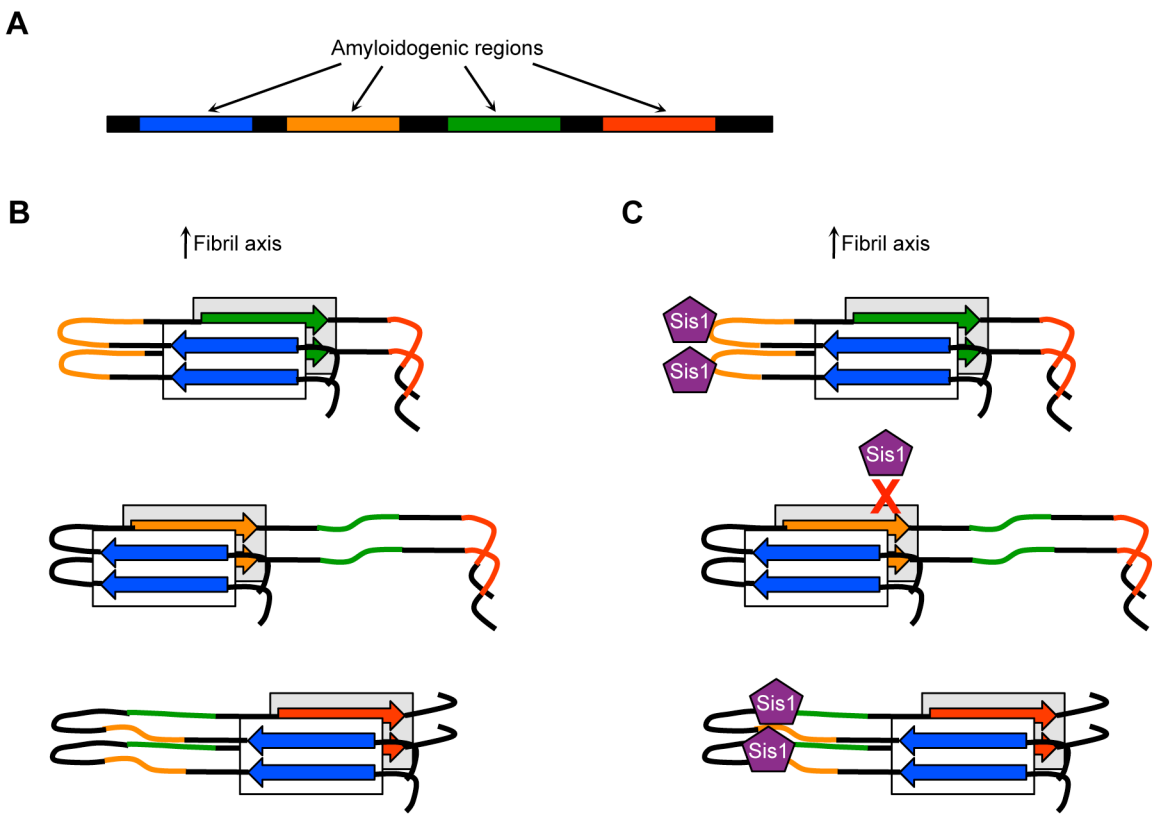

Figure 1. Model showing how distinct amyloidogenic regions could influence amyloid polymorphism and associated phenotypic variation. (A) A single protein can have multiple amyloidogenic regions (colored as blue, orange, green, and red) that are not adjacent in the primary structure. (B) These regions can influence amyloid packing in a variety of ways, with non-adjacent regions possibly forming the amyloid core. (C) If a particular amyloidogenic region represents a chaperone-binding site (e.g. the Hsp40 Sis1 has affinity for the orange region), this region is exposed and available for binding in certain structures (top and bottom), but not others (middle). In addition, chaperone or cofactor binding prior to amyloid folding may influence the range of amyloid structures that can form or propagate, thereby providing a mechanism by which genetic and environmental modifiers may alter amyloid structure.

amyloid structure that forms. These differences are also likely to be true for [*PSI+*] strains [38], and agree with the hypothesis that PrP^{Sc} strains have different interactions with cofactors [39]. Additionally, this provides insight into how changes in extracellular environment may mediate prion strain generation and propagation [40,41]. Hence, variation in amyloid-chaperone sites of interaction is likely a major determinant of the phenotypic differences caused by prion strains.

1.2.6 Amyloid Polymorphism is a Ubiquitous Feature of Disease-Associated Proteins

In recent years, the prevalence of amyloid polymorphism has been extended to many different proteins associated with protein conformational disorders. For instance, based on histopathology and biochemical properties, Aβ forms heterogeneous deposits in the brains of patients with Alzheimer's disease [9]. Heterogeneity was also observed *in vivo* for other proteins, including tau, α-synuclein, and transthyretin, suggesting that the phenomenon of amyloid polymorphism is widespread and not limited to prion proteins [9].

Amyloid polymorphism has also been extensively studied using synthetic polypeptides [42-44]. It was demonstrated that the same sequence could form multiple different steric zipper structures, which were proposed to fall into eight different classes [43]. Furthermore, three different models of polymorphism were postulated to explain the diversity of structures that were observed: packing (different β sheet arrangements of the same sequence), segmental (different sequences form similar β sheet conformation), and heterozipper (different regions that are cross-complementary form the β sheet, either two regions in the same monomer, or between two monomers) [44]. When considering these data in the context of a full-length protein, which can have several amyloidogenic regions, combined with different cofactor requirements [39], it then becomes easier to envision a considerable number of stable amyloid structures that are

theoretically possible. Indeed, one conformation being uniquely thermodynamically stable above all other combinations seems unrealistic simply in terms of probability. Therefore, elucidating the complex interplay of variables that affect the formation and maintenance of polymorphic structures remains a nontrivial, but crucial, task to gain a full understanding of pathological variability and the etiology of protein conformational disorders.

1.3 The [*RNQ*+] Prion: A Model of Both Functional and Pathological Amyloid

Stein KC and True HL (2011) *Prion* 5, 291-8.

1.3.1 Abstract

The formation of fibrillar amyloid is most often associated with protein conformational disorders such as prion diseases, Alzheimer's disease, and Huntington's disease. Interestingly, however, an increasing number of studies suggest that amyloid structures can sometimes play a functional role in normal biology. Several proteins form self-propagating amyloids called prions in the budding yeast *Saccharomyces cerevisiae*. These unique elements operate by creating a reversible, epigenetic change in phenotype. While the function of the non-prion conformation of the Rnq1 protein is unclear, the prion form, [*RNQ*+], acts to facilitate the *de novo* formation of other prions to influence cellular phenotypes. The [*RNQ*+] prion itself does not adversely affect the growth of yeast, but the overexpression of Rnq1p can form toxic aggregated structures that are not necessarily prions. The [*RNQ*+] prion is also involved in dictating the aggregation and toxicity of polyglutamine proteins ectopically expressed in yeast. Thus, the [*RNQ*+] prion provides a tractable model that has the potential to reveal significant insight into the factors that dictate how amyloid structures are initiated and propagated in both physiological and pathological contexts.

1.3.2 Introduction

Protein conformational disorders are associated with the misfolding and aggregation of proteins into cross-β-sheet structures called amyloid [2]. Interestingly, these disorders may result from a common underlying mechanism that has been described as prion-like [45]. Prions are proteins that form a self-propagating, amyloid-like structure that converts protein from its native state into the prion conformation [5]. When the mammalian protein PrP misfolds to its prion conformation, it is infectious. This infectious prion protein is the causative agent of one class of mammalian protein conformational disorders called transmissible spongiform encephalopathies. While the term amyloid is traditionally used in the context of cellular dysfunction and disease, many examples of amyloid structures with normal cellular functions are emerging (reviewed in [10,46,47]). Hence, elucidating how amyloid structures form and propagate is critical to understanding disease pathogenesis and determining how this type of folded structure can have a physiological function.

Much information regarding amyloid formation has been gleaned from the yeast model system and the range of tools it provides. Several unrelated proteins have been demonstrated to form prions in yeast. Yeast prions are associated with changes in phenotype that are inherited epigenetically, thereby showing how amyloid structures can provide a means of regulating cellular functions and phenotypes. Three well-studied yeast prions are [*PSI*+], [*URE3*], and [*RNQ*+], formed by the proteins Sup35, Ure2, and Rnq1, respectively. When the essential translation termination factor Sup35p is sequestered into aggregates in [*PSI*+] cells, it alters translation termination and acts as an omnipotent nonsense suppressor [48,49]. [*PSI*+] provides growth advantages under certain conditions and as such, it is interesting to consider how this

type of element could impact the ability of yeast to adapt to changing environments and ultimately govern the evolution of new traits [15,50-56]. When the transcriptional regulator Ure2p forms the [*URE3*] prion, the transcription of genes involved in nitrogen catabolism is derepressed [57]. This allows the cell to utilize poor nitrogen sources in the presence of good nitrogen sources.

In contrast to Sup35p and Ure2p, the physiological function of the Rnq1 protein has yet to be determined. The [*RNQ*+] prion, however, is required for the *de novo* formation of both [*PSI*+] and [*URE3*], and was originally classified as the [*PIN*+] element, for [*PSI*+] inducible [31,58-61]. The [*RNQ*+] prion has been found in wild yeast isolates [62,63], suggesting that it might not be detrimental in many genetic backgrounds and growth conditions and instead may play some functional role. While [*PSI*+] and [*URE3*] were discovered by phenotype, Rnq1p was identified as a putative prion protein by analyzing the yeast proteome for sequences similar to the glutamine and asparagine (Q/N)-rich prion-forming domains (PFDs) of Sup35p and Ure2p [64]. These domains are defined as the regions that are both necessary and sufficient for prion formation [65]. Definitive confirmation of the prion properties of Rnq1p was shown by transforming *in vitro* generated Rnq1p-PFD fibers (purified, recombinant Rnq1p-(132-405)) into [*rnq*-] yeast to convert cells to [*RNQ*+] [33,66]. Like other yeast prion proteins, as well as those associated with protein conformational disorders, Rnq1p has the propensity to form amyloid *in vitro* with parallel in-register cross-β-sheets [67]. Strikingly, prion proteins can form several unique prion variants (or strains) that have slight differences in their β-sheet structure that constitute distinct amyloid conformations [68,69]. Such different structures are presumably the underlying cause of the diverse phenotypic variation seen in both yeast and in prion diseases

[17,24,31,70]. In the case of Rnq1p, several different [*RNQ*+] variants have been described, and these correspond to different levels to which they facilitate the formation of [*PSI*+] [31].

In this review, we summarize the properties and protein interactions of the [*RNQ*+] prion and highlight its similarities and differences to other yeast prions. This discussion provides a framework to study how [*RNQ*+] may represent another example of a functional amyloid. In addition, we describe how [*RNQ*+] can be used to model pathological amyloid, thereby showing how the same protein may form both toxic and non-toxic aggregates.

1.3.3 The PFD of Rnq1p is complex and may not be confined to the Q/N-rich region

The N-domain of Rnq1p may be involved in [*RNQ*+] *maintenance*

While most polypeptides may be able to form amyloid structures given the right conditions, there are a number of intrinsic factors that determine whether a protein will aggregate under physiological conditions *in vivo* [71]. A high degree of hydrophobicity, minimal net charge, and an intrinsically disordered region often contribute to the propensity of many amyloidogenic proteins, such as PrP and the Alzheimer's disease protein Aβ, to form β-sheets and aggregate [2]. In contrast, polyglutamine (polyQ) proteins are characterized by having a long, highly polar stretch of glutamine residues [72]. The PFDs of many yeast prion proteins are similarly polar as they are enriched in glutamines and asparagines [65]. Thus, our understanding of how amino acid composition influences aggregation and amyloid formation is incomplete.

The PFD of Rnq1p was initially defined as the C-terminal Q/N-rich region (aa153-405) by sequence analysis using the PFDs of Sup35p and Ure2p, and this was later verified experimentally [64]. The N-terminal domain (aa1-152) of Rnq1p, on the other hand, has no known function. To better understand the regions of Rnq1p that are important for [*RNQ*+]

propagation, the effect of a series of *RNQ1* truncations on [*RNQ*+] propagation was tested [73]. With the exception of one construct (aa172-405) that transmitted [*RNQ*+] more efficiently than the entire PFD (aa133-405 in this case), the efficiency of propagation decreased with decreasing fragment lengths. This result provided the first indication that, in addition to the PFD, the N-domain may be involved in maintenance of the [*RNQ*+] prion.

Other studies have also revealed a potential role for the N-domain in the propagation of [*RNQ*+]. An interaction between Rnq1p and the Hsp40 Sis1p is required for [*RNQ*+] propagation [74]. Mutation of one residue in Rnq1p in the putative Sis1p binding site (L94A) disrupts this interaction and eliminates the [*RNQ*+] prion [37,75]. This suggests that the N-terminus of Rnq1p facilitates the interaction with Sis1p to maintain [*RNQ*+]. Additionally, *rnq1* alleles having missense mutations in the N-terminus of Rnq1p destabilize [*RNQ*+] propagation [76,77], further supporting the notion that this domain is involved in [*RNQ*+] propagation. Interestingly, however, these *rnq1* mutants do not disrupt the interaction with Sis1p [76], suggesting that the N-terminal region may contribute functions beyond interaction with Sis1p. Finally, in a screen aimed to identify residues in the Rnq1p-PFD important for [*RNQ*+] propagation, none of the PFD mutants impaired [*RNQ*+] when tested in the context of full-length Rnq1p [78], and only one mutation in the PFD that affects [*RNQ*+] propagation has since been found [76]. Collectively, these data yield conflicting results as to whether the N-terminus of Rnq1p acts as a positive or negative regulator in the maintenance of the [*RNQ*+] prion. Elucidating the role of the N-domain will provide insight into how other intragenic or non-PFD regions may be involved in the formation and propagation of amyloid structures in a pathological or physiological setting.

The Rnq1p-PFD is comprised of multiple recognition elements that act cooperatively

In addition to regions outside of the Rnq1p-PFD being involved in [*RNQ*+] propagation, it seems clear that the Rnq1p-PFD is more complex than the PFDs of Sup35p or Ure2p. The Sup35p-PFD, for example, is much smaller (aa1-123) with two defined regions important for [*PSI*+] propagation: a short Q/N-rich tract (aa5-27) and a region of clearly defined oligopeptide repeats (aa41-95) [24,79]. These regions can be functionally separated into sequences important for prion formation and sequences important for prion propagation [80]. Likewise, the oligopeptide repeats in the mammalian prion protein, PrP, are involved in dictating prion infectivity [81-83]. In contrast, Ure2p does not have any oligopeptide repeats and the Rnq1p-PFD has loosely defined oligopeptide repeats among four largely separated Q/N-rich regions [65]. Hence, the regions that influence the propagation and heritability of Rnq1p aggregates remain poorly defined. None of the four QN-rich regions of the Rnq1p PFD is sufficient to maintain [*RNQ*+] [84]. The presence of either QN2 (aa218-263) or QN4 (aa337-405) is required, but the presence of QN1 (aa185-198) or QN3 (aa279-319) strongly enhances propagation [84]. Thus, the Rnq1p-PFD has multiple sequence determinants that cooperate to propagate [*RNQ*+], thereby creating a complex, composite PFD with ill-defined roles for each of these sequence elements. Defining these roles will help us understand how the primary sequence of a protein is involved in dictating amyloid formation.

1.3.4 [*RNQ*+] *propagation depends on interactions with chaperones*

Differential roles of chaperones on prion propagation

A conserved network of molecular chaperones helps proteins adopt and maintain their proper fold, thereby combating the misfolding and aggregation of proteins that can cause disease [85]. Chaperones also play a major role in the propagation of all yeast prions [86-88]. Proteins in

the Hsp40 and Hsp70 families deliver aggregated substrates to the disaggregase Hsp104p for resolubilization [89,90]. This process serves to fragment prion aggregates into seeds that can be efficiently transmitted from mother to daughter cells during mitosis [91-93]. Both Hsp104p and the essential Hsp40 Sis1p are required for the propagation of [*PSI*+], [*URE3*], and [*RNQ*+] [64,74,94-96]. Several lines of evidence, however, suggest that these chaperones may be differentially involved in propagating these prions. [*PSI*+], [*URE3*], and [*RNQ*+] show distinct sensitivities to both expression levels and mutation of Sis1p and Hsp104p [75,95,97,98]. The overexpression of Hsp104p eliminates [*PSI*+], but does not affect propagation of [*RNQ*+] or [*URE3*] [49,74,94,96]. In contrast, [*RNQ*+] and [*URE3*] are more sensitive to Sis1p levels than [*PSI*+]. Sis1p overexpression does not affect [*RNQ*+] propagation [74], but when Sis1p is downregulated, both [*RNQ*+] and [*URE3*] are lost within 20 generations as compared to >60 generations that it takes to lose [*PSI*+] [95,99]. When Hsp104p is inhibited by guanidine hydrochloride, though, the rate of loss is similar for all three prions and is comparable to the loss of [*RNQ*+] and [*URE3*] when Sis1p is downregulated [95]. One possible explanation as to why these prions show different sensitivities to Sis1p is that one of the other 12 Hsp40s present in yeast could partially compensate for Sis1p in [*PSI*+] propagation. However, none of the other Hsp40s are required for propagation of [*PSI*+], [*URE3*], or [*RNQ*+] [95,100]. Besides Sis1p, the only other Hsp40 shown to bind Rnq1p is Ydj1p [100,101]. Ydj1p is dispensable for [*RNQ*+] propagation [100], but the overexpression of Ydj1p cures some variants of [*RNQ*+] [31]. Such differences in chaperone requirements of [*RNQ*+], [*PSI*+], and [*URE3*] may indicate that the structural differences between different prions and/or variants are responsible for dictating how chaperones recognize or fragment prion aggregates. Our understanding of this highly specific interplay between molecular chaperones and prions is far from complete. Additional mechanistic

studies are required to better understand how chaperones regulate prion propagation – an understanding that could lead to therapeutic development for protein conformational disorders.

Sis1p and [*RNQ+*] *propagation*

Sis1p binds Rnq1p in equimolar ratios in [*RNQ+*] cells and this interaction is required for [*RNQ+*] propagation [37,74,75,100]. Both the human homolog of Sis1p, HDJ1, and the *Drosophila* homolog, DROJ1, can compensate for the loss of Sis1p in viability and [*RNQ+*] propagation, suggesting a conserved function of Sis1p acts in prion propagation [100]. The sequences of Class I and Class II Hsp40s were compared to analyze the specificity of Sis1p in prion propagation [100]. Both types of Hsp40s have an N-terminal J-domain that mediates their interaction with Hsp70s and stimulates Hsp70 ATPase activity [102]. A glycine-rich region is adjacent to the J-domain in both classes as well. In Sis1p, this domain is divided into two parts: a G/F domain rich in glycine and phenylalanine residues and a G/M domain rich in glycine and methionine. The function of these domains is unclear. Following the glycine-rich domain, Class I Hsp40s have a cysteine-rich domain that is not present in Class II Hsp40s like Sis1p. Lastly, both classes have a C-terminal domain (CTD) that can bind unfolded substrates *in vitro* [103]. The G/F domain is the most critical part of Sis1p in [*RNQ+*] propagation as its deletion eliminates [*RNQ+*], although the G/M domain and the CTD are also likely to be involved as deletion of these domains alters aggregates of Rnq1p [74]. The dependence of [*RNQ+*] on the G/F domain helps explain the specificity of Sis1p, as this region is fairly unique among Hsp40s. The region of aa101-113 in the Sis1p G/F domain is not present in other Hsp40s, and is required for [*RNQ+*] propagation: two point mutations in this region (N108I and D110G) impair maintenance of [*RNQ+*] [100]. Interestingly, *in vitro*, Sis1ΔG/F can still bind substrates and stimulate ATPase

activity of the Hsp70 Ssa1p [104], which can interact with Rnq1p [74]. This suggests that these functions of Sis1p are dispensable for [*RNQ*+] propagation, thereby making it unclear as to how Sis1p mediates propagation of [*RNQ*+]. Moreover, downregulation of Sis1p or Hsp104p cures [*RNQ*+] by increasing the size of Rnq1p aggregates in [*RNQ*+] cells [99] beyond a certain threshold that can be effectively transmitted to daughter cells [105]. Perplexingly, the overexpression of Ssa1p also causes an increase in Rnq1p aggregate size [106]. Thus, the chaperone dynamics involved in fragmenting Rnq1p aggregates to propagate [*RNQ*+] are still poorly defined.

1.3.5 [*RNQ*+] *as a functional amyloid: a two-prion system to regulate the formation of new heritable traits*

Discovery of [*PIN*+]

Before Rnq1p was recognized to form the [*RNQ*+] prion [64], it was discovered that the *de novo* formation of [*PSI*+] depended on the presence of [*PIN*+], a non-Mendelian factor that was presumed to be a prion [58,59]. It was later found that [*RNQ*+] was the [*PIN*+] element and that while Δ*rnq1* cells maintained [*PSI*+], the *de novo* formation of [*PSI*+] did not occur in Δ*rnq1* cells [60,61]. Overexpressing other Q/N-rich proteins can also confer the Pin+ phenotype by enhancing the formation of [*PSI*+], but [*RNQ*+] does so most efficiently and does not require the overexpression of *RNQ1* [60,107]. Once [*PSI*+] has formed, both [*RNQ*+] and [*PSI*+] can propagate independently [59,108], and the presence of [*RNQ*+] does not affect [*PSI*+]-mediated nonsense suppression nor most [*PSI*+]-dependent phenotypes [59]. This was the first published example of a productive interaction between heterologous prions [109]. It is interesting, then, to consider the biological consequences of [*RNQ*+] and its influence on [*PSI*+]. The presence of the

[*PSI*+] prion has profound phenotypic effects and confers growth advantages in certain conditions [15,110,111]. Not surprisingly, the reduced efficiency of translation termination can also be detrimental [15,111]. Different [*PSI*+]-mediated phenotypes are observed in different genetic backgrounds [15,111]. Even different stocks of the same strain can show different phenotypes: for instance, different stocks of the strain 74-D694 show phenotypic variation and some have even lost the ability to recover from stress ([15,111] and unpublished data). These differences highlight the complexity of many of these phenotypes and are partly due to additional mutations, but unfortunately, this has been referred to as conflicting evidence for the potential of [*PSI*+] to be beneficial [112,113]. Yet, the molecular nature of some [*PSI*+]-dependent phenotypes has been elucidated [111,114]. As these traits depend on the ability of [*PSI*+] to act as an omnipotent nonsense suppressor, it has been proposed that [*PSI*+] provides an epigenetic means for adapting to changing environments [15,50,51]. It is currently unclear whether [*PSI*+] exists in wild strains, as the primary method used to assay for [*PSI*+] in wild strains (Sup35-PFD-GFP aggregation [62]) is inconclusive as it typically requires the presence of both [*PSI*+] and [*RNQ*+]. For example, some [*PSI*+] [*rnq*-] "BSC" strains (Cox and Tuite [51]) do not show fluorescent foci when expressing Sup35p-PFD-GFP (True and Lindquist, unpublished data). Nevertheless, the existence of [*PSI*+] in the wild would be predicted to be transient and may not easily survive the switch to laboratory cultivation. Since [*RNQ*+] is required for [*PSI*+] to form and is present in wild yeast isolates [62,63], it follows that the [*RNQ*+] prion may serve to poise cells to form [*PSI*+] when environmental conditions change. In this way, this two-prion system may regulate translation and the ability of yeast to quickly adapt by using otherwise unavailable genetic information. More recently, it was discovered that [*RNQ*+] is also required for the formation of [*URE3*] [31,115]. [*URE3*] regulates nitrogen catabolism and may provide growth

advantages in high concentrations of certain ions [116]. As such, the presence of [*RNQ*+] may allow the cell to adapt to environmental changes and utilize a variety of nitrogen sources. Further examination of these interactions may eventually establish the [*RNQ*+] prion as a functional amyloid.

[*RNQ*+] *exists in different aggregated structures*

Distinct aggregated structures of the mammalian prion protein, PrP, form unique prion strains that dictate disease transmissibility and are thought to be the underlying cause of much of the variation in the pathology of prion diseases [17]. Definitive proof that changes in amyloid conformation can cause phenotypic variation came from studies of [*PSI*+] prion variants. Weak [*PSI*+] variants are characterized by lower levels of nonsense suppression and have aggregates that are larger, more stable, and show a slower rate of amyloid formation as compared to fibers that form strong [*PSI*+] variants [26,69,117,118]. A model was proposed to explain the molecular basis of prion variants, positing that fiber stability and the kinetics of amyloid formation were the two primary determinants of the prion variant that propagated [25]. In contrast, for [*RNQ*+] variants similarly formed from transforming *in vitro* fibers, only fiber stability correlates with the proposed model: aggregates of weaker [*RNQ*+] variants are more stable, but exhibit a faster rate of fiber formation [33]. This suggests that the factors that determine the physical basis of [*RNQ*+] variants may not be the same as those that define [*PSI*+] variants [25,33]. Elucidating how different prion variants form and propagate is critical to understanding how different aggregated structures can modulate disease pathology. Indeed, even with one prion protein, different mechanisms may act to generate different classes of prion

strains. Strains formed with PrP, for instance, do not all fit into one simple model that correlates biochemical and biophysical properties to *in vivo* propagation [30,119].

Interestingly, the *de novo* appearance of [*PSI*+] not only depends on the presence of [*RNQ*+], but also on the prion variant of [*RNQ*+]. [*RNQ*+] variants were initially classified by how well they induce [*PSI*+]. [*PSI*+] is induced at a low frequency with the low [*RNQ*+] variant, and increasing levels of [*PSI*+] induction are seen with the medium, high, and very high [*RNQ*+] variants [31]. This classification only partly correlates to the level of aggregated Rnq1p, with decreasing levels of soluble Rnq1p seen from the low [*RNQ*+] to the high [*RNQ*+] variant. The very high [*RNQ*+] variant was an outlier and showed the most soluble Rnq1p of the [*RNQ*+] variants [31]. This change in solubility of the Rnq1 protein in these variants is often difficult to detect [75], however, and not as marked as the changes seen with variants of [*PSI*+]. Moreover, there is no correlation with the size and distribution of Rnq1p aggregates as there is for [*PSI*+] variants: medium [*RNQ*+] and very high [*RNQ*+], for instance, exhibit nearly identical aggregate distributions [108,117]. Another means of categorizing [*RNQ*+] variants is based on the aggregation pattern seen in [*RNQ*+] cells expressing Rnq1p-GFP: single dot (s.d.) for a single focus of fluorescence, or multi dot (m.d.) for cells having multiple foci [120]. Curiously, the relationship between [*RNQ*+] and [*URE3*] does not follow the same trend as [*RNQ*+] and [*PSI*+]. All of the s.d. [*RNQ*+] variants induce [*URE3*] similarly, while m.d. high [*RNQ*+] is unique and has the highest level of [*URE3*] formation [31]. This suggests that [*RNQ*+] interacts differently with Sup35p and Ure2p to promote prion formation. Further investigation of these heterologous prion interactions will help elucidate one means by which prion variants can form *de novo*.

Models of [*RNQ*+]*-mediated* [*PSI*+] *formation*

Two predominant models have been proposed to explain how [*RNQ*+] facilitates the formation of the [*PSI*+] prion [60,61]. The titration model postulates that in [*rnq*-] cells, some factor prevents the formation of [*PSI*+], but the [*RNQ*+] prion sequesters this inhibitor to allow for conversion to [*PSI*+] [60,61]. Alternatively, the cross-seeding model proposes that the Rnq1p aggregates in [*RNQ*+] cells physically interact with Sup35p and serve as an imperfect template for [*PSI*+] formation [60,61]. While these models are not mutually exclusive, no inhibitor has been found to date, even though much work has been directed toward this goal [60]. Additionally, in support of a physical interaction between Rnq1p and Sup35p, fibers of recombinant Rnq1p can seed the amyloid formation of recombinant Sup35p, albeit inefficiently, and Rnq1p and Sup35p have been shown to occasionally colocalize [107,121]. Furthermore, *rnq1* mutations have been identified that have no detectable effect on the structure of Rnq1p aggregates, but impair the formation of [*PSI*+], suggesting that these residues may physically interact with Sup35p to induce [*PSI*+] [78]. Of course, these findings do not exclude the possibility that some cofactor is also involved in this process. Nevertheless, such cross-seeding or co-aggregation of amyloidogenic proteins may play a role in sporadic protein conformational disorders and this model provides the framework to understand how that may occur.

Non-productive amyloid interactions

In addition to facilitating prion formation, [*RNQ*+] is involved in seemingly "non-productive" prion interactions, the purpose of which is unclear. For example, [*RNQ*+] can induce formation of Sup35p aggregates that are not [*PSI*+], termed non-heritable amyloid [122]. Unlike [*PSI*+], which propagates independently after induction, the overexpression of Sup35p and continuous interaction with [*RNQ*+] are required to maintain these non-heritable aggregates,

which may represent by-products of [*PSI*+] formation. Additionally, the presence of [*PSI*+] can enhance the formation of [*RNQ*+] [60].

Interestingly, [*URE3*] and [*PSI*+] can antagonize each other [123]. Shortly after that discovery, it was paradoxically found that certain [*RNQ*+] and [*PSI*+] variants are incompatible [120]. For example, s.d. [*RNQ*+] variants destabilize weak [*PSI*+] by increasing the size of Sup35p aggregates [106,120]. Such destabilization was not seen for the m.d. high [*RNQ*+] variant. This relationship was reciprocal for the s.d. medium [*RNQ*+] and s.d. very high [*RNQ*+] variants, as the cells that did not form unstable [*PSI*+] converted to [*rnq*-] instead. This incompatibility was also seen with newly-induced [*PSI*+]: after inducing the formation of strong [*PSI*+], 70% of s.d. medium [*RNQ*+] cells and 37% of s.d. very high [*RNQ*+] cells became [*rnq*-] [120]. Furthermore, all s.d. medium [*RNQ*+] cells that had stably acquired weak [*PSI*+] became [*rnq*-]. The mechanism behind these incompatible or non-productive prion interactions is unknown, but this may reveal how some protein aggregates can cap other aggregates or compete for cellular resources.

Mutations in *RNQ1* have also been found to negatively affect [*PSI*+] propagation. Deletion of the first 100 amino acids of Rnq1p (Rnq1pΔ100) was found to inhibit the propagation of strong [*PSI*+] [124]. Overexpression of the Rnq1Δ100 protein eliminated both weak and strong [*PSI*+] in a [*RNQ*+]-dependent manner, regardless of any particular [*RNQ*+] variant. Additionally, Rnq1pΔ100 inhibits [*URE3*] propagation and reduces the toxicity of polyQ aggregates [124]. Rnq1pΔ100 was later classified as a prion ([*RNQ1*Δ*100*+]) that induces [*PSI*+], but the Rnq1pΔ100-mediated induction then results in the loss of either [*RNQ1*Δ*100*+] or [*PSI*+] [125].

Most recently, 23 point mutations within the N-terminus of Rnq1p were uncovered that are phenotypically similar to Rnq1pΔ100 [77]. The overexpression of these mutants resulted in the [*RNQ*+]-dependent elimination of [*PSI*+] by increasing the size of Sup35p aggregates [77]. Interestingly, when expressed from the native *RNQ1* promoter, these mutants did not affect [*PSI*+], but impaired [*RNQ*+] propagation [76,77]. Most of these mutations map to the putative α-helical domains of Rnq1p, and while the authors propose that these regions are involved in facilitating protein-protein interactions, the mechanism underlying the antagonistic prion interactions is unclear. One possibility is that disrupting the structure of the N-terminus may cause a gain-of-function effect through non-productive interactions with Sup35p that may result in capping to cure [*PSI*+]. However, one can only speculate how these seemingly non-productive prion interactions relate to the potential role that [*RNQ*+] may play in inducing [*PSI*+] as a means of adapting to fluctuating environments. It is feasible, for example, that the incompatibility between certain protein conformers serves as a bifunctional switch to regulate [*PSI*+]-mediated adaptation.

1.3.6 [*RNQ*+] *as a model for pathological amyloid polyQ aggregation depends on* [*RNQ*+]

A number of inherited human diseases are caused by the expansion of glutamine repeat sequences beyond a certain threshold in particular proteins [72]. These expanded polyQ proteins are prone to aggregation that is associated with cytotoxicity and leads to neurodegeneration and ultimately death. Yeast models were created to provide a tractable means of studying the aggregation mechanisms of these proteins [126-128]. Interestingly, the overexpression of the chaperones intimately involved in prion maintenance (Sis1p, Hsp104p, and Hsp70s) modulated

aggregation of the huntingtin (Htt) protein that had a pathological polyQ expansion [126]. Deletion of *HSP104* effectively eliminated aggregation. The importance of these chaperones in regulating polyQ aggregation was also validated *in vitro* [129]. The role of these chaperones in dictating polyQ aggregation and toxicity is linked to their role in propagating the [*RNQ*+] prion: both deletion of *RNQ1* and curing of [*RNQ*+] suppress polyQ aggregation and its associated toxicity [127]. This also corroborated earlier findings that Pin+ factors enhance the formation of polyQ aggregates [61].

[*PSI*+] also enhances polyQ toxicity and has an additive effect when [*RNQ*+] is present [128], although most yeast models of polyQ aggregation show a stricter dependence on [*RNQ*+]. In a reciprocal fashion, polyQ aggregates can induce aggregation (though not prion formation) of both Rnq1p and Sup35p [130,131], thereby showing how co-aggregation of polyQ and/or Q/N-rich proteins may play a major role in disease pathogenesis. Similarly, while sequences flanking the expanded polyQ repeats can modulate this toxicity, these sequences have the same effect when expressed *in trans*, and other Q-rich proteins also influence polyQ toxicity [132,133]. Importantly, however, all of these effects rely on the presence of the [*RNQ*+] prion.

Insight into how Rnq1p modulates polyQ aggregation and toxicity came from the observation that mutations in endocytic proteins enhance toxicity in a [*RNQ*+]-dependent manner [134]. PolyQ aggregates partially sequester the endocytic machinery and actin, thereby inhibiting endocytosis. This defect was also seen in mammalian cells [134]. It was later discovered that proteins associated with the late stages of the maturing endocytic complexes are recruited into polyQ aggregates [135]. This co-aggregation is most likely due to the polyQ stretches present in many endocytic proteins. Similarly, Rnq1p and multiple chaperones also associate with aggregates of polyQ protein in [*RNQ*+] cells [132,134,136]. These protein interactions may help

initiate polyQ aggregation, and the Q/N-rich Rnq1p aggregates in [*RNQ*+] cells might template this process. Since Rnq1p has no known mammalian homolog, however, it is unclear whether a similar mechanism occurs in human disease. Nevertheless, the yeast model of polyQ aggregation provides a means of determining candidate proteins that may be involved in either suppressing or enhancing polyQ toxicity, and thereby provides a viable approach to identify novel therapeutic targets [137]. As such, the strict dependence of polyQ aggregation on the [*RNQ*+] prion shows how [*RNQ*+] can aid in studying pathological amyloid.

Rnq1p overexpression is toxic in [*RNQ*+] *cells*

In addition to its role in facilitating polyQ toxicity, it was shown that the overexpression of Rnq1p in [*RNQ*+] cells can also result in gain-of-function toxicity [37]. This toxicity required strong overexpression of full-length Rnq1p, as overexpression of either the PFD or the N-domain alone was not toxic. Overexpression of Sup35p in [*PSI*+] cells can also be toxic [24]. In this case, it is clear that the essential termination complex is sequestered into [*PSI*+] aggregates and the toxicity is rescued by overexpression of Sup35p's binding partner, Sup45p [138,139]. Analogously, the overexpression of Sis1p suppresses the toxicity of Rnq1p overexpression [37]. This rescue depends on the translocation of Rnq1p into the nucleus, resulting in increased Rnq1p aggregate formation [140]. Perhaps through a very different mechanism, overexpressing Rnq1p-L94A in [*RNQ*+] cells is also toxic. Sis1p overexpression does not suppress the L94A-induced toxicity since this mutant impairs the Rnq1p-Sis1p interaction [37]. Interestingly, Rnq1p-L94A overexpression is also toxic in [*rnq*-] cells, which can be attributed to its ability to form "off-pathway" aggregates in the absence of [*RNQ*+]. As seen for wild-type Rnq1p, however, directing Rnq1p-L94A to the nucleus via the addition of a nuclear localization signal suppresses toxicity

[140]. Furthermore, nuclear Rnq1p aggregates can act *in trans* to sequester Rnq1p from the cytosol and repress toxicity. It has been proposed that Rnq1p overexpression causes the accumulation of an off-pathway, toxic aggregate in the cytoplasm, but the nucleus provides an environment for more efficient formation into benign aggregates. These nuclear aggregates can also localize polyQ to the nucleus [140]. Yet, instead of suppressing toxicity, nuclear translocation of polyQ enhances toxicity by decreasing the formation of SDS-resistant polyQ aggregates [140]. Hence, while the nucleus may provide a better environment for the formation of a benign amyloid structure for Rnq1p, the nuclear environment renders polyQ more soluble and more toxic.

Ydj1p has also been shown to modulate Rnq1p-associated toxicity. Overexpression of the Rnq1p-PFD is toxic in Δ*ydj1* [*RNQ*+] cells, even though it is not toxic in wild-type cells [101]. In contrast to full-length Rnq1p, this toxicity is associated with the formation of SDS-resistant aggregates. The expression of Ydj1p was suggested to suppress this toxicity by binding to the Rnq1p-PFD and limiting the pool of aggregates. This suppression requires several features of Ydj1p: the zinc finger-like region (ZFLR) that is implicated in transfer of substrates to Hsp70s [141], the C-terminal domain 1 (CTD1), which contains a hydrophobic peptide-binding pocket [142], and farnesylation of the *CAAX* box [101]. Interestingly, these same domains were required for the Ydj1p-dependent suppression of polyQ toxicity [101]. These common mechanisms highlight the utility of Rnq1p as a model to further investigate the cellular machinery that regulates proteotoxicity. Additionally, these models may help to determine what types of protein conformers are toxic to cells.

1.3.7 Conclusions

While the term amyloid is generally associated with the proteins that aggregate in protein conformational disorders, there are an increasing number of examples of amyloid structures having a functional role in normal biology [10,46]. Clearly, some amyloidogenic proteins have the potential to form both toxic and non-toxic structures. From a structural standpoint, this is best detailed with the prion protein Het-s in the filamentous fungi *Podospora anserina*. Structures of Het-s associated with toxicity are amyloids having antiparallel β-sheets, whereas the benign structures identified form parallel β-sheets [143]. Similarly, the [*RNQ*+] prion may simultaneously serve as an example of a functional amyloid and as a model for understanding pathological amyloid, thereby allowing us to examine a number of questions relevant to either a physiological or disease context: What is the toxic protein conformer? How are protein aggregates toxic? What types of heterotypic interactions do amyloidogenic proteins have? How can a single protein form different aggregated structures? How do these various structures cause changes in phenotype? Studying these questions using the [*RNQ*+] prion will further our understanding of protein conformational disorders and perhaps also explain why evolution has preserved proteins that are susceptible to toxic conversion. Indeed, there are examples in biology of balancing selection, in which a certain trait has been conserved even though it is associated with disease, such as the sickle cell trait providing some resistance to malaria [144,145].

1.4 Molecular Chaperones

It has long been recognized that the native folded state of a protein is determined by its sequence [16]. This native state represents a balance between forming a structure that is thermodynamically stable, having nonpolar amino acid residues within the protein's interior, and a structure that has the necessary flexibility to perform its function [146]. However, in order to

find this equilibrium and ensure a properly folded protein, there are significant free energy barriers that must be overcome, especially with larger, more complex proteins [146]. Indeed, exposure of hydrophobic regions increases the propensity of a protein to aggregate [147]. Hence, in order to maintain proteostasis, as defined as a healthy proteome, an elaborate network has evolved that consists of ~1,300 different proteins in mammals that monitor the life cycle of proteins [146]. While there are a variety of cellular machineries that comprise this so-called proteostasis network, one of the largest groups is a class of proteins called molecular chaperones, which act as the cell's means of surveillance to prevent the misfolding and aggregation of protein [146]. The classic group of molecular chaperones are heat shock proteins (HSPs), which are often stress-inducible, and were originally grouped based on their molecular weight, such as Hsp40s, Hsp70s, and Hsp100s [146].

1.4.1 Hsp70 Machinery

The Hsp70 chaperones are ubiquitous, and play a role in all aspects of a protein's life cycle, including folding, re-folding, translocation, and degradation [148]. These proteins are divided into two domains, with an N-terminal adenine nucleotide-binding domain (NBD) and a C-terminal substrate-binding domain (SBD). Processing of client proteins relies on Hsp70 cycling through alternate ATP- and ADP-bound states. Transitioning between these states requires an Hsp40 and usually a nucleotide-exchange factor (NEF). In the ATP-bound state, Hsp70s are in an "open" conformation and interact readily with clients, but have low binding affinity. ATP hydrolysis and conversion to the ADP-bound "closed" conformation is needed to stabilize the interaction between Hsp70s and clients [148]. As the basal Hsp70 ATPase activity is low, Hsp40s are responsible for stimulating the ATPase activity of Hsp70 >1,000 fold to the

ADP-bound state [146]. After substrate processing, dissociation of ADP and exchange for ATP is regulated by NEFs, returning Hsp70 to the "open" conformation and ready to bind another substrate. Thus, the activity of Hsp70 and its involvement in a variety of processes depends on additional molecular chaperones.

In addition to stimulating ATP hydrolysis of Hsp70s, the canonical function of Hsp40s is to deliver substrates to Hsp70 [149]. Interestingly, humans have only 11 Hsp70s, but they have 41 different Hsp40s that have a large amount of sequence variation [148]. This suggests that Hsp40s are specialized proteins, serving to dictate Hsp70 function and selectivity, with particular Hsp40s likely involved in particular cellular functions. There are three classes of Hsp40s that are loosely divided based on domain structure [102]. Common to all three groups is the J domain, so named because it shares homology with DnaJ, the Hsp40 present in *E. coli*. This domain is responsible for the interaction with Hsp70 and stimulating its ATPase activity. For class I Hsp40s, the J domain is N-terminal, followed by a domain that is rich in glycine and phenylalanine residues (G/F), a zinc finger motif, a C-terminal substrate-binding domain, and a dimerization domain at the end of the C-terminus [148]. Class II Hsp40s share a similar domain scheme, but lack the zinc finger motif. By contrast, class III Hsp40s are a non-canonical group that have diverse domain modules. While there is some functional redundancy between various Hsp40s [150], it is clear that the variation present in Hsp40 family members provides the cell and Hsp70 with the ability to handle a wide range of substrates.

1.4.2 Chaperonopathies

Molecular chaperones have a protective role in the cell to help prevent the accumulation of misfolded protein. When a protein misfolds, chaperones will bind the hydrophobic regions of

the substrate that become exposed [151-153] and will determine whether the protein can be refolded or should be degraded. However, the cellular response and capability to handling misfolded substrates can be overwhelmed [154]. Indeed, it is suggested that there is a dramatic decline in the proteostasis network as a cell and organism ages, thereby contributing to the accumulation of protein aggregates and onset of age-related protein conformational disorders [155]. Molecular chaperones have been implicated in a number of these diseases, being found in protein inclusions that might act to sequester these chaperones [156,157]. Interestingly, there are an increasing number mutations being identified in chaperones that cause a variety of distinct disorders [157]. Collectively, these disorders are now being called chaperonopathies [158].

One recently identified chaperonopathy is the limb-girdle muscular dystrophy type 1D (LGMD1D) that is caused by mutations in the Hsp40 DNAJB6 [159-162]. LGMD disorders comprise a heterogeneous group of muscular dystrophies that are characterized by progressive proximal weakness and muscle degeneration and have autosomal patterns of inheritance [163]. In the case of LGMD1D, a major pathological feature is the presence of protein aggregates and vacuoles in the affected skeletal muscle [159]. Interestingly, mutations in other chaperones, including VCP, BAG3, and αB-crystallin, also cause dominantly inherited myopathies that exhibit the accumulation of protein aggregates [164-166]. Hence, it is clear that disrupting chaperone function can lead to significant defects in proteostasis, especially in skeletal muscle, and contributes to the pathogenesis of various diseases.

1.5 Summary and Significance

The formation of amyloid is a common phenomenon, not only occurring as part of the development of several diseases, but also serving as a functional entity in various unrelated

processes [2]. Across this spectrum, there are several generic structural features of amyloid that are independent of the protein determinant. However, on a smaller scale, there are several subtler variations that can occur within the amyloid fiber. This sort of variation associated with amyloid polymorphism can have dramatic consequences in terms of pathological and phenotypic differences. Moreover, molecular chaperones play a critical role in monitoring the formation of these amyloid morphotypes, and protein misfolding in general. Indeed, amyloid and its particular subtypes can overwhelm the activity of molecular chaperones and various mechanisms of protein quality control [154]. Therefore, studying the interplay of amyloid and chaperones, and the underlying mechanisms that influence these interactions, is crucial to gaining a better understanding of protein conformational disorders, and even normal biological processes that involve functional amyloid.

This dissertation is separated into two major parts that both describe the use of yeast prion variants to study the effect of amyloid polymorphism on phenotypic variation. Chapters two and three explore the biochemical, intragenic, and *trans*-acting factors that contribute to the propagation of distinct prion variants of [*RNQ*+] and [*PSI*+]. I show that there are a wide variety of variables involved, including distinct requirements of the primary structure of the aggregating protein as well as different domains of chaperones. Thus, this highlights the complex nature of amyloid polymorphism and the resulting diversity in phenotypes. Then, in Chapters four and five, I explore the effects of mutations in the Hsp40 DNAJB6 that are associated with LGMD1D. Here, I show how amyloid polymorphism might be involved in the pathogenesis of this disorder and provide some mechanistic understanding for how the DNAJB6 mutations might cause disease. Finally, Chapter six describes the broader implications of this work and the important future directions that could provide significant insight into the basis of amyloid polymorphism.

Chapter 2: Extensive Diversity of Prion Strains is Defined by Differential Chaperone Interactions and Distinct Amyloidogenic Regions

Kevin C. Stein and Heather L. True

This chapter is published in the journal *PLOS Genetics* 10, e1004337 (2014).

2.1 Abstract

Amyloidogenic proteins associated with a variety of unrelated diseases are typically capable of forming several distinct self-templating conformers. In prion diseases, these different structures, called prion strains (or variants), confer dramatic variation in disease pathology and transmission. Aggregate stability has been found to be a key determinant of the diverse pathological consequences of different prion strains. Yet, it remains largely unclear what other factors might account for the widespread phenotypic variation seen with aggregation-prone proteins. Here, we examined a set of yeast prion variants of the [*RNQ*+] prion that differ in their ability to induce the formation of another yeast prion called [*PSI*+]. Remarkably, we found that the [*RNQ*+] variants require different, non-contiguous regions of the Rnq1 protein for both prion propagation and [*PSI*+] induction. This included regions outside of the canonical prion-forming domain of Rnq1. Remarkably, such differences did not result in variation in aggregate stability. Our analysis also revealed a striking difference in the ability of these [*RNQ*+] variants to interact with the chaperone Sis1. Thus, our work shows that the differential influence of various amyloidogenic regions and interactions with host cofactors are critical determinants of the phenotypic consequences of distinct aggregate structures. This helps reveal the complex interdependent factors that influence how a particular amyloid structure may dictate disease pathology and progression.

2.2 Author Summary

Protein conformational disorders, including many neurodegenerative diseases, result when a protein misfolds and undergoes a conformational change to form self-templating aggregates, called amyloid. Interestingly, the proteins that misfold in these diseases tend to form

a wide variety of distinct aggregate structures. In prion diseases, these different amyloid conformations are called prion strains. The different conformations of prion strains are responsible for modulating disease progression, pathology, and transmission. Previous work with yeast prions has provided tremendous insight into how distinct prion conformers can cause such phenotypic variability. Here, we used a set of [*RNQ*+] prion variants to show the complex web of interactions involved in the propagation of distinct aggregate structures. We found that several different non-adjacent regions of Rnq1, even outside the prion-forming domain, make varying contributions to the propagation of distinct variants of the [*RNQ*+] prion. Moreover, our data support the hypothesis that the [*RNQ*+] variants differentially interact with the molecular chaperone Sis1. These data strongly suggest that the variable phenotypic manifestations of different aggregate conformations depend upon a unique set of primary structural elements and differential interactions with host cofactors.

2.3 Introduction

The misfolding of proteins to form cross-β sheet amyloid structures is characteristic of a variety of diseases, including many neurodegenerative disorders, such as Alzheimer's disease [1]. Increasing evidence suggests that these protein conformational disorders are caused by a similar etiological mechanism, in which the amyloid that forms represents an infectious, self-templating structure that is often described as prion-like [167,168]. Prion diseases are caused when the native form of the prion protein (PrP^{C}) misfolds and aggregates to form the amyloid structure called PrP^{Sc} [5]. PrP^{Sc} is considered infectious because it transmits its pathogenic conformation by templating the conversion of other native PrP^{C} monomers to PrP^{Sc} in a self-propagating fashion [169].

To add another layer of complexity, it now appears that the proteins that misfold in these disorders can adopt an array of different aggregated conformations, called prion strains in prion diseases [43,44,170]. Prion strains often have unique biochemical properties and encode different degrees of infectivity [17]. These differences are thought to be the underlying cause of the widespread pathological variation seen in prion diseases. It was recently shown that distinct self-propagating structures of α-synuclein, the protein that misfolds in Parkinson's disease, also exist and promote the formation of tau inclusions to different extents [171]. Yet, with estimates that a single amyloidogenic protein like PrP may propagate over 30 distinct aggregate conformers [172], it is unclear what underlying factors contribute to such widespread structural and phenotypic diversity.

A tremendous amount of insight into the physical basis of prion strains, and amyloid polymorphism in general, has come from studying the prion strains that are endogenous to the budding yeast *Saccharomyces cerevisiae* (here also called prion variants). Like mammalian amyloidogenic proteins, yeast prion proteins form self-propagating, β sheet-rich amyloid structures. These self-perpetuating yeast prions exhibit dominant, non-Mendelian inheritance that promotes variation in cellular phenotypes [14]. One of the most well-studied yeast prions is the [*PSI*+] prion, formed from the translation termination factor Sup35. Sup35 is soluble and functional in [*psi*-] cells, but Sup35 misfolds and is sequestered into prion aggregates in [*PSI*+] cells, resulting in a nonsense suppression phenotype [48,49]. Two [*PSI*+] prion variants were initially categorized based on the degree of nonsense suppression [24]. Cells propagating the strong [*PSI*+] variant showed increased nonsense suppression relative to cells propagating the weak [*PSI*+] variant. Yet, like prion strains of PrP^{Sc}, it has become clear that a large continuum of different [*PSI*+] variants also exists [173-175].

Studies of conformationally distinct amyloid fibers of the prion-forming domain (PFD) of Sup35 formed *in vitro* have helped reveal a foundation to explain the structural and phenotypic differences between [*PSI*+] variants [25,26,68,69,176]. Like most yeast prions, and even several disease-associated proteins, Sup35 has a PFD that is rich in glutamine and asparagine (Q/N) residues, and is necessary for the maintenance of [*PSI*+] [8,14,24,177-179]. In distinguishing [*PSI*+] variants, it was shown that the contiguous length of the Sup35-PFD that forms the amyloid core correlates with a set of interdependent biochemical properties, including fiber stability, average aggregate size, and replication kinetics [25,26,69,117,180,181]. Collectively, these parameters dictate a balance between fiber fragmentation and fiber growth, which is the major biophysical determinant of the resulting [*PSI*+] phenotype [25]. In the case of strong [*PSI*+] cells, the shorter and more fragile amyloid core of the Sup35 aggregates gives rise to more fragmentation and greater sequestration of Sup35 into aggregates, thereby resulting in more nonsense suppression. The more stable structure of Sup35 aggregates in weak [*PSI*+] cells, on the other hand, does not as readily fragment or capture monomer; hence, a larger pool of functional protein remains to participate in translation termination. These biochemical parameters have served as the foundation to describe the structural basis of prion strains, and have been shown to apply to various PrP^{Sc} strains [27,182]. However, these correlations do not always hold true for the wide variety of structural variants that are possible for [*PSI*+], PrP^{Sc}, and even another yeast prion, [*RNQ*+] [28,29,32,33,172,183]. Thus, it remains a mystery what other variables help determine the extensive phenotypic differences exhibited by different prion strains.

Interestingly, while [*PSI*+] modulates translation termination, the major phenotypic manifestation of the [*RNQ*+] prion (also called [*PIN*+] and formed from the Rnq1 protein) is

inducing the *de novo* formation of [*PSI*+] [11,58-61,64]. The formation of [*PSI*+], but not its continued propagation, relies on the presence of the [*RNQ*+] prion [59]. Five different variants of the [*RNQ*+] prion have been categorized based on how frequently they facilitate [*PSI*+] formation, from low rates to very high rates [31]. These [*RNQ*+] variants were also classified by the aggregate pattern observed in cells expressing GFP-tagged Rnq1 [120]. Cells predominately showing one fluorescent focus were called single-dot (s.d.) [*RNQ*+], while cells having many foci were called multiple-dot (m.d.) [*RNQ*+]. Recently, it was demonstrated that Rnq1 can form over 40 variants of the [*RNQ*+] prion [32], and different [*RNQ*+] variants were also found in wild yeast isolates [35]. While the mechanism of how [*RNQ*+] affects [*PSI*+] formation remains to be elucidated, a number of studies suggest that [*RNQ*+] acts as an imperfect template that interacts with Sup35 to cross-seed the induction of [*PSI*+] [78,107,121]. Indeed, similar to Sup35, Rnq1 has a Q/N-rich PFD that is necessary for prion propagation and may facilitate the interaction with Sup35 [64,73,78]. However, while some differences in biochemical and cellular properties have been noted between [*RNQ*+] variants, none of these properties explain how [*RNQ*+] variants differentially promote [*PSI*+] formation [31-33,108,120,184].

Here, we set out to determine what factors distinguish [*RNQ*+] prion variants to allow for such dramatic phenotypic differences in [*PSI*+] inducibility. We found that each [*RNQ*+] variant relies on a distinct set of non-adjacent regions for both propagation and interaction with Sup35. While there is normally much emphasis on Q/N-rich prion-like domains, we show that regions outside of the canonical Rnq1-PFD influence [*RNQ*+] propagation in a variant-dependent manner. Furthermore, our data provide striking support for the hypothesis that different interactions between amyloid and molecular chaperones, and potentially other cellular cofactors, influence the phenotypic manifestations of distinct prion variants. This work helps reveal the

structural and biological complexity underlying prion strains, showing that a large set of interdependent factors likely contribute to the ability of distinct aggregate conformations to modulate disease phenotype and transmissibility.

2.4 Results

2.4.1 Fiber fragmentation parameters do not distinguish [*RNQ*+] *variants*

[*PSI*+] variants are easily distinguished by a set of parameters that define an equilibrium between fiber growth and fiber fragmentation [25]. We asked whether these parameters could similarly distinguish a set of previously published [*RNQ*+] variants. This set consisted of four s.d. [*RNQ*+] variants having [*PSI*+] induction levels from low to very high, and one m.d. [*RNQ*+] variant with a high level of [*PSI*+] induction [31]. We first examined whether differences in the fragmentation of the [*RNQ*+] variants could explain the differences in [*PSI*+] inducibility. The properties that dictate fragmentation often include aggregate stability, aggregate size, and chaperone interactions. To test the stability of the Rnq1 aggregates, we subjected [*RNQ*+] [*psi*-] cell lysates to a gradient of increasing temperature, as different amyloid conformations can have different melting temperatures (T_m) [69]. In agreement with previous studies [32,78,108], we found that only the m.d. high [*RNQ*+] variant was thermal labile, having a much lower T_m (~58°C) as compared to the similar T_m (~86°C) of all the s.d. [*RNQ*+] variants (Figure 1A). We also analyzed the sensitivity of Rnq1 aggregates to protease digestion, as work with the mammalian PrP^{Sc} prion has shown that prion strains can display different sensitivities to digestion with proteinase K (PK) [17]. Strains of α-synuclein also show different levels of PK sensitivity [171]. After incubating cell lysates with PK at 37°C, we again found that only m.d.

high [*RNQ*+] was an outlier in displaying increased PK resistance as compared to the s.d. [*RNQ*+] variants (Figure 1B and Figure S1).

We then analyzed the average size distribution of the Rnq1 aggregates using semi-denaturing agarose gel electrophoresis (SDD-AGE), which resolves the Rnq1 aggregated species. By electrophoretically separating the protein longer, we observed some more distinctions between the [*RNQ*+] variants than previously described [108]. There was a gradual decrease in aggregate size between s.d. low, s.d. medium, and s.d. high [*RNQ*+] (notice the aggregates of s.d. low [*RNQ*+] that appear stuck in the well) (Figure 1C). However, both s.d. very high and m.d. high [*RNQ*+] had predominantly larger aggregates.

Another major factor that distinguishes the ability of yeast prion variants to fragment *in vivo* is their interaction with chaperones. Prion replication requires recognition of prion aggregates by the Hsp40 co-chaperone Sis1 and fragmentation by Hsp104 to create "seeds" (or propagons) that cause further monomeric conversion to the prion state [14,90]. Sis1 interacts with Rnq1 specifically in [*RNQ*+] cells [74] and this interaction is required for propagation of [*RNQ*+] [99]. Additionally, more Sis1 is associated with Rnq1 aggregates as compared to Sup35 aggregates [185], which may suggest that Sis1 plays a more significant role in the propagation of [*RNQ*+] as compared to [*PSI*+]. Therefore, as another measure of fragmentability, we asked whether the level of Sis1 associated with Rnq1 differed between [*RNQ*+] variants. To test this, we immunoprecipitated Sis1 from [*rnq*-] cells or cells propagating the [*RNQ*+] variants and immunoblotted for Rnq1. While Sis1 did not co-immunoprecipitate Rnq1 in [*rnq*-] cells, Sis1 and Rnq1 were similarly associated in all [*RNQ*+] cells (Figure 1D), in agreement with a previous study [184]. Furthermore, all the [*RNQ*+] variants depended on Sis1 expression to similar levels for their maintenance (data not shown).

These data do not preclude the possibility that the [*RNQ*+] variants are fragmented to different extents. However, they show that the standard parameters used to monitor fragmentation neither distinguish the [*RNQ*+] variants, as they do for [*PSI*+] variants, nor correlate to [*PSI*+] inducibility.

2.4.2 Fiber growth parameters do not explain phenotypic differences of [*RNQ*+] *variants*

In addition to differences in fiber fragmentation, [*PSI*+] variants also show differences in fiber growth parameters. Knowing the functional role of Sup35 in translation termination allows these differences to be easily monitored phenotypically. The most common means involves colorimetrically measuring the degree of nonsense suppression of the *ade1-14* allele that has a premature stop codon in the *ADE1* gene [186]. The large soluble pool of Sup35 in [*psi*-] cells allows for faithful translation termination at the premature stop codon. This results in the accumulation of a metabolic intermediate and incomplete synthesis of adenine, thereby making these cells unable to grow on medium lacking adenine, and colonies grown on rich media are red. By contrast, Sup35 aggregates in strong [*PSI*+] cells readily recruit and sequester soluble Sup35 into aggregates to cause nonsense suppression [24,118]. Hence, strong [*PSI*+] cells have less soluble Sup35, propagate a mitotically stable aggregate structure, and form light pink or white colonies that grow well on medium lacking adenine. Weak [*PSI*+] cells, on the other hand, have an intermediate phenotype. Thus, the fiber growth characteristics of [*PSI*+] variants are often monitored by: mitotic stability, the amount of soluble protein, and the resulting [*PSI*+] phenotype.

In contrast to Sup35, the functional role of Rnq1 is not known. Hence, in order to phenotypically monitor [*RNQ*+], we previously developed a chimeric protein called the [*RNQ*+]

Reporter Protein (RRP) [78], which consists of the Rnq1-PFD(153-405) fused to the middle and C-terminal domains of Sup35 that provide the GTPase activity required for translation termination [187]. RRP allows us to monitor the [*RNQ*+] prion state by colony color phenotype in a manner analogous to [*PSI*+]. RRP is functional in translation termination in [*rnq*-] cells that remain red, while it co-aggregates with Rnq1 in [*RNQ*+] cells to generate colonies that are phenotypically pink or white [32,33]. Thus, the [*RRP*+] phenotype, like the [*PSI*+] phenotype, serves as a measure of the prion variant-specific sequestration of monomeric protein. Hence, to examine fiber growth parameters, we first determined the [*RRP*+] phenotype for the set of [*RNQ*+] variants studied in this work. Interestingly, we found that the three "higher" [*RNQ*+] variants had a stronger nonsense suppression phenotype as compared to s.d. low and s.d. medium [*RNQ*+] (Figure 2A). Previous work demonstrated that s.d. very high [*RNQ*+] cells had the greatest amount of soluble Rnq1 [31]. Hence, this suggests that, in contrast to other published [*RNQ*+] variants [33], the [*RRP*+] phenotype of the set of [*RNQ*+] variants in this study does not correlate to the level of soluble Rnq1. Moreover, it was surprising that the [*RRP*+] phenotype correlated to [*PSI*+] inducibility for these [*RNQ*+] variants, as this was not the case for other [*RNQ*+] variants [32,33], or for several other prion properties of [*RNQ*+] (this work and [31,108,184]).

The mitotic stability of prion variants is another measure of fiber growth as this property relies on the degree to which monomer is sequestered into aggregates. This property has been shown to distinguish [*PSI*+] variants and other [*RNQ*+] variants [24,32,33]. Hence, to test the mitotic stability of the [*RNQ*+] variants, we plated overnight cultures of cells expressing RRP and propagating each of the [*RNQ*+] variants onto rich media, and then counted the number of colonies that were red or had red sectors (indicating loss of the [*RRP*+] phenotype and the

[*RNQ*+] prion). We found that both s.d. low and s.d. very high [*RNQ*+] showed higher levels of mitotic loss compared to the other three [*RNQ*+] variants (Figure 2B). This loosely correlates with the amount of soluble Rnq1 present in these cells: s.d. low and s.d. very high [*RNQ*+] have been shown to have the greatest amount of soluble Rnq1 [31]. However, because s.d. low [*RNQ*+] has less soluble protein as compared to s.d. very high [*RNQ*+] [31], we would have expected s.d. low [*RNQ*+] to have higher mitotic stability. Hence, mitotic stability did not correlate to either the [*RRP*+] phenotypes or the level of soluble Rnq1 of this set of [*RNQ*+] variants, in contrast to what was shown with [*PSI*+] variants and other [*RNQ*+] variants [33,118].

2.4.3 The region outside of the Rnq1-PFD has variant-specific influence on fiber growth

While regions outside of PFDs remain under-studied, various work has implicated non-PFD regions as affecting prion propagation [180,188]. Indeed, the N-terminal domain that lies outside of the putative Rnq1-PFD can influence the propagation of [*RNQ*+] [76-78]. As such, to gain insight into how the [*RNQ*+] variants are physically distinct, we hypothesized that the Rnq1 N-terminal domain might impact [*RNQ*+] propagation in a variant-specific manner. To address this, we used a modified version of RRP containing full-length (FL) Rnq1 (aa 1-405) fused to the MC domains of Sup35, in contrast to the original version of RRP that contained just the Rnq1-PFD (aa 153-405). Using *sup35Δ* cells that were complemented by episomal *SUP35*, we used a plasmid shuffle technique to replace Sup35 with plasmids expressing RRP, FL RRP, or Sup35. Strikingly, FL RRP was not able to functionally replace Sup35 in cells propagating the m.d. high [*RNQ*+] variant (Figure 2C). Importantly, there was no effect on viability when cells still expressed Sup35. Moreover, the inviability depended on the presence of both the m.d. high [*RNQ*+] variant and the Rnq1 protein, as eliminating (curing) the prion or deleting *RNQ1* before

replacing Sup35 with FL RRP resulted in viable cells (Figures 2C and S2). (As expected, the cells were white in the latter case, indicating that FL RRP propagates the aggregated structure of m.d. high [*RNQ*+] in the absence of the Rnq1 protein since FL Rnq1 is still expressed as part of FL RRP.) In light of previous work showing that m.d. high [*RNQ*+] cells have relatively little soluble Rnq1 [31], these data suggest that the presence of the Rnq1 N-terminus on FL RRP promotes sequestration of FL RRP into Rnq1 aggregates to such a large extent that there is too little soluble FL RRP to function in translation termination. In contrast, [*rnq*-] cells and cells propagating each of the s.d. [*RNQ*+] variants were viable when expressing FL RRP (Figures 2C and S3). In fact, cells propagating each of the s.d. [*RNQ*+] variants and harboring FL RRP were darker pink as compared to the equivalent cells expressing RRP, thus indicating that translation termination was more efficient.

Based on the different phenotypes that resulted from using RRP versus FL RRP, we wanted to more directly test, without the use of RRP, whether the Rnq1 N-terminus influenced the ability of newly synthesized Rnq1 to join pre-existing Rnq1 aggregates. We used a galactose-inducible promoter to express HA-tagged Rnq1 or Rnq1-PFD in cells that are grown in media containing galactose. Then we monitored the ability of Rnq1 monomer to join untagged pre-existing aggregates of the different [*RNQ*+] variants using a well-trap assay. This assay allows us to easily determine the amount of soluble Rnq1 in the cell, as aggregated Rnq1 is retained in the wells of an SDS-PAGE gel when samples are not boiled [189]. As expected for [*rnq*-] cells, upon inducing expression of HA-Rnq1 or Rnq1-PFD, we found that all pre-existing and newly synthesized Rnq1 protein was soluble (Figure 2D). By contrast, all newly synthesized HA-Rnq1 joined the pre-existing aggregates for each of the [*RNQ*+] variants, as indicated by the absence of a band in the unboiled lanes. Interestingly, we saw variant-specific effects when we expressed

just the Rnq1-PFD. For m.d. high [*RNQ*+], newly synthesized Rnq1-PFD, like HA-Rnq1, completely joined the pre-existing aggregates in the given time duration. All of the s.d. [*RNQ*+] variants, on the other hand, maintained a soluble pool of Rnq1-PFD. These data indicate that recruitment of Rnq1-PFD monomers into aggregates occurs more readily for m.d. high [*RNQ*+] in comparison to the s.d. [*RNQ*+] variants. Additionally, it suggests that the Rnq1 N-terminus is important for facilitating monomer addition and fiber growth with the s.d. [*RNQ*+] variants, similar to what we demonstrated above for m.d. high [*RNQ*+] using FL RRP.

Finally, we wanted to test whether this influence of the Rnq1 N-terminal domain on fiber growth was necessary for propagation of the [*RNQ*+] variants. To do this, we deleted *RNQ1* in RRP-expressing yeast cells that were complemented with a *URA3*-marked plasmid expressing *RNQ1*. Cells that lose this plasmid would express only the Rnq1-PFD as part of RRP, and would not express the Rnq1 N-terminal domain. After growing cultures in non-selective media, we plated [*rnq*-] cells and cells propagating each of the [*RNQ*+] variants on media to select for either maintenance (SD-ura) or loss (5-FOA) of the *RNQ1* plasmid. In agreement with our previous results [78], m.d. high [*RNQ*+] did not propagate when Rnq1 was lost, as it was phenotypically [*rnq*-] on 5-FOA medium and did not grow on medium lacking adenine and containing 5-FOA (Figure 2E). This suggests that the Rnq1-PFD is not sufficient to propagate this variant. In stark contrast, all of the s.d. [*RNQ*+] variants could still maintain [*RNQ*+], albeit to varying degrees. This indicates that propagation of m.d. high [*RNQ*+] has a greater reliance on the non-prion-forming N-terminal domain than the s.d. [*RNQ*+] variants. Furthermore, it suggests that propagation of the s.d. [*RNQ*+] variants might differentially depend on the presence of the N-terminal domain. Indeed, we passaged the *rnq1Δ* cells harboring the s.d. [*RNQ*+] variants that had lost the *RNQ1* plasmid and found that, after further growth, these cells did not maintain the

same [*RRP*+] phenotype as the *RNQ1* [*RNQ*+] cells expressing RRP (compare Figure 2A to Figure 2F). For instance, both s.d. low and s.d. medium [*RNQ*+] had a much stronger nonsense suppression phenotype as compared to their phenotype when Rnq1 was present.

Taken together, these data suggest that the [*RNQ*+] variants show differences in fiber growth parameters, which are mediated, in part, by the Rnq1 N-terminal domain. However, despite these differences in properties of fiber growth and fragmentation, these data do not wholly distinguish the [*RNQ*+] variants or explain their differential ability to induce [*PSI*+]. This is in line with previous work that also shows a lack of correlation [184]. Hence, these data highlight the complex nature of both [*PSI*+] induction and the phenotypic consequences that are possible with distinct aggregate structures.

2.4.4 [*RNQ*+] *variants show differential reliance on amyloidogenic regions*

To help elucidate the basis of the structural diversity of the [*RNQ*+] variants and the phenotypic differences they modulate, we postulated that each of the [*RNQ*+] variants, like [*PSI*+], has a different part of the primary structure that is important for prion propagation. Propagation of strong [*PSI*+] incorporates fewer residues of the Sup35-PFD in the amyloid core as compared to weak [*PSI*+], and this difference is tightly correlated to the biochemical and phenotypic differences seen between [*PSI*+] variants [26,176,180]. Hence, determining the regions of Rnq1 that are important for propagation of each of the [*RNQ*+] variants would provide insight into how the [*RNQ*+] variants are structurally different and can mediate differences in [*PSI*+] formation. To help identify these sequence elements, we used five different algorithms that were developed to find regions of a protein predicted to facilitate the formation of amyloid [190-194]. These algorithms found 11 putative amyloidogenic regions spread throughout both

the N-terminal domain and the PFD of Rnq1 (Figure 3). We will refer to these regions hereafter as A1 through A11.

We set out to analyze the influence of these regions on the propagation of the different [*RNQ*+] variants. We mutated each of these regions in its entirety to alanine to make 11 Rnq1 mutant constructs and confirmed expression levels similar to wild-type (WT) Rnq1 (Figure S4). After using a plasmid shuffle technique to replace WT Rnq1 with these mutants in cells propagating each of the [*RNQ*+] variants, we then examined three biochemical properties commonly used to monitor prion replication: 1) the relative distribution of Rnq1 aggregates using SDD-AGE, 2) the amount of soluble Rnq1 by solubility assay, and 3) the thermal stability of Rnq1 aggregates. These assays provide complementary information about the propagation of [*RNQ*+]; for example, detection of monomeric Rnq1 with SDD-AGE is variable for unknown reasons, thus using the solubility assay is informative. Additionally, since these assays examine different aspects of prion propagation, we hypothesized that we might see a difference by one assay and not another. Therefore, collectively, these assays allowed us to make conclusions about how mutation of the amyloidogenic regions in Rnq1 affected [*RNQ*+] propagation.

For each assay, we categorized the reproducible effects of the alanine mutants as mild, moderate, curing [*RNQ*+], or having no effect (Figure S5). Taking all three assays into account, we then scored the overall influence of disrupting the amyloidogenic regions on each [*RNQ*+] variant (Figure 4A). As expected, since our data above showed the involvement of the N-terminus in [*RNQ*+] propagation, we found that the N-terminal alanine mutants revealed regions of both common and unique importance for the [*RNQ*+] variants. For instance, mutation of the A1 or A3 regions both affected the biochemical properties of all of the [*RNQ*+] variants. However, these mutants also showed variant-specific effects. With s.d. high [*RNQ*+], for

example, expression of the A1 and A3 mutants resulted in a dramatic shift in relative aggregate size distribution, but the other N-terminal mutations had minimal effect on propagation of s.d. high [*RNQ*+] (Figure 4B). By contrast, the A3 mutant cured the m.d. high [*RNQ*+] variant, while the A1 mutant resulted in a shift in aggregate size. These data show that particular regions within the non-PFD N-domain have differential roles on prion propagation depending on what [*RNQ*+] variant is present. This indicates that this domain helps define the physical basis of distinct [*RNQ*+] variants.

Prion-forming domains are historically considered the region that forms the amyloid core of prion aggregates [73,80]. As such, PFDs are predicted to encode variant-specific differences, as is the case for weak and strong [*PSI*+] [26,176,180]. Indeed, we have previously shown that deletion of part of the Rnq1-PFD differentially affects the propagation of some [*RNQ*+] variants [78]. Hence, we expected to uncover conformation-specific effects with mutation of the amyloidogenic regions in the Rnq1-PFD. We found that mutation of the A11 region affected propagation of all of the [*RNQ*+] variants, but to varying degrees. For instance, the A11 mutant was the only mutant that cured s.d. low [*RNQ*+] (Figure 4C). On the other hand, none of the PFD alanine mutants cured s.d. medium [*RNQ*+], only mutation of the N-terminal A3 region did (Figure 4D). This suggests that the A3 and A11 regions are the most important of the amyloidogenic regions for propagation of s.d. medium and s.d. low [*RNQ*+], respectively. Strikingly, disruption of 8 of the 11 amyloidogenic regions affected propagation of s.d. very high [*RNQ*+], with several alanine mutants quickly curing this variant (A1, A5, A10, A11) (Figure 4E). Additionally, upon further growth, the s.d. very high [*RNQ*+] variant was also cured by mutation of the A2, A3, A4, and A9 regions. Importantly, loss of [*RNQ*+] was confirmed by the

absence of SDS-resistant aggregates by SDD-AGE after re-transforming a plasmid expressing WT Rnq1 and selecting for loss of the Rnq1 alanine mutant plasmid (Figure S6).

Overall, it has previously been shown that different, non-adjacent Q/N-rich regions of the Rnq1 protein make differential contributions to [*RNQ*+] propagation [84]. Our data now show that a unique set of non-contiguous regions, even regions that are not Q/N-rich, defines the propagation of the [*RNQ*+] variants. This strongly supports the hypothesis that the [*RNQ*+] variants propagate distinct structural conformations and likely mediate differential induction of [*PSI*+] by exposing a different structural template.

2.4.5 [*RNQ*+] *variants have additional Sis1 binding sites*

We wanted to better understand the role that these putative amyloidogenic regions play in propagating the different conformations of [*RNQ*+]. We noted that most of these regions were primarily hydrophobic, with some regions being previously identified as separating the Q/N-rich regions of the Rnq1-PFD [84]. It was unsurprising that the prediction algorithms identified these regions, as hydrophobic residues are generally recognized as sites that facilitate protein interactions, whether normal or abnormal interactions [195]. We conjectured two predominant ways that mutation of these amyloidogenic regions could affect the prion replication cycle of [*RNQ*+]: 1) disrupting the aggregate structure, or 2) disrupting the ability of chaperones to bind the Rnq1 aggregates. Interestingly, one of the amyloidogenic regions of Rnq1, A3 (aa 92-102), was previously identified as containing a binding site for the Hsp40 chaperone Sis1 [37]. Disruption of this site using the Rnq1-L94A mutation impairs Sis1 binding and eliminates the [*RNQ*+] prion [37,75]. Moreover, the bacterial Hsp40 has been predicted to bind several different hydrophobic stretches in each protein of nearly the whole proteome [152,153]. In line with this,

we found that the ANCHOR algorithm, which predicts protein-binding sites in disordered stretches [196,197], identified all of our amyloidogenic regions (except the lone hydrophilic A9 region) to be putative chaperone-binding sites (Figure 5A). As such, we first wanted to test whether Sis1 could bind other regions of Rnq1 outside of the known A3 binding site. To do this, we expressed Rnq1-PFD (which lacks the A3 binding site) in place of full-length Rnq1 in cells propagating each of the [*RNQ*+] variants. Upon immunoprecipitating Sis1, we found that Sis1 could still bind the PFD of Rnq1 in [*RNQ*+] cells, but not in [*rnq*-] cells (Figure 5B), suggesting that some of the amyloidogenic regions in the Rnq1-PFD may serve as additional binding sites for Sis1. Interestingly, in contrast to Figure 1D in which Sis1 bound equal levels of full-length Rnq1 in all of the [*RNQ*+] variants, there was distinctly less Rnq1-PFD bound to Sis1 in the m.d. high [*RNQ*+] variant. While we confirmed that these cells were still [*RNQ*+] at this time point (data not shown), this suggests that propagation of the m.d. high [*RNQ*+] conformer might uniquely require the presence of the A3 binding site. Indeed, this would provide some mechanistic explanation for our finding that the Rnq1-PFD as part of RRP is not sufficient for propagation of the m.d. high [*RNQ*+] variant in particular (Figure 2E).

2.4.6 Rnq1 amyloidogenic regions differentially contribute to the interaction of Sis1 with the [*RNQ*+] *variants*

Since Sis1 only binds Rnq1 in [*RNQ*+] cells, it is challenging to distinguish whether loss of Sis1 binding results in curing [*RNQ*+], or if curing [*RNQ*+] by disrupting some other aspect required for prion propagation results in loss of Sis1 binding. As the A3 region was previously shown to be a major binding site for Sis1, we hypothesized that disruption of this region by the Rnq1-L94A mutation would provide a useful comparison for examining how mutation of the

amyloidogenic regions influences Sis1 binding and propagation of [*RNQ*+]. Therefore, to determine the effect of Rnq1-L94A on [*RNQ*+] propagation, we expressed Rnq1-L94A in place of WT Rnq1 in cells propagating each of the [*RNQ*+] variants and monitored the maintenance of [*RNQ*+] by SDD-AGE. Like the variant-specific differences we observed above, we found that Rnq1-L94A also differentially affected the [*RNQ*+] variants: s.d. very high [*RNQ*+] could still propagate while the other four [*RNQ*+] variants were cured (Figure 5C). However, upon growing cells additional generations, we found that s.d. very high [*RNQ*+] was eventually cured as well (data not shown). This delayed curing suggests that s.d. very high [*RNQ*+] does not rely on the L94 Sis1 binding site in the A3 region to the same extent as the other [*RNQ*+] variants. Importantly, over-expressing Sis1 before replacing WT Rnq1 with Rnq1-L94A rescued propagation of the [*RNQ*+] variants, as an SDS-resistant species was still maintained (Figure 5C) and was transmissible (data not shown). Therefore, these data indicate that over-expression of Sis1 compensates for the disruption of Sis1 binding caused by the Rnq1-L94A mutation.

In using Rnq1-L94A as a model of how disruption of Sis1 binding affects [*RNQ*+], we hypothesized that if mutation of the Rnq1 amyloidogenic regions impaired the binding of Sis1, then Sis1 over-expression would at least partially rescue the propagation of the [*RNQ*+] variants. As a corollary, we postulated that if the mutations instead disrupted the Rnq1 aggregate structure, then these mutants would still cure [*RNQ*+] despite Sis1 being over-expressed. Therefore, as we did using Rnq1-L94A, we over-expressed Sis1 before replacing WT Rnq1 with the alanine mutants and tested whether propagation of the [*RNQ*+] variants was rescued using SDD-AGE to monitor the presence of SDS-resistant aggregates. As expected from our data with Rnq1-L94A, Sis1 over-expression rescued the propagation of m.d. high [*RNQ*+] and s.d. medium

[*RNQ*+] that were both cured by mutation of the A3 region, which encompasses L94 (Figure 5D).

Propagation of s.d. very high [*RNQ*+], on the other hand, was impaired by mutation of several different amyloidogenic regions (Figure 4). This allowed us to gain a more complete picture of how multiple regions of Rnq1 influence propagation of this prion variant. Strikingly, Sis1 over-expression differentially rescued propagation with these mutants, even when comparing N-terminal and C-terminal mutants (Figure 5E). Sis1 over-expression did not rescue s.d. very high [*RNQ*+] propagation when the A4, A5, or A11 regions were mutated to alanine. This suggests that these regions likely disrupt the aggregate structure of s.d. very high [*RNQ*+], thereby impairing the recruitment and conversion of monomeric Rnq1. By contrast, Sis1 over-expression did rescue the propagation of s.d. very high [*RNQ*+] when the N-terminal A1, A2, and A3 regions were mutated, along with the C-terminal A9 and A10 regions. Thus, these data support our hypothesis that mutation of these regions impairs Sis1 binding, which is overcome by Sis1 over-expression.

In order to more finely monitor the degree to which Sis1 over-expression rescued propagation of s.d. very high [*RNQ*+], we determined the amount of soluble Rnq1 using a well-trap assay. As SDD-AGE does not allow us to consistently visualize monomeric Rnq1, the well-trap assay provided a more sensitive measure of soluble Rnq1, and hence, of how much of the Rnq1 protein is not incorporated into aggregates. In agreement with our results using SDD-AGE, we found that in cells originally propagating the s.d. very high [*RNQ*+] variant, all of the Rnq1 protein of the A4, A5, and A11 mutants was in soluble form when Sis1 was over-expressed, and could enter the SDS-PAGE gel in the fraction that was not boiled (Figure 5F). At the other end of this spectrum, all of the Rnq1 protein was in its aggregated form with the A3 and A10

mutants, thus phenocopying WT Rnq1. Mutation of the A1, A2, and A9 regions, on the other hand, resulted in an intermediate amount of soluble Rnq1 when Sis1 was over-expressed. These data show that Sis1 over-expression rescues propagation of s.d. very high [*RNQ*+] to widely varying degrees when the different amyloidogenic regions are mutated. We hypothesize that mutation of the A1, A2, and A9 regions likely allosterically impact Sis1 binding, and so are only partially rescued by Sis1 over-expression. The A3 and A10 regions, on the other hand, may represent direct binding sites for Sis1 in the context of the s.d. very high [*RNQ*+] conformation. In fact, the peptide-binding array that discovered the affinity of Sis1 for the L94 region (A3) of Rnq1 also showed some affinity, albeit weaker, for the A10 region [37]. This further supports our hypothesis that the [*RNQ*+] variants expose different parts of the Rnq1 protein to interact with Sis1.

2.4.7 [*RNQ*+] *variant conformation dictates dependence on Sis1 binding sites*

The data above suggest that propagation of the s.d. very high [*RNQ*+] variant likely relies on Sis1 binding to both the A3 and A10 regions. The other [*RNQ*+] variants, however, clearly show a difference in the importance of these regions for prion replication. Both the s.d. medium and m.d. high [*RNQ*+] variants were cured when the A3 region was mutated, but these conformations could still propagate with the A10 mutant (Figure 4). By contrast, mutation of neither of these regions eliminated the aggregates of s.d. low or s.d. high [*RNQ*+]. As such, we hypothesized that the A3 and A10 regions might have some redundancy with these [*RNQ*+] variants, whereby the A10 region serves as another Sis1 binding site, as our data suggest for s.d. very high [*RNQ*+], albeit to a lesser degree. To test this, we created the double mutant of Rnq1 having both the A3 and A10 regions mutated to alanine, termed Rnq1-A3+A10. We then

replaced WT Rnq1 and confirmed similar expression (Figure S4). Upon continual growth, we monitored how quickly [*RNQ*+] was cured using SDD-AGE. Interestingly, mutation of both regions cured s.d. low and s.d. high [*RNQ*+], but at different rates: s.d. high [*RNQ*+] was cured much faster than s.d. low [*RNQ*+] (Figure 6). Furthermore, the double mutant cured both s.d. medium and m.d. high [*RNQ*+] faster than either single mutant (data not shown). These results indicate that both putative Sis1 binding sites in the A3 and A10 regions influence propagation of the [*RNQ*+] variants, but the extent to which these regions are utilized is variant-specific.

2.4.8 Rnq1 amyloidogenic regions have [*RNQ*+] *variant-dependent effects on* [*PSI*+] *formation*

By identifying the Rnq1 amyloidogenic regions as major factors in distinguishing the ability of the [*RNQ*+] variants to propagate, we next wanted to determine whether these differences had any functional consequence on the differential ability of the [*RNQ*+] variants to induce [*PSI*+]. We envisioned two ways that these regions could affect the formation of [*PSI*+] in a variant-specific manner: 1) through mediating the differential binding of Sis1, where Sis1 plays a role in facilitating interaction with Sup35, and 2) having a different set of Rnq1 residues that facilitate the interaction with Sup35 through cross-seeding.

To test the first possibility, we asked whether over-expression of Sis1 would enhance the rate of spontaneous [*PSI*+] formation, as it has been shown to do for [*URE3*] [115]. The spontaneous conversion to [*PSI*+] is normally a rare event, occurring at a rate of ~5.8×10^{-7} [56]. We transformed [*rnq*-] [*psi*-] cells or [*psi*-] cells propagating m.d. high, s.d. high, or s.d. very high [*RNQ*+] with a plasmid that over-expressed Sis1 or an empty vector control. We then selected for nonsense suppressors and screened for cells that had spontaneously converted to [*PSI*+]. We found that Sis1 over-expression significantly increased the level of spontaneous

[*PSI*+] formation in [*RNQ*+] cells, but not in [*rnq*-] cells (Figure 7A). The apparent increase in [*PSI*+] formation was not due to any noticeable difference in the distribution of [*PSI*+] variants obtained (data not shown). Moreover, there were no significant differences in the levels of Hsp104 or Ssa, both of which are known to modulate the existence of [*PSI*+] (Figure S7) [94,198]. This indicates that Sis1 helps facilitate the formation of [*PSI*+], thereby suggesting that the differential interaction between Sis1 and the [*RNQ*+] variants might contribute to their different capabilities of cross-seeding Sup35.

Next, we wanted to determine if the [*RNQ*+] variants might have different regions of Rnq1 involved in facilitating [*PSI*+] formation. Previously, we have shown that some mutations in Rnq1 that have no detectable effect on the Rnq1 aggregate structure can decrease the ability of [*RNQ*+] to induce [*PSI*+] [78]. This suggested that these residues are involved in facilitating the interaction and cross-seeding of Sup35 to form [*PSI*+]. Thus, we asked whether disruption of the Rnq1 amyloidogenic regions would show variant-specific effects on [*PSI*+] induction. In cells propagating each of the [*RNQ*+] variants and harboring the Rnq1 alanine mutants in place of WT Rnq1, we over-expressed Sup35, which greatly enhances the *de novo* formation of [*PSI*+]. We then analyzed [*PSI*+] formation by monitoring growth on media lacking adenine. Strikingly, we found that disruption of the Rnq1 amyloidogenic regions had a variety of effects on [*PSI*+] induction (Figures 7B-E and S8). As we expected, we found that some mutations that affected [*RNQ*+] also affected the formation of [*PSI*+]. For instance, mutation of the N-terminal A1 region affected propagation of all of the [*RNQ*+] variants. While we anticipated that this destabilization would cause decreased formation of [*PSI*+], it actually enhanced [*PSI*+] formation for the s.d. low, s.d. medium, and m.d. high [*RNQ*+] variants, as we saw an increase in Ade+ colonies (Figure 7B). By contrast, mutation of the A7 region had very little effect on

propagation of any of the [*RNQ*+] variants, but it enhanced [*PSI*+] induction in most of them (Figure 7C). This suggests that this region might have general importance in facilitating the interaction with Sup35. Moreover, disruption of the A9 region showed quite varied effects, greatly decreasing [*PSI*+] formation with s.d. high [*RNQ*+], but increasing it with s.d. low and m.d. high [*RNQ*+] (Figure 7D), despite not grossly affecting the overall structures of these three [*RNQ*+] variants (Figure 4A). Overall, these variant-specific effects indicate that the [*RNQ*+] variants have different regions of the Rnq1 protein that are important for [*PSI*+] induction (Figure 7E). Moreover, these regions are not confined to the Rnq1-PFD.

2.5 Discussion

It has previously been shown that a single amyloidogenic protein, Rnq1, can form a wide variety of different prion variants, many of which differentially influence the formation of [*PSI*+] [31,32]. Similarly, it is estimated that PrP^{Sc} likely exists in over 30 different prion strains [172]. However, the physical and mechanistic basis underlying different prion strains and their associated phenotypes has only been elucidated using two variants of the [*PSI*+] prion. Our work reveals additional layers of complexity that help explain the widespread diversity of amyloid polymorphism and phenotypic variation. Here, we show *in vivo* that different amyloidogenic regions, both within and outside of the putative PFD, as well as different interactions with cofactors, are key determinants in distinguishing, and likely generating, distinct prion variants. This provides significant insight into how certain prion strains can be biochemically indistinguishable, but confer different pathological consequences [30].

Previous work has emphasized the importance of fiber stability in distinguishing prion variants [25,27,33,69,182]. The less stable Sup35 fibers of strong [*PSI*+] cause increased

fragmentation into a greater number of smaller prion seeds that recruit more Sup35 monomer [25]. Similarly, less stable prion strains of PrP^{Sc} correlated with shorter incubation periods [27,182]. In this study, we show a similar trend with the m.d. high [*RNQ*+] variant. This [*RNQ*+] variant propagated less stable Rnq1 aggregates as compared to the s.d. [*RNQ*+] variants (Figure 1A). This correlated with several properties that show that m.d. high [*RNQ*+] cells readily sequester Rnq1 monomer: solubility [31], mitotic stability, [*RRP*+] phenotype, and inviability with FL RRP (Figure 2). Hence, we propose that the decreased stability of m.d. high [*RNQ*+], like strong [*PSI*+], results in an increased number of propagons, as previously reported [184], which then enhances the ability of Rnq1 monomer to join pre-existing aggregates.

However, the decreased fiber stability does not explain all the properties of m.d. high [*RNQ*+], nor all the differences between the [*RNQ*+] variants. Despite the lower stability, which is predicted to increase fiber fragmentation into smaller aggregates, m.d. high [*RNQ*+] propagated aggregates of a larger average size than other [*RNQ*+] variants (Figure 1C). Also, both s.d. high and s.d. very high [*RNQ*+] were more thermal stable, which is predicted to cause less nonsense suppression, but these variants caused a similarly strong nonsense suppression phenotype as compared to m.d. high [*RNQ*+] (Figures 1 and 2). Therefore, our data suggest that thermal stability, while a crucial parameter, does not serve as a perfect measure of fiber fragmentation, and cannot explain the existence of many different aggregate structures, nor the large variability in phenotype. Moreover, our work and that of another group show that many additional properties that helped elucidate the physical basis of [*PSI*+] variants, similarly do not distinguish the [*RNQ*+] variants and their phenotypic effects on [*PSI*+] [31,32,108,184]. These data indicate that additional factors influence prion strain propagation and the resulting phenotypes, and highlight the wide variety of polymorphic structures that can exist [44], with

[*PSI*+] and [*RNQ*+] variants possibly exhibiting different types of polymorphism (e.g. packing versus segmental).

Several studies have examined the primary structural elements that are important for prion propagation, with particular emphasis on the prion-forming domains. A different length of the same stretch of contiguous residues of Sup35 was found to be protected in the amyloid structure of different [*PSI*+] variants [26]. Other work has shown that prion transmission involves the differential contribution and cooperation of discontinuous intragenic regions of the Rnq1-PFD [84]. Our data extend these findings, as we showed that disruption of certain discontinuous amyloidogenic regions in the Rnq1-PFD show variant-specific effects on [*RNQ*+] propagation (Figures 4 and S5). For instance, mutation of the A11 region, despite impairing propagation of all the [*RNQ*+] variants we analyzed, did so to varying degrees. Also, mutation of the A9 region eliminated s.d. very high [*RNQ*+] and affected propagation of s.d. medium [*RNQ*+], but had no noticeable impact on the other [*RNQ*+] variants, in agreement with some of our previous work [78]. Importantly, there were no reproducibly significant differences in protein expression of the alanine mutants that could explain their differential effects (Figure S4). Hence, these data clearly establish that the involvement and cooperation of non-adjacent regions of the PFD can vary with the type of prion variant that propagates.

In addition to the Rnq1-PFD, we found that the often-overlooked N-terminal non-Q/N-rich domain of Rnq1 has a prion variant-dependent influence on prion propagation (Figures 2 and 4). Sequences flanking the aggregation-prone part of proteins, even between regions that are far apart in the primary structure, have previously been implicated in influencing aggregation dynamics [188,199-205]. For instance, amyloid fibers formed with Sup35NM as compared to those formed with full-length Sup35 have morphologically and biochemically distinct properties

[206-208]. Similarly, it was recently shown that the region outside of the amyloid core has different structural dynamics for different [*PSI*+] variants [38]. Two models have been proposed to explain how regions outside the PFDs may be involved in amyloid assembly and propagation: 1) serving to dock monomers, with the PFD forming the amyloid core and the non-PFD outside, or 2) incorporating within the core of the fiber assembly itself [188]. Our data strongly suggest that the non-PFD domain of Rnq1 helps facilitate monomer addition into aggregates (Figure 2). However, we also show that mutation of N-terminal amyloidogenic regions differentially disrupted propagation of the [*RNQ*+] variants (Figure 4). Hence, we propose that both of these models could be correct, depending on what prion variant is propagating. In fact, as our work indicates that regions outside the unstructured Q/N-rich domains can have a major influence on propagation of particular prion variants, our data may help explain particular inconsistencies when using the full-length protein or truncated derivatives to examine the *in vivo* and *in vitro* properties of prion variants [118,184].

Along with the influence on prion propagation, we also show that different primary structural elements likely dictate different phenotypic and pathological ramifications of prion strains. We found that mutation of certain amyloidogenic regions of Rnq1 causes variant-dependent alterations in the interaction with Sup35, thereby altering the degree of [*PSI*+] formation (Figures 7 and S8). In several cases, there was minimal to no detectable effect on maintenance of Rnq1 aggregates. Hence, while it is proposed that amino acid composition, rather than the exact sequence, is the primary driver of amyloid maintenance [209,210], our data suggest that even relatively subtle variation in primary sequence can have profound effects on some properties of prion variants, but not others. Therefore, we have now established that the contribution of different regions of an amyloidogenic protein can help account for the biological

differences seen between prion strains, such as the variation in [*PSI*+] formation mediated by the [*RNQ*+] variants.

We also discovered a striking difference in the relationship of the [*RNQ*+] variants with Sis1. Mutation of the A10 region in the Rnq1-PFD eliminated the ability of only the s.d. very high [*RNQ*+] variant to propagate (Figure 4), but this was rescued by over-expression of Sis1 (Figure 5), suggesting that the A10 region might be a secondary Sis1 binding site, in agreement with a previous peptide-binding array [37]. Interestingly, s.d. very high [*RNQ*+] was also the least affected by mutation of the known Sis1 binding site in the A3 region (using the Rnq1-L94A mutant). At the other end of this spectrum, s.d. medium [*RNQ*+] and m.d. high [*RNQ*+] were most sensitive to disruption of the A3 region, but there was no detectable effect when the A10 region was mutated. In stark contrast, for s.d. low and s.d. high [*RNQ*+], it was only when both the A3 and A10 regions were mutated that these prion variants were eliminated, with propagation of s.d. high [*RNQ*+] being abolished faster than s.d. low [*RNQ*+] (Figure 6). Surprisingly, disruption of the known Sis1 binding site using the A3 mutant did not entirely phenocopy the effects of Rnq1-L94A. We hypothesize that this might be attributed, at least in part, to higher steady state levels of Rnq1-L94A (Figure S4), and possibly in addition, how the residues surrounding L94 that are mutated in the A3 mutant are involved in propagation of particular [*RNQ*+] variants. Collectively, while we cannot definitively exclude the possibility that the Rnq1 alanine mutants are affecting multiple factors important for prion propagation, our data strongly support the hypothesis that propagation of the [*RNQ*+] variants relies on Sis1 differentially binding various sites exposed by the distinct Rnq1 aggregate structures. As we demonstrated that the over-expression of Sis1 can enhance the formation of [*PSI*+] in [*RNQ*+]

cells (Figure 7A), we propose that such differential binding may influence the phenotypic impact of the [*RNQ*+] variants on [*PSI*+] inducibility.

It is suggested that similar chaperone dynamics might also influence the physical basis of [*PSI*+] variants. As Hsp104 can bind Sup35 in [*PSI*+] cells [90] and is required for propagation of the [*PSI*+] prion [94], one would predict that abrogation of the Hsp104 binding site in Sup35 would eliminate the ability of [*PSI*+] to propagate. However, propagation of a strong [*PSI*+] variant was maintained, albeit impaired, when Hsp104 binding was disrupted using *sup35Δ129-148* [211]. This suggests that Hsp104 must be able to bind other sites in Sup35. Moreover, recent work shows that this binding site can adopt different conformations for different [*PSI*+] variants, which might influence Hsp104 binding [38]. In fact, particular [*PSI*+] variants have been isolated that require increased levels of Hsp104 to stably propagate [212,213]. Our work now provides a mechanistic explanation of these previous findings, supporting the hypothesis that different chaperone dependencies may be dictated by the exposure or conformation of different regions of the protein [214]. Indeed, these different amyloid-chaperone relationships likely explain why differences in the host environment, due to different genetic backgrounds or environmental conditions, can modulate prion propagation [41,215]. Moreover, our data support the hypothesis that different host cofactors might interact with different amyloid structures to influence pathology [39].

With such a large variety of distinct structures that can be adopted with the same protein [42-44,172], it was unclear how general the model that elegantly explains the physical basis of [*PSI*+] variants might be. We found that the parameters that define this model do not distinguish a set of [*RNQ*+] variants or explain their phenotypic effects. Our work now shows that disparate, non-adjacent amyloidogenic regions and complex interactions with chaperones contribute to

defining the propagation of distinct prion variants. These data help elucidate what factors are involved in determining a wide array of structural differences and their associated phenotypic consequences. This may provide insight as to why some prion strains are indistinguishable based on typical biochemical properties, but have very different pathological phenotypes [30]. Furthermore, our study highlights the intricate interplay between several factors, including cofactor-amyloid interactions, which likely underlie the ability of distinct amyloid structures to co-aggregate with different proteins and cause variation in disease pathology.

2.6 Materials and Methods

2.6.1 Yeast Strains and Media

All yeast strains used in this study were derivatives of 74-D694 (*ade1-14 ura3-52 leu2-3,112 trp1-289 his3-Δ200*) and are described in Table S1. Yeast were grown and manipulated using standard techniques. As indicated, cells were grown in YPD (1% yeast extract, 2% peptone, 2% dextrose) or synthetic media (0.67% yeast nitrogen base without amino acids, 2% dextrose or 2% galactose+1% raffinose) lacking one or more nutrients (e.g. SD-his lacks histidine) to select for appropriate plasmids. YPD+3mM guanidine hydrochloride (GdnHCl) was used to test prion curability. The plasmid shuffle technique was used by plating cells on media containing 1mg/mL 5-fluoroorotic acid (5-FOA) to counterselect against cells that maintained *URA3*-containing plasmids. Reverse plasmid shuffle of WT Rnq1 was performed by transforming these Ura- cells with a *URA3* plasmid, and screening for Ura+ His- cells.

Wild-type [*rnq*-] and [*RNQ*+] yeast strains (L1751, L1943, L1945, L1767 [*psi*-], L1953, L1749) were a kind gift from Dr. Susan Liebman [31,108]. Derivatives of these strains expressing *RRP* were constructed as described previously using pRS306-*RRP* [78]. Integration of

RRP in the *SUP35* locus was confirmed by PCR and western blot. The *rnq1Δ::kanMX4* strains were made as described previously [78]. The *sup35Δ::hphMX4* strains were made by first passaging *Mat a* and *Mat* α 74-D694 [*PSI*+] [*RNQ*+] *sup35Δ::hphMX4* strains on YPD+3mM GdnHCl. These were confirmed to be [*psi*-] by maintaining a red color when streaked back to YPD, and also confirmed to be [*rnq*-] by well-trap assay. These strains were then mated to *RNQ1* plasmid shuffle strains containing pRS313-*RNQ1* and propagating one of the [*RNQ*+] prion variants. Diploids were sporulated and colonies that were $HygB^R$, Ura+, $5\text{-}FOA^s$, $G418^s$, and His- were selected. The [*RNQ*+] variant was confirmed by well-trap assay and [*PSI*+] induction.

2.6.2 Plasmid Construction

All plasmids used in this study were confirmed by sequencing and are listed in Table S2, and all oligonucleotides are listed in Table S3. Construction of pRS306-*RRP*, pRS313-*RNQ1*, pRS316-*RNQ1*, pRS413*GPD-L94A*, and pEMBL-*SUP35* were described previously [32,75,78]. The following plasmids were gifts: pRS414*GPD-SIS1* (S. Lindquist [74]), pYK810 (M. Tuite [83]), and pYES2-*GAL-HA-RNQ1* (E. Craig [99]). Galactose-inducible *RNQ1(153-405)* was made by amplification using oligonucleotides 1626 and 0040, digestion with HindIII/XhoI, and ligation into pYES2-*GAL-HA-RNQ1*.

To create pRS315-*SUP35* and pRS315-*RRP*, the *SUP35* promoter was first amplified using oligonucleotides 1367 and 0316. This product and pRS315 were digested with SalI/BamHI and ligated to make pRS315-*SUP35p*. The *SUP35* open-reading frame and terminator were then amplified using oligonucleotides 1348 and 0322, digested with BamHI/XbaI, and ligated into pRS315-*SUP35p*. A BamHI/SacI fragment of *RRP* was digested from pRS316-*RRP* that was previously described [78] and ligated into pRS315-*SUP35p*. To make pRS315-full-length-*RRP*,

full-length *RNQ1* was amplified using oligonucleotides 0477 and 0320, digested with BamHI/SacII and ligated with pRS316-*RRP*. Full-length *RRP* with the *SUP35* promoter and terminator were then amplified using oligonucleotides 1366 and 0322, digested with XhoI/SacI, and ligated into pRS315.

All *RNQ1* alanine mutants were cloned using bridge PCR. The N-terminus of *RNQ1* was amplified using oligonucleotide 0488 and the oligonucleotide containing the corresponding *rnq1* mutant. The C-terminus of *RNQ1* was amplified using the reverse complement of the mutant-specific oligonucleotide with 0489. The two amplicons were then used as a template to amplify the full-length *rnq1* mutant using oligonucleotides 0488 and 0489. This product was digested with EcoRV/SalI and ligated into the previously described pRS313 plasmid containing the *RNQ1* promoter and terminator [78], thereby expressing the Rnq1 mutants at protein levels close to WT (Figure S4). As an exception, *rnq1-A11* and the *RNQ1* terminator were amplified using oligonucleotide 0491 in place of 0489 and digested with EcoRV/XhoI. The N-terminus of *rnq1-A3+A10* was amplified using oligonucleotides 0488 and 0018 with pRS413*TPI1-rnq1-A3* as the template, while the C-terminus was amplified using oligonucleotides 0014 and 0489 with pRS313-*rnq1-A10* as the template. Similar to what we previously saw with Rnq1-L94A [75], the *rnq1* mutants *A1*, *A3*, and *A3+A10* were cloned into pRS413*TPI1* as these mutants had lower steady state protein levels as compared to WT Rnq1 when expressed from the endogenous *RNQ1* promoter. Expression from the *TPI1* promoter resulted in slightly higher protein levels for Rnq1-A1 as compared to WT Rnq1, but WT protein levels for Rnq1-A3 and Rnq1-A3+A10 (Figure S4). Furthermore, the A1, A2, and A11 mutants consistently ran higher than WT Rnq1 by SDS-PAGE despite having the same number of amino acids. To make pRS413*TPI1*, the *TPI1* promoter was amplified using oligonucleotides 1429 and 1430, digested with SacI/XbaI, and

ligated into pRS413*ADH* cut with the same enzymes to replace the *ADH1* promoter. Finally, pRS413*TEF-RNQ1(132-405)* was cloned with oligonucleotides 1436 and 0489 and digested with EcoRV/SalI.

2.6.3 Protein Analysis

Sedimentation of Rnq1 by solubility assay and SDD-AGE were performed using established methods [32,78]. For well-trap and thermal stability assays, yeast cell lysates were prepared by vortexing with glass beads in buffer (100mM Tris pH 7.5, 200mM NaCl, 1mM EDTA, 5% glycerol, 0.5mM DTT, 3mM PMSF, 50mM N-Ethylmaleimide (NEM), complete protease inhibitor from Roche). Lysates were pre-cleared by centrifugation at 3,300*g* for 15 sec. For well-trap assays, protein concentration was normalized, and samples were treated in sample buffer (50mM Tris-HCl pH 6.8, 10% glycerol, 2% SDS, 100mM DTT) for 5 minutes at room temperature or 100°C. For thermal stability assays, samples were also incubated at a temperature gradient (45°C to 95°C) for 5 minutes. Samples were then analyzed by SDS-PAGE and western blot using a polyclonal αRnq1 antibody.

2.6.4 Limited Proteolysis

[*RNQ*+] cell lysates were prepared as above for well-trap assays, with the exception of adding PMSF to the buffer. Protein concentration was normalized to ~3µg/µl, followed by addition of proteinase K (Sigma-Aldrich) to varying concentrations. Samples were incubated at 37°C in a water bath for 30 min or 1 hr as indicated. The reaction was stopped by adding sample buffer and boiling samples at 100°C for 5 min, followed by SDS-PAGE and western blot using an αRnq1 antibody. Cell lysates propagating the m.d. high [*RNQ*+] variant consistently showed

higher starting concentrations of the Rnq1 protein, likely because the very thermal stable Rnq1 aggregates of s.d. [*RNQ*+] were not completely broken down.

2.6.5 Immunoprecipitation

For co-immunoprecipitation of Sis1 and Rnq1, cultures were grown overnight, washed, and lysed by vortexing in buffer (50mM Tris pH 8, 150mM NaCl, 1mM EDTA, 0.2% Triton X-100, 1mM PMSF, 50mM NEM, complete protease inhibitor from Roche) containing glass beads. Lysates were pre-cleared by centrifugation at 9,300*g* for 30 sec at 4°C. Protein was normalized to 1mg/mL. Following incubation with or without αSis1 antibodies for 1 hr at 4°C, Protein G Sepharose (GE Healthcare) beads were added and incubated for 1 hr at 4°C. Beads were pelleted by centrifugation at 800*g* for 30 sec, followed by washing three times, and boiling at 100°C for 5 min. Samples were analyzed by SDS-PAGE and western blot using αRnq1 and αSis1 antibodies.

2.6.6 Phenotypic Colorimetric Assays

Taking advantage of the ability of [*RNQ*+] cells harboring *RRP* to suppress *ade1-14*, we monitored [*RRP*+] phenotypes as done previously [32]. Equal numbers of cells were normalized by OD_{600}, serially diluted five-fold, and spotted to the indicated media. SD-ade plates were incubated at 30°C for 6 days, while all other types of media were incubated for 3 days, followed by overnight at 4°C for color development. Mitotic stability assays were performed as before with at least three independent cultures for each [*RNQ*+] variant [33].

2.6.7 Joining Assay

Cells were transformed with pYES2-*GAL-HA-RNQ1* or pYES2-*GAL-RNQ1(153-405)*. Overnight cultures grown in glucose-based selection media were washed and diluted to OD_{600} 0.3 in induction media containing 2% galactose + 1% raffinose, followed by harvesting after 3 hrs of growth. Cell lysates were prepared and analyzed by well-trap assay.

2.6.8 [*PSI*+] *Formation*

To monitor the spontaneous conversion to [*PSI*+], cells were first transformed with pRS414*GPD-SIS1* or an empty vector control. Then, using suppression of *ade1-14* to monitor [*PSI*+] formation, at least three independent cultures were grown overnight and 200µl of culture was plated on SD-ade-trp and 200µl of a 1:10,000 dilution was plated on SD-trp. SD-ade-trp plates were grown overnight at 30°C, followed by two weeks at 4°C, then two weeks at 30°C, as it has been reported that cold enhances prion formation [60]. To calculate the number of cells plated on SD-ade-trp, the colonies on SD-trp were counted, averaged, and multiplied by the dilution factor of 10,000. Over $7.1x10^6$ cells were plated on SD-ade-trp for each condition. Ade+ colonies were then scored as [*PSI*+] by spotting to YPD and SD-ade, as well as YPD+3mM GdnHCl to confirm curability. The rate of [*PSI*+] formation was then calculated as the ratio of [*PSI*+] colonies to the total number of cells plated.

The induction of [*PSI*+] by over-expression of Sup35 was performed as previously described [32]. Briefly, cells expressing the indicated Rnq1 construct were transformed with pEMBL-*SUP35*. Overnight cultures were normalized by OD_{600} and spotted in five-fold serial dilutions to SD-his, SD-ade, and SD-ade-his. At least five independent experiments were performed. As previously reported, over 88% of colonies are bona fide [*PSI*+] [78].

2.7 Acknowledgments

We thank the following people for reagents: S. Liebman, S. Lindquist, M. Tuite, and E. Craig. We are also grateful to A. Cashikar and members of the True Lab for providing valuable comments on the manuscript.

2.8 Figures

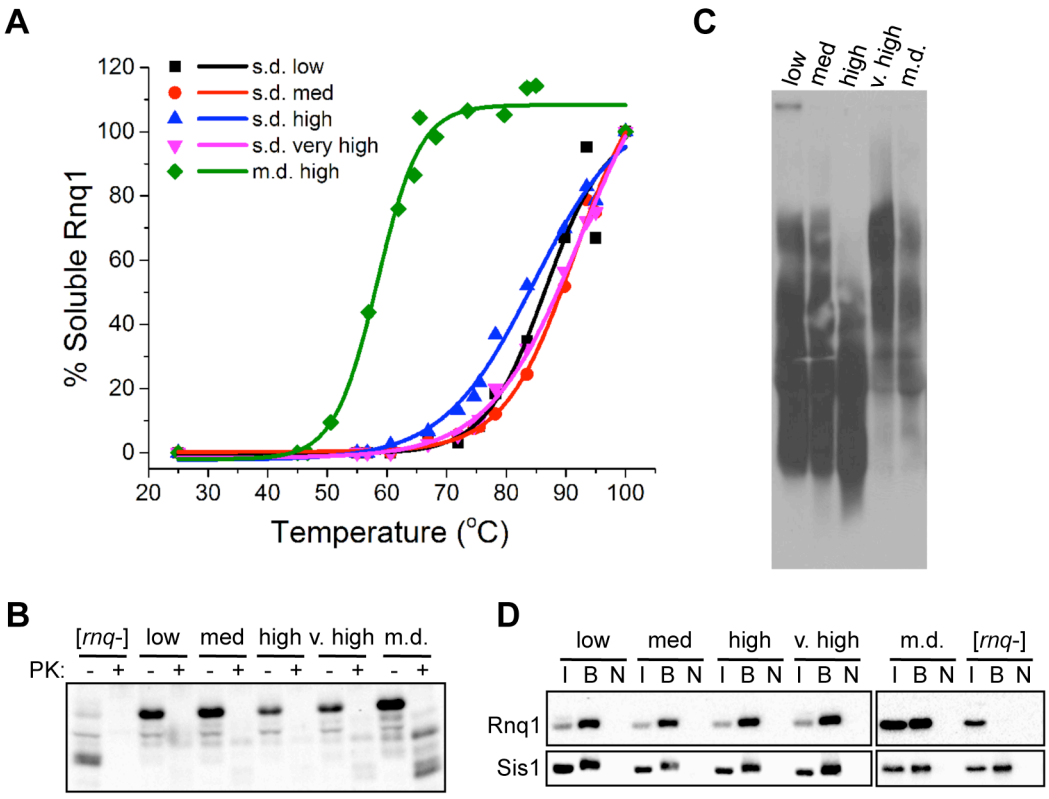

Figure 1. Biophysical parameters associated with fiber fragmentation do not distinguish [*RNQ*+] variants. (A) Rnq1 aggregates of s.d. [*RNQ*+] variants have similar thermal stability and are more stable than m.d. high [*RNQ*+]. Lysates were treated with a temperature gradient, followed by SDS-PAGE and western blot using an αRnq1 antibody. Rnq1 was quantified using ImageJ, normalized to the 100°C band, and plotted using Origin 9.0 software. Data are representative of at least five independent experiments. (B) Rnq1 aggregates of m.d. high [*RNQ*+] have increased protease resistance as compared to the s.d. [*RNQ*+] variants. Lysates of [*rnq*-] cells or cells propagating the indicated [*RNQ*+] variant were incubated with 2μg/mL proteinase K (PK) at 37°C for 1 hr, followed by SDS-PAGE and western blot with an αRnq1 antibody. (C) Relative Rnq1 aggregate distribution for each [*RNQ*+] variant does not correlate to rate of [*PSI*+] induction. Lysates of yeast cells propagating s.d. low, s.d. medium, s.d. high, s.d.

very high, and m.d. high (m.d.) [*RNQ*+] were subjected to SDD-AGE and western blot using an αRnq1 antibody. Data are representative of at least three independent experiments. (D) Co-immunoprecipitation of Sis1 and Rnq1. Sis1 was immunoprecipitated from cell lysates using an αSis1 antibody (gift from E. Craig), analyzed by SDS-PAGE, and immunoblotted with αRnq1 and αSis1 antibodies. The input of the total cell lysate (I) represents 10% of the sample that was bound by the αSis1 antibody (B). The bound fraction from the same sample not incubated with antibody (N) was used as a control.

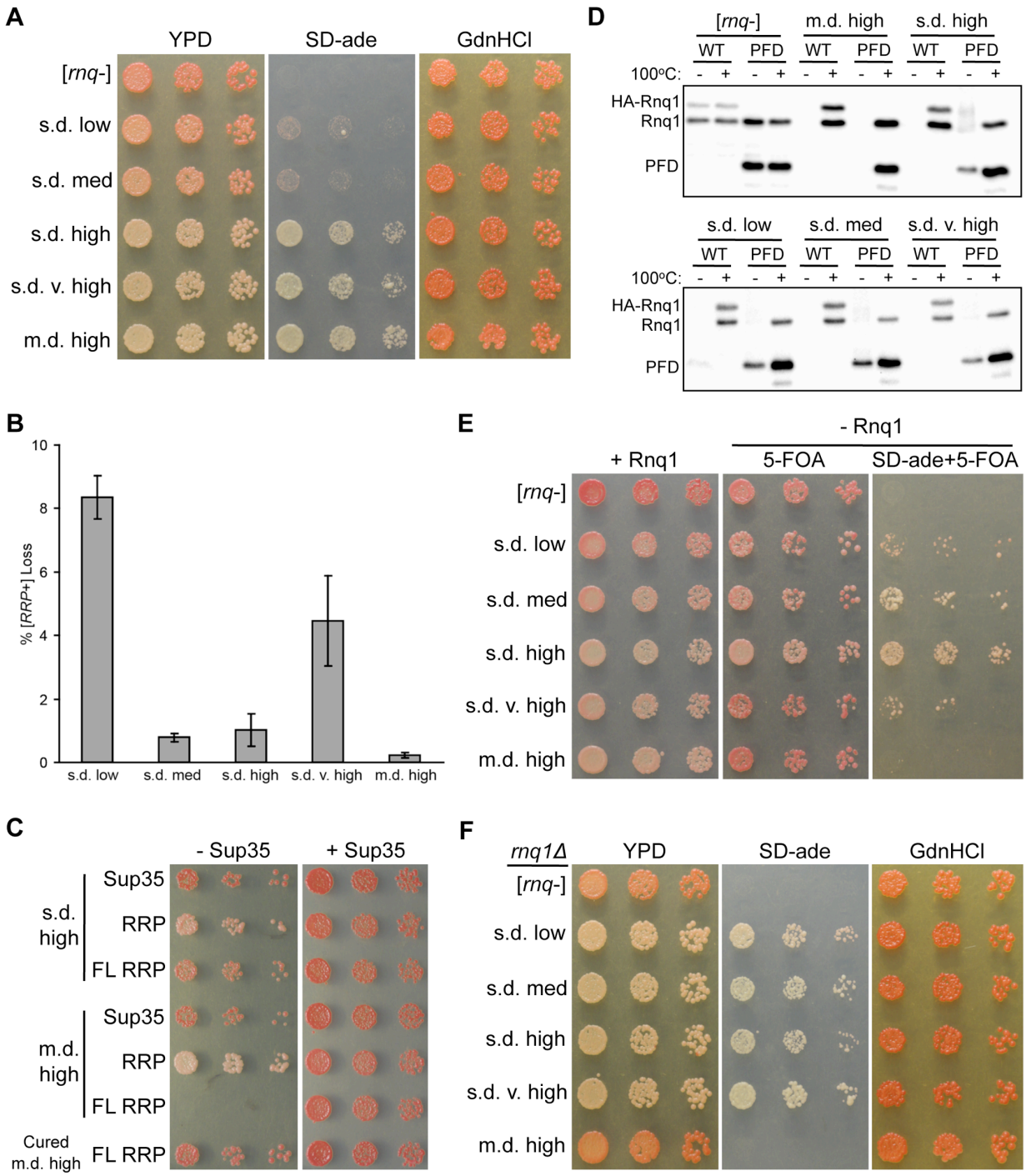

Figure 2. The non-prion forming domain of Rnq1 shows variant-specific influence on fiber growth. (A) Higher [*RNQ*+] variants confer stronger [*RRP*+] phenotypes. Cells harboring RRP and the indicated [*RNQ*+] variant were normalized by OD_{600}, serially diluted five-fold, and spotted onto YPD, SD-ade, and YPD+3mM GdnHCl (GdnHCl). Representative spottings are

shown. (B) Mitotic stability of [*RNQ*+] variants. Averages indicate the percentage of colonies that lost [*RRP*+] and error bars represent standard error of the mean calculated from at least three independent experiments. (C) Expression of full-length (FL) RRP in m.d. high [*RNQ*+] cells is lethal. Normalized numbers of yeast cells propagating s.d. high [*RNQ*+], m.d. high [*RNQ*+], or cured of m.d. high [*RNQ*+], and expressing Sup35, RRP, or FL RRP were serially diluted five-fold and spotted to select for loss (- Sup35) or co-expression (+ Sup35) of wild-type Sup35. Representative spottings are shown. (D) Rnq1-PFD readily joins pre-existing Rnq1 aggregates of m.d. high [*RNQ*+] as compared to s.d. [*RNQ*+] variants. Cells transformed with plasmids expressing *HA-RNQ1* or *RNQ1-PFD* from the *GAL1* promoter were subcultured in galactose media. Lysates were incubated for five minutes at 100°C (+) or at room temperature (-), followed by SDS-PAGE and western blot using an αRnq1 antibody. Data are representative of three independent experiments. (E) RRP is not sufficient to propagate m.d. high [*RNQ*+] without expression of Rnq1. Normalized numbers of *rnq1Δ* cells harboring RRP were serially diluted five-fold and spotted to select for maintenance of Rnq1 expression (+ Rnq1), or loss of Rnq1 (- Rnq1) on media to monitor color (5-FOA) and nonsense suppression (SD-ade+5-FOA) phenotypes. Representative spottings are shown. (F) Loss of Rnq1 results in altered [*RRP*+] phenotypes. Normalized numbers of *rnq1Δ* cells harboring RRP that lost Rnq1 expression, as shown in (E), were serially diluted five-fold and spotted onto YPD, SD-ade, and GdnHCl media to monitor the stable [*RRP*+] phenotypes. Representative spottings are shown.

A

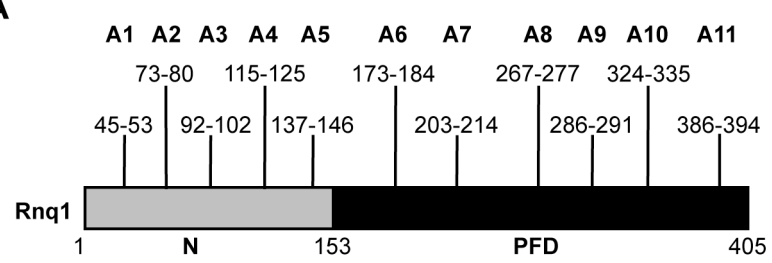

B

	Residues	Sequence	1	2	3	4	5
A1	45-53	LIQKIAGYV	+	+	+	+	+
A2	73-80	SSFMNTLM	+		+	+	
A3	92-102	GKLALLATVMT	+	+	+	+	
A4	115-123	DVGTVMSML	+	+	+	+	
A5	137-146	GLAALASQFF	+		+	+	
A6	173-184	SFTALASLASSF	+		+	+	
A7	203-214	SFGALASMASSF	+		+	+	
A8	267-277	FSSLASMAQSY	+			+	
A9	286-291	NQQQYN					+
A10	324-335	SFSALASMASSY	+		+	+	
A11	386-394	SFNFSGNFS	+				

Figure 3. Consensus amyloidogenic regions of Rnq1 identified by prediction algorithms. (A) Diagram of the Rnq1 protein highlighting the N-terminal domain (N) between residues 1-152, the putative prion-forming domain (PFD) between 153-405, and the identified amyloidogenic regions. (B) Residues and sequences of the predicted amyloidogenic regions and which algorithm identified that region: 1) Zyggregator (http://www-vendruscolo.ch.cam.ac.uk/zyggregator.php); 2) PASTA (http://biocomp.bio.unipd.it/pasta/); 3) TANGO (http://tango.crg.es/); 4) Aggrescan (http://bioinf.uab.es/aggrescan/); 5) WALTZ (http://waltz.switchlab.org/).

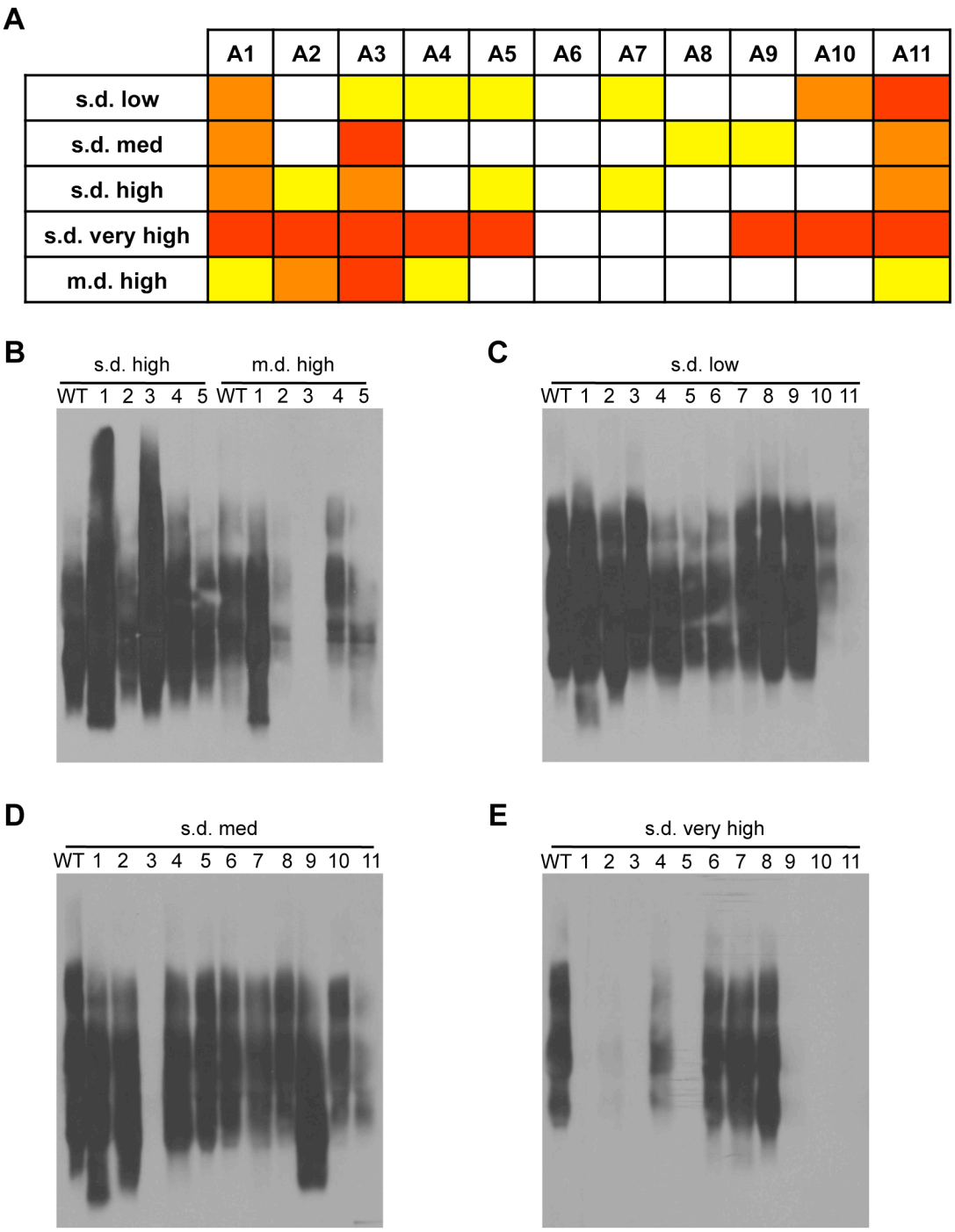

Figure 4. Distinct regions of Rnq1 are important for each [*RNQ*+] variant. (A) Summary of how disruption of the amyloidogenic regions by alanine mutations affects propagation of the [*RNQ*+] variants. Mutants are categorized as having no effect (white), mild effect (yellow), moderate effect (orange), or not propagating [*RNQ*+] (red) after successive passaging. These

effects on [*RNQ*+] propagation were summarized from at least three independent experiments of each of the following assays: solubility assay, thermal stability, and SDD-AGE. See Figure S5 for more detail. If only one assay showed mild effects, e.g. SDD-AGE of s.d. low [*RNQ*+] cells harboring the A6 mutant, this was scored as having no effect in this summary table. (B) Mutation of the Rnq1 N-terminal domain shows [*RNQ*+] variant-dependent effects. Lysates from cells propagating s.d. high or m.d. high [*RNQ*+] and expressing wild-type (WT) Rnq1 or the N-terminal alanine mutants (A1 - A5) were resolved by SDD-AGE, followed by western blot using an αRnq1 antibody. (C – E) Mutation of Rnq1 amyloidogenic regions differentially affects [*RNQ*+] variants. Yeast lysates propagating (C) s.d. low [*RNQ*+], (D) s.d. medium [*RNQ*+], or (E) s.d. very high [*RNQ*+] expressing WT Rnq1 or the set of alanine mutants (A1 - A11) were analyzed by SDD-AGE and western blot with an αRnq1 antibody.

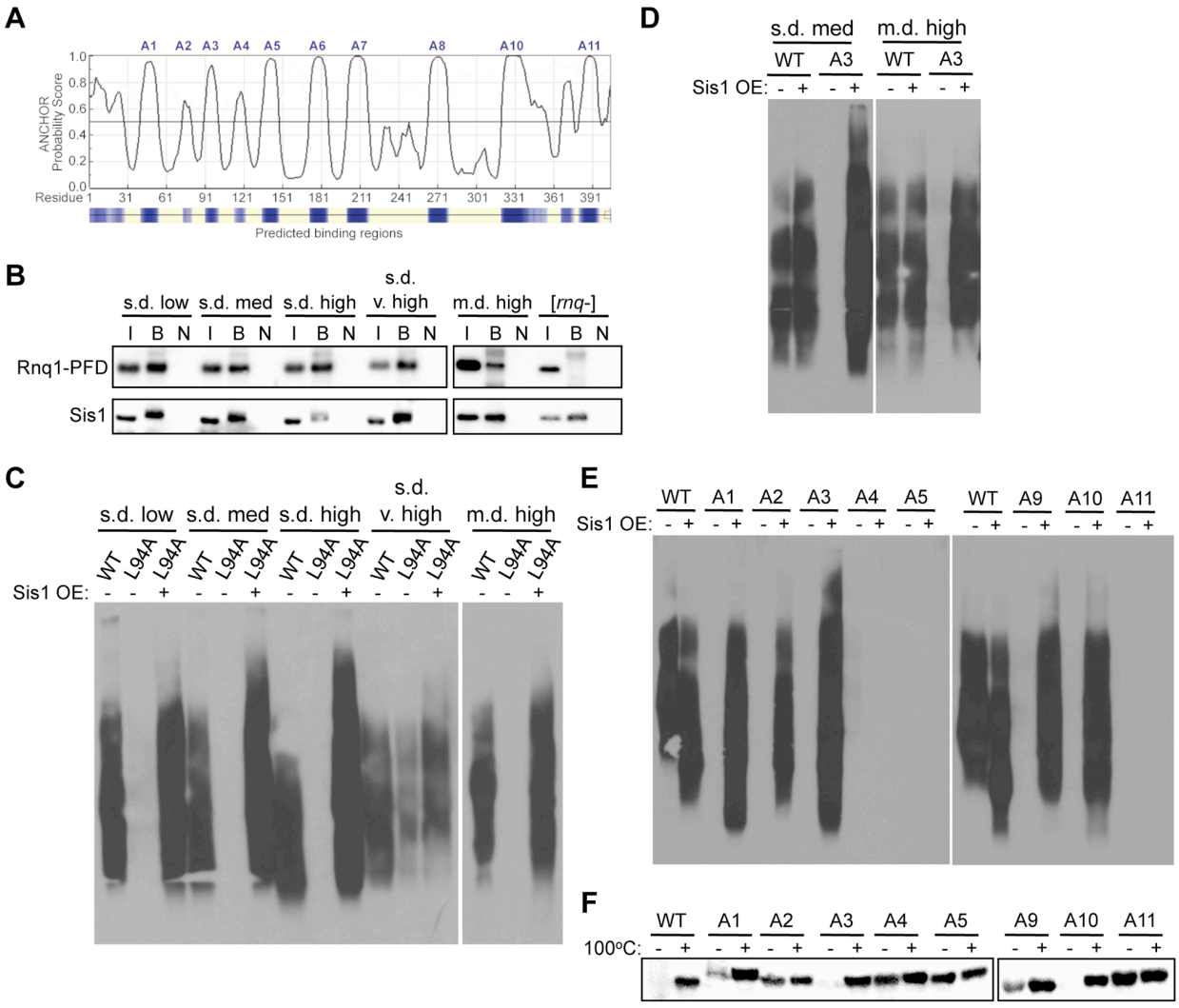

Figure 5. Rnq1 amyloidogenic regions differentially modulate interactions with Sis1. (A) Prediction of protein interaction sites in Rnq1 using the ANCHOR algorithm (http://anchor.enzim.hu/). Denoted at the top are the amyloidogenic regions A1 – A11. (B) Co-immunoprecipitation of Sis1 and Rnq1(132-405). Sis1 was immunoprecipitated using an αSis1 antibody (gift from E. Craig) from cell lysates expressing Rnq1(132-405) in place of WT Rnq1, followed by SDS-PAGE and immunoblotting with αRnq1 and αSis1 antibodies. The input of the total cell lysate (I) represents 10% of the sample that was bound by the αSis1 antibody (B). The bound fraction from the same sample not incubated with antibody (N) was used as a control. (C)

Rnq1-L94A differentially affects [*RNQ*+] variant propagation and is rescued by Sis1 over-expression. Cell lysates with (+) or without (-) over-expression (OE) of Sis1 and propagating the indicated [*RNQ*+] variant with WT Rnq1 or Rnq1-L94A were subjected to SDD-AGE and western blot using an αRnq1 antibody. (D – F) Elimination of [*RNQ*+] by mutation of Rnq1 amyloidogenic regions is differentially rescued by Sis1 over-expression. As in (C) for (D) cells propagating s.d. medium [*RNQ*+] or m.d. high [*RNQ*+] and expressing WT Rnq1 or the A3 mutant, or (E) cells propagating s.d. very high [*RNQ*+] expressing WT Rnq1 or mutants A1 - A5 or A9 - A11. (F) Yeast lysates propagating s.d. very high [*RNQ*+], over-expressing Sis1, and expressing WT Rnq1, or mutants A1 - A5 or A9 - A11 were incubated for five minutes at 100°C (+) or at room temperature (-), followed by SDS-PAGE and western blot using an αRnq1 antibody. Data are representative of at least three independent experiments.

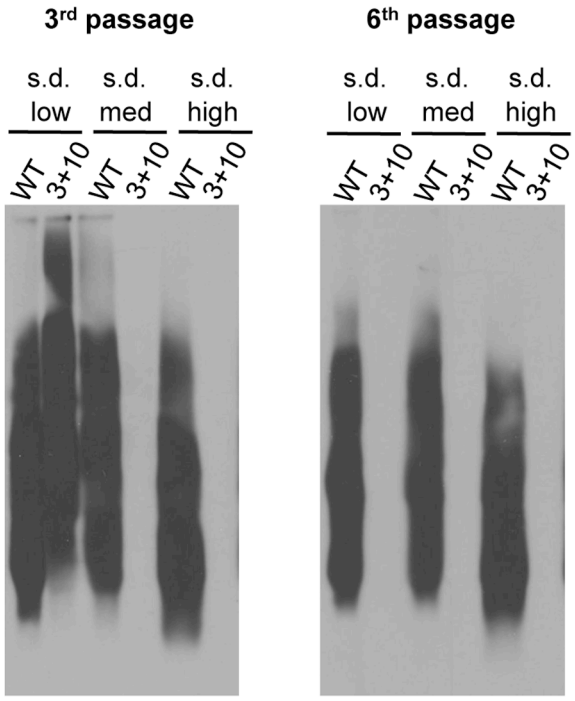

Figure 6. [*RNQ*+] variants rely on putative Sis1 binding sites to different extents.

Propagation of s.d. high [*RNQ*+] is eliminated faster than s.d. low [*RNQ*+] when Rnq1-A3+A10 is expressed. Yeast cells propagating the indicated [*RNQ*+] variant and expressing either WT Rnq1 or Rnq1-A3+A10 were successively passaged three or six times after plasmid shuffle. Cell lysates were subjected to SDD-AGE and western blot using an αRnq1 antibody, and are representative of three independent experiments.

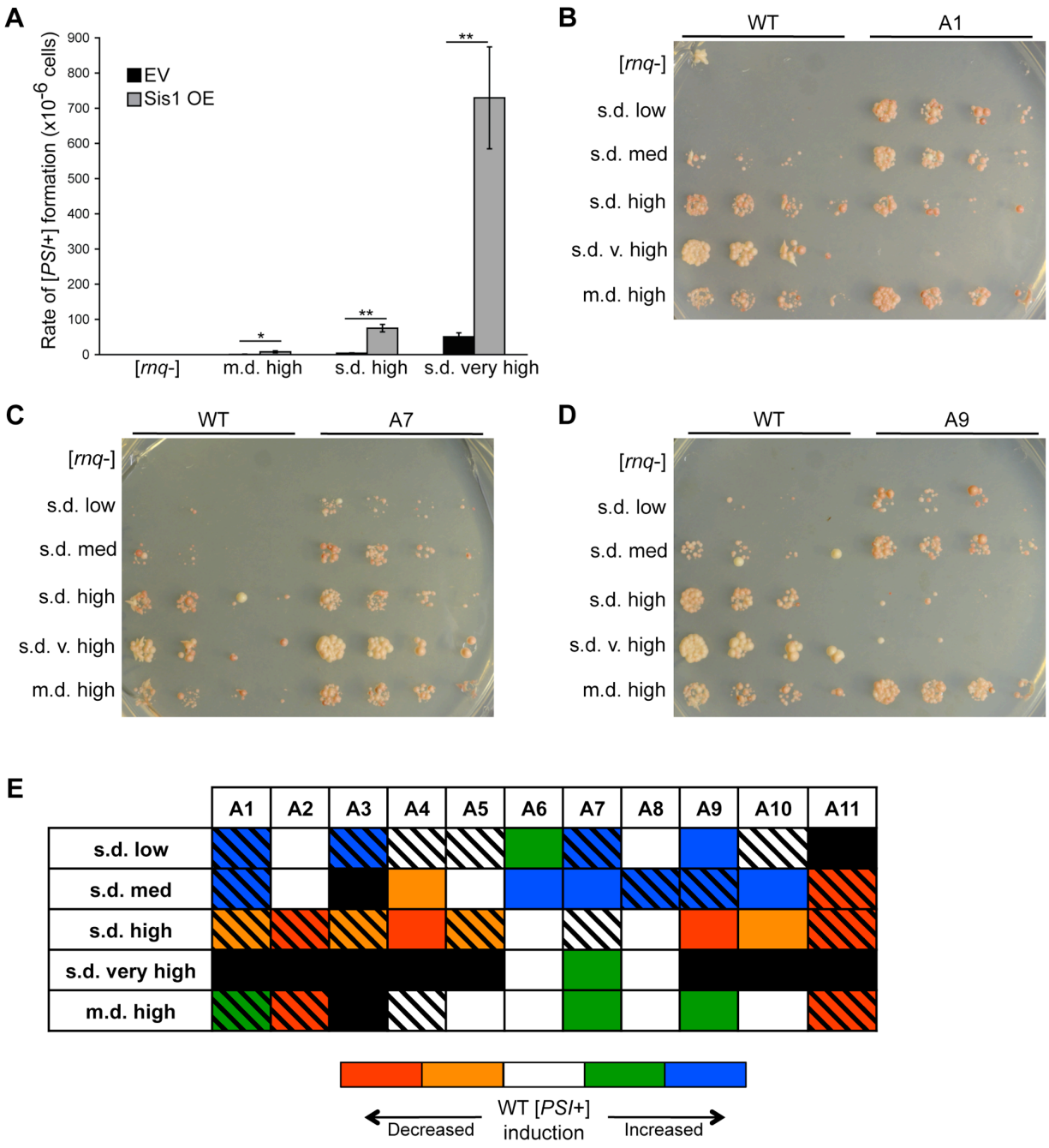

Figure 7. Sis1 over-expression and Rnq1 amyloidogenic regions influence the formation of [*PSI*+]. (A) Over-expression of Sis1 enhances the spontaneous formation of [*PSI*+] in [*RNQ*+] cells. [*rnq*-] [*psi*-] and [*RNQ*+] [*psi*-] cells were transformed with a Sis1 over-expressing plasmid (Sis1 OE) or an empty vector control (EV). Cultures were plated on medium that selected for [*PSI*+] cells as well as a non-selective medium to determine the total number of cells plated.

Averages and error bars representing standard error of the mean were calculated from at least three independent experiments. Statistical significance was assessed using Student's *t*-test (*$p < 0.05$, **$p < 0.01$). (B – E) Cells expressing WT Rnq1 or the indicated mutant Rnq1 were transformed with a plasmid to over-express Sup35. [*PSI*+] induction was monitored by spotting five-fold serial dilutions of normalized cell numbers on SD-ade and SD-ade-his. Representative spottings are shown of cells expressing the mutants (B) A1, (C) A7, or (D) A9 in comparison to expression of WT Rnq1. (E) Summary of data showing how disruption of the amyloidogenic regions by alanine mutations affects [*PSI*+] induction in each of the [*RNQ*+] variants. Mutants were categorized as having no effect (white), < 5-fold increase (green) or decrease (orange) in [*PSI*+] induction, or > 5-fold increase (blue) or decrease (red) in [*PSI*+] induction. Black boxes indicate that [*RNQ*+] was eliminated, while black hash marks indicate that [*RNQ*+] propagation was altered (see Figure 4). Data are summarized from at least five independent experiments.

2.9 Supplemental Figures and Tables

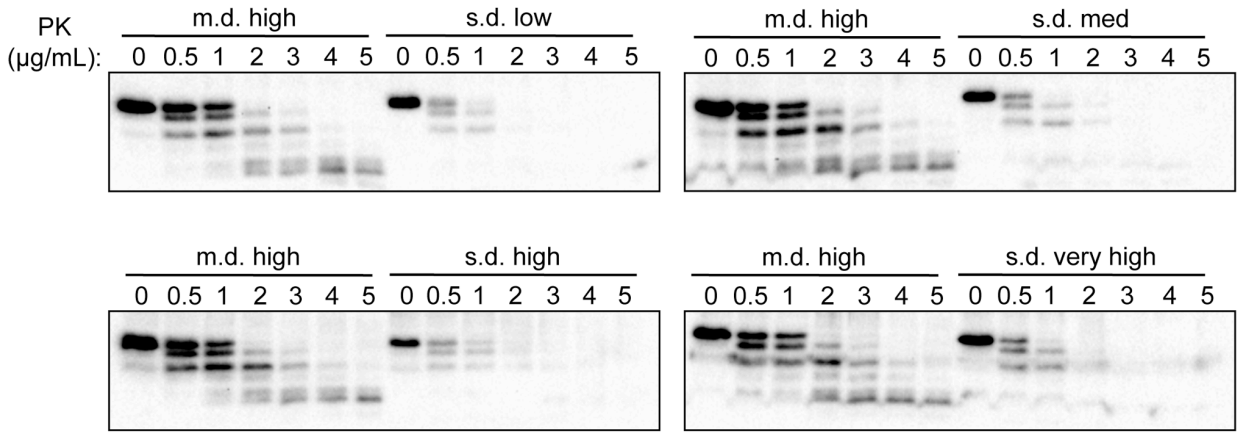

Figure S1. Differential proteinase K resistance of Rnq1 in [*RNQ*+] variants. Rnq1 aggregates of the m.d. high [*RNQ*+] variant reproducibly show enhanced protease resistance as compared to s.d. [*RNQ*+] variants. Lysates of cells propagating the indicated [*RNQ*+] variant were incubated with a gradient of different proteinase K (PK) concentrations at 37°C for 30 min, followed by SDS-PAGE and western blot analysis using an αRnq1 antibody.

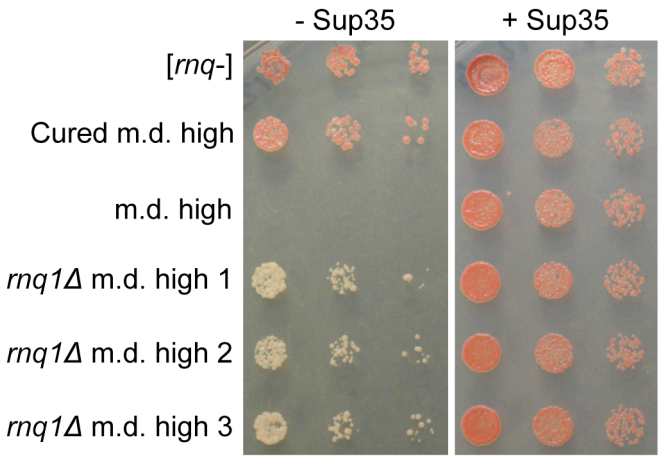

Figure S2. Inviability of FL RRP in m.d. high [*RNQ*+] cells depends on Rnq1 expression. Cultures of three different clones of *rnq1Δ* cells propagating m.d. high [*RNQ*+], along with controls of [*rnq*-] cells, cells cured of m.d. high [*RNQ*+], and m.d. high [*RNQ*+] cells, all expressing FL RRP were normalized by OD_{600}, serially diluted five-fold, and spotted on media to select for loss (- Sup35) or co-expression (+ Sup35) of wild-type Sup35. Representative spottings are shown.

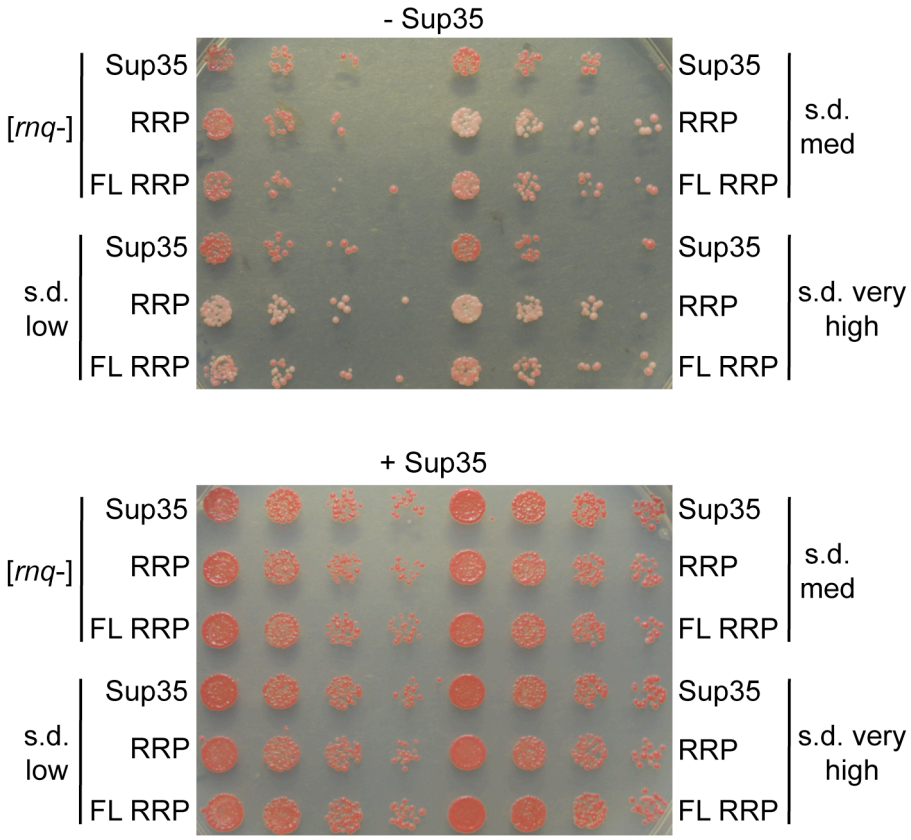

Figure S3. Expression of FL RRP in cells propagating s.d. [*RNQ*+] variants. Cultures of [*rnq*-] cells or cells propagating s.d. low, s.d. medium, or s.d. very high [*RNQ*+] and expressing Sup35, RRP, or full-length (FL) RRP were normalized by OD_{600}, serially diluted five-fold, and spotted to select for loss (- Sup35) or co-expression (+ Sup35) of wild-type Sup35. Representative spottings are shown.

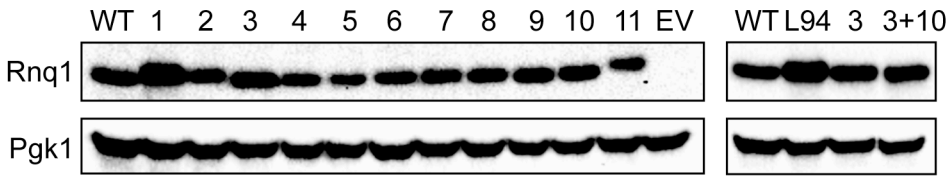

Figure S4. Protein expression of Rnq1 alanine mutants. Normalized protein from cell lysates expressing the indicated Rnq1 alanine mutant, or an empty vector (EV), in place of WT Rnq1, was subjected to SDS-PAGE and western blot using an αRnq1 antibody.

A

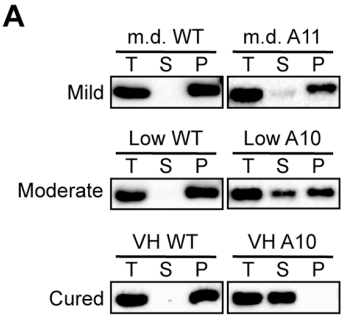

B

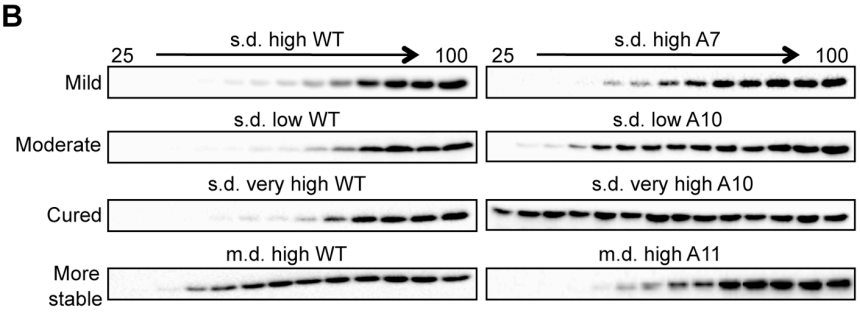

C

		s.d. low	s.d. med	s.d. high	s.d. very high	m.d. high
A1	SDD-AGE	Aggregate shift	Aggregate shift	Aggregate shift		Aggregate shift
	Thermal stability					
	Solubility assay					
A2	SDD-AGE		Aggregate shift			
	Thermal stability					
	Solubility assay					
A3	SDD-AGE			Aggregate shift		
	Thermal stability					
	Solubility assay					
A4	SDD-AGE					
	Thermal stability					More stable
	Solubility assay					
A5	SDD-AGE					
	Thermal stability			More stable		
	Solubility assay					
A6	SDD-AGE					
	Thermal stability					
	Solubility assay					
A7	SDD-AGE			Aggregate shift		Aggregate shift
	Thermal stability					
	Solubility assay					
A8	SDD-AGE					
	Thermal stability					
	Solubility assay					
A9	SDD-AGE		Aggregate shift			
	Thermal stability					
	Solubility assay					
A10	SDD-AGE					
	Thermal stability					
	Solubility assay					
A11	SDD-AGE					
	Thermal stability					More stable
	Solubility assay					

Figure S5. Summary of effects on [*RNQ*+] propagation by mutation of Rnq1 amyloidogenic regions according to assay. For the indicated assay, mutants are categorized as having no effect (white), mild effect (yellow), moderate effect (orange), or not propagating [*RNQ*+] (red) after successive passaging. (A) Examples of how the Rnq1 solubility assay was scored. Cells propagating m.d. high [*RNQ*+] (m.d.), s.d. low [*RNQ*+] (Low), or s.d. very high [*RNQ*+] (VH), and harboring either wild-type (WT) Rnq1 or the indicated Rnq1 alanine mutant, were fractionated by high-speed ultracentrifugation into total (T), supernatant (S), and pellet (P) fractions, followed by SDS-PAGE and western blot using an αRnq1 antibody. Mutants were characterized as follows: 1) mild effect, if there was a slight increase in the amount of soluble Rnq1; 2) moderate effect, if the supernatant and pellet fractions contained roughly equal amounts of Rnq1; or 3) cured, if all of Rnq1 accumulated in the supernatant. (B) Examples of how the thermal stability of Rnq1 aggregates was scored. Cells propagating the indicated [*RNQ*+] variant with either WT Rnq1 or the indicated Rnq1 alanine mutant were lysed and treated with a temperature gradient, followed by SDS-PAGE and western blot using an αRnq1 antibody. Mutants were characterized as follows: 1) mild effect, if there was a slight, but reproducible shift in the more intense bands; 2) moderate effect, if the number of intense bands shifted by four or more lanes; 3) cured, if there was roughly equal amounts of Rnq1 in each lane, which was confirmed by well-trap assay; or 4) more stable, if Rnq1 was reproducibly present in fewer lanes. (C) Summary table of the effects of Rnq1 mutants on [*RNQ*+] propagation. Unless the phenotypic change is noted, colors indicate: decreased aggregate densitometry (SDD-AGE), decreased stability (Thermal stability), or increased pool of soluble Rnq1 (Solubility assay). Data are summarized from at least three independent experiments.

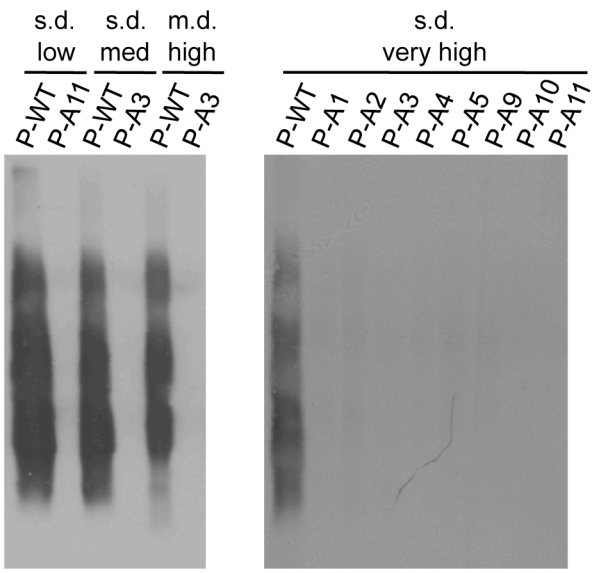

Figure S6. Disruption of Rnq1 amyloidogenic regions eliminates propagation of [*RNQ*+] variants. Cells originally propagating the indicated [*RNQ*+] variant and expressing WT Rnq1 or a Rnq1 alanine mutant from a *HIS*-marked plasmid (as in Figure 4) were transformed with a *RNQ1 URA3*-marked plasmid. These cells were then screened for loss of the indicated Rnq1 construct in order to express WT Rnq1 from the *URA3*-marked plasmid as the only copy of Rnq1. For instance, P-WT and P-A3 refer to post (P) expression of the *HIS*-marked copy of WT Rnq1 and Rnq1-A3, respectively, and now both expressing WT Rnq1. The presence of Rnq1 aggregates in these Ura+ his- cells was then monitored using SDD-AGE and western blot using an αRnq1 antibody.

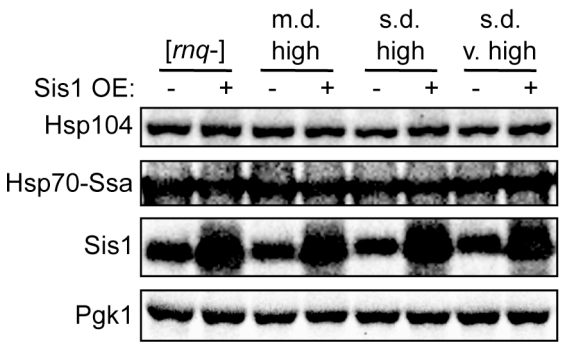

Figure S7. Expression levels of Ssa and Hsp104 are unchanged when Sis1 is over-expressed. Cells with the indicated [*RNQ*+] status were transformed with a Sis1 over-expressing plasmid (+) or an empty vector control (-). Lysates were subjected to SDS-PAGE and western blot using αHsp104, αHsp70-Ssa, αSis1, and αPgk1 antibodies.

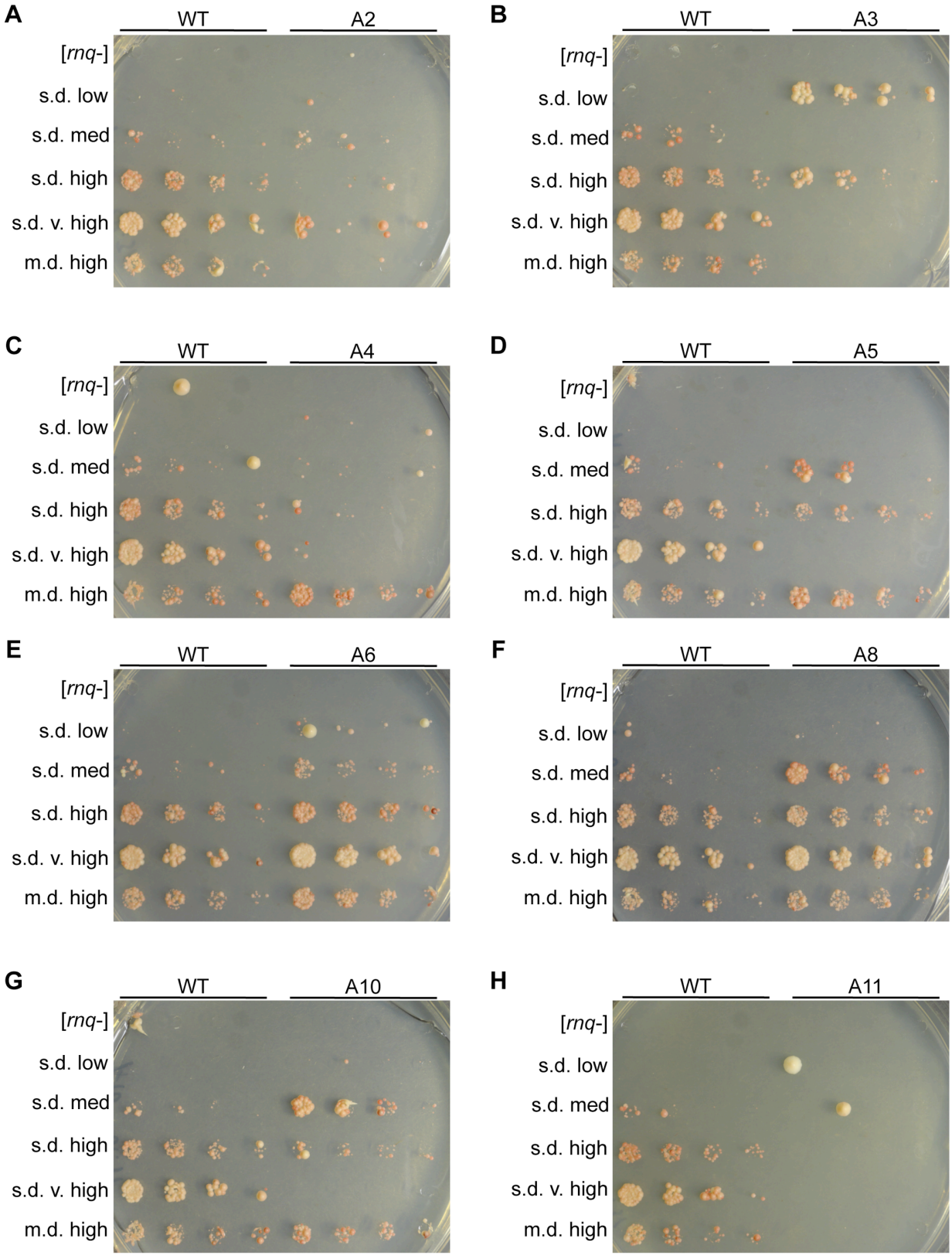
A
WT
A2
[rnq-]
s.d. low
s.d. med
s.d. high
s.d. v. high
m.d. high
B
WT
A3
[rnq-]
s.d. low
s.d. med
s.d. high
s.d. v. high
m.d. high
C
WT
A4
[rnq-]
s.d. low
s.d. med
s.d. high
s.d. v. high
m.d. high
D
WT
A5
[rnq-]
s.d. low
s.d. med
s.d. high
s.d. v. high
m.d. high
E
WT
A6
[rnq-]
s.d. low
s.d. med
s.d. high
s.d. v. high
m.d. high
F
WT
A8
[rnq-]
s.d. low
s.d. med
s.d. high
s.d. v. high
m.d. high
G
WT
A10
[rnq-]
s.d. low
s.d. med
s.d. high
s.d. v. high
m.d. high
H
WT
A11
[rnq-]
s.d. low
s.d. med
s.d. high
s.d. v. high
m.d. high

Figure S8. Formation of [*PSI*+] is altered by mutation of Rnq1 amyloidogenic regions. [*rnq*-] cells or cells propagating the indicated [*RNQ*+] variant and expressing WT Rnq1 or mutants (A) A2, (B) A3, (C) A4, (D) A5, (E) A6, (F) A8, (G) A10, or (H) A11 were transformed with a plasmid over-expressing Sup35. [*PSI*+] induction was monitored by spotting five-fold serial dilutions of normalized numbers of cells on SD-ade and SD-ade-his. Representative spottings from at least five independent experiments are shown.

Table S1. Yeast strains used in this study.

Strain	Description	Reference
1060	*Mat a ade1-14 ura3-52 leu2-3,112 trp1-289 his3-Δ200 sup35Δ::RMC* [*rnq*-]	[78]
693	*Mat a ade1-14 ura3-52 leu2-3,112 trp1-289 his3-Δ200 sup35Δ::RMC* s.d. low [*RNQ*+]	[33]
694	*Mat a ade1-14 ura3-52 leu2-3,112 trp1-289 his3-Δ200 sup35Δ::RMC* s.d. medium [*RNQ*+]	[33]
2311	*Mat a ade1-14 ura3-52 leu2-3,112 trp1-289 his3-Δ200 sup35Δ::RMC* s.d. high [*RNQ*+]	This study
2042	*Mat a ade1-14 ura3-52 leu2-3,112 trp1-289 his3-Δ200 sup35Δ::RMC* s.d. very high [*RNQ*+]	This study
459	*Mat a ade1-14 ura3-52 leu2-3,112 trp1-289 his3-Δ200 sup35Δ::RMC* m.d. high [*RNQ*+]	[33,78]
2043	*Mat a ade1-14 ura3-52 leu2-3,112 trp1-289 his3-Δ200 sup35Δ::RMC rnq1Δ::kanMX4* [*rnq*-]	This study
2044	*Mat a ade1-14 ura3-52 leu2-3,112 trp1-289 his3-Δ200 sup35Δ::RMC rnq1Δ::kanMX4* s.d. low [*RNQ*+]	This study
2045	*Mat a ade1-14 ura3-52 leu2-3,112 trp1-289 his3-Δ200 sup35Δ::RMC rnq1Δ::kanMX4* s.d. medium [*RNQ*+]	This study
2369	*Mat α ade1-14 ura3-52 leu2-3,112 trp1-289 his3-Δ200 sup35Δ::RMC rnq1Δ::kanMX4* s.d. high [*RNQ*+]	This study
2053	*Mat a ade1-14 ura3-52 leu2-3,112 trp1-289 his3-Δ200 sup35Δ::RMC rnq1Δ::kanMX4* s.d. very high [*RNQ*+]	This study
2047	*Mat a ade1-14 ura3-52 leu2-3,112 trp1-289 his3-Δ200 sup35Δ::RMC rnq1Δ::kanMX4* m.d. high [*RNQ*+]	This study
1890	*Mat a ade1-14 ura3-52 leu2-3,112 trp1-289 his3-Δ200 sup35Δ::hphMX4* [*psi*-] [*rnq*-]	This study
2259	*Mat a ade1-14 ura3-52 leu2-3,112 trp1-289 his3-Δ200 sup35Δ::hphMX4* [*psi*-] s.d. low [*RNQ*+]	This study
2260	*Mat a ade1-14 ura3-52 leu2-3,112 trp1-289 his3-Δ200 sup35Δ::hphMX4* [*psi*-] s.d. medium [*RNQ*+]	This study
2416	*Mat α ade1-14 ura3-52 leu2-3,112 trp1-289 his3-Δ200 sup35Δ::hphMX4* [*psi*-] s.d. high [*RNQ*+]	This study
2262	*Mat a ade1-14 ura3-52 leu2-3,112 trp1-289 his3-Δ200 sup35Δ::hphMX4* [*psi*-] s.d. very high [*RNQ*+]	This study
2261	*Mat α ade1-14 ura3-52 leu2-3,112 trp1-289 his3-Δ200 sup35Δ::hphMX4* [*psi*-] m.d. high [*RNQ*+]	This study
2055	*Mat a ade1-14 ura3-52 leu2-3,112 trp1-289 his3-Δ200 rnq1Δ::kanMX4* [*psi*-] [*rnq*-]	This study
831	*Mat α ade1-14 ura3-52 leu2-3,112 trp1-289 his3-Δ200 rnq1Δ::kanMX4* [*psi*-] s.d. low [*RNQ*+]	[78]
833	*Mat α ade1-14 ura3-52 leu2-3,112 trp1-289 his3-Δ200 rnq1Δ::kanMX4* [*psi*-] s.d. medium [*RNQ*+]	[78]
2310	*Mat a ade1-14 ura3-52 leu2-3,112 trp1-289 his3-Δ200*	This study

	rnq1Δ::kanMX4 [*psi*-] s.d. high [*RNQ*+]	
2057	*Mat a ade1-14 ura3-52 leu2-3,112 trp1-289 his3-Δ200 rnq1Δ::kanMX4* [*psi*-] s.d. very high [*RNQ*+]	This study
835	*Mat α ade1-14 ura3-52 leu2-3,112 trp1-289 his3-Δ200 rnq1Δ::kanMX4* [*psi*-] m.d. high [*RNQ*+]	[78]
L1751	*Mat a ade1-14 ura3-52 leu2-3,112 trp1-289 his3-Δ200* [*psi*-] [*rnq*-]	[31]
L1943	*Mat a ade1-14 ura3-52 leu2-3,112 trp1-289 his3-Δ200* [*psi*-] s.d. low [*RNQ*+]	[31]
L1945	*Mat a ade1-14 ura3-52 leu2-3,112 trp1-289 his3-Δ200* [*psi*-] s.d. medium [*RNQ*+]	[31]
L1767 [*psi*-]	*Mat a ade1-14 ura3-52 leu2-3,112 trp1-289 his3-Δ200* [*psi*-] s.d. high [*RNQ*+]	[108]
L1953	*Mat a ade1-14 ura3-52 leu2-3,112 trp1-289 his3-Δ200* [*psi*-] s.d. very high [*RNQ*+]	[31]
L1749	*Mat a ade1-14 ura3-52 leu2-3,112 trp1-289 his3-Δ200* [*psi*-] m.d. high [*RNQ*+]	[31]

Table S2. Plasmids used in this study.

Plasmid	Description	Reference
5245	pRS306-*RRP*	[78]
6246	pRS315-*SUP35*	This study
6501	pRS315-*RRP*	This study
6479	pRS315-full-length-*RRP*	This study
SL6602	pRS414*GPD-SIS1*	[74]
6244	pEMBL-*SUP35*	This study
5908	p413*GPD-rnq1-L94A*	[75]
6312	pRS313-*RNQ1*	[78]
6352	pRS413*TPI1-rnq1-A1*	This study
6392	pRS313-*rnq1-A2*	This study
6389	pRS413*TPI1-rnq1-A3*	This study
6322	pRS313-*rnq1-A4*	This study
6411	pRS313-*rnq1-A5*	This study
6477	pRS313-*rnq1-A6*	This study
6478	pRS313-*rnq1-A7*	This study
6397	pRS313-*rnq1-A8*	This study
6165	pRS313-*rnq1-A9*	This study
6398	pRS313-*rnq1-A10*	This study
6416	pRS313-*rnq1-A11*	This study
6548	pRS413*TPI1-rnq1-A3+A10*	This study
6357	pRS413*TEF-RNQ1(132-405)*	This study
5195	pRS316-*RNQ1*	[78]
5049	pYK810	[83]
6545	pYES2-*GAL-HA-RNQ1*	[99]
6613	pYES2-*GAL-RNQ1(153-405)*	This study

Table S3. Oligonucleotides used in this study.

Oligonucleotide	Description	Sequence
1366	5’ Sup35prom-XhoI	5'CGCCTCGAGGACGACGCGTCACAGTG
1367	5’ Sup35prom-SalI	5'CGCGTCGACGACGACGCGTCACAGTG
0316	3’Sup35prom-BamHI	5'CCCGGATCCTGTTGCTAGTGGGCAGATATAG
1348	5’ Sup35-BamHI-SpeI	5'CGCGGATCCACTAGTATGTCGGATTCAAACCAAGG
0322	3’Sup35(124-685)term-SacI	5’GGGGAGCTCGTGATTGAAGGAGTTGAAACCTTGC
0014	5'-TO-RNQ-4	5'GGTGGCAACGGTGGTTACC
0018	3'-TO-RNQ-8	5'AAAGCACCACCAGATTGTCC
0477	5’ Rnq1-BamHI	5'CCCGGATCCATGGATACGGATAAGTTAATCTCAGAGG
0320	3’RNQ1(153-405)-SacII	5'GGGCCGCGGGTAGCGGTTCTGGTTGCCGTTATTG
0488	5' Rnq1-EcoRV	5'GGGGATATCATGGATACGGATAAGTTAATCTCAGAGG
0489	3' Rnq1-SalI	5'CCCGTCGACTCAGTAGCGGTTCTGGTTGCCG
0491	3' Rnq1 terminator-XhoI	5'CCCCTCGAGGCAACACATACCTTACAAAGC
1429	5’ TPI1prom-SacI	5’GCGGAGCTCCTACGTATGGTCATTTCTTC
1430	3’ TPI1prom-XbaI	5’GCGTCTAGATTTTAGTTTATGTATGTG
1244	5' Rnq1-A1	5'CAAATGTCAACTATTGAATCAGCAGCTGCAGCAGCCGCAGCAGCCGCCATGGACAACCGTAGT
1245	3' Rnq1-A1	5'CACCACTACGGTTGTCCATGGCGGCTGCTGCGGCTGCTGCAGCTGCTGATTCAATAGTTGACATTTG
1472	5’ Rnq1-A2	5'GTGGTGGTGCAGCTGCTGCGGCCGCTGCAGCGGCAGACTCTAAGGGTTC
1473	3’ Rnq1-A2	5'GAGTCTGCCGCTGCAGCGGCCGCAGCAGCTGCACCACCACCAGCAGCACG
1442	5’ Rnq1-A3	5'GCAGCAGCAGCTGCGGCAGCCGCAGCGGCGGCACACTCATCAAATAAAGG
1443	3’ Rnq1-A3	5'TGCCGCCGCTGCGGCTGCCGCAGCTGCTGCTGCTAGTTGCGTTTGGGAAG
1426	5’ Rnq1-A4	5’CTTCTAACAGAGGGTTTGCCGCAGCGGCTGCCGCGGCAGCGGCAAGTGGTTCTGGCGGC
1427	3’ Rnq1-A4	5’GCCGCCAGAACCACTTGCCGCTGCCGCGGCAGCCGCTGCGGCAAACCCTCTGTTAGAAG
1474	5’ Rnq1-A5	5'GTGCTTCCGCCGCGGCTGCCGCGGCTGCTGCAGCCGCTAAGTCAGGTAACAATTCCC

1475	3’ Rnq1-A5	5'CTTAGCGGCTGCAGCAGCCGCGGCAGCCGCGGCGGAAGCACCCATACTTTG
1444	5’ Rnq1-A6	5'GCTGCTGCTGCTGCGGCGGCTGCGGCTGCAGCTGCCATGAATTCCAACAAC
1445	3’ Rnq1-A6	5'GGCAGCTGCAGCCGCAGCCGCCGCAGCAGCAGCAGCACCTTGACCTTGACCTTGTCCTTGACCTTGACC
1547	5’ Rnq1-A7	5’GCTCCGGTGGTTCCGCCGCTGCAGCAGCGGCTGCTGCGGCAGCCGCTGCTATGCATTCCAATAATAATC
1548	3’ Rnq1-A7	5’GATTATTATTGGAATGCATAGCAGCGGCTGCCGCAGCAGCCGCTGCTGCAGCGGCGGAACCACCGGAGC
1478	5’ Rnq1-A8	5'GCTGCTGCCGCAGCGGCCGCCGCGGCTGCAGCTGCCTTAGGTGGTGGACAAACTC
1479	3’ Rnq1-A8	5'CTAAGGCAGCTGCAGCCGCGGCGGCCGCTGCGGCAGCAGCACCACCAGATTGTCCC
1246	5' Rnq1-A9	5'GGTGGTGGACAAACTCAATCCGCCGCAGCGGCAGCCGCTCAACAAGGCCAAAACAACCAGCAGCAA
1247	3' Rnq1-A9	5'TTGCTGCTGGTTGTTTTGGCCTTGTTGAGCGGCTGCCGCTGCGGCGGATTGAGTTTGTCCACCACC
1480	5’ Rnq1-A10	5'GTGCAGCCGCAGCTGCGGCTGCCGCGGCAGCTGCCGCCCTGGGCAATAACTCCAATTC
1481	3’ Rnq1-A10	5'CAGGGCGGCAGCTGCCGCGGCAGCCGCAGCTGCGGCTGCACTGGAGTGGCCTTGTTGC
1498	3’ Rnq1-A11	5’GAGCAGCGGCGGCAGCAGCAGCGGCGGCTTCGTGCTGTCCATTGGAG
1525	5’ Rnq1-A11	5’CGAAGCCGCCGCTGCTGCTGCCGCCGCTGCTCAACAGAACAATAACGGC
0040	3'-XhoI-RNQ	5'CCGCTCGAGTCATCAGTAGCGGTTCTGGTTGCC
1626	5’Rnq1-153-405-HindIII	5’GCGAAGCTTATGCAAGGTCAGGGACAAGG
1436	5’Rnq1-del131	5'GCGGATATCATGAGTATGGGTGCTTCCGGC

Chapter 3: Comparative Analysis of Yeast Prion Variants Reveals Conformation-Specific Requirements for Chaperone Machinery

Kevin C. Stein and Heather L. True

This chapter is a manuscript under review for publication in the journal *Molecular Microbiology*.

3.1 Abstract

Molecular chaperones act as a major cellular line of defense through monitoring and processing misfolded substrates. This system helps prevent the aggregation of proteins that is associated with protein conformational disorders like Alzheimer's disease and prion diseases. In these diseases, a variety of different aggregate structures can form, called prion strains or variants, which cause variation in disease pathogenesis. Hence, chaperones are tasked with recognizing and processing a large spectrum of misfolded substrates to maintain proteostasis. Here, we use the yeast prion variants [*RNQ*+] and [*PSI*+] to explore the interactions of chaperones with distinct aggregate structures. We found that prion variants show striking variation in their relationship with Hsp40s. Specifically, the yeast Hsp40 Sis1 and its human ortholog Hdj1 had differential capacities to process prion variants. Such selectivity involves different domains of Sis1, with some prion conformers having a greater dependence on particular Hsp40 domains. Moreover, [*PSI*+] was more sensitive to modulation of Hsp70 activity as compared to [*RNQ*+] variants, which depended on Hsp70 and Hsp104 to similar extents. Collectively, these data indicate that Hsp40 selectivity has changed through evolution and that distinct chaperone machinery is required to process different aggregate structures. Elucidating the intricacies of chaperone-aggregate interactions will be crucial to understanding how this system can go awry in disease and contribute to the pathological variation observed in many protein conformational disorders.

3.2 Introduction

The aggregation of several different proteins is associated with the development of protein conformational disorders, including various neurodegenerative diseases like Alzheimer's

disease, Parkinson's disease, and prion diseases [2]. Interestingly, the proteins that aggregate in these disorders can misfold to form a variety of aggregate structures having distinct conformations [20]. In prion diseases, these different self-perpetuating structures, called prion strains, cause changes in pathological phenotypes and dictate disease transmissibility. It is the responsibility of molecular chaperones, as the master regulators of protein quality control from bacteria to humans, to recognize and process these diverse misfolded substrates and mitigate the devastating consequences these aggregates can have on cellular homeostasis [216]. Yet, how chaperone machinery can handle a large array of substrate conformations remains unclear.

Yeast prion strains (called prion variants) have served as a valuable model for examining the interactions between chaperones and distinct amyloid structures [14]. The [*PSI*+] and [*RNQ*+] prions are two of the best-studied yeast prions. [*PSI*+] is formed from the translation termination factor Sup35 [48,49]. Sequestration of Sup35 in prion aggregates results in modulating the efficiency of translation termination, causing readthrough of stop codons, called nonsense suppression [217]. Different variants of [*PSI*+] sequester Sup35 to different degrees. Hence, [*PSI*+] variants are associated with different amounts of soluble Sup35, and consequently, different levels of nonsense suppression [24,118]. Stronger [*PSI*+] variants cause more nonsense suppression (less faithful translation termination) as compared to cells propagating weaker [*PSI*+] variants. The [*RNQ*+] prion, on the other hand, is formed from the Rnq1 protein that has no clear function [11]. However, [*RNQ*+] is responsible for inducing the *de novo* formation of the [*PSI*+] prion [60,61], and [*RNQ*+] variants are distinguished based on how readily [*PSI*+] forms in [*RNQ*+] cells [31].

Just as molecular chaperones play a pivotal role in processing substrates in humans, chaperones process the aggregates of the [*PSI*+] and [*RNQ*+] prions. This processing is required

for transmission of the prion state to daughter cells and its continued maintenance in a yeast population [218]. A combination of chaperones from the Hsp40 and Hsp70 families, along with the disaggregase Hsp104, is involved in the proper maintenance of yeast prions [89,90]. Hsp104 is a AAA+ ATPase that assembles into a ring-shaped hexamer having a central pore to thread a variety of substrates [219,220]. Such substrate threading fragments large prion aggregates into smaller seeds that can be inherited by daughter cells [86]. Expression of Hsp104 is required for propagation of both [*PSI*+] and [*RNQ*+] as fragmentation is a necessary feature for prion maintenance [64,94]. However, proper processing of prion aggregates relies on Hsp70s, which act to transfer substrates to Hsp104 [86]. Like Hsp104, Hsp70s like Ssa1, which plays a major role in prion propagation [221], are ATPases whose activity relies on a constant cycling between nucleotide binding states [148]. Hsp70s will bind substrates in the ADP-bound state and release substrates in the ATP-bound state. Other chaperones are required to mediate this ATPase cycle. Nucleotide exchange factors (NEFs) promote the ATP-bound state, exchanging ADP for ATP and causing Hsp70 to have low affinity for non-native polypeptides. By contrast, Hsp40s are responsible for transferring substrates to Hsp70 and stimulating the Hsp70 ATPase activity [148]. Thus, Hsp40s promote the ADP-bound state of Hsp70s, thereby causing Hsp70s to have high affinity for non-native polypeptides and allowing further substrate processing. Interestingly, Hsp40s are proposed to be the predominant regulator dictating Hsp70 function and substrate selectivity.

Sis1 is the Hsp40 that is required for propagation of [*PSI*+] and [*RNQ*+] [90,95,99]. Sis1, like its human ortholog Hdj1, is a Type II Hsp40 that is divided into four major domains. The N-terminal J domain, a region conserved by all Hsp40 proteins, is required for Hsp70 interaction and stimulation, as well as for yeast viability [102,150,222]. Additionally, Sis1 has a C-terminal

domain (CTD) responsible for binding substrates [223], with the last 15 residues of the protein comprising the dimerization domain (DD) [224]. In between the J domain and CTD is a region rich in glycine and phenylalanine residues (G/F) followed by a region rich in glycine and methionine (G/M) residues. These regions are generally viewed as linker regions, but their function remains poorly understood. Interestingly, the G/F domain is required for propagation of [*RNQ*+], and we found that this was true for several different [*RNQ*+] variants (Stein et al., in review). Propagation of [*PSI*+] variants, on the other hand, differentially depends on this domain (Stein et al., in review) and Sis1 expression [215]. Moreover, mutations in the G/F domain associated with a myopathy show variant-dependent effects (Stein et al., in review). Yet, it remains unclear whether prion variants are differentially sensitive to changes in other Sis1 domains or have various other chaperone requirements.

Here, we explored the relationship between molecular chaperones and their interactions with different aggregate structures. We found striking differences in the chaperone interactions required for propagation of the [*PSI*+] and [*RNQ*+] prions and their associated structural variants. Hdj1 was unable to fully complement the function of Sis1 in propagating every prion variant of [*PSI*+] and [*RNQ*+]. This was likely because propagation of different prion variants relied on the presence of different domains of Sis1. In general, the [*RNQ*+] variants were more sensitive to changes in Sis1 and how it interacts with Hsp70, while [*PSI*+] variants were more sensitive to changes in Hsp70-Ssa1. These data indicate that distinct aggregate structures require different chaperone interactions for proper processing. Hence, gaining insight into the complex nature of these interactions is necessary in order to fully understand how defects in the proteostasis network can lead to disease.

3.3 Results

3.3.1 Sis1 and its Human Ortholog Hdj1 show Distinct Conformer Specificity

Hsp40s are suggested to dictate much of the substrate specificity of the chaperone network [148]. As Sis1 is capable of propagating a large spectrum of prion conformations ([95,215] and Stein et al., in review), we wondered whether its human ortholog, Hdj1, can functionally substitute for Sis1 in propagating different types of prion variants. To test this, we used four different prion conformers of the [*PSI*+] prion, representing two weaker [*PSI*+] variants (Sc37 and weak [*PSI*+]) and two stronger [*PSI*+] variants (Sc4 and strong [*PSI*+]) [24,69]. Since [*PSI*+] modulates translation termination, [*PSI*+] variants are easily distinguished based on colony color using the *ade1-14* allele, which has a premature stop codon in the *ADE1* gene [186]. Cells propagating distinct [*PSI*+] variants have different amounts of soluble Sup35 [118], and thus differentially suppress *ade1-14* to cause different amounts of red pigment to accumulate. Stronger [*PSI*+] colonies, having less soluble Sup35 and more nonsense suppression, are whiter in color as compared to colonies propagating weaker [*PSI*+] variants that are darker pink. All Sup35 is soluble in [*psi*-] cells, which makes these colonies red.

To determine if Hdj1 was capable of propagating these distinct [*PSI*+] variants, we used *sis1Δ* cells that expressed *SIS1* from a *URA3* plasmid, and used the plasmid shuffle technique to express Hdj1 or WT Sis1. Interestingly, the [*PSI*+] variants showed striking differences in their sensitivity to Hdj1 expression. While the weaker [*PSI*+] variants were darker pink when WT Sis1 was expressed, these cells were red and phenotypically [*psi*-] when Hdj1 was expressed (Fig. 1A). By contrast, expression of Hdj1 in stronger [*PSI*+] cells appeared to have no phenotypic consequences, as lighter pink colonies were seen when either Sis1 or Hdj1 was expressed. To confirm these results, we used SDD-AGE, which resolves aggregated Sup35 from

soluble Sup35 and has shown that [*PSI*+] variants have different aggregate distributions: Sup35 aggregates in weaker [*PSI*+] cells have a larger average aggregate size as compared to stronger [*PSI*+] cells [117]. In agreement with our phenotypic results, both weaker [*PSI*+] variants had no Sup35 aggregates when Hdj1 was expressed (Fig. 1B). However, Hdj1 expression caused a minor shift in the aggregate distribution with the stronger [*PSI*+] variants, despite being phenotypically similar to cells expressing Sis1. Nevertheless, these results indicate that the [*PSI*+] variants show drastically different sensitivity to Hdj1 expression, suggesting that Hdj1 is unable to propagate weaker [*PSI*+] conformers.

Next, we asked if Hdj1 showed differential capabilities in handling [*RNQ*+] variants. Previously, it was shown that expression of Hdj1 was fully capable of propagating an uncharacterized [*RNQ*+] variant [100]. Here, we used five different [*RNQ*+] variants that show differences in their ability to induce the formation of the [*PSI*+] prion [31]. Moreover, these [*RNQ*+] variants show differences in their *in vivo* distribution of aggregates using Rnq1-GFP, where single-dot (s.d.) [*RNQ*+] variants have one focus of fluorescence, while multiple-dot (m.d.) cells have multiple foci [120]. Hence, cells propagating the s.d. low [*RNQ*+] variant have the s.d. pattern of fluorescence and induce the formation of [*PSI*+] at low levels. In performing SDD-AGE to analyze the propagation of these variants as we did for [*PSI*+], we found that Hdj1 had diverse capabilities in maintaining the [*RNQ*+] variants (Fig. 1C). Like weak [*PSI*+], s.d. medium [*RNQ*+] was mostly eliminated by expression of Hdj1 and showed the presence of few aggregates. Moreover, propagation of all of the other s.d. [*RNQ*+] variants was impaired, as indicated by the presence of fewer aggregates, while m.d. high [*RNQ*+] appeared to be unaffected by Hdj1 expression. Collectively, these data suggest that Sis1 and Hdj1 have different specificity in processing distinct prion conformers.

3.3.2 Differential Dependence on Hsp40 Domains Dictates Conformer Specificity

As Hdj1 and Sis1 had differential ability to propagate particular prion variants, we hypothesized that there might be distinct differences in domain functionality of these Hsp40s. Thus, we wanted to determine what domains might underlie these differences. To gain insight into this question, we created a suite of chimeras having various combinations of the four major domains present in Hdj1 and Sis1, and confirmed comparable expression as the wild-type (WT) proteins (Fig. S1). We refer to these chimeras by delineating the origins of each domain, with "S" for Sis1 and "H" for Hdj1 (Fig. 2A). As Hdj1 was unable to propagate certain prion variants, these chimeras allowed us to ask which Sis1 domains would rescue this defect.

Using *sis1Δ* cells propagating weak [*PSI*+] or Sc37, as these prion structures were eliminated when Hdj1 was expressed, we replaced WT Sis1 with one of the chimeric proteins. Interestingly, we found that the chimeras were differentially capable of propagating these structures, despite both being weaker [*PSI*+] variants (Fig. 2B,C). For instance, the chimera HSHH expressed the Sis1 G/F domain in place of that of Hdj1. This chimera largely rescued propagation of Sc37, as indicated by the presence of less soluble Sup35 as compared to expression of Hdj1, based on phenotype (Fig. 2B) and SDD-AGE (Fig. 2C). However, HSHH provided very little rescue of propagation of weak [*PSI*+], as these cells were phenotypically similar to [*psi*-] cells and had a greatly reduced aggregate band by SDD-AGE. Moreover, replacing additional Hdj1 domains with those of Sis1 (e.g. HSSH, HHSS, and SSSH) also partially rescued both prion variants. Yet, HHSS was more capable of propagating Sc37 than weak [*PSI*+], as there was a large soluble pool of Sup35 with weak [*PSI*+] cells expressing HHSS that was not seen with cells propagating Sc37. However, none of the chimeras completely

rescued propagation of Sc37, while SSSH appeared to fully rescue propagation of weak [*PSI*+], as indicated by a lack of soluble Sup35.

We also tested whether the Sis1-Hdj1 chimeras would rescue propagation of the s.d. low and s.d. medium [*RNQ*+] variants that were most impaired by Hdj1 expression. Using SDD-AGE, we found that propagation of these variants showed dramatic differences in terms of what chimera was capable of mediating prion propagation (Fig. 2D). For s.d. medium [*RNQ*+], it was only the two chimeras that contained the Sis1 CTD (HHHS and HHSS) that rescued propagation as compared to Hdj1. Strikingly, HHHS did not rescue propagation of s.d. low [*RNQ*+], but several other chimeras did (Fig. 2D). Collectively, these data indicate that propagation of both [*PSI*+] and [*RNQ*+] variants relies on distinct domains of the Hsp40 machines.

3.3.3 Propagation of Different Prion Variants Relies on Distinct Regions of Sis1

As a complementary approach to asking whether particular prion variants differentially require the presence of certain Sis1 domains, we took advantage of a variety of Sis1 mutants that have previously been used to interrogate the importance of Sis1 regions on prion propagation [74,97,100]. This included deletion mutants of major Sis1 domains that supported viability in *sis1Δ* cells (Sis1-ΔG/F, Sis1-ΔG/M, Sis1-ΔCTD), the dimerization domain (Sis1-ΔDD), smaller regions of the G/F domain (Sis1-Δ86-96 and Sis1-Δ101-113), and a point mutation in the G/F domain (Sis1-D110G). We transformed each of these mutants to replace WT Sis1in *sis1Δ* cells that propagated one of the [*PSI*+] or [*RNQ*+] variants.

For both weaker [*PSI*+] variants, we found that deletion of the G/F or G/M domains impaired prion propagation, as these cells were phenotypically darker pink as compared to cells expressing WT Sis1 (Fig. 3A), and there was an increase in soluble Sup35 according to SDD-

AGE (Fig. 3B). Additionally, deletion of the Sis1 CTD had a major impact on prion propagation, mostly eliminating both variants, while deletion of the DD and residues 86-96 had minimal effect. However, paradoxically, deletion of residues 101-113 had a greater effect on propagation of weak [*PSI*+] as compared to Sc37, with a complete loss of Sup35 aggregates in weak [*PSI*+] cells, but a point mutation within this stretch of Sis1, D110G, impaired propagation of Sc37 to a larger extent, as indicated by the darker pink color and a dramatic shift in the average aggregate distribution (Fig. 3). These data again suggest that the weaker [*PSI*+] variants are differentially sensitive to mutations in Sis1. Moreover, Sis1 mutants showed very minimal effect on propagation of stronger [*PSI*+] variants, with the greatest impact being the toxicity of Sis1-ΔCTD in the presence of stronger [*PSI*+] (Fig. S2), as seen previously [97].

Next, we tested how the Sis1 mutants affected propagation of the [*RNQ*+] variants using a sedimentation assay that separated cell lysates into soluble and insoluble fractions. In the [*RNQ*+] state with WT Sis1, almost all Rnq1 protein is sequestered into aggregates and accumulates in the insoluble fraction, whereas any impairment in prion propagation results in an increased soluble pool of Rnq1 [74]. Some prion variants, such as s.d. very high [*RNQ*+] have a larger pool of soluble Rnq1 than others [31]. As we previously found, deletion of the G/F domain eliminated all five [*RNQ*+] variants (Fig. 3C and Stein et al., in review). Interestingly, other than Sis1-ΔG/F, both s.d. high [*RNQ*+] and m.d. high [*RNQ*+] were particularly resistant to changes in Sis1. There was some increased soluble Rnq1 when Sis1-Δ101-113 was expressed in s.d. high [*RNQ*+] cells, but it was only deletion of the G/M domain that really impaired propagation of these two [*RNQ*+] variants (Fig. 3C). Sis1-ΔG/M also affected propagation of the three other [*RNQ*+] variants, thereby showing the general importance of this domain in prion propagation. However, deletion of this domain showed varying degrees of impairment, minimally increasing

the soluble pool of Rnq1 in s.d. low [*RNQ*+] cells and mostly eliminating the propagation of s.d. medium and s.d. very high [*RNQ*+]. Interestingly, s.d. medium and s.d. very high [*RNQ*+] were particularly sensitive to deletion of the Sis1 CTD and the DD. Moreover, deletion of residues 86-96 resulted in increased soluble Rnq1 for only s.d. very high [*RNQ*+] cells, suggesting that this region is important for propagation of only the s.d. very high [*RNQ*+] prion variant. Collectively, these data suggest that Sis1 utilizes distinct domains in order to propagate a wide spectrum of aggregated structures.

3.3.4 [*RNQ*+] *Variants all depend on the Interaction of Hsp40 with Hsp70*

A complex of chaperones is often required to process misfolded substrates. It is suggested that Hsp40s, in general, are responsible for recognizing substrates [148]. Then, in the case of yeast prions, Sis1 in combination with an Hsp70, such as Ssa1, will transfer substrates to Hsp104 for fragmentation and continued propagation [90]. While the Sis1 J domain is critical for the interaction of Sis1 with the nucleotide-binding domain of Hsp70s [225], part of the Sis1 CTD interacts with the EEVD motif in the substrate-binding domain of Hsp70s [226-228]. Indeed, a mutation in the Sis1 CTD (L268P) was previously found to impair the interaction of Sis1 and Ssa1 *in vitro*, which inhibited the propagation of an uncharacterized [*RNQ*+] variant [104].

Using Sis1-L268P as a means of disrupting the Sis1-Hsp70 interaction, we asked whether all prion variants similarly relied on the Sis1-Hsp70 interaction for proper maintenance. We expressed Sis1-L268P in place of WT Sis1 in *sis1Δ* cells propagating one of the [*RNQ*+] or [*PSI*+] variants. Unexpectedly, despite the [*RNQ*+] variants showing dramatic differences in sensitivity to changes in Sis1, the Sis1-L268P construct eliminated the propagation of all five [*RNQ*+] variants, as all of the Rnq1 protein accumulated in the soluble fraction after

ultracentrifugation (Fig. 4). By contrast, propagation of the stronger [*PSI*+] variants was unchanged, while propagation of the weaker [*PSI*+] variants was impaired, but not eliminated (data not shown). This suggests that propagation of all [*RNQ*+] variants depends on the interaction between Sis1 and Hsp70, but propagation of [*PSI*+] does not absolutely require this interaction.

3.3.5 [*RNQ*+] *Variants do not show the Same Sensitivity to Modulating the Hsp70 ATPase Cycle as* [*PSI*+]

As Hsp70s clearly play an important role in substrate processing, we next wanted to determine whether altering Hsp70 function differentially affected propagation of prion variants. The Hsp70-dependent processing of substrates depends on an iterative nucleotide-binding cycle between ADP- and ATP-bound states that depends on the activity of Hsp40 and NEFs [148]. We asked whether modulation of Hsp70 activity might affect particular [*RNQ*+] variants to different extents, as has been observed with [*PSI*+] variants [229].

To address this, we first utilized a mutant of Ssa1, called Ssa1-21, that is known to dominantly affect propagation of the [*PSI*+] prion [230]. Ssa1-21 harbors the L483W mutation, which resides in the C-terminal substrate-binding domain of Ssa1 and causes elevated ATPase activity [231]. In order to examine the effect of Ssa1-21, we created *ssa2Δ* [*RNQ*+] strains as loss of Ssa2 enhances the effect of Ssa1-21 [230,232]. We then transformed these cells with a plasmid expressing *SSA1-21* from the endogenous *SSA1* promoter, along with an *SSA1* plasmid or an empty vector as controls. To monitor the influence on prion propagation, we performed well-trap assays, which allows us to easily determine the amount of soluble Rnq1 in the cell, since aggregated Rnq1 is retained in the wells of an SDS-PAGE gel when cell lysate fractions

are not boiled [189]. Interestingly, there was no increased pool of soluble Rnq1 in cells propagating any of the [*RNQ*+] variants when Ssa1-21 was expressed (Fig. 5A). Importantly, as genetic background is a critical variable for revealing the effects of Ssa1-21 [233], we found that an isogenic *ssa2Δ* strain propagating strong [*PSI*+] showed that [*PSI*+] propagation was impaired with Ssa1-21 expression as compared to Ssa1-expressing cells and empty vector controls (Fig. 5B). However, [*PSI*+] was not cured as previous studies had shown [230,232,234].

Despite not seeing an effect using the Ssa1-21 construct, we hypothesized that over-expression of Ssa1 might impair propagation of certain [*RNQ*+] variants. Additionally, as NEF activity is an important modulator of Hsp70 activity, we also wanted to determine whether the [*RNQ*+] variants would be differentially sensitive to over-expression or deletion of the NEF *SSE1*, as is the case for other prions and prion variants [229,233]. Using well-trap assays, we found that neither over-expression of Ssa1 nor Sse1 altered the amount of soluble Rnq1, as compared to empty vector controls, for any of the [*RNQ*+] variants (Fig. 5C). Furthermore, deletion of *SSE1* also had no effect on [*RNQ*+] propagation (Fig. 5D), despite the previous finding that [*PSI*+] variants are sensitive to deletion of *SSE1* to different extents [229]. These data suggest that [*RNQ*+] is less sensitive to the alterations in Hsp70 activity as compared to [*PSI*+].

3.3.6 [*RNQ*+] *Variants Similarly Rely on Hsp104-ClpB Chimeras*

Along with Sis1, the other protein that is essential for propagation of all known yeast prions is Hsp104 [64,94,96,235]. Upon transfer of substrates from Hsp40-Hsp70, Hsp104 fragments prion aggregates into smaller seeds that are transmissible to daughter cells and maintain the prion state [236]. Hsp104 has been divided into an N-terminal domain with no clear

function along with two ATPase domains that are separated by a coiled-coil middle (M) domain [237]. The M domain is responsible for mediating the physical interaction with the Hsp70 machinery [238-240]. Interestingly, the *E. coli* ortholog of Hsp104, ClpB, is unable to cooperate with the yeast co-chaperones to propagate [*PSI*+], [*RNQ*+], and [URE3], unless the Hsp104 M domain is present [90,241]. We have recently shown that modulating the activity of the Hsp104 M domain differentially affects [*RNQ*+] and [*PSI*+] variants [242], possibly through altering interactions with co-chaperones. Therefore, we wondered whether these differences between ClpB and Hsp104 would similarly affect all [*RNQ*+] variants. Hence, we took advantage of a set of chimeras that consisted of different combinations of domains from Hsp104 and ClpB [90] to ask if distinct prion structures showed differential dependence on other regions of Hsp104.

We used [*RNQ*+] *hsp104Δ* yeast strains and replaced WT Hsp104 with one of the ClpB-Hsp104 chimeras, along with WT ClpB, WT Hsp104, and an empty vector as controls. We then monitored [*RNQ*+] propagation by the presence of aggregates using SDD-AGE. Unexpectedly, we found that only WT Hsp104 and the chimera 444B were able to maintain Rnq1 aggregates (Fig. 6). The chimera 444B was the only chimera that was previously shown to propagate a stronger [*PSI*+] variant [90]. This indicates that the second ATPase domain of ClpB is able to functionally substitute for that of Hsp104. Moreover, these data suggest that the propagation of the [*RNQ*+] variants relies similarly on the different domains of Hsp104.

3.4 Discussion

Our study highlights the extent to which molecular chaperones differentially interact with various aggregate conformations. Previous work has focused on the fact that different prions or prion variants show distinct sensitivity to chaperone levels [215,229,243]. We have recently

shown that propagation of several different [*RNQ*+] variants all require the presence of the Sis1 G/F domain, while [*PSI*+] variants show differential dependence on this domain (Stein et al., in review). Here, we show that other domains of Sis1 are also important in a prion variant-dependent manner. This suggests that substrate conformation, not simply the substrate protein, is a critical determinant of how chaperone machinery interacts and processes substrates. In fact, we recently found that the [*RNQ*+] variants likely have different regions of the Rnq1 protein that are available for chaperone binding [34].

Hsp40s are responsible for interacting with non-native polypeptides and mediating the functional specificity of Hsp70s [148]. We showed that prion variants of [*RNQ*+] showed differences in sensitivity to only variation in Sis1, and not in Hsp70 or Hsp104. Moreover, we found that such specificity also extends to the direct orthologs of Sis1 and Hdj1 (Fig. 1). Hdj1 was unable to propagate weaker [*PSI*+] variants and s.d. medium [*RNQ*+], and impaired the propagation of the other s.d. [*RNQ*+] variants. Previous work with the bacterial DnaJ protein suggested that the G/F domain mediated substrate specificity [244]. However, our work clearly shows that other domains of Sis1 also play an important role. In the case of the weaker [*PSI*+] variants, the Sis1 CTD is necessary for propagation (Fig. 3), which agrees with this being the substrate-binding domain [224]. However, the deletion of the Sis1 DD did not affect propagation of either of these variants, suggesting that dimerization is not essential for propagation. By contrast, we found that propagation of the [*RNQ*+] variants relied on the G/M domain to different extents, in particular s.d. medium and s.d. very high [*RNQ*+]. Interestingly, these variants were the only structures eliminated by deletion of the CTD, and propagation was even affected by the DD (Fig. 3C). Moreover, it was only the Sis1-Hdj1 chimeras that had the Sis1 CTD that rescued propagation of s.d. medium [*RNQ*+] (Fig. 2). As the dimerization of Sis1 is proposed to increase

the affinity of Sis1 for substrates or for transfer to Hsp70, we suggest that s.d. medium and s.d. very high [*RNQ*+] are particularly recalcitrant substrates, such that Sis1 must function as a dimer in order for these variants to be properly processed.

Structurally, X-ray crystallography has shown that the structures of the J domain and CTD of Sis1 and Hdj1 are very similar [225]. The CTD of these homo-dimeric proteins [224], forms a U-shaped cleft that binds substrate proteins [223] and part of the substrate-binding domain of Hsp70 [228]. Interestingly, this cleft is smaller in Hdj1, in which the distance between the monomer subunits is shorter as compared to Sis1 [245]. This might indicate that the decreased ability of Hdj1 to process all prion conformers is because its CTD has lower flexibility to bind larger, or more recalcitrant, substrates. Furthermore, the putative narrower range of clients for Hdj1 as compared to Sis1 might suggest that, through evolution from yeast to humans that included a large increase in the number of Hsp40s [148], Hdj1 may have become more specialized.

A previous study had observed that expression of Hdj1 was synthetically lethal with the presence of strong [*PSI*+] [97], which we did not reproduce here. However, as shown in that previous study [97], expression of Sis1-ΔCTD was toxic in strong [*PSI*+] cells (Fig. S2). We suggest that these differences are likely due to variation in genetic background, which is an important consideration in analyzing chaperone-amyloid interactions [215]. Nevertheless, as aggregates can sequester various chaperone machinery [246,247], it is feasible that Sup35 aggregates in strong [*PSI*+] cells sequester Sis1 more than other prion variants, such that the already reduced capability of Sis1-ΔCTD (or Hdj1 in the previous work [97]) cannot maintain the essential functions of Sis1 in yeast.

We had previously shown that mutations in the Hsp104 M domain affect propagation of the [*RNQ*+] variants differently [242]. However, in this study, we found that the ClpB-Hsp104 chimeras similarly affected propagation of the [*RNQ*+] variants, with only the 444B chimera able to maintain Rnq1 aggregates. In light of the dramatic differences in sensitivity that the [*RNQ*+] variants have to alterations in Sis1, we now propose that the differential effects of mutations in the Hsp104 M domain are likely mediated through disrupting the interactions with co-chaperones, particularly Sis1. Indeed, the s.d. high and m.d. high [*RNQ*+] variants were the most resistant to changes in the Hsp104 M domain [242], just as they were the most resistant to mutations in Sis1 (Fig. 3). This would agree with the finding that co-chaperones bind to and mediate the activity of the Hsp104 M domain [238].

It has long been recognized that [*PSI*+] is the only prion that is cured by over-expression of Hsp104 [243], which is due to Hsp104 outcompeting Ssa1 for binding to Sup35 aggregates, thus resulting in a non-productive interaction [221]. Our data further indicate that [*PSI*+] is more sensitive to changes in Hsp70 activity as compared to [*RNQ*+] (Fig. 5). By contrast, while the weaker [*PSI*+] variants show some dependence on Sis1 alterations, unlike the stronger [*PSI*+] variants, the [*RNQ*+] variants all show even more dependence on Sis1 as these structures were all eliminated by expression of Sis1-ΔG/F. Moreover, [*PSI*+] is less sensitive to Sis1-L268P, as compared to [*RNQ*+], indicating that [*RNQ*+] depends on the Sis1-Ssa1 interaction to a greater extent than [*PSI*+]. Taken together, these data make a strong argument that Sis1 plays a more intimate role in propagation of [*RNQ*+] as compared to [*PSI*+], which depends more on Ssa1 and Hsp104.

Genetic and environmental changes can influence the formation and maintenance of distinct aggregate structures ([32,34,40,41] and Stein et al., in review). Indeed, many of these

changes are likely due to altering the ability of molecular chaperones to monitor protein quality control. Our study indicates that substrate processing of not only different substrates, but also different substrate conformers, can depend on a distinct set of chaperone machinery. Therefore, with the vital role that molecular chaperones play in maintaining proteostasis, elucidating the complex nature of chaperone-aggregate interactions is crucial to understanding protein conformational disorders and the pathological variation that is often observed.

3.5 Materials and Methods

3.5.1 Yeast Strains and Media

All yeast strains described in this study were derived from 74-D694 (*ade1-14 ura3-52 leu2-3,112 trp1-289 his3-Δ200*) and are listed in Table S1. Standard culturing techniques were used throughout with ¼ YEPD (0.25% yeast extract, 2% peptone, 2% dextrose) or synthetic defined (SD) media (0.67% yeast nitrogen base without amino acids, 2% dextrose) lacking one or more nutrients to select for appropriate plasmids. Medium containing 1mg/mL 5-fluoroorotic acid (5-FOA) was used to select against *URA3* plasmids in order to replace wild-type (WT) proteins with mutant constructs using the plasmid shuffle technique.

WT yeast strains were kind gifts from S. Liebman (L1751, L1943, L1945, L1767 [*psi*-], L1953, L1749, S12600, S12606) [24,31,108] and J. Weissman (2397, 2398) [69]. Construction of the *sis1Δ* strains containing pRS316-*SIS1* (see Table S2 for plasmids used in this study) and the *hsp104Δ* strains containing pRS316-*HSP104p-HSP104* were described previously (Stein et al., in review and [242]). To create the *ssa2Δ* strains, the *kanMX4* cassette having flanking homology to the *SSA2* promoter and terminator was amplified from pFA6a using oligonucleotides 0978 and 0979 (see Table S3 for oligonucleotides used in this study), followed

by transformation into yeast cells, and selecting for resistance to G418. To create the *sse1Δ* strains, the plasmid-based disruption cassette *sse1Δ::LEU2* was digested with SacII/PstI, transformed into yeast, and Leu+ transformants were selected. All gene deletions were confirmed by colony PCR.

3.5.2 Plasmid Construction

The following plasmids were kind gifts (see Table S2): Hsp104-ClpB constructs from J. Weissman [90], Sis1 mutant constructs from E. Craig, S. Lindquist, and D. Masison [74,97,100,104], pRS424*GPD-HDJ1* from E. Craig [100], pRS315-*SSA1* and pRS315-*SSA1-21* from D. Masison [234], pRS413*GPD-FLAG-SSE1* and the *sse1Δ::LEU2* disruption cassette from K. Morano [248]. Construction of pRS314-*SIS1* was described previously (Stein et al., in review). To create pRS415*GPD-SSA1*, *SSA1* was amplified using oligonucleotides 0219 and 0220, digested with SpeI/HindIII, ligated with pRS415*GPD* digested with the same enzymes, and confirmed by sequencing.

Construction of the Sis1-Hdj1 chimeras was performed using bridge PCR with the indicated oligonucleotides and pRS316-*SIS1* or pRS424*GPD-HDJ1* as templates, unless otherwise noted: *SHHH* (*S* with 0229 and 1581, *HHH* with 1580 and 1471), *HSHH* (*H* with 1466 and 1467, *S* with 1468 and 1469, *HH* with 1470 and 1471), *HHSH* (*HH* with 1466 and 1500, *S* with 1499 and 1566, *H* with 1565 and 1471), *HHHS* (*HHH* with 1466 and 1502, *S* with 1501 and 0230), *HSSH* (*HS* with 1466 and 1583 using pRS414*GPD-HSHH* as template, *SH* with 1582 and 1471 using pRS414*GPD-HHSH* as template), *HHSS* (*HH* with 1466 and 1500, *SS* with 1499 and 0230), *SSSH* (*SSS* with 0229 and 1566, *H* with 1565 and 1471). Sis1 domains were demarcated as follows: J domain (1-66), G/F (67-121), G/M (122-179), CTD (180-352). Hdj1 domains were

demarcated as follows: J domain (1-66), G/F (67-108), G/M (109-161), CTD (162-340). All constructs with digested with SpeI/ClaI, ligated into pRS414*GPD* digested with the same enzymes, and confirmed by sequencing.

3.5.3 Phenotypic Colorimetric Analysis

Overnight yeast cultures were normalized to OD_{600} 0.4, serially diluted five-fold, and spotted to the indicated media. Plates were grown at 30°C for 6 days for SD-ade-leu, and for 3 days for all other media, followed by overnight at 4°C for additional color development.

3.5.4 Protein Analysis

Semi-denaturing detergent agarose gel electrophoresis (SDD-AGE) for both Rnq1 and Sup35 proteins was performed as described previously with the indicated antibodies [32,242]. The solubility assay of Rnq1 was described elsewhere [78]. Briefly, cell lysates in detergent-containing lysis buffer were subjected to ultracentrifugation at 80,000 rpm for 30 min at 4°C to separate into soluble and insoluble fractions that were analyzed by SDS-PAGE and western blot with a polyclonal αRnq1 antibody. Well-trap assays were performed as described [34]. Additional antibodies used to analyze protein expression included: two different αSis1 antibodies (here referred to as αSis1.1 (COP-COP-080051, Cosmo Bio Co.) and αSis1.2 (a kind gift from E. Craig)), αHdj1 (ADI-SPA-400, Enzo Life Sciences), and αPgk1 (A6457, Molecular Probes).

3.6 Acknowledgments

We are grateful to the following for reagents: S. Liebman, S. Lindquist, E. Craig, J. Weissman, K. Morano, and D. Masison. This work was supported, in whole or in part, by the

National Institutes of Health: F31AG040899 and T32GM007067 to KCS and GM072778 to HLT.

3.7 Figures

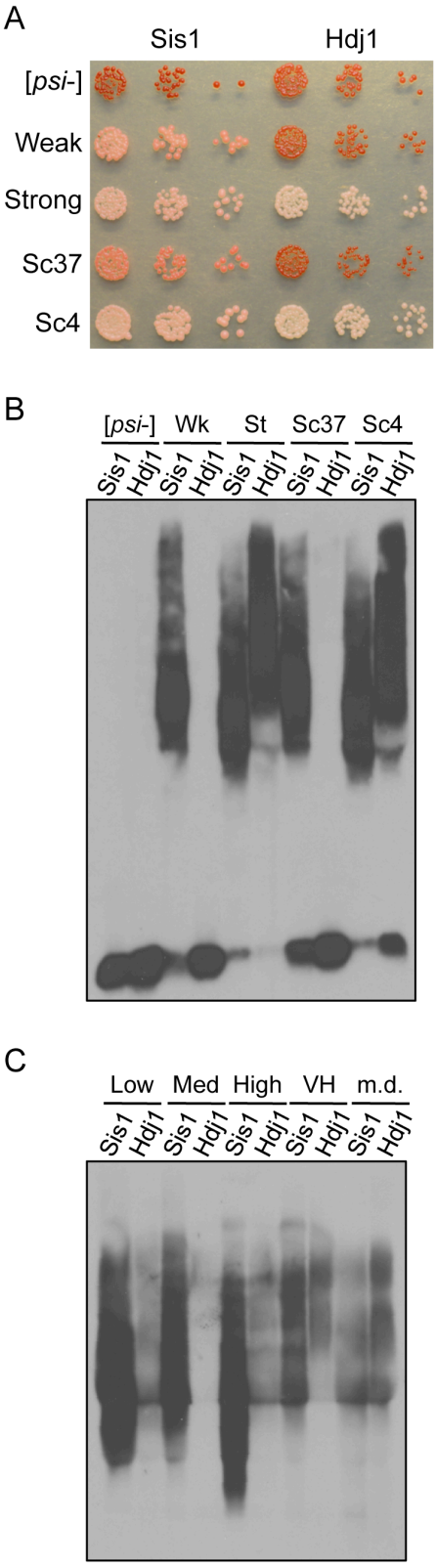
A
Sis1
Hdj1
[psi-]
Weak
Strong
Sc37
Sc4
B
[psi-]
Wk
St
Sc37
Sc4
Sis1
Hdj1
C
Low
Med
High
VH
m.d.

Figure 1. Hdj1 cannot maintain propagation of all prion variants of [*PSI*+] and [*RNQ*+]. (A) Normalized numbers of yeast *sis1Δ* cells expressing Sis1 or Hdj1 and propagating the indicated [*PSI*+] variant, as compared to [*psi*-] cells, were serially diluted five-fold and spotted on ¼ YEPD to monitor prion propagation by colony color. (B) [*PSI*+] and [*psi*-] cell lysates expressing Sis1 or Hdj1 were subjected to SDD-AGE and western blot using an αSup35 antibody. (C) As in (B) with cells propagating the indicated [*RNQ*+] variant and using an αRnq1 antibody.

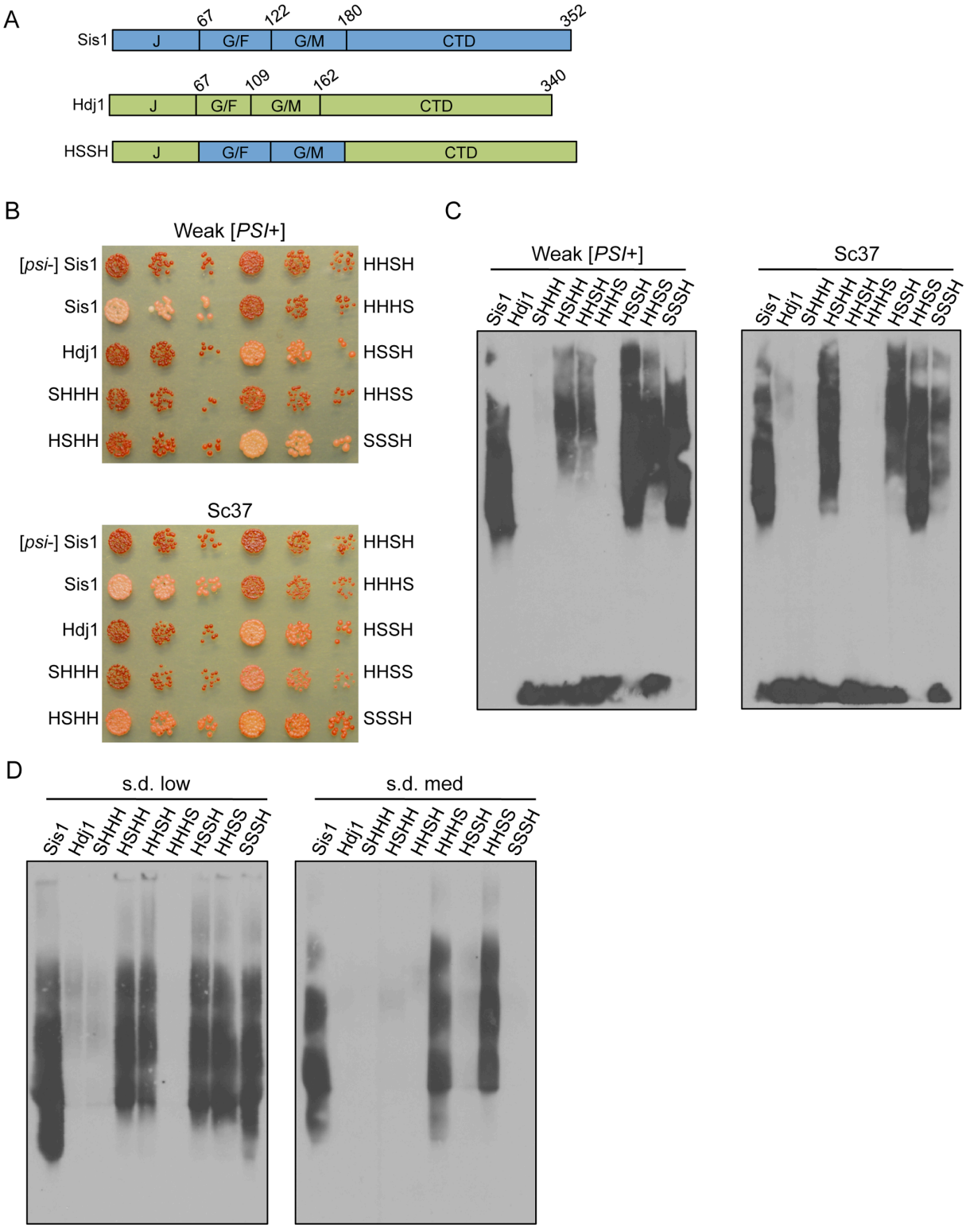

Figure 2. Prion propagation shows variant-specific dependence on Sis1-Hdj1 chimeras. (A) Schematic diagram of domain structure of Sis1, Hdj1, and one of the Sis1-Hdj1 chimeras, HSSH.

(B) Normalized numbers of yeast *sis1Δ* cells expressing Sis1, Hdj1, or the indicated Sis1-Hdj1 chimera and propagating weak [*PSI*+] or Sc37, with [*psi*-] *SIS1* cells as a control, were serially diluted five-fold and spotted on ¼ YEPD to monitor prion propagation by colony color. (C) Cell lysates propagating weak [*PSI*+] or Sc37 and expressing the indicated constructs were subjected to SDD-AGE and western blot using an αSup35 antibody. (D) As in (C) with cells propagating the s.d. low or s.d. medium [*RNQ*+] variants and using an αRnq1 antibody.

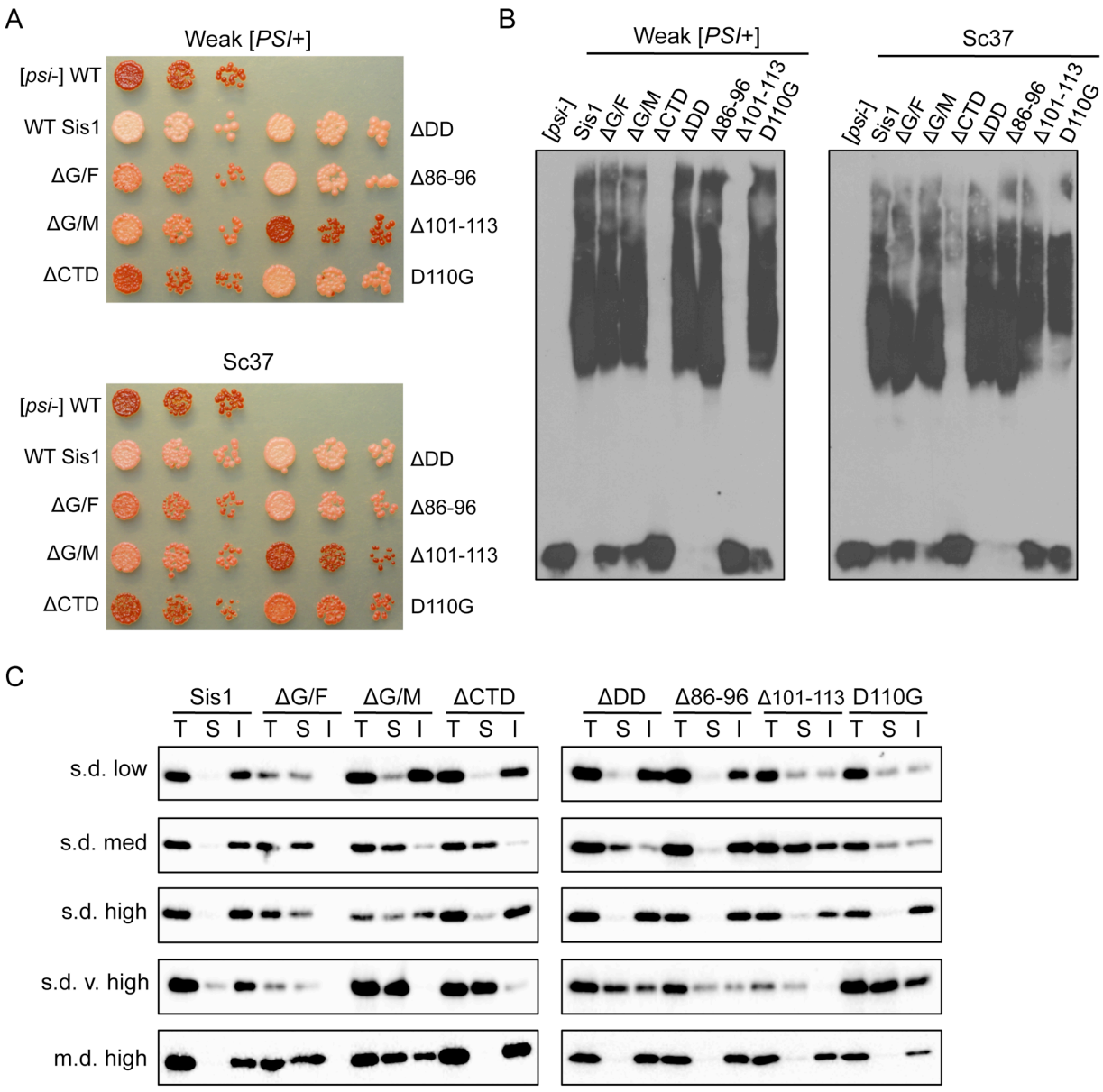

Figure 3. Distinct Sis1 domains are involved in defining conformer specificity. (A) Normalized numbers of yeast *sis1Δ* cells expressing WT Sis1 or the indicated Sis1 mutant, and propagating weak [*PSI*+] or Sc37, with [*psi*-] *SIS1* cells as a control, were serially diluted five-fold and spotted on ¼ YEPD to monitor prion propagation by colony color. (B) Cell lysates propagating weak [*PSI*+] or Sc37 and expressing the indicated constructs, along with [*psi*-] cells expressing WT Sis1, were subjected to SDD-AGE and western blot using an αSup35 antibody.

(C) Cell lysates propagating the indicated [*RNQ*+] variant and expressing WT Sis1 or the indicated Sis1 mutant, were separated by high-speed ultracentrifugation into total (T), soluble (S), and insoluble (I) fractions, followed by SDS-PAGE and western blot using an αRnq1 antibody.

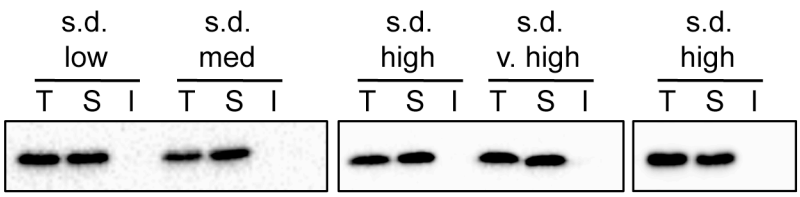

Figure 4. Sis1-Hsp70 interaction is required for propagation of all [*RNQ*+] variants. Cell lysates propagating the indicated [*RNQ*+] variant and expressing in place of WT Sis1 the Sis1-L268P construct, which disrupts the interaction of Sis1 with Ssa1 *in vitro* [104], were separated by high-speed ultracentrifugation into total (T), soluble (S), and insoluble (I) fractions, followed by SDS-PAGE and western blot using an αRnq1 antibody.

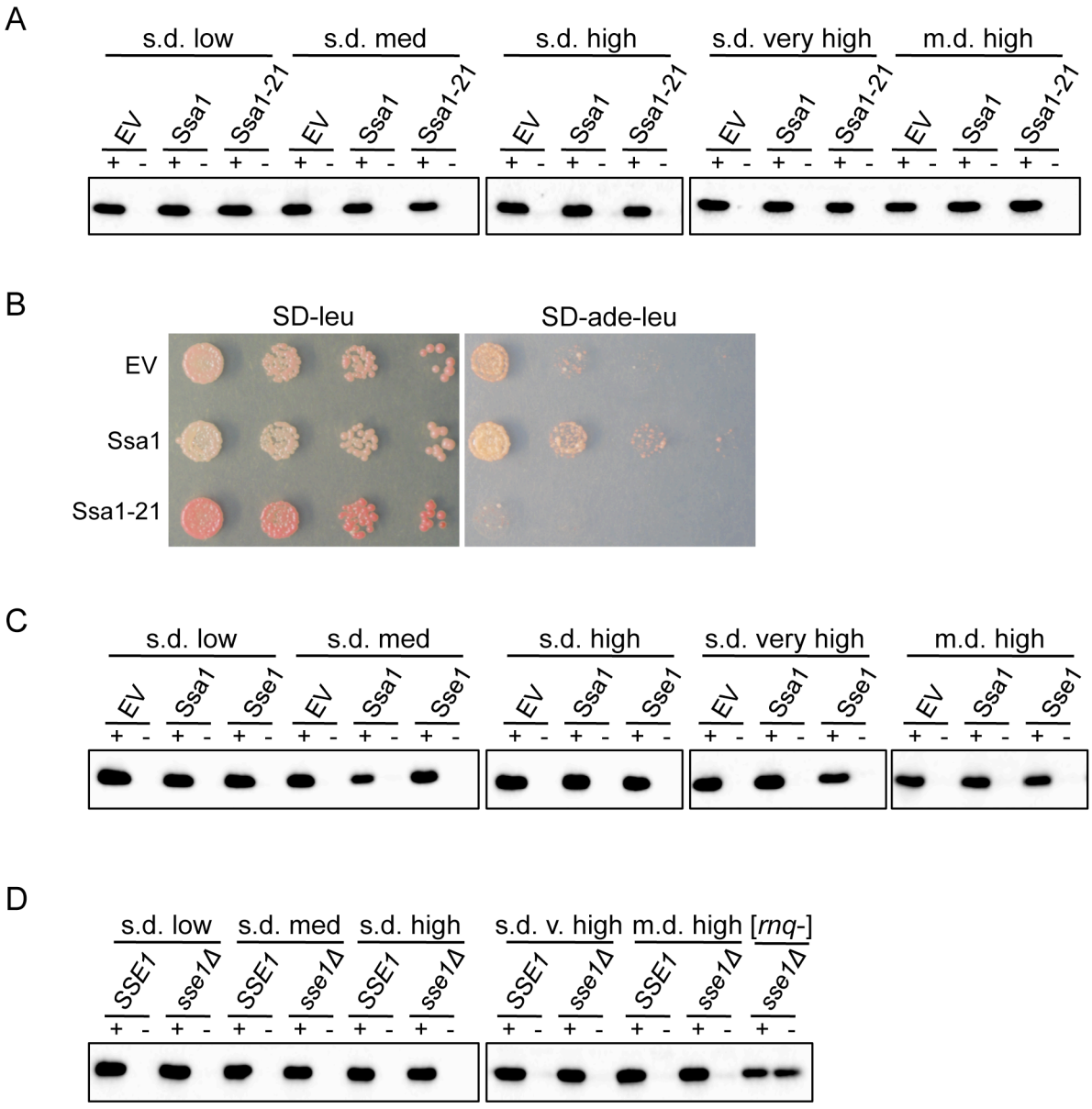

Figure 5. [*PSI*+] variants, but not [*RNQ*+] variants, are sensitive to alterations in the Hsp70 ATPase cycle. (A) The amount of soluble Rnq1 protein in *ssa2Δ* cells propagating the indicated [*RNQ*+] variant and expressing an extra copy of Ssa1 or Ssa1-21, or an empty vector (EV) control, was analyzed by well-trap assay. Cell lysates were incubated at 100°C (+) or room temperature (-) and subjected to SDS-PAGE and western blot using an αRnq1 antibody. (B) Normalized numbers of *ssa2Δ* cells propagating strong [*PSI*+] and expressing an extra copy of

Ssa1 or Ssa1-21, or an empty vector (EV) control, were serially diluted five-fold and spotted onto the indicated media to monitor prion propagation by colony color (SD-leu) or cell growth (SD-leu-ade). (C) Wild-type cell lysates propagating the indicated [*RNQ*+] variant and over-expressing Ssa1 or Sse1, as compared to an EV, were analyzed by well-trap assay as in (A). (D) *SSE1* and *sse1Δ* cell lysates propagating the indicated [*RNQ*+] variant, as compared to [*rnq*-] *sse1Δ* cells, were analyzed by well-trap assay as described in (A).

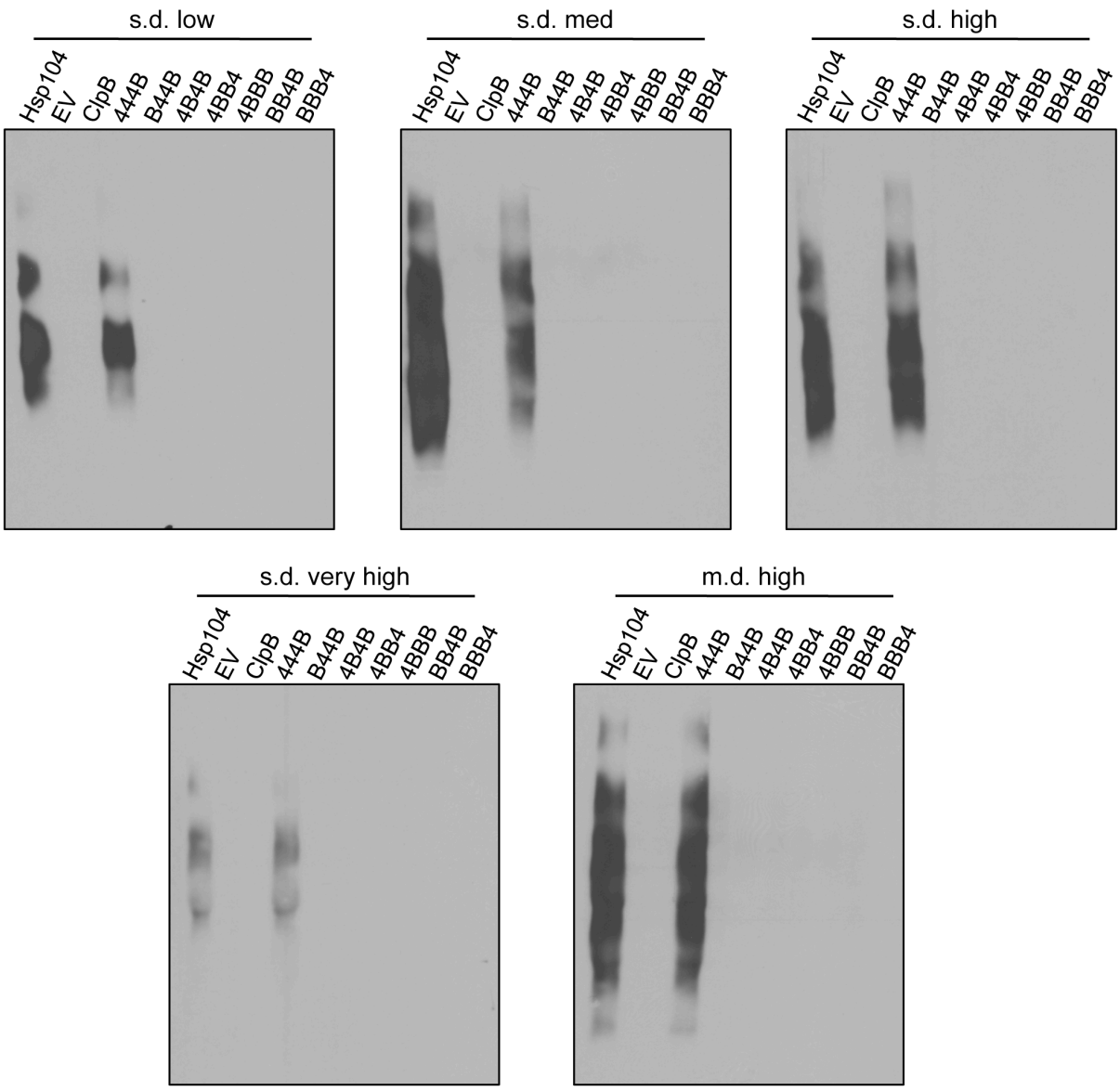

Figure 6. [*RNQ*+] variants similarly rely on Hsp104-ClpB chimeras. Yeast *hsp104Δ* cells, propagating the indicated [*RNQ*+] variant, had WT Hsp104 replaced with ClpB or the indicated Hsp104-ClpB chimeras, with WT Hsp104 and an empty vector (EV) as controls. Cell lysates were subjected to SDD-AGE and western blot using an αRnq1 antibody.

3.8 Supplemental Figures and Tables

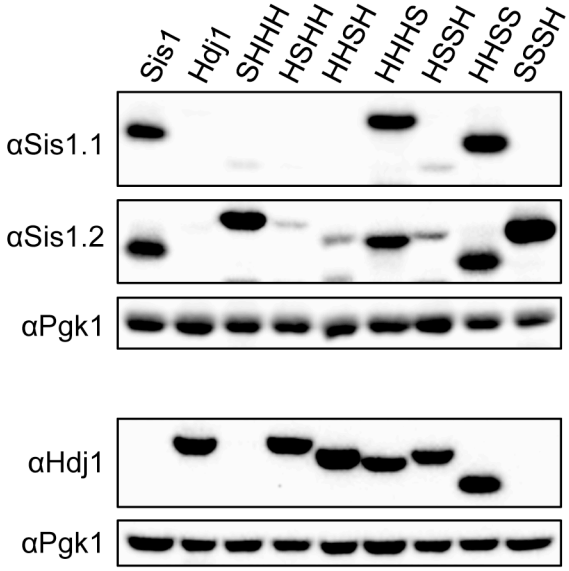

Figure S1. Protein expression levels of Sis1-Hdj1 chimeras. Normalized concentrations of protein from cell lysates harboring the indicated construct was subjected to SDS-PAGE and western blot using two different αSis1 antibodies (αSis1.1 and αSis1.2 as described in the Materials and Methods), an αHdj1 antibody, and an αPgk1 antibody as a loading control.

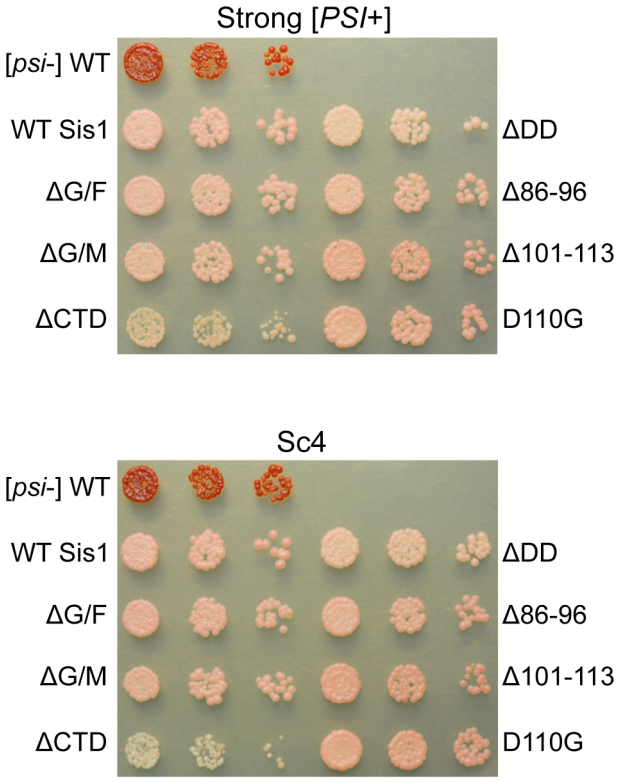

Figure S2. Effect of Sis1 mutations on propagation of strong [*PSI*+] and Sc4. Normalized numbers of yeast *sis1Δ* cells expressing WT Sis1 or the indicated Sis1 mutant, and propagating strong [*PSI*+] or Sc4, with [*psi*-] *SIS1* cells as a control, were serially diluted five-fold and spotted on ¼ YEPD to monitor prion propagation by colony color.

Table S1. Yeast strains used in this study.

Strain	Description	Reference
2879	74-D694 *Mat α sis1Δ::hphMX4* [*psi*-] [*rnq*-]	Stein et al., in review
2384	74-D694 *Mat α sis1Δ::hphMX4* [*psi*-] s.d. low [*RNQ*+]	Stein et al., in review
2386	74-D694 *Mat α sis1Δ::hphMX4* [*psi*-] s.d. medium [*RNQ*+]	Stein et al., in review
2468	74-D694 *Mat α sis1Δ::hphMX4* [*psi*-] s.d. high [*RNQ*+]	Stein et al., in review
2470	74-D694 *Mat α sis1Δ::hphMX4* [*psi*-] s.d. very high [*RNQ*+]	Stein et al., in review
2242	74-D694 *Mat α sis1Δ::hphMX4* [*psi*-] m.d. high [*RNQ*+]	Stein et al., in review
2244	74-D694 *Mat α sis1Δ::hphMX4* weak [*PSI*+]	Stein et al., in review
2240	74-D694 *Mat α sis1Δ::hphMX4* strong [*PSI*+]	Stein et al., in review
2248	74-D694 *Mat a* sis1Δ::hphMX4 [*PSI*+] Sc4	Stein et al., in review
2246	74-D694 *Mat a sis1Δ::hphMX4* [*PSI*+] Sc37	Stein et al., in review
2549	74-D694 *Mat α ssa2Δ::kanMX4* [*psi*-] s.d. low [*RNQ*+]	This study
2638	74-D694 *Mat α ssa2Δ::kanMX4* [*psi*-] s.d. medium [*RNQ*+]	This study
2692	74-D694 *Mat α ssa2Δ::kanMX4* [*psi*-] s.d. high [*RNQ*+]	This study
2689	74-D694 *Mat α ssa2Δ::kanMX4* [*psi*-] s.d. very high [*RNQ*+]	This study
2639	74-D694 *Mat α ssa2Δ::kanMX4* [*psi*-] m.d. high [*RNQ*+]	This study
2818	74-D694 *Mat α ssa2Δ::kanMX4 weak* [*PSI*+]	This study
2756	74-D694 *Mat α ssa2Δ::kanMX4* strong [*PSI*+]	This study
0116	74-D694 *Mat α sse1Δ::LEU2* [*psi*-] [*rnq*-]	This study
0076	74-D694 *Mat α sse1Δ::LEU2* [*psi*-] s.d. low [*RNQ*+]	This study
0078	74-D694 *Mat α sse1Δ::LEU2* [*psi*-] s.d. medium [*RNQ*+]	This study
0477	74-D694 *Mat α sse1Δ::LEU2* [*psi*-] s.d. high [*RNQ*+]	This study
0182	74-D694 *Mat α sse1Δ::LEU2* [*psi*-] s.d. very high [*RNQ*+]	This study
0103	74-D694 *Mat α sse1Δ::LEU2* [*psi*-] m.d. high [*RNQ*+]	This study
2641	74-D694 *Mat α hsp104Δ::hphMX4* [*psi*-] s.d. low [*RNQ*+]	[242]
2642	74-D694 *Mat α hsp104Δ::hphMX4* [*psi*-] s.d. medium [*RNQ*+]	[242]
2646	74-D694 *Mat α hsp104Δ::hphMX4* [*psi*-] s.d. high [*RNQ*+]	[242]
2645	74-D694 *Mat α hsp104Δ::hphMX4* [*psi*-] s.d. very high [*RNQ*+]	[242]
2643	74-D694 *Mat α hsp104Δ::hphMX4* [*psi*-] m.d. high [*RNQ*+]	[242]
L1751	74-D694 *Mat a* [*psi*-] [*rnq*-]	[31]

L1943	74-D694 *Mat a* [*psi*-] s.d. low [*RNQ*+]	[31]
L1945	74-D694 *Mat a* [*psi*-] s.d. medium [*RNQ*+]	[31]
L1767 [*psi*-]	74-D694 *Mat a* [*psi*-] s.d. high [*RNQ*+]	[108]
L1953	74-D694 *Mat a* [*psi*-] s.d. very high [*RNQ*+]	[31]
L1749	74-D694 *Mat a* [*psi*-] m.d. high [*RNQ*+]	[31]
S12600	74-D694 *Mat a* weak [*PSI*+]	[24]
S12606	74-D694 *Mat a* strong [*PSI*+]	[24]
2397	74-D694 *Mat a* [*PSI*+] Sc4	[69]
2398	74-D694 *Mat a* [*PSI*+] Sc37	[69]

Table S2. Plasmids used in this study.

Plasmid	Description	Reference
5687	pRS316-*SIS1* (alias pYW17, YCp50-SIS1)	[74]
6404	pRS314-*SIS1*	Stein et al., in review
6331	p424*GPD-HDJ1*	[100]
6687	pRS414*GPD-SHHH*	This study
6453	pRS414*GPD-HSHH*	This study
6504	pRS414*GPD-HHSH*	This study
6455	pRS414*GPD-HHHS*	This study
6683	pRS414*GPD-HSSH*	This study
6454	pRS414*GPD-HHSS*	This study
6685	pRS414*GPD-SSSH*	This study
S16928	pRS314-*sis1-ΔG/F* (alias PYW116)	[74]
S17036	pRS314-*sis1-ΔG/M*	[100]
S16927	pRS314-*sis1-ΔCTD* (alias PYW66)	[74]
6408	pRS314-*sis1-ΔDD*	[97]
6341	pRS314-*sis1-Δ86-96*	[100]
6337	pRS314-*sis1-Δ101-113*	[100]
6334	pRS314-*sis1-D110G*	[100]
6544	pRS314-*sis1-L268P*	[104]
6524	pRS315-*SSA1*	[234]
6525	pRS315-*SSA1-21*	[234]
6526	*sse1Δ::LEU2*	[248]
6391	pRS415*GPD-SSA1*	This study
6529	p413*GPD-FLAG-SSE1*	[248]
6240	pRS315-*HSP104p-ClpB*	[90]
6241	pRS315-*HSP104p-444B*	[90]
6242	pRS315-*HSP104p-BBB4*	[90]
6509	pRS315-*HSP104p-HSP104*	[90]
6511	pRS315-*HSP104p-4BBB*	[90]
6512	pRS315-*HSP104p-B44B*	[90]
6513	pRS315-*HSP104p-BB4B*	[90]
6514	pRS315-*HSP104p-4B4B*	[90]
6516	pRS315-*HSP104p-4BB4*	[90]
6517	pRS316-*HSP104p-HSP104*	[90]

Table S3. Oligonucleotides used in this study.

Oligonucleotide	Description	Sequence
0219	5' SpeI-Ssa1	5'GCACTAGTATGTCAAAAGCTGTCGG
0220	3' HIII-Ssa1	5'GGGAAGCTTTTAATCAACTTCTTCAACG
0229	5'SIS1-Spe1	5'ATACTAGTATGGTCAAGGAGACAAAA
0230	3'SIS1-Cla1	5'TGATCGATATTTGCTTAGGATTACTATTAAA
0978	5'SSA2-KO	5'CCAACAGATCAAGCAGATTTTATACAGAAAT ATTTATACATCGTACGCTGCAGGTCGAC
0979	3'SSA2-KO	5'AGTAAAACTTTTCGGATATTTTACAGGGCGAT CGCTAAGCATCGATGAATTCGAGCTCG
1466	5' HDJ1-J-SpeI	5'GCGACTAGTATGGGTAAAGACTACTAC
1467	3' HDJ1-J-sis1	5'CTAGCAGCCTCGAGACCGTAGCGGTCGAAGA TCTCGC
1468	5' SIS1-G/F-hdj1	5'GCGAGATCTTCGACCGCTACGGTCTCGAGGC TGCTAG
1469	3' SIS1-G/F-hdj1	5'GGTGTCAAAGGGATTTCTGCCGCCAAAGAAT TGTG
1470	5' HDJ1-G/M-sis1	5'CACAATTCTTTGGCGGCAGAAATCCCTTTGAC ACC
1471	3' HDJ1-ClaI	5'GCGATCGATCTATATTGGAAGAACCTG
1499	5' Sis1-G/M-hdj1-G/F	5'GCTGAGTTCTTCGGTGGCAGTTCCCCATTCGG TGGTGC
1500	3' HDJ1-G/F-sis1-G/M	5'CACCACCGAATGGGGAACTGCCACCGAAGA ACTCAGC
1501	5' Sis1-CTD-hdj1-G/M	5'CCGCCCGAAAGAAGCAAGATGAAACAGTTC AAGTTAATTTAC
1502	3' HDJ1-G/M-sis1-CTD	5'GTAAATTAACTTGAACTGTTTCATCTTGCTTC TTTCGGGCG
1565	5'Hdj1-CTD-sis1-G/M	5'CCCACGTATCCAGAGGAACCCCCAGTCACCC ACGACCTTC
1566	3'Sis1-G/M-hdj1-CTD	5'GGTCGTGGGTGACTGGGGGTTCCTCTGGATA CGTGGGAG
1579	3'Hdj1-J-sis1-G/F	5'CTAGCAGCCTCGAGACCGTAGCGGTCGAAGA TCTCGCGC
1580	5'Hdj1-G/F-sis1-J	5'CTCAAAAAAGGGAAATATATGATCAATACGG GGAGGAAGGCCTAAAG
1581	3'Sis1-J-hdj1-g/f	5'CTTTAGGCCTTCCTCCCCGTATTGATCATATA TTTCCCTTTTTTG
1582	5'Sis1-G/M	5'CACAATTCTTTGGCGGCAGTTCCCCATTCGGT GGTG
1583	3'Sis1-G/F	5'CACCACCGAATGGGGAACTGCCGCCAAAGA ATTGTG

Chapter 4: Myopathy-Causing Mutations in an Hsp40 Chaperone Disrupt Processing of Specific Client Conformers

Kevin C. Stein, Rocio Bengoechea, Matthew B. Harms,

Conrad C. Weihl, and Heather L. True

This chapter is a manuscript in revision for publication in the *Journal of Biological Chemistry*.

Data presented in this chapter was contributed by Rocio Bengoechea.

Author Contributions: KCS, CCW, and HLT designed the study, interpreted the results, and wrote the manuscript. KCS performed the yeast experiments. RB performed the cell culture experiments and interpreted the results. MBH contributed novel reagents and helped interpret results.

4.1 Abstract

The molecular chaperone network protects against the toxic misfolding and aggregation of proteins. Disruption of this network leads to a variety of protein conformational disorders. One such recently discovered example is limb-girdle muscular dystrophy type 1D (LGMD1D), which is caused by mutation of the HSP40 chaperone DNAJB6. All LGMD1D-associated mutations localize to the conserved G/F domain of DNAJB6, but the function of this domain is largely unknown. Here, we exploit the yeast Hsp40 Sis1, which has known aggregation-prone client proteins, to gain insight into the role of the G/F domain and its significance in LGMD1D pathogenesis. Strikingly, we demonstrate that LGMD1D mutations in a Sis1-DNAJB6 chimera differentially impair the processing of specific conformers of two yeast prions – [*RNQ*+] and [*PSI*+]. Importantly, these differences do not simply correlate to the sensitivity of these prion strains to changes in chaperone levels. Additionally, we analyzed the effect of LGMD1D-associated DNAJB6 mutations on TDP-43, a protein known to form inclusions in LGMD1D. We show that the DNAJB6 G/F domain mutants disrupt the processing of nuclear TDP-43 stress granules in mammalian cells. These data suggest that the G/F domain mediates chaperone-substrate interactions in a manner that extends beyond recognition of a particular client and to a subset of client conformers. We propose that such selective chaperone disruption may lead to the accumulation of toxic aggregate conformers and result in the development of LGMD1D and perhaps other protein conformational disorders.

4.2 Introduction

Maintenance of cellular homeostasis requires that proteins adopt a proper tertiary structure. Both genetic and sporadic modifications can impair this process, leading to protein

misfolding and the formation of protein aggregates that are present in many neuro- and myodegenerative diseases. Molecular chaperones, such as heat shock proteins (HSPs), help combat such aggregation, serving to refold substrates or target them for degradation. Consequently, dysfunction of this protective network of chaperones contributes to a variety of disorders.

Dominantly inherited mutations in the HSP40 chaperone DNAJB6 cause a progressive, late-onset degenerative myopathy called limb-girdle muscular dystrophy type 1D (LGMD1D) [159-162]. DNAJB6 is expressed as two isoforms, DNAJB6a and DNAJB6b, with DNAJB6b suggested to be the principal mediator of LGMD1D pathogenesis [160]. DNAJB6b has three distinct domains that are conserved in many HSP40 proteins present from yeast to humans. The N-terminal J domain and C-terminal substrate-binding domain facilitate the interaction and processing of client proteins in cooperation with HSP70 [148]. In between these domains is a poorly understood region called the G/F domain that is rich in glycine and phenylalanine residues. All known LGMD1D-associated mutations localize to an eight amino acid stretch within the G/F domain. Disruption of the conserved G/F domain of DNAJB6 and similar DNAJ proteins can alter interactions with substrates, thereby highlighting the importance of the G/F domain [74,160,244]. However, it is unclear how this domain modulates HSP40 function and how mutation of this region can cause disease.

Recently, the RNA-binding protein TDP-43 has emerged as a sensitive and specific marker of myodegeneration, and has been shown to form inclusions in LGMD1D [159,249]. Interestingly, TDP-43 has a domain that is rich in glutamine and asparagine (Q/N) residues that is reminiscent of the prion-forming domains (PFDs) of several yeast prion proteins [14,250]. This domain facilitates aggregation of TDP-43 into stress granules during heat shock and can be

functionally replaced with the Q/N-rich PFD of the Rnq1 protein that forms the prion [*RNQ*+] in the budding yeast *Saccharomyces cerevisiae* [64,250].

Yeast prions are self-propagating aggregate structures that template the conversion and recruitment of monomers, acting as epigenetic elements of inheritance to modulate cellular phenotypes [14]. This same conformational change underlies the mechanistic basis of prion diseases in mammals, and likely several other degenerative disorders [2]. One striking feature of prion proteins lies in their innate ability to form a variety of amyloid structures, called prion strains, each having a different aggregate conformation that differentially influences cellular and pathological phenotypes [20]. This property is not specific to prion proteins, however. In fact, many amyloidogenic proteins exist in a multitude of distinct self-propagating amyloid conformations [43,44], which likely contributes to the pathological variability observed in many amyloid disorders [251].

Genetic and environmental modifiers likely play a role in the generation and selection of different amyloid conformers, a characteristic we recently described with the [*RNQ*+] prion [32,34,35,41]. Like the regulation of proteostasis in humans, molecular chaperones are intimately involved in the propagation of yeast prions. The Hsp40 Sis1 binds prion aggregates and, in cooperation with Hsp70 and Hsp104, fragments these aggregates into smaller seeds that can be transmitted to daughter cells [86]. Hence, such processing results in, and is required for, the continued maintenance of the prion state. Interestingly, the DNAJB6 G/F domain shares more homology with the G/F domain of Sis1 than any other yeast Hsp40 [159]. Moreover, the Sis1 G/F domain modulates protein aggregation [74]. Yet, the role that this domain plays in substrate processing remains unclear.

Here, we used the LGMD1D mutations in DNAJB6 with a combination of mammalian and yeast models to investigate how the G/F domain contributes to protein homeostasis. We found that these mutations impaired the chaperone-client interaction in a manner that showed striking dependence on not only the client, but also the specific conformation of the substrate. Additionally, G/F domain mutations in another member of the HSP40 family, DNAJB1, resulted in loss of yeast viability, likely due to a loss-of-function in handling essential substrates. Collectively, our data suggest that the G/F domain of DNAJB6 plays a crucial role in recognizing particular client conformers. Such loss of surveillance activity might lead to the accumulation of a toxic species that contributes to LGMD1D pathogenesis. In addition, the conformer-specific effects may be one factor that underlies the observed variation in disease progression, a hallmark of prion strains and the variability observed in prion diseases.

4.3 Results

4.3.1 Homologous LGMD1D mutations in DNAJB1 impair cell growth and propagation of the [*RNQ*+] *prion*

To examine the role of G/F mutations on LGMD1D pathogenesis, we turned to the yeast system, which has provided significant mechanistic insight into many human diseases [252,253]. The yeast Hsp40 Sis1 shares homology with DNAJB6 through the G/F domain (Fig. 1A). While DNAJB6b could not functionally replace the essential role of Sis1 in yeast cells (data not shown), the closest human homolog to Sis1, the HSP40 DNAJB1, can complement for loss of Sis1 [100]. In addition to yeast viability, DNAJB1 can complement for the required role that Sis1 plays in the maintenance of the yeast prion [*RNQ*+] [74,100]. This function in protein aggregate processing requires Sis1's G/F domain and, in particular, a subdomain of the G/F domain not

present in the yeast Hsp40 Ydj1 that is comprised of the amino acid stretch containing all three LGMD1D mutant residues in DNAJB6 [100]

Therefore, we created each of the LGMD1D mutations in DNAJB1 to test their effect on [*RNQ*+] propagation using *sis1Δ* yeast cells. Strikingly, we found that cells expressing DNAJB1-F90I (homologous to DNAJB6-F89I) were unable to grow without Sis1 expression, similar to the vector control (Fig. 1B). Moreover, cells expressing DNAJB1-P98R (homologous to DNAJB6-P96R) had a slow growth phenotype even when *SIS1* was co-expressed. By contrast, cells expressing DNAJB1-F94L (homologous to DNAJB6-F93L) showed no defect in viability. Thus, we assessed the propagation of the [*RNQ*+] prion in cells expressing DNAJB1-F94L in the absence of WT Sis1 using sedimentation analysis. The [*RNQ*+] state can be monitored by assessing the amount of soluble versus insoluble Rnq1 after fractionating cell lysates with high-speed ultracentrifugation. As most all of the Rnq1 protein is sequestered into aggregates in [*RNQ*+] cells, Rnq1 accumulates in the pellet fraction [64]. In cells expressing WT DNAJB1, we found that the [*RNQ*+] prion was maintained as most of Rnq1 was in its aggregated, insoluble form (Fig. 1C), in agreement with previous work [100]. In stark contrast, much of Rnq1 was soluble in cells expressing DNAJB1-F94L, indicating that DNAJB1-F94L can functionally replace the essential roles of Sis1, but is defective in propagation of [*RNQ*+].

4.3.2 DNAJB6 mutations differentially impair prion propagation of [*RNQ*+] *strains*

Because two of the LGMD1D mutations in DNAJB1 impaired cell growth, we created a chimeric protein to test the effect of all of the disease-linked mutations on [*RNQ*+] propagation. This chimera has the G/F domain of DNAJB6 in place of Sis1's, leaving intact the other

functional domains of Sis1 (Fig. 2A). Hereafter, this chimera is referred to as SDSS, denoting the origins of each domain with "S" for Sis1, or "D" for DNAJB6.

Using *sis1Δ* yeast cells, we replaced Sis1 with WT SDSS or LGMD1D mutant SDSS constructs. As controls, we used cells expressing WT Sis1 or Sis1-ΔG/F, which has the G/F domain deleted and is unable to propagate [*RNQ*+] [74]. We then monitored [*RNQ*+] propagation using sedimentation assays. In contrast to cells expressing WT Sis1, where most of Rnq1 was insoluble, expression of Sis1-ΔG/F resulted in a shift of Rnq1 to the soluble fraction, as expected from earlier studies [74] (Fig. 2B). This suggests that the presence of the G/F domain is required for Sis1 to recognize and maintain the self-propagating Rnq1 aggregate structure. Importantly, expression of WT SDSS phenocopied WT Sis1, indicating that this chimera can functionally replace WT Sis1 in maintaining the [*RNQ*+] prion. To our surprise, no soluble Rnq1 was detected in lysates of cells expressing the LGMD1D mutant SDSS constructs. This suggests that the mutant chimera has no defect in the recognition and processing of the Rnq1 aggregates.

However, amyloidogenic proteins, including Rnq1, exist in a variety of different self-propagating structures [9,11,32,35]. Prion strains of [*RNQ*+] have been classified largely on two properties: their ability to induce the formation of the [*PSI*+] prion (low to very high rates), and the *in vivo* aggregation pattern observed by expressing Rnq1-GFP [31,120]. Cells propagating a single-dot (s.d.) [*RNQ*+] strain have predominantly one focus present, while multiple-dot (m.d.) [*RNQ*+] cells exhibit multiple foci. Thus, we hypothesized that the DNAJB6 G/F domain and the LGMD1D mutations might be differentially important in processing distinct aggregate structures. While we initially analyzed the m.d. high [*RNQ*+] strain (Fig. 2B), we extended our analysis to examine the propagation of four different [*RNQ*+] strains (Fig. 2C). First, we found that expression of WT SDSS resulted in most of the Rnq1 protein accumulating in the insoluble

fraction (s.d. low and s.d. very high [*RNQ*+] contain a small pool of soluble Rnq1 that is larger than that of other [*RNQ*+] strains [31]). Deletion of the G/F domain resulted in accumulation of Rnq1 in the soluble fraction for all [*RNQ*+] strains, indicating that the G/F domain is universally important for the maintenance of different Rnq1 aggregate structures. Remarkably, however, we found that the LGMD1D mutations differentially impaired the propagation of the [*RNQ*+] strains, despite being expressed at similar levels (Fig. S1A). Like m.d. high [*RNQ*+], the amount of soluble Rnq1 did not change in s.d. low [*RNQ*+] cells expressing any of the mutants. In contrast, in s.d. medium [*RNQ*+] cells, SDSS-F89I phenocopied the deletion of the entire G/F domain. There was also an accumulation of soluble Rnq1 in s.d. medium [*RNQ*+] cells expressing SDSS-P96R. Moreover, the F89I mutation eliminated the majority of Rnq1 aggregates in s.d. very high [*RNQ*+] cells and increased the amount of soluble Rnq1 in s.d. high [*RNQ*+] cells. However, the P96R mutation did not affect s.d. high or s.d. very high [*RNQ*+]. These data suggest that LGMD1D mutations impair the role of the G/F domain in processing particular aggregate conformations of Rnq1.

We next examined the effect of the LGMD1D mutations on the prion strain-specific distribution of Rnq1 aggregates using fluorescence microscopy with cells harboring WT or mutant SDSS and propagating either s.d. medium or m.d. high [*RNQ*+]. We found that expression of SDSS-F89I in s.d. medium [*RNQ*+] cells caused all of Rnq1-GFP to be diffuse, similar to [*rnq*-] cells harboring WT SDSS (Fig. 3). By contrast, the distribution of puncta was unchanged in mutant cells propagating m.d. high [*RNQ*+] (Fig. S1B), thereby confirming our solubility assay results.

4.3.3 [*RNQ*+] *strains rely on Sis1 expression to different degrees*

As chaperone-mediated substrate processing is an intricate process, changes in chaperone expression have been shown to differentially affect strains of another yeast prion called [*PSI*+] [94,215]. As such, we hypothesized that the differential effects of the LGMD1D mutations may simply be due to [*RNQ*+] prion strains having different sensitivities to changes in Sis1 expression. To test this, we down-regulated *SIS1* and monitored the rate at which the Rnq1 aggregates were lost using semi-denaturing agarose gel electrophoresis (SDD-AGE), a technique that resolves aggregates. Despite being unaffected by the LGMD1D mutations, we found that m.d. high [*RNQ*+] cells had a dramatic loss in Rnq1 aggregates by the fifth generation. By contrast, a comparable loss of Rnq1 aggregates was delayed in s.d. medium [*RNQ*+] cells, which was most affected by LGMD1D mutations, and occurred at the seventh generation (Fig. 4A). Moreover, the sensitivity to Sis1 expression of the other s.d. [*RNQ*+] strains, which were variably affected by the LGMD1D mutations, was similar to s.d. medium [*RNQ*+] (Fig. S1C). Importantly, steady state levels of Sis1 were similarly down-regulated to 2% of WT by the seventh generation (Fig. 4B). This indicates that the effect of the LGMD1D mutations on the propagation of the [*RNQ*+] strains does not correlate to the sensitivity of these prion strains to Sis1 expression.

4.3.4 DNAJB6 mutations differentially impair propagation of [*PSI*+] *strains*

We then asked if the LGMD1D mutations affected another known Sis1 substrate, the [*PSI*+] prion, which is formed by the translation termination factor Sup35 [24,95]. The presence of [*PSI*+], by sequestering Sup35 into aggregates, modulates translation termination. Thus, it is easily monitored using auxotrophic markers that have a premature termination codon (PTC), such as the *ade1-14* allele [14]. [*psi*-] cells have soluble Sup35 that faithfully terminates

translation at the PTC. Thus, these cells cannot complete the adenine biosynthetic pathway and accumulate a metabolic intermediate that gives [*psi*-] colonies a red color. In contrast, [*PSI*+] cells can read through the PTC (called nonsense suppression), thus preventing accumulation of the red pigment. Interestingly, different prion strains of [*PSI*+] are linked to different levels of nonsense suppression: cells propagating stronger [*PSI*+] strains have more nonsense suppression and are light pink as compared to cells propagating weaker [*PSI*+] strains that are darker pink [24].

To test how the G/F domain and the LGMD1D mutations affect [*PSI*+] propagation, we used *sis1Δ* cells propagating four different [*PSI*+] structures: two weaker [*PSI*+] strains (Sc37 and weak [*PSI*+]) and two stronger [*PSI*+] strains (Sc4 and strong [*PSI*+]) [24,25]. We first noted that all [*PSI*+] strains propagated, to some degree, when Sis1-ΔG/F was expressed, as indicated by a pink or white colony color that was distinct from [*psi*-] cells (Fig. 5A). As all [*RNQ*+] strains were eliminated by expression of Sis1-ΔG/F (Fig. 2), this suggests that Sup35 contrasts with Rnq1 as a Sis1 substrate, and thereby provides a good means of expanding our analysis. However, unlike previous reports [95], propagation of both weaker [*PSI*+] strains was impaired, as indicated by cells having a darker pink color on rich media. Propagation of Sc4 and strong [*PSI*+] was not affected by expression of Sis1-ΔG/F. This indicates that the G/F domain of Sis1 plays a more significant role in propagation of weaker [*PSI*+] strains as compared to stronger [*PSI*+] strains, but [*RNQ*+] has the greatest dependence on this domain.

Next, we analyzed the effect of the LGMD1D mutations in SDSS on [*PSI*+] propagation. None of the mutations affected the stronger [*PSI*+] strains (Fig. 5B). However, like the deletion of the G/F domain, the F89I mutation impaired the propagation of Sc37 and weak [*PSI*+]. Furthermore, as prion strains have different biochemical properties, we hypothesized that the

LGMD1D mutations might affect these properties without necessarily affecting the [*PSI*+] phenotype. Previously, it was shown that one of the major distinguishing features of [*PSI*+] strains is that weaker [*PSI*+] strains typically consist of larger Sup35 aggregates as compared to stronger [*PSI*+] strains and have more soluble Sup35 [117,118]. Therefore, in order to gain additional insight into how the LGMD1D mutations affect prion propagation, we analyzed aggregate size and soluble Sup35 using SDD-AGE. In agreement with our phenotypic analysis, we found that for Sc37 and weak [*PSI*+], expression of either SDSS-F89I or Sis1-ΔG/F resulted in a loss of aggregated Sup35 as well as an increased monomer pool (Fig. 5C and Fig. S2). Moreover, while expression of SDSS-P96R did not result in any detectable phenotypic change in cells propagating these weaker [*PSI*+] strains, lysates showed increased soluble Sup35. By contrast, the Sup35 aggregate size and amount of soluble Sup35 of cells propagating Sc4 and strong [*PSI*+] was not affected by expression of the LGMD1D mutations in SDSS. Therefore, like [*RNQ*+], these data show that the G/F domain and the LGMD1D mutants differentially affect propagation of distinct [*PSI*+] prion strains.

4.3.5 LGMD1D mutations in DNAJB6 alter TDP-43 nuclear aggregation and disaggregation

In order to examine the G/F domain mutations in a mammalian model of LGMD1D, we used TDP-43 as a pathological correlate, as it is known to aggregate in LGMD1D [159]. Moreover, TDP-43 contains a prion-like domain that mediates its aggregation [254]. This domain can be functionally replaced by the prion-forming domain of Rnq1 [250,254], thereby further connecting our yeast studies to a mammalian substrate. To test whether mutations in DNAJB6 affected TDP-43 aggregation, we heat shocked HeLa cells expressing TDP-43-mCherry and WT or LGMD1D mutant DNAJB6b-GFP, which leads to the formation of nuclear

stress bodies of TDP-43 [250]. During heat shock and the following recovery, we monitored the presence and co-localization of TDP-43 nuclear stress bodies with DNAJB6b. Interestingly, we found that WT DNAJB6b and all mutant constructs similarly translocated to the nucleus during heat shock and co-localized with TDP-43 nuclear stress bodies (Fig. 6A and Fig. S3A). During recovery, we found that WT DNAJB6b enhanced the dissolution of these stress bodies, as compared to GFP controls (Fig. 6B,C). However, despite no defect in localization to TDP-43 aggregates or differences in expression (Fig. S3B), every DNAJB6b mutant enhanced the formation and persistence of TDP-43 stress bodies (Fig. 6B,C).

In addition, we monitored the amount of insoluble TDP-43 using differential detergent extraction and centrifugation. With expression of WT DNAJB6b or our GFP control, we found that TDP-43 entered an insoluble fraction upon heat shock and became soluble upon recovery (Fig. 6D). However, consistent with our immunofluorescence data, when LGMD1D mutants or DNAJB6b-ΔG/F was expressed, more TDP-43 was present in the insoluble fraction under normal conditions and upon heat shock, and persisted during the recovery period (Fig. 6D).

We then performed a similar analysis without DNAJB6 over-expression, using fibroblasts derived from three independent LGMD1D patients harboring the DNAJB6-F93L mutation, as compared to three patient control fibroblasts. Importantly, these cells expressed DNAJB6b at similar levels (Fig. S3C). Again, upon heat shock and during recovery, we found that the mutant fibroblasts showed enhanced formation and delayed dissolution of TDP-43 nuclear stress bodies (Fig. 7), a pattern also seen with endogenous TDP-43 (Fig. S3D,E). These data indicate that LGMD1D mutations abrogate the ability of DNAJB6b to resolve nuclear TDP-43 stress granules, resulting in the persistence of TDP-43 aggregates.

4.4 Discussion

Taken together, our study demonstrates that the LGMD1D mutations in the G/F domain of DNAJB6 disrupt client processing in both a substrate- and conformation-specific manner. This defines a novel disease pathomechanism in a protein aggregate disorder, as it is the first time, to our knowledge, that mutations associated with a chaperonopathy have client conformer-specific effects. Specifically, when placed in the context of Sis1, DNAJB6's G/F domain can efficiently recognize and process multiple protein aggregate conformers of the same protein (e.g. Rnq1 and Sup35). However, a single disease point mutation in this previously underappreciated region of DNAJ proteins abrogates processing of distinct protein aggregate conformers.

One potential mammalian aggregation-prone protein with specificity to protein aggregate myopathies is TDP-43. We have previously established that TDP-43 accumulates in LGMD1D patient muscle and that TDP-43 is a potential DNAJB6 client protein [159,250]. Persistence of TDP-43 aggregates in DNAJB6-expressing cells and patient fibroblasts further demonstrates a DNAJB6-TDP-43 client interaction. In the context of a human protein aggregate disorder, our data now emphasize the expanded and crucial role that the G/F domain plays in protein aggregation by acting as the major regulator of substrate and conformer selectivity. This agrees with previous data with the bacterial DnaJ protein [244]. Two possibilities might explain the selectivity: either the G/F domain directly binds substrates, or it modulates the neighboring J domain and the interaction of this domain with Hsp70. Future studies will be necessary in order to distinguish between these two scenarios. In either case, we suggest that LGMD1D mutations in DNAJB6 do not abolish all of its chaperone function, but instead confer impaired chaperone surveillance in human skeletal muscle of distinct protein aggregate conformers, such as TDP-43 or some other important client. Selectively disrupting substrate processing might then lead to the

accumulation of these particular aggregate conformers, followed by toxicity, and ultimately muscle degeneration (Fig. 8).

DNAJB6 has previously been implicated in modulating the turnover of a number of different proteins [250,255-257]. Interestingly, many proteins can populate a variety of different aggregated structures or different folding intermediates [20,258]. Hence, the chaperone network is charged with the task of handling a large spectrum of substrate conformations in order to maintain cellular homeostasis. Moreover, while there are some common pathogenic mechanisms involved in protein misfolding disorders, there is also tremendous tissue specificity. DNAJB6 is one of the more abundant HSP40s in skeletal muscle, yet it is ubiquitously expressed and is more abundant in other tissues [259]. Therefore, it is intriguing to speculate that certain tissue-specific protein conformers, whether aggregated or simply unfolded, are more refractory to dissolution and cannot be resolved by DNAJB6 G/F domain mutants.

By analyzing the LGMD1D mutations in a yeast model, we found striking differences between these mutations on phenotypic consequences. Expression of the homologous mutation of F89I showed the greatest effect in terms of cell viability using DNAJB1 and propagation of [*RNQ*+] and [*PSI*+] using SDSS. Indeed, previous work in zebrafish similarly showed that the F89I mutation caused more severe muscle degeneration than the F93L mutation [160]. This is also consistent with human LGMD1D: while the disease is typically late onset, patients with the F89I mutation have been reported to present with childhood onset weakness [260]. It is important to note, however, that even though there was no effect of SDSS-F93L on propagation of the m.d. high [*RNQ*+] strain, the homologous F94L mutation present in DNAJB1 impaired propagation. Therefore, we propose that different mutations may be associated with variation in disease severity by impairing Hsp40 function to different degrees.

Mutations in other DNAJ proteins have also been shown to cause disease, and the involvement of these proteins has been implicated in many other disorders [157]. As this family of chaperones has over 40 members in humans, there likely is a high level of specificity in cellular functions [148]. A variety of factors can influence this functional specificity. Here, we show that the Hsp40 G/F domain plays a major role in substrate conformer selectivity. Hence, when examining the mechanistic basis of chaperonopathies, our data suggest that substrate conformation is another important variable that may contribute to disease progression.

4.5 Materials and Methods

4.5.1 Yeast strains and media

All yeast strains used in this study are derivatives of 74-D694 (*ade1-14 his3-Δ200 leu2-3,112 trp1-289 ura3-52*). [*RNQ*+] and [*PSI*+] yeast strains were kind gifts from S. Liebman [24,31] and J. Weissman [25]. Standard culturing techniques were used. Rich media consisted of YPD (1% yeast extract, 2% peptone, 2% dextrose) or ¼ YPD (0.25% yeast extract, 2% peptone, 2% dextrose) as indicated. Synthetic defined (SD) media (0.67% yeast nitrogen base without amino acids, 2% dextrose) lacking the specified nutrients was used to select for plasmids. To make the *sis1Δ* yeast strains, [*rnq*-] [*psi*-] cells were transformed with pRS316-*SIS1*. *SIS1* was then deleted by first amplifying the *hphMX4* cassette from pAG32 using oligonucleotides 1415 and 1416 (see oligonucleotides listed in Table S1), having flanking homology to the *SIS1* promoter and terminator. The purified product was then transformed and cells resistant to hygromycin B were selected. Deletion of *SIS1* was confirmed by the inability to grow on solid medium containing 1mg/mL 5-fluoroorotic acid (5-FOA), as expression of *SIS1* is essential. These cells were then mated to [*PRION*+] cells, followed by sporulation of the diploids, and

selection of haploids that were resistant to hygromycin B. Replacement of WT Sis1 with the DNAJB1, SDSS, or Sis1 constructs was then performed by a plasmid shuffle technique using media containing 5-FOA to select against cells containing the *URA3*-marked *SIS1* plasmid.

4.5.2 Plasmid construction

Plasmids pRS314-*sis1-ΔG/F* and pRS316*CUP1-RNQ1(153-405)-GFP* were kind gifts from S. Lindquist [74], and plasmids p*TETr-SIS1*, pRS316-*SIS1*, and pRS424*GPD-DNAJB1* were kind gifts from E. Craig [99,100]. Oligonucleotides used to clone the yeast plasmids are listed in Table S1. The endogenous *SIS1* promoter was amplified with oligonucleotides 1454 and 1455 and digested with SacI/SpeI, and the endogenous *SIS1* terminator was amplified with 1456 and 1457 and digested with ClaI/XhoI. These products were ligated into pRS314 to make an intermediate plasmid used to clone the other constructs. To make pRS314-*SIS1*, *SIS1* was amplified with oligonucleotides 0229 and 0230, followed by SpeI/ClaI digestion and ligation. pRS314-*SDSS* was created by bridge PCR amplifying the N-terminal part with oligonucleotides 0229 and 1618. The C-terminal part of this construct was amplified in two parts, using oligonucleotides 1617 and 0230, followed by using this PCR product as a template with oligonucleotides 1619 and 0230 to create the rest of the DNAJB6 G/F domain. The full-length SDSS construct was then amplified using the N-terminal and C-terminal products with oligonucleotides 0229 and 0230, followed by SpeI/ClaI digestion and ligation. Using pRS314-*SDSS*, the LGMD1D mutations were created by bridge PCR using the following oligonucleotides: 1567 and 1568 (F89I), 1620 and 1621 (F93L), 1569 and 1570 (P96R). The SDSS chimera consists of Sis1 amino acid residues 1-84 and 124-352 flanking the DNAJB6 G/F domain residues 72-108. DNAJB1 mutants were made by bridge PCR using the following

oligonucleotides: 1539 and 1540 (F90I), 1492 and 1493 (F94L), 1541 and 1542 (P98R), followed by digestion with SpeI/ClaI and ligation with pRS424*GPD*. Finally, mammalian constructs of DNAJB6b were cloned using site-directed mutagenesis, digested with HindIII/XhoI, and ligated into vector pcDNA3.1 containing a GFP tag. DNAJB6b-ΔG/F consisted of a deletion of amino acid residues 87-97.

4.5.3 Protein analysis

Sedimentation analysis of Rnq1 was performed as described previously [75], and assessed by SDS-PAGE and western blot using an αRnq1 antibody. SDD-AGE for [*PSI+*] yeast cells was performed as described elsewhere [242], and analyzed by western blot using an αSup35 antibody. For extraction and immunoblotting of mammalian cells, cells were washed twice with cold PBS, lysed in cold RIPA buffer (50mM Tris pH 8.0, 150mM NaCl, 1% Nonidet-p40 (IGEPAL), 0.5% sodium deoxycholate, 0.1% SDS, 1mM phenylmethylsulfonyl fluoride, and protease inhibitor cocktail) for 30 min, and centrifuged at 10,000 rpm at 4^{o}C for 10 min. Equal amounts of total protein (10µg/sample) were resolved by 10% SDS-PAGE and analyzed by western blot according to standard procedures. Antibodies used included: polyclonal rabbit αTDP-43 (Proteintech, 10782-2-AP, 1:1500), monoclonal mouse αDNAJB6 (Novus Biologicals, H00010049-M01, 1:500), monoclonal mouse αHSP70 (Enzo Life Sciences, ADI-SPA-810, 1:1000), polyclonal rabbit αGAPDH (Cell Signaling Technologies, 2118, 1:1000), and Goat αMouse-HRP and Goat αRabbit-HRP (Jackson Immunoresearch Laboratories, 1:5000).

For the TDP-43 sedimentation assay, HeLa cells ($5x10^4$) were seeded into 6-well plates and incubated in DMEM containing 10% FBS and 1% Pen/Strep at 37°C and 5% CO_2. After an overnight incubation, the cells were co-transfected with Cherry-TDP-43-FL and either WT or

mutant versions of DNAJB6b. After a post-transfection period (24h), the cells were lysed in RIPA buffer. The lysates were fractionated first with sonication (10 cycles of 30" on, 30" off) followed by centrifugation at 40,000 rpm for 30 min at 4°C. The insoluble pellets were dissolved in Urea buffer (7M urea, 2M thiourea, 4% CHAPS, and 30mM Tris pH 8.5), subjected to SDS-PAGE and western blotting using a polyclonal αTDP-43 antibody. For unknown reasons, the TDP-43-mCherry construct migrates as a doublet between 50-75 kDa, as previously described [261,262].

4.5.4 Prion analysis by fluorescence microscopy

Imaging of live yeast cells was performed on a Zeiss Axiovert 200 Inverted Microscope equipped with a Zeiss 100x/1.4 NA oil objective. Overnight liquid cultures of cells harboring pRS316*CUP1-RNQ1(153-405)-GFP* were diluted to an OD_{600} of 0.2. After 1 hr of growth, 50μM $CuSO_4$ was added to cultures and cells were imaged after ~2.5 hrs of induction. Representative images of at least three independent experiments are shown.

4.5.5 Time-course of prion loss

Yeast *sis1Δ* cells expressing p*TETr-SIS1* in place of pRS316-*SIS1* were used to repress *SIS1*, as previously described [99]. p*TETr-SIS1* expresses *SIS1* from a tetracycline-repressible promoter, allowing for down-regulation of *SIS1* by growing cells in media containing doxycycline, a tetracycline analog. Cultures were maintained in log phase and grown in the presence of 5μg/mL doxycycline. Samples were subjected to SDD-AGE and western blot using an αRnq1 antibody following established protocols for the [*RNQ*+] prion [32], which does not

reliably show Rnq1 monomer for unknown reasons. SDS-PAGE and western blot was used with an αSis1 antibody (gift of E. Craig) and quantified by ImageJ.

4.5.6 Yeast phenotypic assays

To monitor cell growth or the [*PSI*+] status of yeast cells, overnight cultures were normalized by OD_{600}, serially diluted five-fold, and spotted on the indicated media. The [*PSI*+] status was assessed by colony color on ¼ YPD plates that were incubated for 3 days at 30°C, followed by overnight incubation at 4°C for additional color development. Representative images of at least three independent experiments are shown.

4.5.7 Mammalian cell culture and heat shock

HeLa cells were cultured in high glucose formulation of Dulbecco's modified Eagle's medium (high glucose + glutamine, no sodium pyruvate) supplemented with 10% (vol/vol) fetal bovine serum and penicillin/streptomycin. Primary fibroblast cell lines were derived from patient skin biopsies and grown in FGM™-2 Fibroblast Growth Medium-2 (Lonza CC-4126) that is developed to support the growth of most primary human fibroblasts.

For heat shock experiments, cells were transfected with Cherry-TDP-43 and either wild-type or mutant versions of the GFP-DNAJB6b constructs, and maintained at 37°C. 24 hrs after transfection, cells were subjected to heat shock (42°C, 1 hr), then allowed to recover at 37°C for the indicated times (0–3 hrs). Imaging of cells was performed as described previously [250].

4.6 Acknowledgments

We thank R. Stewart and R. Wilkinson for microscopy assistance. For reagents, we are grateful to S. Liebman, S. Lindquist, E. Craig, and J. Weissman. We thank A. Cashikar, D. Summers, and L. Westergard for helpful comments on the manuscript. This work was supported, in whole or in part, by the National Institutes of Health (AG040899 to KCS, GM072778 to HLT, AG031867 and AG042095 to CCW), the Muscular Dystrophy Association (CCW), and the Hope Center for Neurological Disorders (CCW, HLT).

4.7 Figures

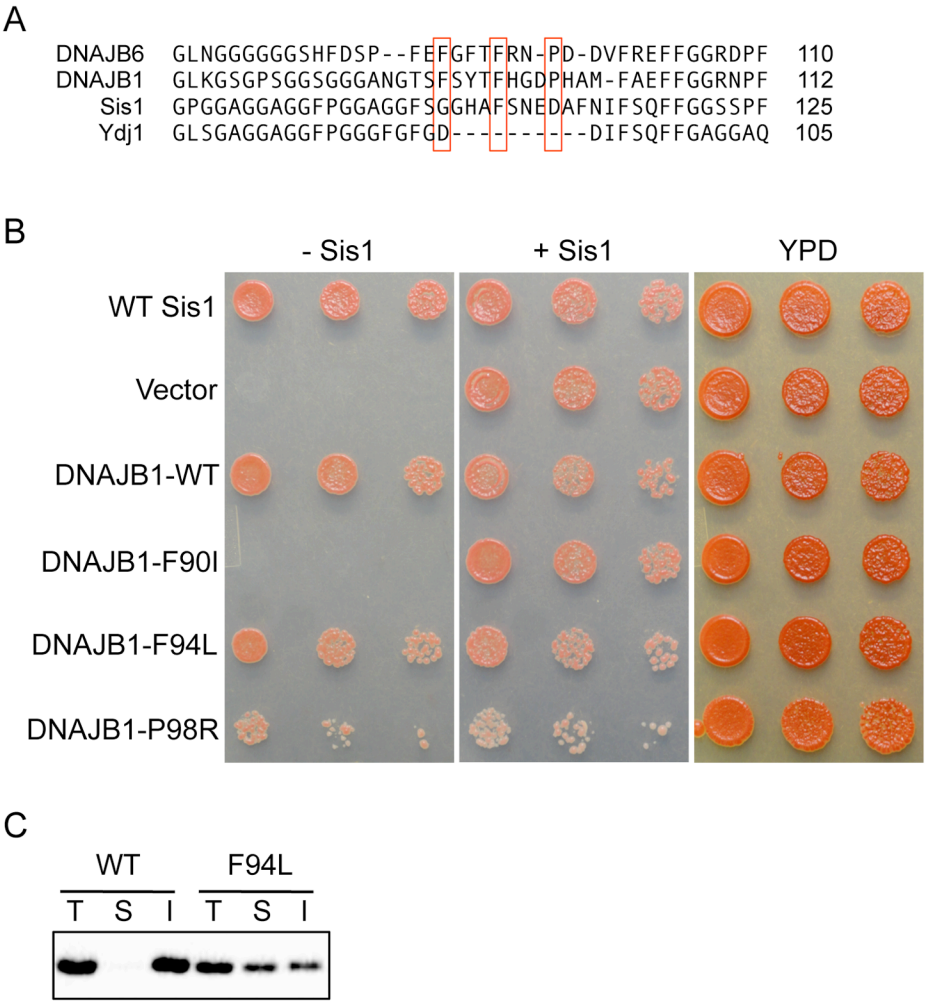

Figure 1. Homologous LGMD1D mutations in DNAJB1 impair cell growth and [*RNQ*+] prion propagation. (A) Sequence comparison of the G/F domains of DNAJB6, DNAJB1, Sis1, and another yeast Hsp40 Ydj1, aligned with ClustalW2. Boxes surround the disease-linked mutations. (B) Yeast *sis1Δ* cells propagating m.d. high [*RNQ*+] and expressing the indicated construct were serially diluted five-fold and spotted onto rich media (YPD), or on media to select for loss (- Sis1) or co-expression (+ Sis1) of WT Sis1. (C) m.d. high [*RNQ*+] cell lysates expressing WT DNAJB1 or DNAJB1-F94L in place of Sis1 were separated by ultracentrifugation into total (T), soluble (S), and insoluble (I) fractions that were then subjected to SDS-PAGE and western blot using an αRnq1 antibody. Data are representative of $n \geq 3$.

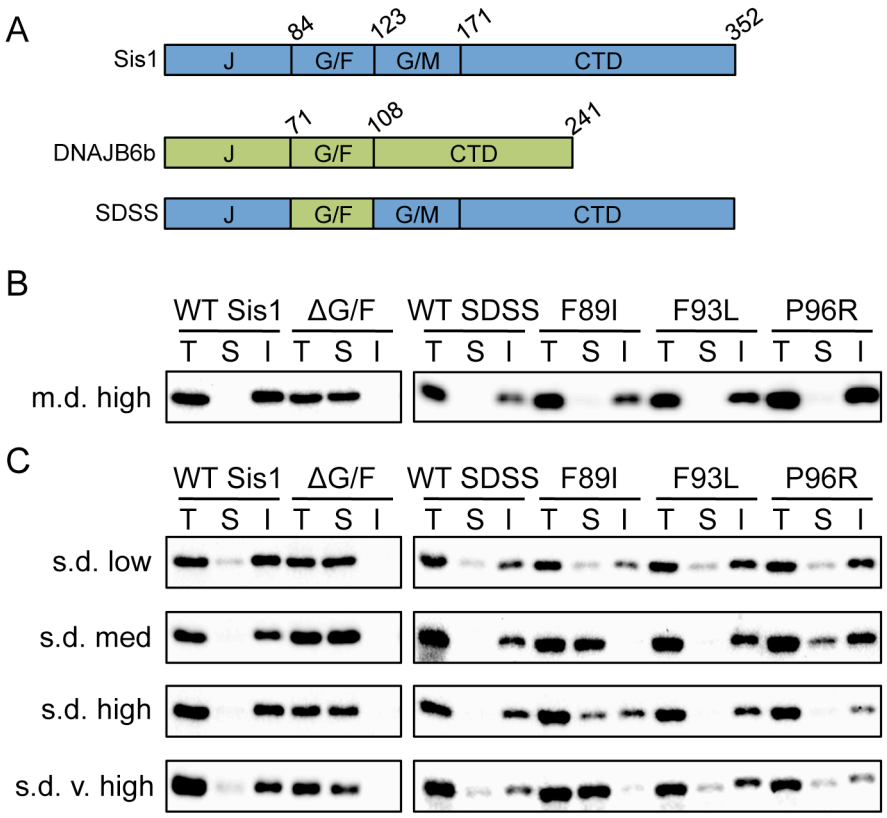

Figure 2. Maintenance of different [*RNQ*+] strains is differentially impaired by LGMD1D mutations in SDSS. (A) Domain structures of Sis1, DNAJB6b, and chimera SDSS. (B) m.d. high [*RNQ*+] cell lysates expressing WT Sis1, Sis1-ΔG/F, or the indicated SDSS construct were fractionated as in Fig. 1C, followed by SDS-PAGE and western blot using an αRnq1 antibody. Data are representative of n ≥ 3. (C) As in (B) with cells propagating the indicated [*RNQ*+] strain.

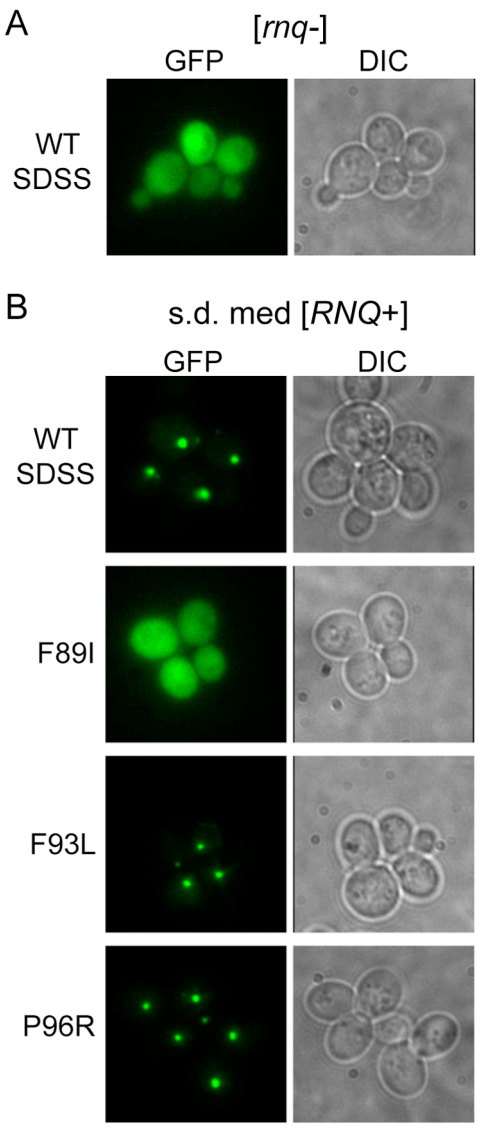

Figure 3. LGMD1D mutations modulate the aggregation pattern of Rnq1 *in vivo*. The Rnq1 aggregation pattern in (A) [*rnq*-] cells or (B) s.d. medium [*RNQ*+] cells harboring the indicated SDSS construct and copper-inducible Rnq1-GFP.

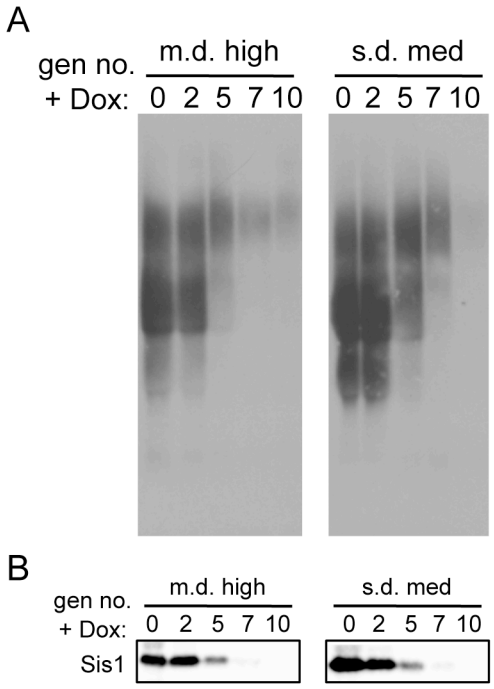

Figure 4. Effect of LGMD1D mutations does not correlate to the sensitivity of [*RNQ*+] strains to Sis1 expression. (A) Cells propagating m.d. high or s.d. medium [*RNQ*+] had endogenous *SIS1* replaced by p*TETr-SIS1*. Cells grown in the presence of doxycycline (Dox) had samples taken at the indicated number of generations (gen no.), followed by SDD-AGE and western blot using an αRnq1 antibody. Data are representative of n = 3. (B) Western blot analysis of (A) with an αSis1 antibody.

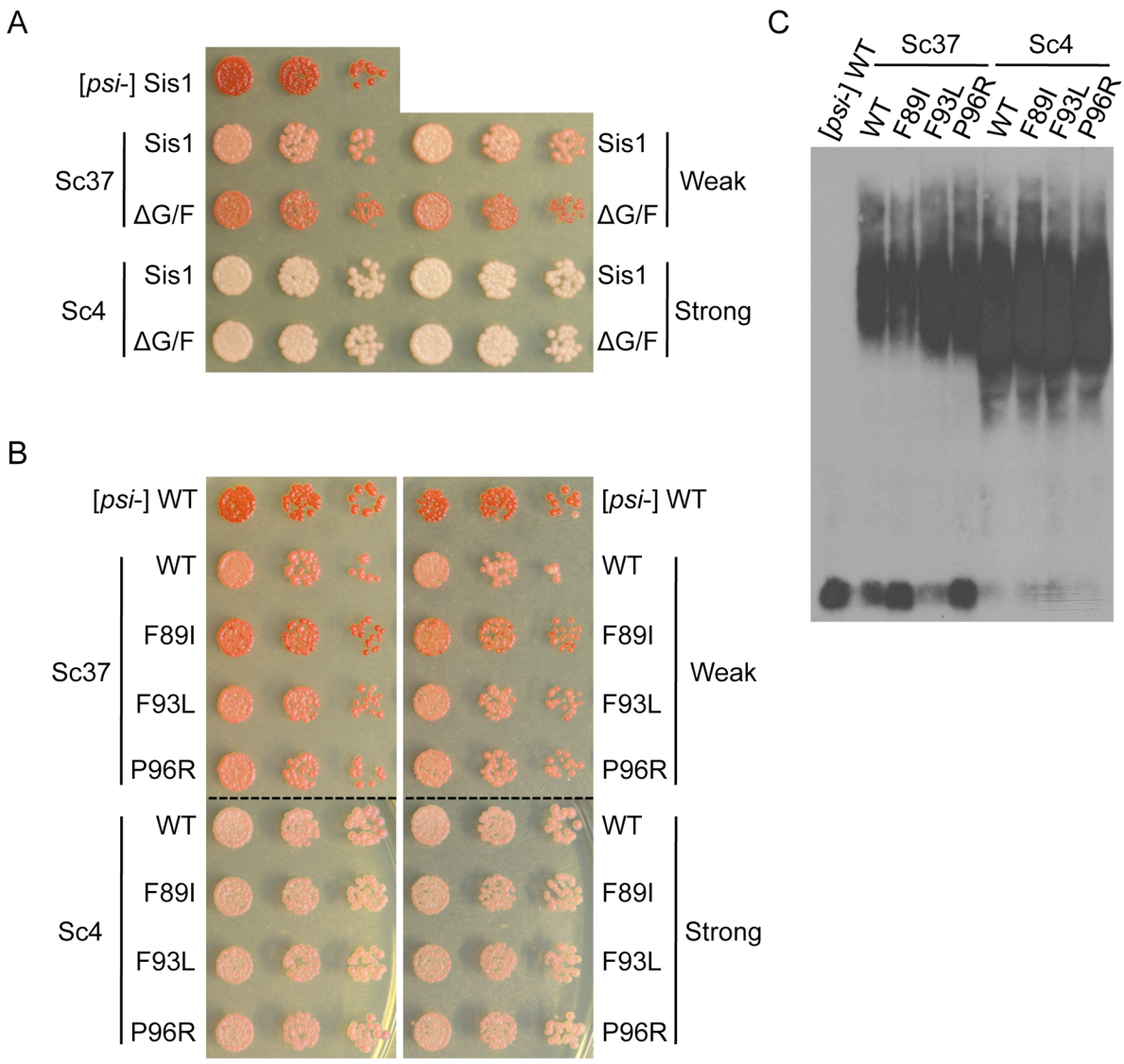

Figure 5. LGMD1D mutations in SDSS differentially impair propagation of [*PSI*+] strains. (A) Equivalent numbers of *sis1Δ* cells expressing WT Sis1 or Sis1-ΔG/F with the indicated [*PSI*+] status were serially diluted five-fold and spotted onto rich media to monitor the [*PSI*+] phenotype by color. (B) As in (A) with the indicated SDSS construct. Dotted lines represent different parts of the same plate cropped for clarity. (C) SDD-AGE analysis of cell lysates expressing the indicated SDSS construct. Data are representative of n = 4.

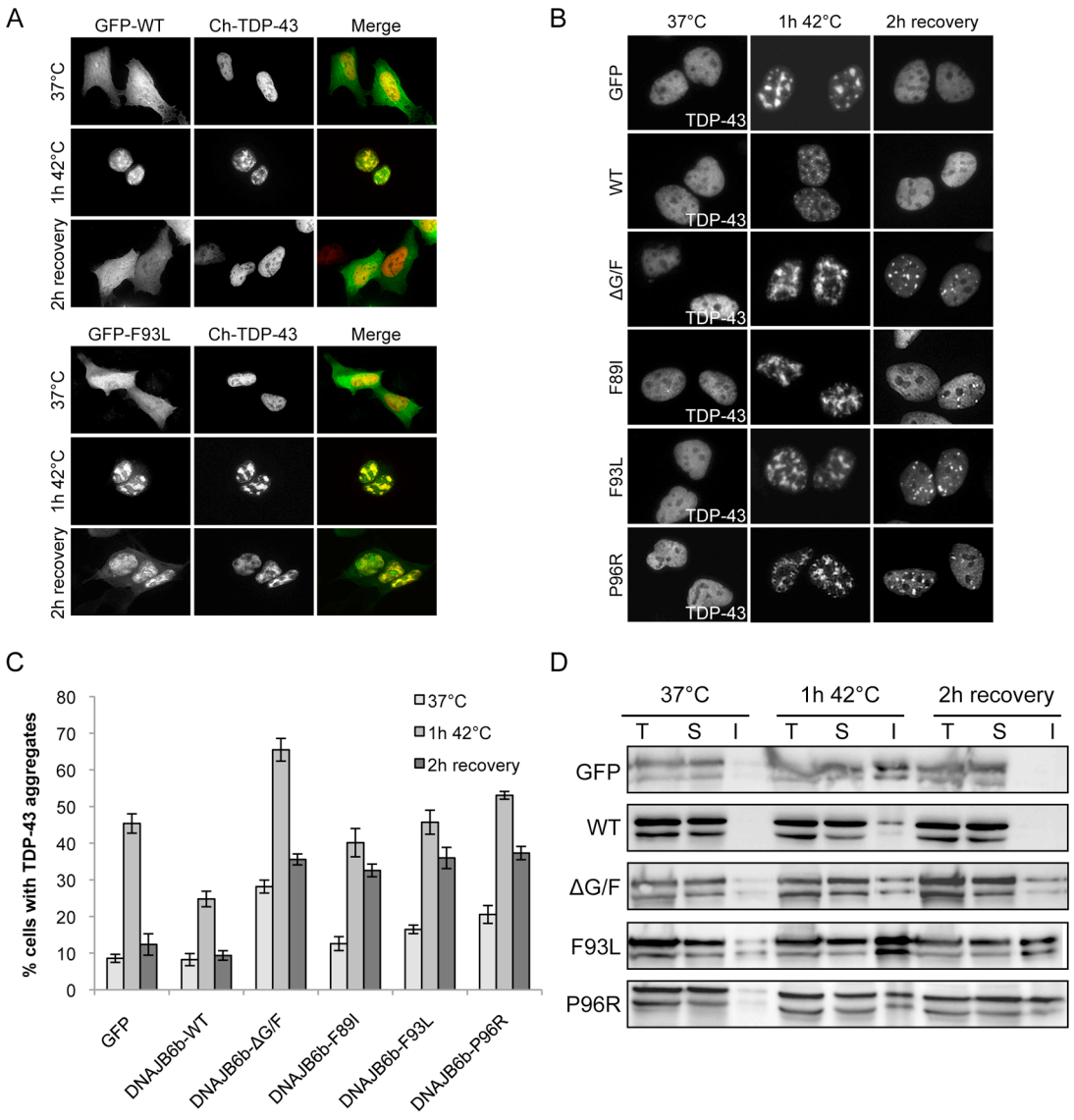

Figure 6. LGMD1D mutations in DNAJB6 alter TDP-43 nuclear aggregation and disaggregation. (A) Nuclear co-localization of DNAJB6b and TDP-43 upon heat shock. HeLa cells were co-transfected with TDP-43-mCherry and DNAJB6b-GFP (WT or F93L), subjected to heat shock at 42°C for 1 hr, followed by recovery for 2 hrs at 37°C. (B and C) As in (A), TDP-43 nuclear stress body formation (B) and quantitation (C) in HeLa cells transfected with the indicated DNAJB6b construct. Data are represented as mean ± SEM with n = 4. (D) HeLa cells expressing the indicated construct were treated as in (A), lysed, and separated into total (T),

soluble (S), and insoluble (I) fractions that were then subjected to SDS-PAGE and western blot using an αTDP-43 antibody.

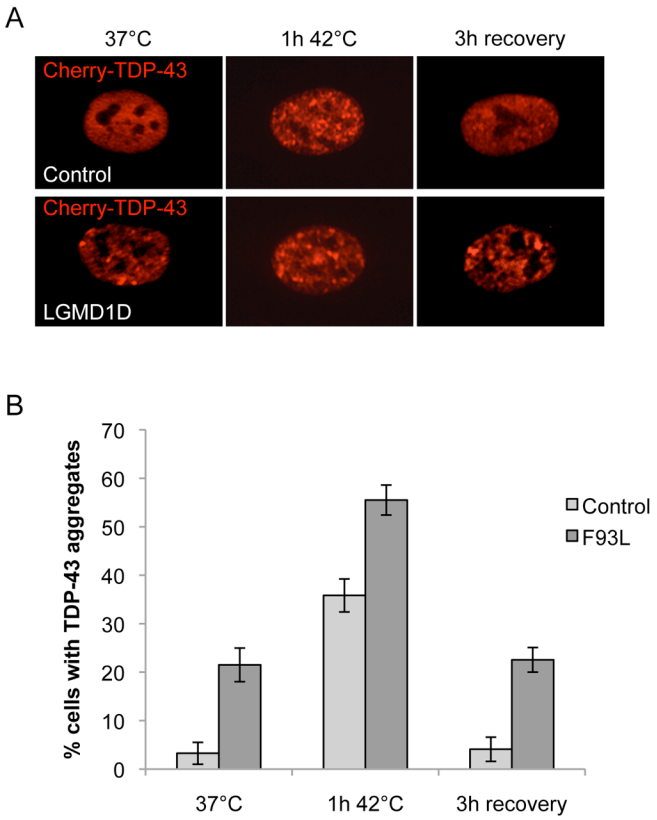

Figure 7. Dissolution of TDP-43 stress granules is disrupted in patient fibroblasts. TDP-43 nuclear stress body formation (A) and quantitation (B) in LGMD1D patient (F93L) or control fibroblasts. Cells were transfected with TDP-43-mCherry and treated as in Fig. 6A with a 3 hr recovery. Data are represented as mean ± SEM with $n \geq 4$.

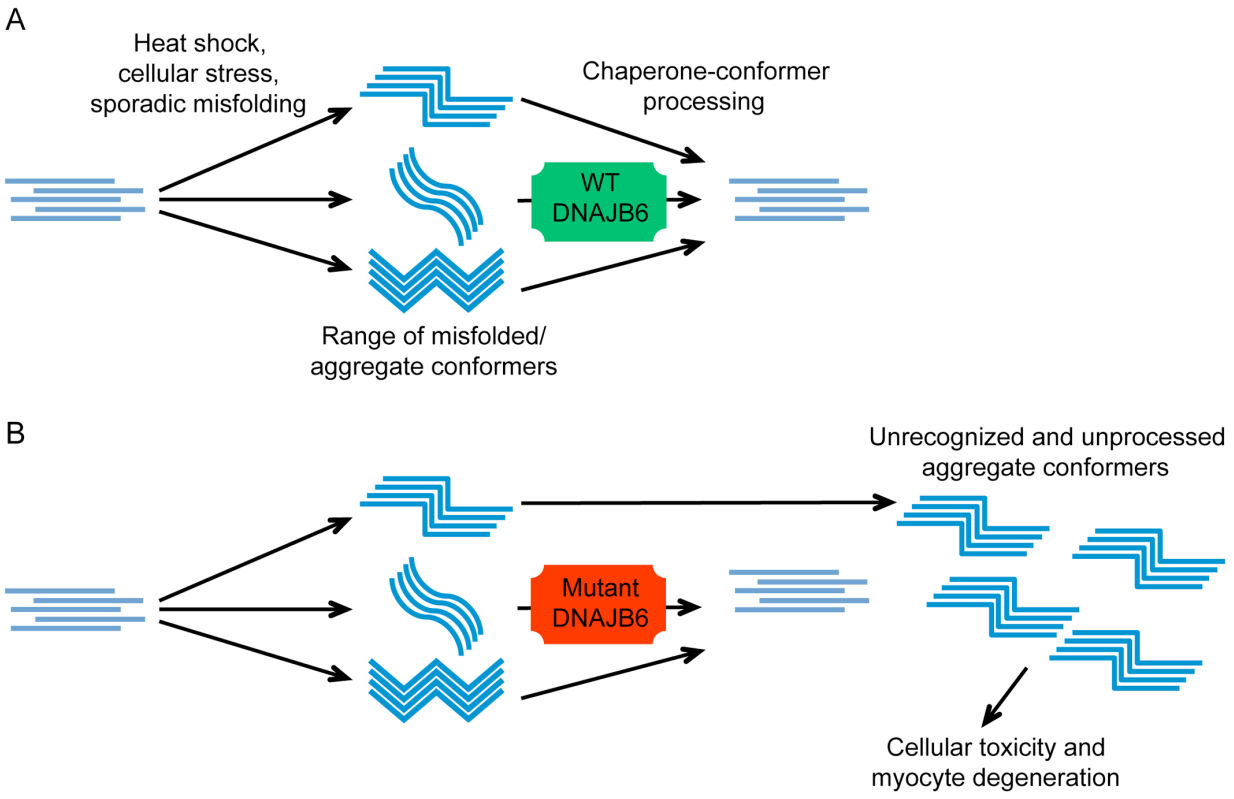

Figure 8. Schematic model of how mutations in DNAJB6 may contribute to LGMD1D pathogenesis. In skeletal muscle, various insults may lead to the misfolding of a substrate into a range of distinct aggregate conformers. (A) Wild-type (WT) DNAJB6 is capable of properly processing these misfolded conformers, which might include refolding the substrate into its native conformation. (B) In the case of LGMD1D, mutations in DNAJB6 impair the processing of particular conformers. This leads to the accumulation of this specific aggregate conformer, and ultimately to cellular toxicity and myocyte degeneration.

4.8 Supplemental Figures and Tables

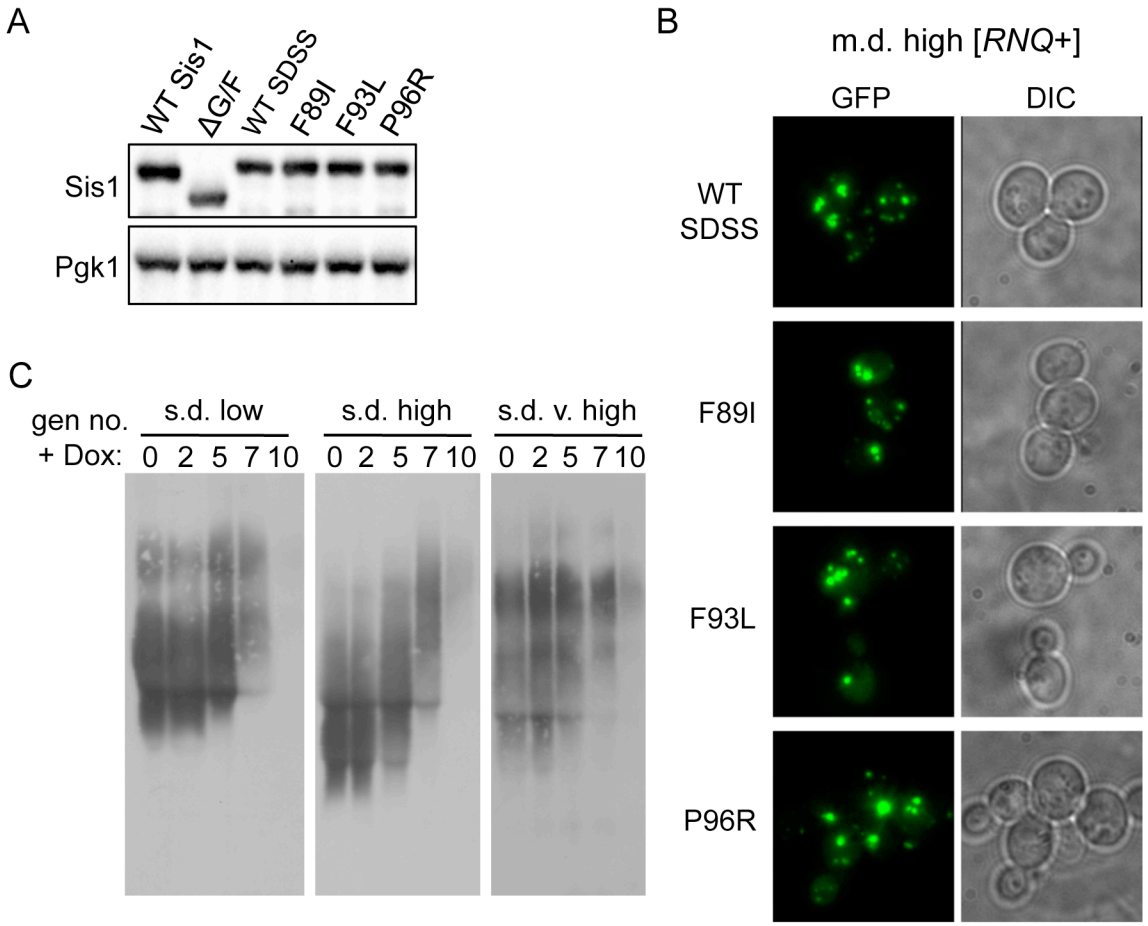

Figure S1. Maintenance of different [*RNQ*+] strains is differentially impaired by LGMD1D mutations in SDSS. (A) Western blot analysis of Sis1 and SDSS mutants in yeast cells. Cell lysates harboring the indicated construct were subjected to SDS-PAGE and western blot with an αSis1 antibody along with an αPgk1 antibody as a loading control. (B) Representative images of the Rnq1 aggregation pattern in m.d. high [*RNQ*+] cells harboring the indicated SDSS construct and expressing copper-inducible Rnq1-GFP. (C) Cells propagating the indicated [*RNQ*+] strain had endogenous *SIS1* replaced by p*TETr-SIS1*. Cells were grown in the presence of doxycycline (Dox) with samples taken at the indicated number of generations (gen no.). Lysates were subjected to SDD-AGE and western blot using an αRnq1 antibody. Data are representative of n = 3.

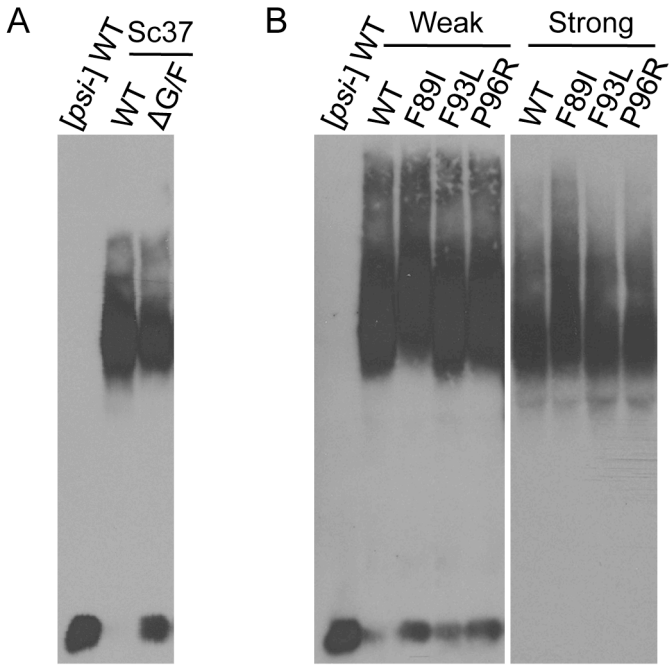

Figure S2. LGMD1D mutations in SDSS differentially impair propagation of [*PSI*+] strains. (A) Sc37 [*PSI*+] or [*psi*-] cell lysates expressing wild-type Sis1 or Sis1-ΔG/F were subjected to SDD-AGE and western blot using an αSup35 antibody. (B) Weak and strong [*PSI*+] cells or [*psi*-] cells harboring the indicated SDSS construct were subjected to SDD-AGE and western blot using an αSup35 antibody. Data are representative of $n \geq 3$.

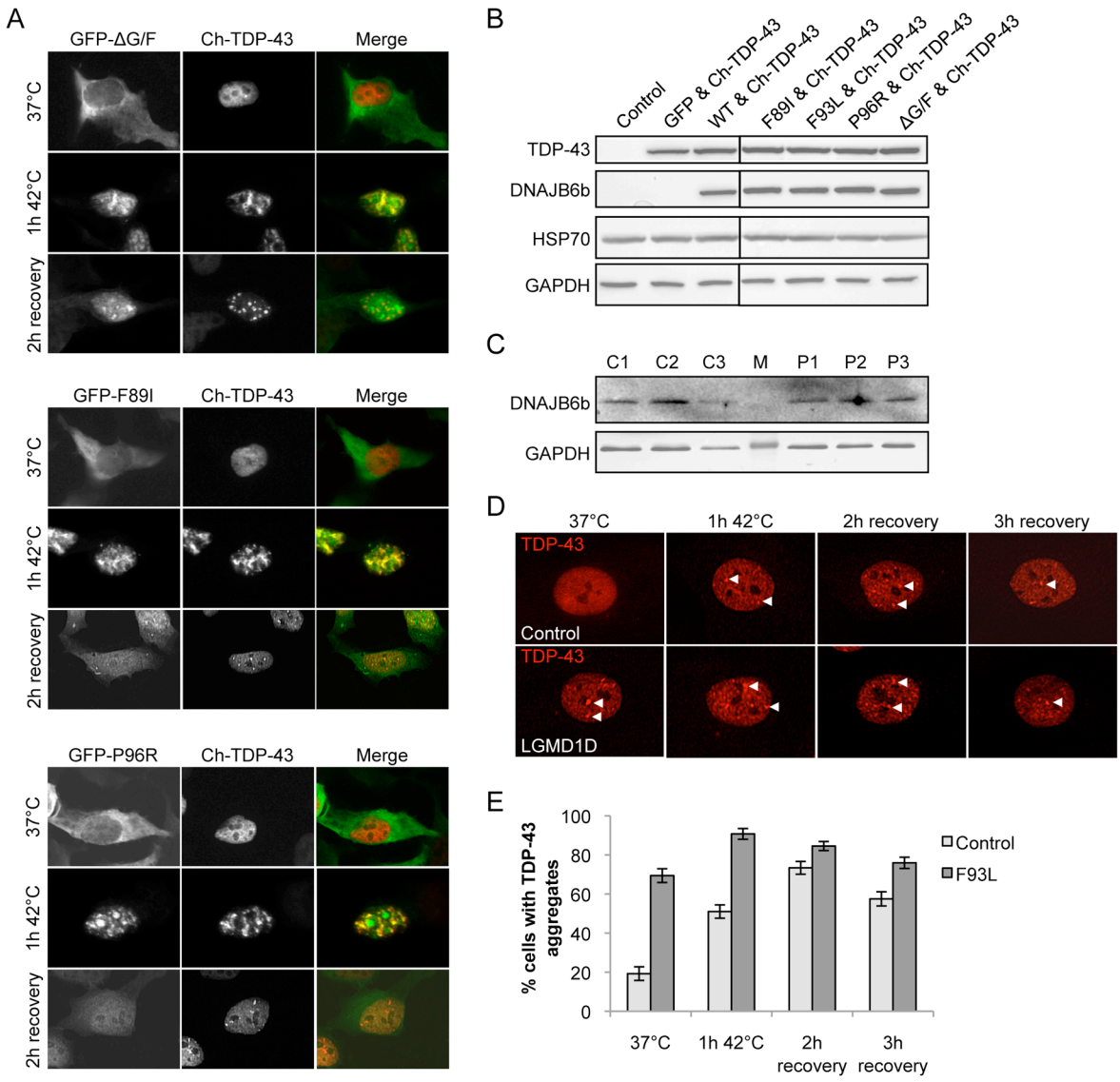

Figure S3. LGMD1D mutations in DNAJB6 alter TDP-43 nuclear aggregation and disaggregation. (A) Nuclear co-localization of DNAJB6b and TDP-43 upon heat shock. HeLa cells were co-transfected with TDP-43-mCherry and the indicated GFP-DNAJB6b mutant for 24 hours and then subjected to heat shock at 42°C for 1 hr, or 42°C for 1 hr followed by recovery for 2 hrs at 37°C. (B) Western blot analysis of HeLa cell extracts transfected with the indicated constructs as compared to untransfected cells (control), using antibodies against TDP-43, DNAJB6b, and HSP70, along with GAPDH as a loading control. All samples were run on the

same gel, but have been cropped for clarity. (C) Western blot analysis of patient fibroblasts from three independent control patients (C1, C2, C3) and three different patients from the same family having the DNAJB6-F93L mutation (P1, P2, P3), using antibodies against DNAJB6b and GAPDH. M: marker. (D and E) Nuclear stress body formation (D) and quantitation (E) of endogenous TDP-43 in LGMD1D patient (F93L) or control fibroblast lines, subjected to heat shock at 42^{o}C for 1 hr, or 42^{o}C for 1 hr followed by recovery for 2 or 3 hrs at 37^{o}C. Data are represented as mean ± SEM with n = 4.

Table S1. Oligonucleotides used in this study.

Oligonucleotide	Description	Sequence
1454	5’ Sis1prom-SacI	5'CGCGAGCTCGCTAGTCGTTACTTTTC
1455	3’ Sis1prom-SpeI	5'CGCACTAGTTATTAGTTCTGTATACTATAC
1456	5’ Sis1term-ClaI	5'CGCATCGATTAGTAATCCTAAGCAAATATAA
1457	3’ Sis1term-XhoI	5'CGCCTCGAGTTGGACTTACAAAAACTTC
0229	5' Sis1-SpeI	5'ATACTAGTATGGTCAAGGAGACAAAAC
0230	3' Sis1-ClaI	5'TGATCGATATTTGCTTAGGATTACTATTAAA
1618	3' SDSS	5’CTGTCAAAATGACTTCCACCTCCTCCTCCACCATTTAATCCAGGACCACCAGGACCAAAGCTTG
1617	5' SDSS	5’CCGTAACCCAGATGATGTCTTCAGGGAATTTTTTGGTGGAAGGGACCCATTCGGTGGTGCTGATGAC
1619	5' SDSS linker	5’GGTGGAAGTCATTTTGACAGTCCATTTGAATTTGGCTTCACATTCCGTAACCCAGATGATGTCTTC
1567	5’ dnajB6-F89I	5’GACAGTCCATTTGAAATTGGCTTCACATTCCGTAAC
1568	3’ dnajB6-F89I	5’GTTACGGAATGTGAAGCCAATTTCAAATGGACTGTC
1620	5’ dnajB6-F93L	5’GAATTTGGCTTCACACTCCGTAACCCAGATGATG
1621	3’ dnajB6-F93L	5’CATCATCTGGGTTACGGAGTGTGAAGCCAAATTC
1569	5’ dnajB6-P96R	5’GGCTTCACATTCCGTAACCGAGATGATGTCTTCAGGG
1570	3’ dnajB6-P96R	5’CCCTGAAGACATCATCTCGGTTACGGAATGTGAAGCC
1415	5’ Sis1 KO	5’CATTCACATCAATATAATAGAGTATAGTATACAGAACTAATACAGCTGAAGCTTCGTACGC
1416	3’ Sis1 KO	5’GTGATAAATTTATTTGAGTTTATAATTATATTTGCTTAGGATTACTAGCATAGGCCACTAGTGGATCTG
1539	5’ dnajb1-F90I	5’GTGCCAATGGTACCTCTATCAGCTACACATTCCATG
1540	3’ dnajb1-F90I	5’CATGGAATGTGTAGCTGATAGAGGTACCATTGGCAC
1492	5’ dnajb1-F94L	5’CTCTTTCAGCTACACACTCCATGGAGACCCTCATG
1493	3’ dnajb1-F94L	5’CATGAGGGTCTCCATGGAGTGTGTAGCTGAAAGAG
1541	5’ dnajb1-P98R	5’CACATTCCATGGAGACCGTCATGCCATGTTTGCTG
1542	3’ dnajb1-P98R	5’CAGCAAACATGGCATGACGGTCTCCATGGAATGTG

Chapter 5: DNAJB6 Mutations that Cause Limb-Girdle Muscular Dystrophy Alter Select Hsp40 Functions

Kevin C. Stein and Heather L. True

This chapter is a manuscript in preparation for publication.

5.1 Abstract

A wide range of cellular activity depends on the function of molecular chaperones. Through modulating the activity of Hsp70s, Hsp40 proteins are proposed to be major regulators of several aspects of protein quality control. Mutations in the Hsp40 DNAJB6 G/F domain disrupt the proteostasis network and cause the limb-girdle muscular dystrophy type 1D (LGMD1D), which exhibits an accumulation of protein aggregates and vacuoles in skeletal muscle. Recently, we have shown that these mutations selectively alter the processing of particular aggregate conformers. Here, we use yeast and the DNAJB6 ortholog Sis1 to explore what other Hsp40 functions are altered by the LGMD1D-associated mutations. We demonstrate that these mutations do not disrupt the role of Hsp40 in luciferase refolding or Sis1-mediated protein degradation. However, we found that over-expression of the LGMD1D-associated mutations exhibits Hsp70-dependent toxicity, likely through dysregulation of processing essential substrate proteins. Moreover, modulating the Hsp70 ATPase cycle partially suppressed the impaired processing of the [*RNQ*+] prion. We propose that the LGMD1D-associated mutations might cause hyperstimulation of Hsp70 activity and aberrant client processing. Hence, this work provides additional mechanistic insight into how the LGMD1D-associated mutations might disrupt DNAJB6 function, which could lead to more targeted therapeutic approaches.

5.2 Introduction

From translation to degradation, molecular chaperones monitor multiple aspects of the life cycle of a protein. The family of Hsp70 proteins consists of key players in maintaining the health of the proteome. As proteins are innately susceptible to misfolding and aggregation, a major function of Hsp70s is to refold these substrates or mediate the degradation of terminally

misfolded proteins. However, while Hsp70s function on the frontline to protect the cell, the family of Hsp40 co-chaperones serves as the functional operators [148]. Indeed, the large number of Hsp40s (41 in humans as compared to 11 Hsp70s [148]), with their distinct tissue expression patterns [259], provides a tremendous amount of specificity in dictating Hsp70 function.

Hsp40s are categorized into three classes [102]. The presence of a highly conserved J domain is the common feature among all three classes. This domain facilitates the interaction with Hsp70s and the stimulation of Hsp70 ATPase activity and substrate processing [263]. The structural features outside of the J domain determine the class of Hsp40. In general, class A (type I) proteins have a domain rich in glycine and phenylalanine (G/F), a zinc finger motif, and a C-terminal substrate-binding domain. The generic structure of class B (type II) Hsp40s is similar without the zinc finger motif. All class A and several class B proteins also have a dimerization domain at the extreme C-terminus that facilitates Hsp40 dimerization and increases the affinity for substrates [264]. Type III (class C) Hsp40s, on the other hand, do not fall into one of these categories and consist of a number of disparate domains that help increase the functional specificity of the Hsp40 family [148].

While some Hsp40s function in particular organelles or have specific client proteins, others act as general housekeeping proteins that can interact with a wide range of substrates [148]. However, it is suggested that the capacity of Hsp40s, and molecular chaperones in general, to monitor protein folding can be overwhelmed. Indeed, a loss of proteostatic control can occur through an increased burden of misfolded proteins that leads to protein aggregation [154]. There is a large number of unrelated proteins that aggregate and are associated with numerous diseases called protein conformational disorders [2]. Interestingly, a subset of protein

conformational disorders, called chaperonopathies, highlight the importance of molecular chaperones in protein quality control, as these diseases are caused by a mutation in a molecular chaperone, including a number of different Hsp40 proteins [157]. One such example is a type of myopathy called limb-girdle muscular dystrophy type 1D (LGMD1D), which is caused by mutations in the Hsp40 DNAJB6 [159-162].

DNAJB6 is involved in regulating the turnover of several different substrates, indicating it likely plays a general role in protein quality control [250,255-257,265-268]. Indeed, one of the striking features of LGMD1D is the aggregation of several different proteins [159,160]. Interestingly, all of the LGMD1D-associated mutations that have been identified to date have been found in a short stretch of the G/F domain of DNAJB6 ([159-162] and personal communication). In addition to DNAJB6, disruption of the G/F domain in similar DNAJ proteins can impair substrate processing [74,244,269]. Recently, we extended the results of these studies, showing that mutations in the G/F domain not only affect the processing of particular substrates, but particular conformations of those substrates (Stein et al., in review). Yet, the underlying mechanism for how the G/F mutations impair Hsp40 function remains unclear.

In this study, we take advantage of the yeast system and the homology between DNAJB6 and the yeast Hsp40 Sis1, to provide mechanistic insight into how the LGMD1D-associated mutations affect DNAJB6 function. Despite showing that the G/F domain is involved in refolding heat-denatured luciferase *in vivo*, we show that the LGMD1D mutations do not affect processing of this substrate. Moreover, we found that there is no impact on Sis1-mediated protein degradation or induction of the heat shock response. However, the LGMD1D-associated mutations show striking toxicity when over-expressed that relies on an interaction with Hsp70, suggesting that the mutants cause aberrant processing of essential substrates. We propose that the

LGMD1D-associated mutations in DNAJB6 might cause hyperstimulation of Hsp70 ATPase activity, which leads to dysregulation of the turnover of certain substrates, or substrate conformers, that play a critical role in maintaining the integrity of skeletal muscle.

5.3 Results

5.3.1 LGMD1D Mutations do not affect Luciferase Refolding

Hsp40s are proposed to dictate the specificity of substrate processing and monitoring protein quality control [148]. In line with this, we have previously shown that LGMD1D-associated mutations impair the propagation of particular conformers of the [*RNQ*+] and [*PSI*+] prions in yeast (Stein et al., in review). We now wanted to test the extent to which these mutations impaired Hsp40 processes. First, we explored the selectivity of the LGMD1D mutations in altering substrate processing. Prion aggregates are considered to be rich in β sheets [20]. Hence, we asked if the mutations would similarly affect the processing of aggregated substrates that are not β sheet-rich. One substrate commonly used is heat-denatured luciferase, the refolding of which is an Hsp40-dependent process [89,104,270].

To test whether LGMD1D-associated mutations affect the refolding of luciferase, we used *sis1Δ* yeast cells that expressed in place of WT Sis1 our previously described Sis1-DNAJB6 chimeras, referred to as SDSS. As controls, we used WT Sis1 and the deletion construct Sis1-ΔG/F, which was shown to impair the refolding of luciferase *in vitro* [104]. We grew each of these strains at 44°C in order to denature luciferase, followed by monitoring the efficiency of luciferase refolding during a two hour recovery period at 30°C. As expected, Sis1-ΔG/F reduced the ability of cells to refold luciferase as compared to WT Sis1 (Fig. 1), which agrees with the previous *in vitro* studies [104]. However, we found that none of the SDSS chimeras, WT or

mutant, significantly altered the ability to refold luciferase in [*rnq*-] cells (Fig. 1). The same was true in cells propagating the m.d. high [*RNQ*+] prion variant (data not shown), which we had previously shown was maintained in the presence of the SDSS chimeras (Stein et al., in review). This suggests that the LGMD1D-associated mutations might selectively alter interactions with substrates that are prone to forming aggregates rich in β sheets.

5.3.2 Sis1-Mediated Protein Degradation is not altered by LGMD1D Mutations

In response to heat shock, DNAJB6b translocates to the nucleus and aids in resolving stress granules containing TDP-43 [250]. Similarly, Sis1 mediates the nuclear translocation and processing of cytosolic substrates [140,271], as well as the cytosolic degradation of other substrates [272]. Such Sis1-mediated translocation and degradation was recently shown using the model substrate, CG*, which consists of the cytosolic carboxypeptidase Y* fused to GFP [271]. Hence, we asked if the LGMD1D-associated mutations might impair the function of Sis1 in mediating the degradation of CG*. To test this, we monitored the kinetics of CG* turnover in [*rnq*-] and m.d. high [*RNQ*+] cells expressing WT Sis1, Sis1-ΔG/F, or the SDSS chimeras. When WT Sis1 was expressed, we found that CG* degraded rapidly (Fig. 2). Interestingly, none of the Sis1 constructs affected the turnover of CG*, even when the entire G/F domain was deleted. Moreover, these effects were independent of [*RNQ*+], as both [*rnq*-] and m.d. high [*RNQ*+] cells showed similar rates of CG* turnover. We had previously shown that the LGMD1D-associated mutations in DNAJB6 did not affect the translocation of DNAJB6 to the nucleus (Stein et al., in review). As CG* is translocated to the nucleus [271], our data agree with our previous results that the LGMD1D-associated mutations do not affect nuclear translocation. However, unlike our previous data using TDP-43 (Stein et al., in review), processing of CG* was unaffected.

5.3.3 Cellular Heat Shock Response is Normal in the Presence of LGMD1D Mutations

In response to stress, cells will induce the expression of molecular chaperones, and particularly heat shock proteins, to counteract any cellular damage to proteins [273]. The transcription factor Hsf1 is the master regulator of the heat shock response, acting to induce expression of genes that have a heat shock element (HSE) in their promoter [273]. Interestingly, Hsf1 activity is regulated by Hsp70s, which repress Hsf1 activity under basal conditions, as well as activate the heat shock response when stress is sensed [274]. Therefore, as Hsp40s modulate the activity of Hsp70s, we asked whether the LGMD1D-associated mutations affected induction of the cellular heat shock response. We transformed [*rnq*-] and m.d. high [*RNQ*+] cells with a plasmid that expresses *LacZ* under the control of a promoter containing four heat shock elements. With the use of this plasmid, β-galactosidase activity serves as a direct measure of the heat shock response. After growing cells expressing each of the Sis1 and SDSS constructs at 39°C for one hour and measuring the β-galactosidase activity, we found that there were no significant changes in the heat shock response with any of the constructs (Fig. 3 and data not shown). This suggests that the role of the LGMD1D-associated mutations in causing disease is not through alteration of the Hsp70-dependent induction of the heat shock response.

5.3.4 Toxic Over-Expression of LGMD1D Mutants is Hsp70-Dependent

It has been shown that over-expressing Sis1-ΔG/F dominantly impairs yeast cell viability and propagation of the [*RNQ*+] prion [104], indicating the importance of the G/F domain in substrate processing. We wondered whether the LGMD1D-associated mutations would similarly affect cell viability. To test this, we made the homologous Sis1 mutations in the residues that are

conserved between Sis1 and DNAJB6. This included Sis1-F106L (homologous to DNAJB6-F93L) and Sis1-F115I (homologous to DNAJB6-F100I). We then over-expressed these mutants, along with WT Sis1, in [*rnq*-] and m.d. high [*RNQ*+] cells. Strikingly, while cells over-expressing WT Sis1 grew similar to the empty vector control, over-expression of both Sis1 mutants greatly inhibited cell growth (Fig. 4). Such toxicity was independent of [*RNQ*+] status and could not be explained by any differences in expression (Fig. S1).

Interestingly, a secondary mutation in Sis1 was previously identified that suppressed the toxicity of Sis1-ΔG/F over-expression [104]. This mutation, Sis1-L268P, resides in the C-terminal substrate-binding domain of Sis1 and was demonstrated to disrupt the interaction of Sis1 with the Hsp70 Ssa1 *in vitro* [104]. Therefore, we hypothesized that this mutation might also suppress the toxicity caused by the LGMD1D-associated mutations in Sis1. Indeed, making the second-site L268P mutation completely rescued the toxicity (Fig. 4). However, deletion of the Sis1 dimerization domain [224] did not suppress toxicity of the Sis1-F115I mutation. Taken together, these data suggest that over-expression of the LGMD1D-associated mutations in Sis1 impairs cell viability in a manner that depends on the interaction of Sis1 with Hsp70, but not on Sis1 dimerization.

5.3.5 Loss of Hsp70 Nucleotide Exchange Factor Partially Rescues Prion Propagation

We have demonstrated that the LGMD1D-associated mutations can impair propagation of particular prion conformers, especially s.d. medium [*RNQ*+] (Stein et al., in review). Similar to the Sis1-DNAJB6 chimeras that we had tested previously, we found that expression of Sis1-F115I also eliminated the ability of s.d. medium [*RNQ*+] to propagate, as indicated by using a well-trap assay (Fig. 5). This assay determines the amount of Rnq1 protein that is soluble: for

[*RNQ*+] samples that have Rnq1 in an aggregated form, the aggregates will not break down in unboiled fractions and will not be able to enter an SDS-PAGE gel [189]. By contrast, the soluble Rnq1 in [*rnq*-] cells will enter the gel even in the unboiled fraction.

Since we found that the toxicity of the LGMD1D-associated mutations in Sis1 was mediated through the interaction with Hsp70, we asked whether modulating Hsp70 activity would rescue prion propagation. While Hsp40s promote an ADP-bound state of Hsp70 that has high affinity for substates, nucleotide exchange factors (NEFs) also play a crucial role in the Hsp70 ATPase cycle by stimulating the exchange of ADP to ATP to release substrates and allow for additional substrate binding [148]. Therefore, we deleted *SSE1*, one of the primary Hsp70 NEFs in yeast, and used a well-trap assay to test the effect of Sis1-F115I on propagation of s.d. medium [*RNQ*+]. Like *SSE1* cells, we found that all of the Rnq1 protein was in its aggregated state in *sse1Δ* cells when WT Sis1 was expressed, as indicated by the absence of Rnq1 in the unboiled fraction, suggesting that loss of *SSE1* did not affect prion propagation of s.d. medium [*RNQ*+] (Fig. 5). Moreover, all of the Rnq1 protein is soluble and can enter the SDS-PAGE gel in the unboiled fractions of [*rnq*-] *sse1Δ* cells, along with *SSE1* cells propagating s.d. medium [*RNQ*+] and expressing Sis1-F115I. However, there is significantly less soluble Rnq1 protein in *sse1Δ* cells expressing Sis1-F115I, indicating it is sequestered in Rnq1 aggregates. This suggests that loss of *SSE1* delays the loss of the s.d. medium [*RNQ*+] prion. This provides additional evidence to support the role of Hsp70 in mediating the effects of the LGMD1D-associated mutations.

5.4 Discussion

Here, we have provided additional mechanistic insight into the effects of the mutations associated with LGMD1D, and how they might contribute to pathogenesis. It was previously demonstrated that DNAJB6 can process substrates having of a polyglutamine expansion [256,275,276] and that LGMD1D-associated mutations can impair such processing of these aggregation-prone substrates [160]. This was also seen using the RNA-binding protein TDP-43 that formed nuclear stress granules (Stein et al., in review). We had extended these studies by showing that LGMD1D-associated mutations in DNAJB6 orthologs show tremendous selectivity and disrupt the processing of only particular conformers of the [*RNQ*+] and [*PSI*+] prions (Stein et al., in review). We now show additional specificity of these mutations.

We found that the LGMD1D-associated mutations do not alter the processing of heat-denatured luciferase (Fig. 1). Unlike the previously analyzed substrates, luciferase represents another aggregated substrate, but one that is not thought to form an ordered β sheet-rich structure. Moreover, the LGMD1D mutations did not affect the role that Sis1 plays in mediating the proteasomal degradation of a model misfolded cytosolic protein (Fig. 2). As this model substrate is degraded in the nucleus [271], this would suggest that the LGMD1D-associated mutations do not affect Hsp40 localization, which agrees with our previous results with DNAJB6 (Stein et al., in review). Collectively, these data support the view that Hsp40s are major determinants of functional specificity in the cell [148]. We propose that the LGMD1D-associated mutations impair certain Hsp40 functions (e.g. processing of substrates that form ordered aggregates), but not other functions (e.g. processing of particular amorphous substrates).

In addition to the selectivity that occurs between Hsp40s and substrates, another layer of selectivity operates through the interaction of Hsp40s with Hsp70s. While Hsp40s can act independently of Hsp70s, the general view is that Hsp40 function is often determined through its

interaction with Hsp70 [148]. The J domain of Hsp40s, in particular an HPD motif within the J domain, is required for stimulating the activity of Hsp70 [222]. In the case of Sis1, its interaction with Hsp70 is essential to yeast viability, as disruption of the HPD motif with the H34Q mutation causes inviability [150]. Moreover, the ability of Hsp40s to bind substrates is also essential, as loss of the substrate-binding domains of Sis1 and a related Hsp40 Ydj1 reduces cell growth when these domains are lost separately, and results in inviability when both domains are lost as there is some overlap in function between these Hsp40s [277]. Hence, it is clear that Hsp70-dependent substrate processing is an essential Hsp40 function in yeast. We found that over-expression of the LGMD1D-associated mutations in the G/F domain of Sis1 is toxic (Fig. 4), and this is suppressed by a secondary mutation in the substrate-binding domain of Sis1, L268P, that impairs the interaction with Hsp70 [104]. These data suggest that the LGMD1D-associated mutations likely disrupt the processing of essential substrates. We propose that these mutations might cause hyperstimulation of Hsp70 ATPase activity. In the case of Hsp40 over-expression, the stoichiometric ratios of Hsp40 and Hsp70 are altered, causing aberrant processing of essential proteins that is mitigated by disrupting the interaction between Sis1 and Hsp70 using the L268P mutation.

Additionally, such aberrant processing might also be the underlying factor for processing prion aggregates. When maintaining the normal stoichiometric ratios of Hsp40 and Hsp70, the LGMD1D-associated mutations disrupt the processing of particular prion variants (Stein et al. in review, and data not shown). This might result from certain prion conformers being sensitive to over-stimulation of Hsp70. Loss of NEF activity would slow the ATPase cycle and thus the recycling of Hsp70 monomer, potentially allowing for normal substrate processing. This would explain why deletion of the NEF *SSE1* partially rescues prion propagation in the presence of

Sis1-F115I (Fig. 5). There are at least two possibilities that could explain how mutations in the Hsp40 G/F domain cause hyperstimulation of Hsp70: 1) disrupting the spatial orientation of the Sis1 domains and consequently the interaction with Hsp70, or 2) altering Hsp70 interaction if the G/F domain binds to Hsp70 directly. Nevertheless, *in vitro* studies are necessary to specifically look at the relationship between DNAJB6 and Hsp70 to test these possibilities.

There are 11 Hsp70s in humans, but 41 different Hsp40s [148], and Hsp40s have very different tissue expression and activity [259]. In addition to the 13 different NEFs, this indicates that a complex network acts to modulate the function and ATPase cycle of Hsp70, and its involvement in many aspects of protein quality control. Indeed, the selectivity provided by Hsp40s may contribute to the increasing number of disorders, that have varying pathological features, that are linked to mutations in Hsp40 proteins [157]. Moreover, the role of DNAJB6 in causing LGMD1D indicates that myopathies can no longer be viewed simply as diseases caused by defects in scaffold proteins [278]. Our study highlights the selectivity of the LGMD1D-associated mutations, indicating how dysregulation of only certain Hsp40 functions can lead to disease.

5.5 Materials and Methods

5.5.1 Yeast Strains, Plasmids, and Media

All yeast strains used in this study are derived from 74-D694 (*ade1-14 his3-Δ200 leu2-3,112 trp1-289 ura3-52*) and were grown using standard techniques. YPD media (1% yeast extract, 2% peptone, 2% dextrose) or synthetic defined (SD) media (0.67% yeast nitrogen base without amino acids, 2% dextrose) lacking a particular nutrient to select for plasmids, was used as indicated. Wild-type (WT) [*RNQ*+] and [*rnq*-] strains were kind gifts from S. Liebman [31].

Construction of *sis1Δ* [*rnq*-] and [*RNQ*+] strains was described previously (Stein et al., in review). Replacement of WT Sis1 was performed by a plasmid shuffle technique using media containing 1mg/mL 5-fluoroorotic acid (5-FOA) that selects against the *URA3*-marked *SIS1* plasmid. The s.d. medium [*RNQ*+] *sse1Δ* strain was made using a plasmid-based *sse1Δ*::*LEU2* disruption construct (kind gift from K. Morano [248]) that was digested with SacII/PstI and transformed into *sis1Δ* cells propagating s.d. medium [*RNQ*+] and expressing *SIS1* from a *URA3*-marked plasmid. Transformants were selected on SD-leu and deletion of *SSE1* was confirmed by colony PCR.

The following plasmids were kind gifts: pRS314-*sis1-ΔG/F* from S. Lindquist [74], and pRS316-*SIS1* and pRS314-*sis1-L268P* from E. Craig [100,104]. Construction of pRS314-*SIS1* and *SDSS* chimeras was described previously (Stein et al., in review). Mutations in *SIS1* were created using bridge PCR with the indicated oligonucleotides, digested with SpeI/ClaI and ligated with the indicated vector, and confirmed by sequencing: *SDSS-F100I* (5'GTAACCCAGATGATGTCATCAGGGAATTTTTTGG and 5'CCAAAAAATTCCCTGATGACATCATCTGGGTTAC), *sis1-F106L* (5'GATTCTCCGGAGGACATGCGCTCAGTAATGAGGATGC and 5'GCATCCTCATTACTGAGCGCATGTCCTCCGGAGAATC), *sis1-F115I* (5'GATGCTTTCAATATTATTTCACAATTCTTTGGC and 5'GCCAAAGAATTGTGAAATAATATTGAAAGCATC), double mutations with *sis1-L268P* (5'GTTTCTCTAGTTATCCATCTG and 5'GTTTCTCTAGTTATCCATCTG using pRS314-*sis1-F106L*, pRS314-*sis1-F115I*, or pRS314-*sis1-L268P* as templates as necessary). To create pRS414*GPD-sis1-ΔDD-F115I*, 5'ATACTAGTATGGTCAAGGAGACAAAAC and

5'CGCATCGATTTATGGATAGTCCACTTTATATTTTAC were used, followed by digestion with SpeI/ClaI, and ligation with pRS414*GPD* that was digested with the same enzymes.

5.5.2 Luciferase Refolding

Yeast expressing the indicated construct from the pRS314 vector in place of pRS316-*SIS1* were transformed with pRS316*GPD-luciferase*, a kind gift from B. Bukau [220]. Refolding of luciferase was then monitored as described in previous studies [90,242]with modifications. Yeast cultures were grown to mid-logarithmic phase at 30°C, followed by growth at 37°C for one hour, then heat shocked at 44°C for one hour to induce aggregation of luciferase. 20µg/mL cycloheximide (Sigma) was added to each culture 50 min into heat shock. After heat shock, cells recovered at 30°C with 100µl samples taken at the indicated times, added to 50µl of 1mM beetle luciferin (Promega). Luminescence was measured on a single tube luminometer (Berthold Detection Systems) with a delay time of 2 sec and a read time of 6 sec. Luminescence was normalized to the pre-heat shock value taken after growth at 37°C.

5.5.3 CG Degradation Assay*

Monitoring CG* turnover was performed as described previously [271]. Yeast expressing the indicated construct from the pRS314 vector in place of pRS316-*SIS1* were transformed with pRS313-*CG**, a kind gift from U. Hartl [271]. Cultures were grown at 30°C until mid-logarithmic phase. 100µg/mL cycloheximide (Sigma) was added to each culture and samples were removed at the indicated times. Cell pellets were lysed by alkaline lysis that was adapted from previous studies [272,279]. Briefly, cells were resuspended in 0.1M NaOH and incubated at room temperature for 5min, followed by washing in H_2O and pelleting at 3,000 rpm for 3 min.

Cells were resuspended in denaturing lysis buffer (60mM Tris-HCl pH 6.8, 2% SDS, 2mM DTT), boiled at 100°C for 10 min, and pre-cleared at 3,000 rpm for 3 min. Equal volumes of cell lysates and sample buffer (60mM Tris-HCl pH 6.8, 2% SDS, 10% glycerol, 2mM EDTA, 5% β-mercaptoethanol, bromophenol blue) were analyzed by SDS-PAGE and western blot using an αGFP antibody (Roche).

5.5.4 Heat Shock Response

The indicated yeast strains were transformed with a plasmid expressing *LacZ*, from a promoter having four heat shock elements, a kind gift from S. Lindquist. Cultures were grown until mid-logarithmic phase at 30°C, followed by growth at 39°C for one hour. Samples were then lysed and luminescence was measured as described previously [280], followed by normalization to protein concentration.

5.5.5 Genetic Analysis

WT yeast strains that were [*rnq*-] or harboring m.d. high [*RNQ*+] were transformed with the indicated pRS414*GPD* constructs (pRS414*GPD-SIS1* was a kind gift from S. Lindquist [74]). Overnight cultures were normalized to OD_{600}, followed by spotting five-fold serial dilutions onto YPD and SD-trp and growth at 30°C for 3 days.

5.5.6 Protein Analysis

Yeast samples were lysed with glass beads in buffer (100mM Tris pH 7.5, 200mM NaCl, 1mM EDTA, 5% glycerol, 0.5mM DTT, 3mM PMSF, 50mM N-Ethylmaleimide (NEM), complete protease inhibitor from Roche) and pre-cleared at 6,000 rpm for 15 sec. Protein

concentration of cell lysates was then normalized. For well-trap assays, samples were incubated for 5 min at room temperature or 100°C in sample buffer (50mM Tris-HCl pH 6.8, 10% glycerol, 2% SDS, 100mM DTT), then analyzed by SDS-PAGE and western blot using an αRnq1 antibody. Expression of Sis1 mutants was determined similarly using αSis1 (a kind gift from E. Craig) and αPgk1 antibodies.

5.6 Acknowledgments

We thank the following people for reagents: S. Liebman, K. Morano, S. Lindquist, E. Craig, B. Bukau, and U. Hartl. This work was supported, in whole or in part, by the National Institutes of Health (F31AG040899 and T32GM007067 to KCS, GM072778 to HLT) and the Hope Center for Neurological Disorders (HLT).

5.7 Figures

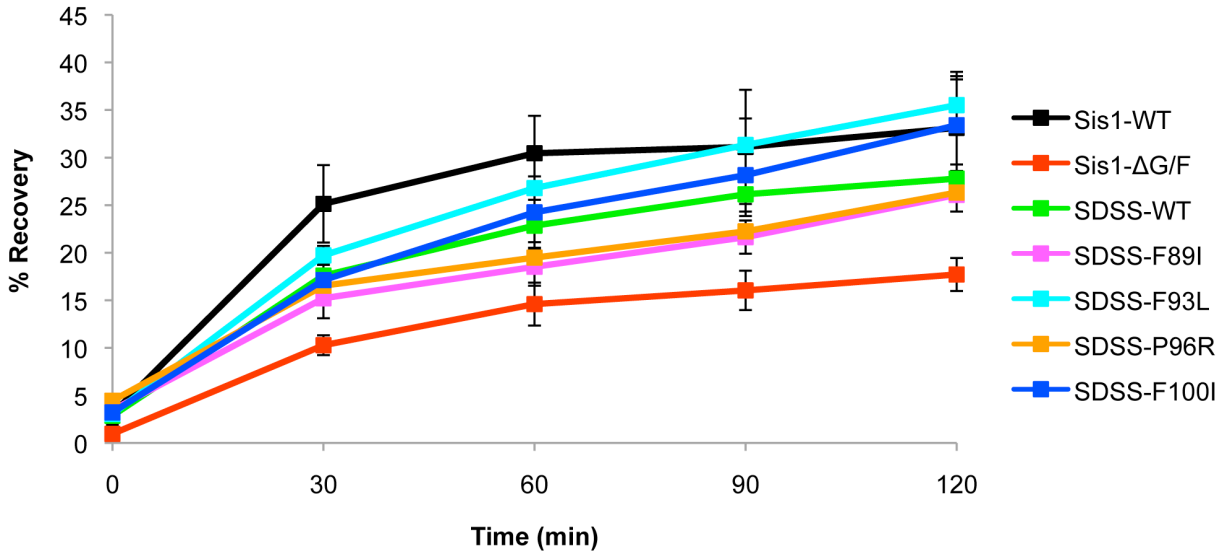

Figure 1. Luciferase refolding is unaffected by LGMD1D mutations. The capability of refolding luciferase was measured in [*rnq*-] *sis1Δ* yeast cultures harboring the indicated construct and a plasmid expressing luciferase. Yeast were subjected to heat shock to induce luciferase aggregation, followed by recovery at 30°C. Luminescence was measured at the indicated times during recovery and normalized to the luminescence before heat shock, with the amount of luciferase refolding plotted as the % recovery and represented as mean ± SEM with n = 4.

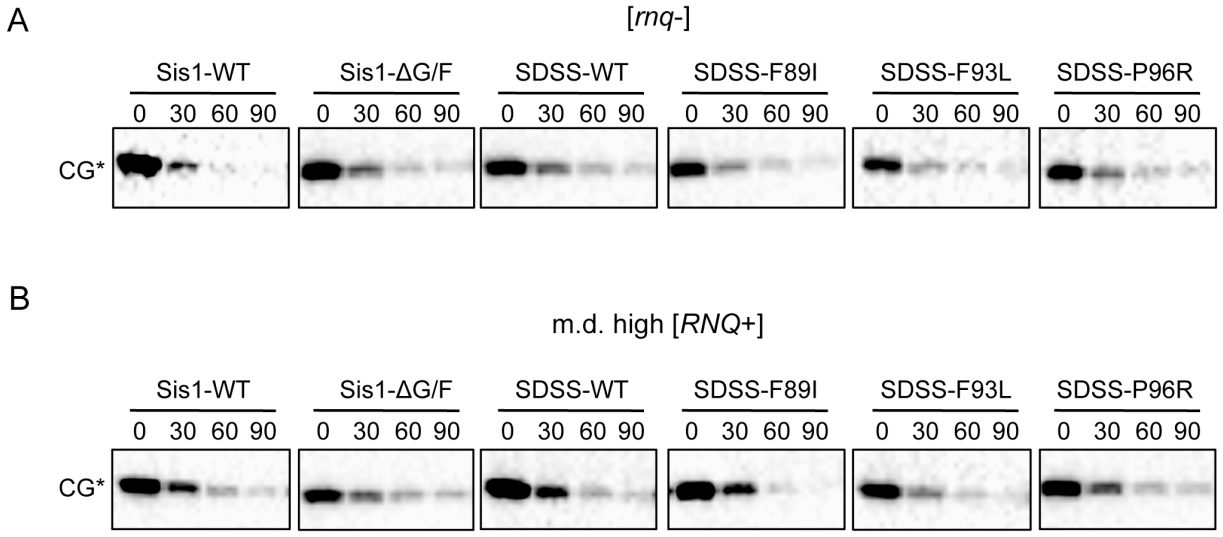

Figure 2. LGMD1D mutations do not impair Sis1-mediated protein degradation. The ability to mediate protein turnover was monitored in (A) [*rnq*-] and (B) m.d. high [*RNQ*+] *sis1Δ* yeast cultures harboring the indicated construct and a plasmid expressing CG*. After addition of cycloheximide, samples were harvested at the indicated times, lysed, and subjected to SDS-PAGE and western blot using an αGFP antibody that detects CG*.

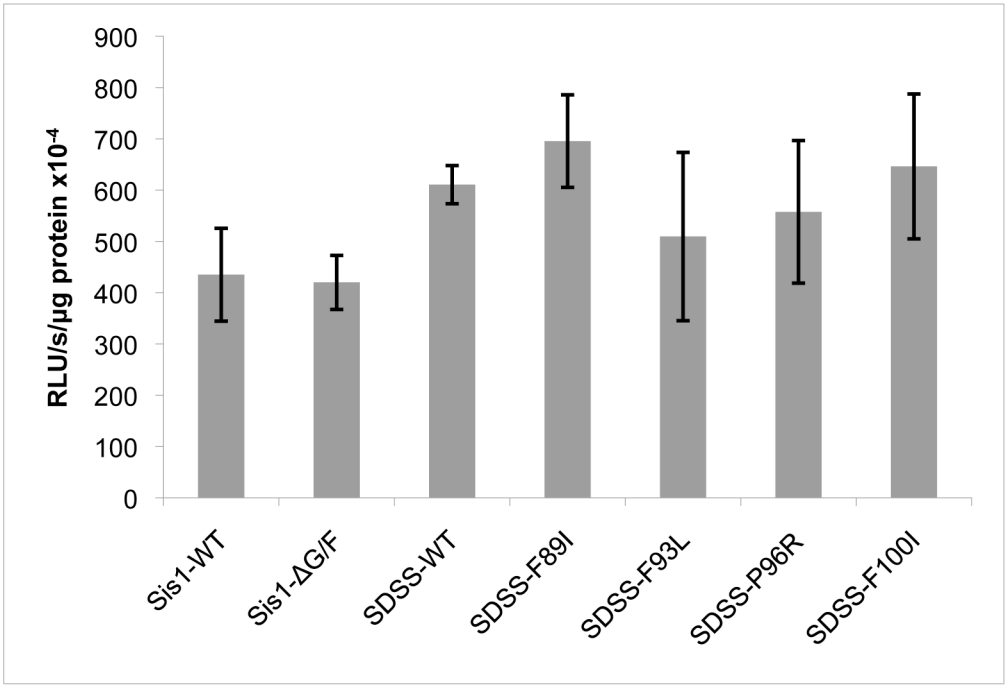

Figure 3. The heat shock response is unchanged in the presence of LGMD1D mutations. [*rnq*-] *sis1Δ* yeast cultures expressing the indicated construct, along with a plasmid expressing *LacZ* from a promoter containing four heat shock elements, were grown at 39°C for one hour to induce the heat shock response. Samples were harvested, lysed, and β-galactosidase activity was measured and normalized to protein concentration to give random luminescence units (RLU)/s/µg protein. Data are represented as mean ± SEM with n = 3, with no significant differences in the heat shock response between samples.

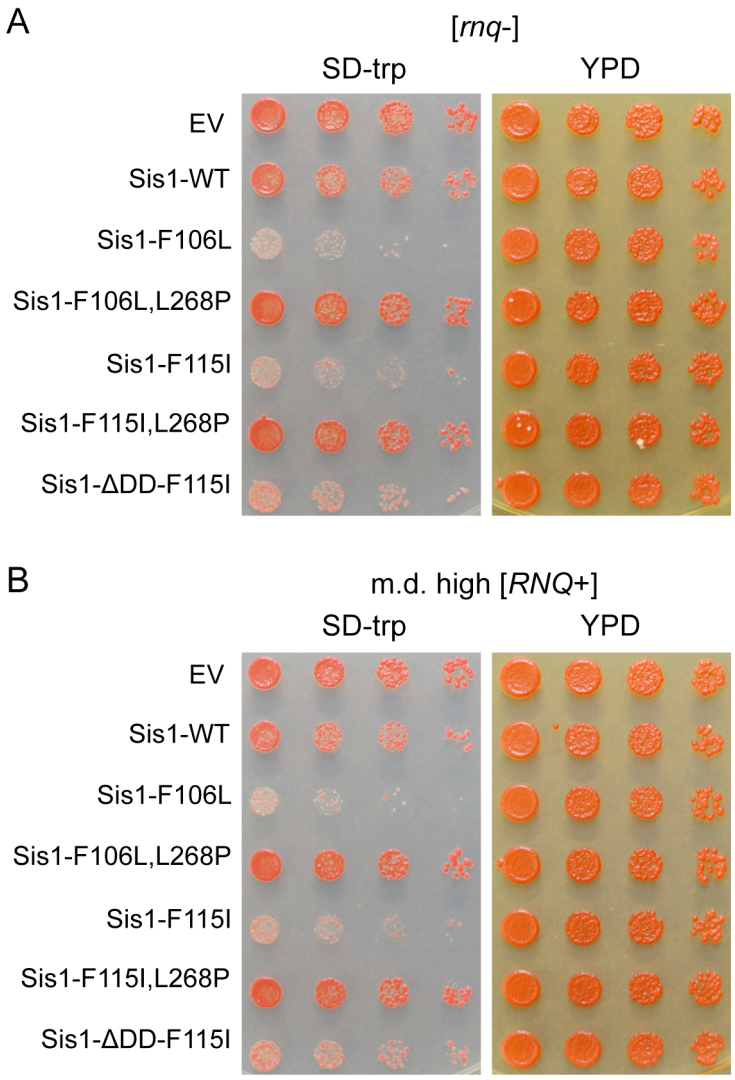

Figure 4. Impaired Hsp40-Hsp70 interaction rescues the toxicity associated with over-expressing homologous LGMD1D mutations in Sis1. Wild-type [*rnq*-] and m.d. high [*RNQ*+] yeast cells were transformed with plasmids that over-expressed the indicated Sis1 construct, or an empty vector control (EV). Cultures were normalized and five-fold serial dilutions were spotted on medium to select for the plasmid (SD-trp), or medium that provides no selection (YPD). Images are represented of at least three independent experiments.

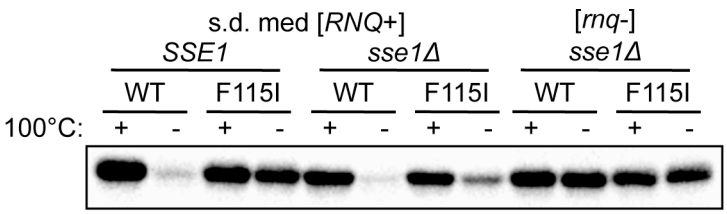

Figure 5. Deletion of *SSE1* suppresses the prion loss caused by a homologous LGMD1D mutant. Analysis of prion propagation in *SSE1* and *sse1Δ* strains harboring s.d. medium [*RNQ*+], along with a [*rnq*-] *sse1Δ* strain, expressing either WT Sis1 or Sis1-F115I. Cell lysates were incubated at room temperature (-) or 100°C and subjected to SDS-PAGE and western blot using an αRnq1 antibody. Rnq1 that is not sequestered in aggregates will enter the gel in the unboiled sample and indicates destabilization of the [*RNQ*+] prion.

5.8 Supplemental Figures

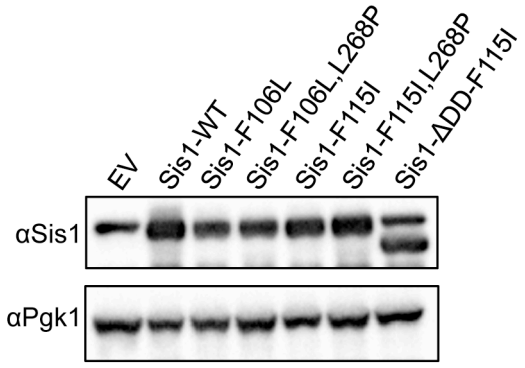

Figure S1. Expression of homologous LGMD1D-associated mutations in Sis1. Western blot analysis showing expression of the indicated Sis1 constructs. Cell lysates were subjected to SDS-PAGE and western blot using antibodies against Sis1, along with Pgk1 as a loading control.

Chapter 6: Conclusions and Future Directions

6.1 Summary

6.1.1 Prion Variants and Molecular Chaperones

Amyloid polymorphism and its effects on phenotypic variation can be viewed from a variety of different levels, from biophysical and biochemical levels to genetic and cellular levels. In Chapters two and three, I utilized concepts from each of these areas to examine the structural variation of prion strains. Yeast prion variants of [*PSI*+] have served as the foundation for studying amyloid polymorphism for several years. I extended this analysis by using the prion variants of [*RNQ*+] to study the structural diversity of amyloid in comparison to [*PSI*+]. In so doing, I broadened the foundation for examining prion strains, and demonstrated that a large network of factors can modulate amyloid polymorphism and the associated phenotypic consequences.

The overarching principle that was proposed from the work with [*PSI*+], is that prion propagation relies on an equilibrium between the fragmentation of aggregates and the ability of monomer to join a preexisting aggregate (fiber growth) [25]. This principle is likely applicable to both the pathological amyloid of protein conformational disorders and to the functional amyloid associated with a variety of different cellular processes. From an intuitive standpoint, this principle makes sense. If fiber growth is increased relative to fragmentation, then larger aggregates accumulate that have reduced ability to spread spatially and propagate. However, if fiber fragmentation is increased relative to growth, then this may result in the clearance of the aggregate. This balance was proposed to explain how prion strains can influence phenotype: different prion strains have different equilibrium points and thus distinct abilities to catalyze conformational conversion and sequester monomer [25]. Arguably, neither my work, nor any work from other groups using other proteins, refutes this principle. However, what I have

demonstrated, along with others, is that the factors that dictate this equilibrium are complex and not as simple as what was originally proposed [28,34,38]. The novel factors that I found to influence this equilibrium include a role for non-canonical sequence elements, distinct chaperone binding sites, and different dependencies on chaperone interactions and processing.

It was previously suggested that the balance between fiber fragmentation and growth was dictated by the stability of the aggregates and the size of the amyloid core [25,26]. The less stable Sup35 aggregates of strong [*PSI*+] had a high degree of fragmentation and growth, resulting in a small soluble pool of Sup35 as much of the Sup35 in the cell is incorporated into aggregates. Using the [*RNQ*+] variants, I found that s.d. very high [*RNQ*+] provides the most striking counterexample [34]. Utilizing RRP to analyze [*RNQ*+] in an analogous fashion as [*PSI*+], s.d. very high [*RNQ*+] had a similarly strong phenotype as strong [*PSI*+], but propagated a stable structure and had a relatively large soluble pool of Rnq1. Moreover, m.d. high [*RNQ*+], while also having a strong phenotype, a small pool of soluble protein, and low stability, had a larger aggregate size, in contrast to the trends of strong [*PSI*+]. These examples show that the amount of soluble protein, aggregate size, and aggregate stability do not always correlate or predict where the equilibrium point is between fragmentation and growth. Indeed, this might suggest that this equilibrium is not simply between monomeric protein and aggregated protein, but of multiple oligomeric intermediates.

Unlike [*PSI*+] variants, which are proposed to have a contiguous stretch of Sup35 that forms the aggregate structure, I found that the [*RNQ*+] variants have a surprising amount of diversity in the sequence elements that are important for prion propagation. First, these amyloidogenic regions of Rnq1 that are involved in prion propagation are not contiguous, suggesting that Rnq1 might utilize a different category of packing arrangement as compared to

Sup35. Second, the region outside of the Rnq1 prion-forming domain (PFD) played a strain-dependent role in prion propagation, at least in part, through facilitating monomer addition to aggregates. This suggests that the so-called prion-like domains that are Q/N-rich, which have been identified in numerous human proteins [8], are likely not the only important part of the primary structure that influences the aggregation of disease-related proteins. This agrees with the fact that other prion proteins, such as PrP and HET-s, are not Q/N-rich [2].

In addition to the direct effect on propagation of distinct prion variants, I found that the Rnq1 amyloidogenic regions were also important for modulating the phenotypic manifestations of [*RNQ*+] [34]. More specifically, mutation of certain regions influenced how well [*RNQ*+] induced the formation of [*PSI*+], with particular mutations enhancing [*PSI*+] formation. It is possible that the large Q/N-rich PFD of Rnq1 allows for a level of redundancy not seen when analyzing shorter peptides or proteins that are not Q/N-rich. This redundancy may allow for a moveable amyloid core, whereby the Rnq1 protein can still aggregate despite disruption of so-called 'nonessential regions' that are not needed for nucleated conversion, but the structure has been slightly altered. This might suggest that Rnq1 can form a larger spectrum of different prion variants than other proteins that have less sequence redundancy, which would be quite striking considering the wide variety of structures already observed for other proteins [172,173].

The other major factor that my work reveals as contributing to the equilibrium between aggregate fragmentation and growth, is the diversity in which chaperones interact and process different structures. While a binding site in Rnq1 for the Hsp40 chaperone Sis1 had been previously identified [37], I found that Sis1 was capable of binding other parts of the Rnq1 protein [34]. Moreover, it appeared that the dependence of these alternative sites varies in a prion variant-dependent fashion. For instance, propagation of the s.d. very high [*RNQ*+] variant

showed striking reliance on the C-terminal A10 amyloidogenic region (a putative Sis1 binding site), more so than any of the other [*RNQ*+] variants. This suggests that prion conformation determines the exposure of chaperone binding sites, or how these sites are used.

In addition, I found that the chaperone machinery that utilizes these chaperone binding sites can vary. One interesting example is that faithful propagation of s.d. medium [*RNQ*+] and s.d. very high [*RNQ*+] depended on the dimerization domain of Sis1. Also, the [*PSI*+] variants showed greater dependence on Hsp70 function as compared to Sis1. Hence, in addition to prion variants having different exposed sites for interaction, these data indicate several other possible ways of influencing the equilibrium between fiber fragmentation and growth: 1) what chaperone(s) bind the exposed sites, 2) the affinity with which chaperone(s) bind, and 3) the ability (or inability) of chaperones to process the prion aggregates and whether other co-chaperones are needed. These factors, in part, might help explain the distinct cofactor requirements of various PrP^{Sc} strains [39].

Collectively, Chapters two and three showed other important variables that distinguish prion variants. For the prion protein, this might include different, non-adjacent regions of the prion protein that 1) serve as the template to catalyze conformational conversion, 2) facilitate monomer addition, or 3) are available for chaperone binding. Moreover, the different requirements of the chaperone machinery for distinct prion variants is another important factor. Hence, in addition to biochemical properties influencing the prion variant-dependent balance of fiber fragmentation and growth, these other variables play a major role in dictating structural variation and its associated phenotypic variation.

6.1.2 DNAJB6 and LGMD1D

Mutations in the Hsp40 DNAJB6 cause the protein aggregate myopathy known as limb-girdle muscular dystrophy type 1D (LGMD1D). These mutations all localize to a short stretch in the G/F domain of DNAJB6 [159-162]. In Chapters four and five, I exploited the conservation of the G/F domain that is present in DNAJB6 and the yeast Sis1, both type II Hsp40s, to gain insight into the pathogenesis of LGMD1D. Furthermore, this demonstrated the application of my findings from Chapters two and three and the broad utility of the yeast prion model.

By making the homologous disease-associated mutations in Sis1, DNAJB1, the chimera SDSS, as well as DNAJB6, I demonstrated the crucial role that the mutated residues play in modulating the function of Hsp40s and the G/F domain. First, mutation of DNAJB6 impaired its ability to resolve nuclear stress granules of TDP-43. Second, mutation of DNAJB1 and Sis1 resulted in slow growth phenotypes, likely through disrupting the Hsp70-mediated processing of essential substrates. Finally, mutation of SDSS disrupted the propagation of particular prion variants.

In demonstrating that the LGMD1D-associated mutations do not alter other Hsp40 functions, these data suggest that the G/F domain is involved in mediating the selectivity of substrate processing in an Hsp70-dependent fashion. In the case of muscle tissue, where protein quality control is highly regulated [281], chaperones are constantly responsible for the turnover of proteins. It is easy to envision that these proteins are damaged or misfolded to form a variety of different conformations having different regions of the protein exposed and available for chaperone binding. The LGMD1D-associated mutations might alter the ability of DNAJB6 to bind these different conformers or properly transfer them to Hsp70 to be processed. Indeed, as I showed that disrupting the interaction of mutant Hsp40 with Hsp70 could rescue particular growth phenotypes, this suggests that the LGMD1D mutations alter the regulation of the Hsp40-

Hsp70 complex. Moreover, since we found differential effects between the mutants, it is conceivable that there are different degrees of Hsp40-Hsp70 dysfunction depending on the DNAJB6 mutant.

Taken together, in light of the mutation- and conformer-specific effects seen with disruption of the G/F domain, my data indicate that subtle differences in the interplay between the proteostasis network with particular client conformers might contribute to the observation that patients with LGMD1D show a range of disease onset and pathology [159,163]. Hence, these data suggest that amyloid polymorphism, or even different conformations of folding intermediates, is an important consideration when studying chaperonopathies in the future.

6.2 Elucidate the Biophysical and Biochemical Basis of Prion Strains

6.2.1 Structural Polymorphism in [*RNQ*+] *Variants*

The ability of structural differences to manifest as variation in phenotype is a widespread phenomenon [20]. An increasing number of examples are likely to be found both with pathological amyloid as well as functional amyloid. In order to elucidate how structure dictates phenotype, it is important to extend beyond the numerous biochemical and genetic assays, which have provided significant information, but act as surrogates of structural information. Accomplishing this with the large, insoluble amyloid structures remains technically challenging, but there are certain strategies that have proven fruitful.

To determine how the [*RNQ*+] variants are structurally distinct and can induce the formation of [*PSI*+] to different extents, Rnq1 aggregates should be first isolated from [*RNQ*+] yeast cells and used to seed the aggregate formation of recombinant full-length Rnq1 in order to obtain a large quantity of purified aggregates. As I have shown the importance of the N-terminal

non-PFD, it will be crucial to use the full-length Rnq1 protein rather than just the Rnq1-PFD, as is generally done. After confirming that the same aggregate conformation has been maintained by transforming the aggregates back into yeast cells and testing variant-dependent properties (e.g. [*PSI*+] induction), structural data can be obtained using hydrogen-deuterium exchange combined with mass spectrometry or NMR. This will help indicate which amino acid residues are protected in the β sheet amyloid core. Also, magic-angle spinning NMR could be used to interrogate the structure of the [*RNQ*+] variants by determining the dynamics of particular residues, as recently done with fibers of Sup35NM [38].

Additionally, as Rnq1 does not contain any endogenous cysteine residues, cysteine mutations can be made throughout the protein to use in combination with structural probes. Isolated Rnq1 aggregates from yeast cells would be used to seed the conformational change of the cysteine mutants. It will be important to confirm that such mutations do not grossly alter the amyloid structure by determining that the biochemical properties of the [*RNQ*+] variants are maintained. These Rnq1 mutants can then be coupled to the fluorophores pyrene or acrylodan to monitor the exposure of these residues to solvent using fluorescence. The cysteine residues could also be coupled to a paramagnetic spin label for use with EPR to determine the dynamics of these residues.

There are some alternative approaches that are less direct ways of getting structural information, but would still help determine how regions of the protein are packed. By generating a variety of monoclonal antibodies that recognize a particular peptide region in Rnq1, an ELISA could be performed to probe the regions of the Rnq1 aggregates that are exposed and available to bind the antibody, as well as detecting the affinity with which the antibody binds. In fact, I have already determined that one of the polyclonal αRnq1 antibodies that we generated does not

recognize the PFD of Rnq1, which would provide a good starting point to probe the packing of the N-terminal domain in different [*RNQ*+] variants. This assay could then be adapted for use with a denaturant, as done with the conformation-dependent immunoassay (CDI), to determine what regions become exposed when the aggregates break down with increasing concentrations of denaturant.

As another less direct way of identifying structural differences, isolated Rnq1 aggregates could be used to seed recombinant mutant Rnq1 having certain amyloidogenic regions disrupted. If the region of interest were typically incorporated in the amyloid core of a given [*RNQ*+] variant, then the wild-type aggregates would have a reduced ability to catalyze the conformational change and aggregate formation of the mutant monomer. This could easily be monitored using the amyloid-binding dye Thioflavin T. These assays should help elucidate the exact role of the amyloidogenic regions of Rnq1 in prion propagation.

Finally, a major complementary question in the field is determining the size or nature of the aggregate species that is responsible for prion transmission. A different size of species might be important for propagation of distinct strains. Indeed, as the [*RNQ*+] variants have a large distribution of aggregate sizes, it is conceivable that the size of the "infectious" species is different for each [*RNQ*+] variant. As such, yeast lysates should be fractionated by sucrose gradient, isolated, and transformed into naïve [*rnq*-] cells expressing RRP to determine which fraction is most infectious for each of the [*RNQ*+] variants. This would provide insight into how the [*RNQ*+] variants might differentially interact with Sup35 (see below) by showing the size of Rnq1 aggregate that is the interacting partner. It would also be informative as to the role of oligomeric species with different conformations in amyloid diseases.

6.2.2 Analysis of PrP^{Sc} Strains in Yeast

Studies with [*PSI*+] were the first to provide a biochemical and biophysical explanation for how variation in Sup35 aggregates causes differences in phenotype. With PrP^{Sc} strains, there are many correlations made between the biochemical properties and pathology, but a causal connection remains lacking. Moreover, certain PrP^{Sc} strains are biochemically similar [30], as I showed was also true for some [*RNQ*+] variants. By using chimeric proteins that fuse PrP to the MC domains of Sup35, this would provide a much more tractable system for analyzing the link between PrP^{Sc} structural variation and phenotype. Strains of PrP^{Sc} could be transformed into cells expressing the PrP-MC fusion and analyzed in an analogous fashion as [*PSI*+]. Moreover, changing the allele of PrP, would provide an easy and quick means of testing the strength of the species barrier, which is especially a concern nowadays since chronic wasting disease is endemic to populations of deer and elk in the United States and Canada [282].

6.3 Determine how Heterologous Prion Proteins Interact to Influence Strain-Mediated Phenotypes and Prion Transmission

6.3.1 Influence of [*RNQ*+] *on Formation of* [*PSI*+]

Understanding the biophysical basis of structural differences is crucial to elucidating how the [*RNQ*+] variants influence phenotypic variation by inducing the formation of [*PSI*+] to different extents. However, the other important factor that dictates this phenotypic variability is how Sup35 interacts with the [*RNQ*+] variants. Interestingly, it is postulated that one contributing factor in the pathogenesis of protein conformational disorders is the co-aggregation of heterologous proteins, and a variety of different proteins have been found in amyloid plaques [283]. Moreover, distinct strains of α-synuclein have been shown to induce the formation of tau

inclusions to different extents [171]. Hence, understanding the underlying mechanism of how heterologous proteins interact could provide significant insight into disease etiology.

One model for how [*RNQ*+] induces [*PSI*+] formation suggests that Rnq1 aggregates physically interact with Sup35 to cross-seed [*PSI*+][60]. We have genetic evidence to support this model (Stein and True, unpublished results). In order to gain additional support and determine what regions of Sup35 and Rnq1 interact, Rnq1 aggregates should be isolated from yeast cells propagating distinct [*RNQ*+] variants, and amplified using recombinant Rnq1 as mentioned above. Then, cross-linking assays should be performed with these aggregates and recombinant Sup35. The cross-linked products could then be digested with trypsin and analyzed by mass spectrometry. This would provide the best evidence to date that polymorphic amyloid structures differentially interact with other proteins.

Besides the direct interaction between Rnq1 aggregates and [*PSI*+], we have shown that over-expression of Sis1 can enhance [*PSI*+] formation [34], suggesting that it might act as a cofactor to facilitate conversion to [*PSI*+]. To identify other cofactors that might also be involved, a library of plasmids over-expressing much of the yeast genome could be transformed into cells propagating the s.d. medium [*RNQ*+] variant and screened for enhanced (or reduced) levels of [*PSI*+] formation. This could then be checked in cells propagating the other [*RNQ*+] variants to determine if the cofactors are similarly involved. Additionally, as most of the yeast deletion library is [*RNQ*+] [284], this library could be screened for enhanced (or reduced) formation of [*PSI*+]. These assays would help identify novel factors that might contribute to the differential ability of the [*RNQ*+] variants to induce [*PSI*+], and furthermore, what factors might be involved in the aggregation of disease-related proteins.

6.3.2 Conservation of [*RNQ*+] *and the Species Barrier*

Of the yeast prions, the [*RNQ*+] prion is the one that is found most commonly in wild yeast isolates [285]. We recently identified different [*RNQ*+] variants in these wild isolates [35]. Interestingly, many different genetic polymorphisms have also been found in the *RNQ1* gene [286], and different fungal species have different *RNQ1* alleles as compared to the reference sequence in *Saccharomyces cerevisiae*. These different alleles could be expressed in *S. cerevisiae* propagating different [*RNQ*+] variants, followed by determining whether the [*RNQ*+] prion is maintained. This information would serve two purposes: 1) it would further elucidate what primary structure elements are important for the [*RNQ*+] variants, and 2) it would help determine what types of structures (if any) could exist with a particular *RNQ1* allele in the wild. This information would reveal what parts of the Rnq1 protein help control the species barrier, and the extent to which [*RNQ*+], as a regulatory epigenetic element, is phylogenetically conserved.

6.4 Elucidate how Interactions between Molecular Chaperones and Substrates are modulated

6.4.1 Interplay between Sis1 and [*RNQ*+] *Variants*

My work and that of others demonstrates that molecular chaperones and other cofactors can differentially interact with polymorphic amyloid structures [34,39]. While this phenomenon is clear, the basis of these differences is still poorly understood; for instance, how Sis1 interacts and processes different aggregate structures. As such, it is first important to obtain definitive evidence that the [*RNQ*+] variants expose different chaperone binding sites and Sis1 binds to different regions of the Rnq1 protein. To do this, Sis1 should be immunoprecipitated from wild-

type [*RNQ*+] cells, cross-linked, digested with trypsin, and analyzed by mass spectrometry. This would help confirm whether Sis1 binds different amyloidogenic regions of Rnq1 depending on the [*RNQ*+] variant. A complementary approach was presented above in which isolated Rnq1 aggregates should be used to seed the aggregate formation of mutant Rnq1 having one of the amyloidogenic regions mutated, and monitoring aggregation using Thioflavin T. If these regions act as chaperone binding sites, then the rate at which aggregates form should be comparable to the self-seeding of wild-type Rnq1.

Chaperones might also have distinct affinities for the same binding site, depending on the aggregate structure. My work suggests this might be the case with Sis1 and Rnq1. This hypothesis should be tested using isothermal titration calorimetry with Sis1 (recombinant or purified from yeast) titrated with purified wild-type or mutant Rnq1 aggregates of different [*RNQ*+] variants. Comparing the [*RNQ*+] variants with just wild-type Rnq1 would show whether Sis1 has different affinity for Rnq1 as a whole. However, disrupting particular putative binding sites should help show the degree to which Sis1 binds these regions as compared to wild-type Rnq1. Moreover, this could be done with various Sis1 mutants to determine the importance of particular Sis1 domains in binding Rnq1. In addition, it might also be feasible to make cysteine mutations at candidate regions in Rnq1 and Sis1 and perform cross-linking assays. This could help reveal, for instance, whether the Sis1 G/F domain physically binds substrates, or if its critical role in [*RNQ*+] propagation is through modulating other Hsp40 functions. Collectively, this information would provide mechanistic details for how chaperones bind and interact with distinct substrate conformers.

With regards to the Sis1 G/F domain, it was striking to find that all of the [*RNQ*+] variants required the presence of the Sis1 G/F domain for propagation, while the [*PSI*+] variants

showed less dependence on this domain. It would be interesting to screen for a novel [*RNQ*+] variant that does not rely on the Sis1 G/F domain and perform biochemical and structural studies on this novel prion variant. This could be done by expressing Sis1-ΔG/F in [*rnq*-] cells that express RRP, and selecting for cells that have spontaneously converted to [*RRP*+], similar to what we have done previously (Appendix A) [32]. Comparing this prion variant to the other [*RNQ*+] variants I have characterized might show what is structurally different about these latter variants that necessitates the presence of the Sis1 G/F domain.

Finally, to determine novel parts of Sis1 that influence the relationship between Sis1 and [*RNQ*+], mutations in *SIS1* that disrupt [*RNQ*+] propagation could be identified by first randomly mutating *SIS1* by error-prone PCR. Then, this mutant library should be expressed in place of wild-type Sis1 in [*RNQ*+] cells expressing RRP to screen for cells that can no longer propagate [*RNQ*+]. A similar test could be done with [*PSI*+]. Moreover, I found a number of Sis1 mutants that impaired the variant-specific propagation of [*RNQ*+]. Screening for rescue of these phenotypes would help determine the mechanism of how these Sis1 regions are involved in propagating specific [*RNQ*+] variants. As both *cis*- and *trans*-acting factors could be involved in mediating the effects of the Sis1 mutants, the screens could involve the use of an over-expression plasmid library, mutating yeast with EMS, or with a second-site suppressor mutant Sis1 library for Sis1 mutants of particular interest.

6.4.2 Factors of the Proteostasis Network that Influence Propagation of Prion Strains

Interestingly, the genetic background influences the interaction of Sis1 with [*RNQ*+] [215], suggesting that the proteostasis network might be altered in different cell types. At the most basic level, this could simply be differences in gene or protein expression, as was shown

with Sis1 [215]. Hence, genomic analysis, including genome sequencing and RNA-Seq, should be performed between genetic backgrounds of interest (e.g. 74-D694 and W303) to identify novel factors that could influence prion propagation.

In thinking about species and organism differences, recently it was found that the Hsp110 from the malarial parasite *Plasmodium falciparum* prevented aggregation of Sup35, and it was suggested that this chaperone has a particularly potent ability in handling Q/N-rich substrates [287]. To gain a better understanding of the apparent enhanced functionality of this chaperone, it could be expressed in yeast to determine if it is similarly capable of handling different prion and non-prion aggregates, and even whether it can functionally replace the role of Hsp104 as a disaggregase. Furthermore, purifying recombinant Hsp110 would allow for the biochemical characterization of this chaperone that would provide additional insight into its function and ability to handle misfolded substrates having distinct conformations. Comparing this information to human chaperones might reveal ways in which chaperone activity should be modulated and enhanced.

6.4.3 Effects of LGMD1D-Associated Mutations on DNAJB6 Function

Despite my work demonstrating the selective impairment of LGMD1D-associated mutations on Hsp40 functions, there are several areas that need to be addressed in order to obtain a clear picture of the effects of these mutations. First, how the mutations in DNAJB6 affect the interaction with Hsp70 should be analyzed *in vitro* with recombinant protein. It is important to determine whether the mutations affect the binding to Hsp70 and Hsp70 ATPase activity. Additionally, a variety of substrates could be used to analyze Hsp70-mediated substrate refolding

in vitro. These assays would elucidate whether the role that the LGMD1D-associated mutations play in disease could involve a disrupted interaction between DNAJB6 and Hsp70.

If any alteration in Hsp70 function is observed, there are a number of chemical compounds that could be analyzed that modulate specific aspects of Hsp70 function [288]. These compounds could be used in an attempt to rescue the deficits caused by the DNAJB6 mutations. Additionally, screening for secondary *cis* or *trans* factors that rescue the defects in substrate processing would provide significant insight into the mechanistic underpinnings of LGMD1D and how mutations in DNAJB6 cause disease. One of the best tools to accomplish this would be using the DNAJB1-F90I mutant that caused inviability when expressed in yeast (Chapter 4). Second-site suppressors could be identified in DNAJB1 after mutagenizing this construct using error-prone PCR. Additionally, the over-expression plasmid library should also be screened for novel *trans*-acting factors. My preliminary results using over-expression of various candidate proteins (including an Hsp70 and nucleotide exchange factors) were all negative.

In addition to the interaction of DNAJB6 with other chaperones, another important variable that likely contributes to the development of LGMD1D is what substrates are being misprocessed. Expression of DNAJB1-P98R, as well as over-expression of the LGMD1D-associated mutations in Sis1, does not cause inviability, but still causes a slow-growth phenotype. This is likely due to the sequestration or aberrant processing of essential substrates. It is possible that these substrates are aggregating or concentrating in particular locations in the yeast cell. As such, using a sedimentation assay and mass spectrometry, these essential substrates could be identified, which might reveal particular types of substrates that are misprocessed and contribute to muscle degeneration in LGMD1D patients. Additionally, conducting a similar

proteomic analysis on the aggregates in patient tissue would also provide significant information into disease pathogenesis.

Finally, while I demonstrated the conformer-specificity of the LGMD1D-associated mutations using yeast prion variants, it is important to translate these findings to mammalian cells and determine if the same phenomenon exists. In order to do this, distinct conformers of TDP-43 or another DNAJB6 client must be isolated. Then, it can be tested whether the DNAJB6 mutants are defective in the refolding or resolution of these conformers.

6.5 Determine Cellular Processes and *Trans*-Acting Factors that Influence Formation and Propagation of Prion Strains

6.5.1 Influence of Translation Efficiency on Prion Formation

Most cases of protein conformational disorders are sporadic [2]. Hence, it remains unclear what causes proteins to misfold and aggregate in these cases, and form different amyloid structures. As nascent polypeptides are considered to be more thermodynamically unstable as compared to folded proteins, I hypothesize that variation in translation and the ribosome quality control machinery might be a contributing factor. One means of testing this is by using constructs having the same amino acid sequence, but changing the codons in order to disrupt the organism-specific codon bias (i.e. organisms have a greater preference for particular codons than others, likely in part, because of differences in tRNA levels) [289]. We have designed constructs of Rnq1 having codons optimized for use in yeast, which should enhance the rate of translation, and disoptimized codons, which should cause ribosomes to pause. Interestingly, I have preliminary evidence that the disoptimized construct of Rnq1 spontaneously forms the [*RNQ*+] prion at the highest rate, followed by wild-type Rnq1, and then the optimized Rnq1 (Stein and

True, unpublished results). This suggests that slowing translation enhances prion formation. Determining whether the distribution of prion variants that forms changes when the translation rate is altered would help shed light on how prion variants sporadically form. Similarly, deletion or over-expression of particular candidates of the ribosome quality control machinery to determine the effect on prion formation and propagation would also help elucidate the role that mRNA translation plays in protein misfolding and the formation of prion strains.

6.5.2 Cellular Factors that Contribute to Prion Formation

I have shown that over-expression of Sis1 enhances [*PSI*+] formation in [*RNQ*+] cells [34]. Other groups have focused on the ability of over-expressed Q/N-rich proteins or chaperones to modulate the formation of [*PSI*+] and [URE3] [60,115,290]. Yet, in these cases, there remains a dependence on a Q/N-rich protein to act as the nucleating factor for prion formation, with [*RNQ*+] often serving as the Q/N-rich entity. Hence, it remains unclear what other factors might influence the spontaneous formation of prions, specifically of [*RNQ*+]. Analyzing what factors influence the ability of Rnq1 to convert to its prion state would provide a means of identifying novel factors that regulate aggregate formation. To do this, the over-expression plasmid library expressing most all of the yeast genome could be transformed into [*rnq*-] cells harboring RRP and screened for enhanced spontaneous formation of [*RNQ*+], which we have shown is generally a pretty rare event (~$3x10^{-6}$) [32]. The distribution of prion variants that forms could also be determined for a subset of candidates to determine if certain cellular factors bias the formation of particular aggregate conformers, as we have shown to be true by altering extracellular growth conditions [41]. As I have demonstrated that Sis1 interacts with [*RNQ*+] variants differently, one intriguing possibility is that increased (or decreased) expression of Sis1 might bias the formation

of different [*RNQ*+] variants. Follow-up studies could then analyze certain factors in mammalian cells with any number of disease-related proteins.

One interesting candidate is human SERF1a (MOAG-4 in *Caenorhabditis elegans*, YDL085C-A in *S. cerevisiae*), which is a small, highly conserved protein having an undefined function, but which promotes amyloid formation [291,292]. Deletion or over-expression of SERF1a or YDL085C-A in yeast and determining the distribution of prion variants that form would show whether this protein could be involved in modulating amyloid polymorphism and the pathological variation observed with protein conformational disorders. Additionally, identifying novel factors involved in the propagation of prion variants is also an important area for investigation, as this might provide new targets for intervention of the amyloid cascade. Hence, it should be tested whether deletion of YDL085C-A alters the propagation of particular prion variants.

6.5.3 Influence of Localization and Clearance on Prion Variants

Another mechanism that might influence the ability of distinct aggregate structures to dictate phenotypic variation is where the aggregates localize. It is easy to envision that aggregates of one prion variant might localize predominantly to one part of the cell, whereas aggregates of another prion variant might localize to a different part of the cell. This would result in distinct interactions with subcellular organelles, and likely different cellular responses. It has been recognized that yeast have distinct compartments to partition misfolded proteins called the JUNQ and the IPOD [293]. Substrates that are ubiquitinated and targeted for proteasomal degradation are targeted to the JUNQ, whereas terminally aggregated substrates, such as both the [*RNQ*+] and [URE3] prions, have been found to localize to the IPOD [293]. However, an

uncharacterized [*RNQ*+] variant was used in this analysis. Interestingly, manipulation of the ubiquitin proteasome system can direct substrates from one compartment to the other compartment. Therefore, the dynamics of localization between the JUNQ and the IPOD should be determined for particular prion variants of [*PSI*+] or [*RNQ*+], and whether they localize to other parts of the cell. To minimize the possibility of artifacts that can arise with over-expression of tagged proteins, ideally this would be performed using immunohistochemistry.

Additionally, just as prion variants can have distinct abilities to incorporate monomeric protein into aggregates, it is also possible that the clearance mechanisms of certain aggregate structures are different. My work has already shown that chaperones differentially interact with distinct conformers [34], but other parts of protein quality control might also be different. Hence, using pulse-chase studies, it should be tested whether the turnover of Rnq1 is different in cells propagating different [*RNQ*+] variants. Additionally, Rnq1 could also be differentially ubiquitinated when a certain [*RNQ*+] variant is present. If the clearance mechanisms are altered for different prion variants, this could influence how quickly monomer is sequestered, or in the case of human disease, how quickly the aggregates spread.

6.6 Conclusions

The phenomenon of amyloid polymorphism is a feature that spans numerous disease-related proteins, and is also present in functional amyloid [2,10,20,294]. The work presented in this dissertation reveals the complicated nature underlying the variation in amyloid structure and how it influences phenotypic variability. In the coming years, it will be important to gain a better understanding of precisely what the structural differences are and how such variation modulates the interaction with the proteostasis network. This will be critical to elucidating how amyloid

polymorphism influences variation in pathology in the case of protein conformational disorders, or phenotype in the case of the regulatory processes that involve functional amyloid.

REFERENCES

1. Selkoe DJ (2003) Folding proteins in fatal ways. Nature 426: 900–904. doi:10.1038/nature02264.

2. Chiti F, Dobson CM (2006) Protein misfolding, functional amyloid, and human disease. Annu Rev Biochem 75: 333–366. doi:10.1146/annurev.biochem.75.101304.123901.

3. Taylor JP, Hardy J, Fischbeck KH (2002) Toxic proteins in neurodegenerative disease. Science 296: 1991–1995. doi:10.1126/science.1067122.

4. Prusiner SB (2013) Biology and Genetics of Prions Causing Neurodegeneration. Annu Rev Genet 47: 601–623. doi:10.1146/annurev-genet-110711-155524.

5. Colby DW, Prusiner SB (2011) Prions. Cold Spring Harbor Perspectives in Biology 3: a006833. doi:10.1101/cshperspect.a006833.

6. Brundin P, Melki R, Kopito R (2010) Prion-like transmission of protein aggregates in neurodegenerative diseases. Nat Rev Mol Cell Biol 11: 301–307. doi:10.1038/nrm2873.

7. Biasini E, Turnbaugh JA, Unterberger U, Harris DA (2011) Prion protein at the crossroads of physiology and disease. Trends Neurosci: 1–12. doi:10.1016/j.tins.2011.10.002.

8. King OD, Gitler AD, Shorter J (2012) The tip of the iceberg: RNA-binding proteins with prion-like domains in neurodegenerative disease. Brain research 1462: 61–80. doi:10.1016/j.brainres.2012.01.016.

9. Eisenberg D, Jucker M (2012) The Amyloid State of Proteins in Human Diseases. Cell 148: 1188–1203. doi:10.1016/j.cell.2012.02.022.

10. Fowler DM, Koulov AV, Balch WE, Kelly JW (2007) Functional amyloid--from bacteria to humans. Trends Biochem Sci 32: 217–224. doi:10.1016/j.tibs.2007.03.003.

11. Stein KC, True HL (2011) The [RNQ+] prion: a model of both functional and pathological amyloid. Prion 5: 291–298. doi:10.4161/pri.18213.

12. Halfmann R, Lindquist S (2010) Epigenetics in the extreme: prions and the inheritance of environmentally acquired traits. Science 330: 629–632. doi:10.1126/science.1191081.

13. Shorter J, Lindquist S (2005) Prions as adaptive conduits of memory and inheritance. Nat Rev Genet 6: 435–450. doi:10.1038/nrg1616.

14. Liebman SW, Chernoff YO (2012) Prions in yeast. Genetics 191: 1041–1072. doi:10.1534/genetics.111.137760.

15. True HL, Lindquist SL (2000) A yeast prion provides a mechanism for genetic variation and phenotypic diversity. Nature 407: 477–483. doi:10.1038/35035005.

16. Dobson CM (2003) Protein folding and misfolding. Nature 426: 884–890. doi:10.1038/nature02261.

17. Collinge J, Clarke AR (2007) A general model of prion strains and their pathogenicity. Science 318: 930–936. doi:10.1126/science.1138718.

18. Bessen RA, Marsh RF (1994) Distinct PrP properties suggest the molecular basis of strain variation in transmissible mink encephalopathy. J Virol 68: 7859–7868.

19. Requena JR, Wille H (2014) The structure of the infectious prion protein: Experimental data and molecular models. Prion 8: 60–66. doi:10.4161/pri.28368.

20. Toyama BH, Weissman JS (2011) Amyloid Structure: Conformational Diversity and Consequences. Annu Rev Biochem 80: 557–585. doi:10.1146/annurev-biochem-090908-120656.

21. Surewicz WK, Apostol MI (2011) Prion protein and its conformational conversion: a structural perspective. Topics in current chemistry 305: 135–167. doi:10.1007/128_2011_165.

22. Smirnovas V, Baron GS, Offerdahl DK, Raymond GJ, Caughey B, et al. (2011) Structural organization of brain-derived mammalian prions examined by hydrogen-deuterium exchange. Nat Struct Mol Biol 18: 504–506. doi:10.1038/nsmb.2035.

23. Kim C, Haldiman T, Cohen Y, Chen W, Blevins J, et al. (2011) Protease-Sensitive Conformers in Broad Spectrum of Distinct PrPSc Structures in Sporadic Creutzfeldt-Jakob Disease Are Indicator of Progression Rate. PLoS Pathog 7: e1002242. doi:10.1371/journal.ppat.1002242.t001.

24. Derkatch IL, Chernoff YO, Kushnirov VV, Inge-Vechtomov SG, Liebman SW (1996) Genesis and variability of [PSI] prion factors in Saccharomyces cerevisiae. Genetics 144: 1375–1386.

25. Tanaka M, Collins SR, Toyama BH, Weissman JS (2006) The physical basis of how prion conformations determine strain phenotypes. Nature 442: 585–589. doi:10.1038/nature04922.

26. Toyama BH, Kelly MJS, Gross JD, Weissman JS (2007) The structural basis of yeast prion strain variants. Nature 449: 233–237. doi:10.1038/nature06108.

27. Colby DW, Giles K, Legname G, Wille H, Baskakov IV, et al. (2009) Design and construction of diverse mammalian prion strains. Proc Natl Acad Sci USA 106: 20417–20422. doi:10.1073/pnas.0910350106.

28. Cobb NJ, Apostol MI, Chen S, Smirnovas V, Surewicz WK (2014) Conformational stability of mammalian prion protein amyloid fibrils is dictated by a packing polymorphism within the core region. J Biol Chem 289: 2643–2650. doi:10.1074/jbc.M113.520718.

29. Ayers JI, Schutt CR, Shikiya RA, Aguzzi A, Kincaid AE, et al. (2011) The strain-encoded relationship between PrP replication, stability and processing in neurons is predictive of the incubation period of disease. PLoS Pathog 7: e1001317. doi:10.1371/journal.ppat.1001317.

30. Angers RC, Kang H-E, Napier D, Browning S, Seward T, et al. (2010) Prion strain mutation determined by prion protein conformational compatibility and primary structure. Science 328: 1154–1158. doi:10.1126/science.1187107.

31. Bradley ME, Edskes HK, Hong JY, Wickner RB, Liebman SW (2002) Interactions among prions and prion "strains" in yeast. Proc Natl Acad Sci USA 99 Suppl 4: 16392–16399. doi:10.1073/pnas.152330699.

32. Huang VJ, Stein KC, True HL (2013) Spontaneous Variants of the [RNQ+] Prion in Yeast Demonstrate the Extensive Conformational Diversity Possible with Prion Proteins. PLoS ONE 8: e79582. doi:10.1371/journal.pone.0079582.

33. Kalastavadi T, True HL (2010) Analysis of the [RNQ+] prion reveals stability of amyloid fibers as the key determinant of yeast prion variant propagation. J Biol Chem 285: 20748–20755. doi:10.1074/jbc.M110.115303.

34. Stein KC, True HL (2014) Extensive Diversity of Prion Strains is Defined by Differential Chaperone Interactions and Distinct Amyloidogenic Regions. PLoS Genet 10: e1004337. doi: 10.1371/journal.pgen.1004337.

35. Westergard L, True HL (2014) Wild yeast harbour a variety of distinct amyloid structures with strong prion-inducing capabilities. Mol Microbiol 92: 183–193. doi:10.1111/mmi.12543.

36. Belli M, Ramazzotti M, Chiti F (2011) Prediction of amyloid aggregation in vivo. EMBO Rep 12: 657–663. doi:10.1038/embor.2011.116.

37. Douglas PM, Treusch S, Ren H-Y, Halfmann R, Duennwald ML, et al. (2008) Chaperone-dependent amyloid assembly protects cells from prion toxicity. Proc Natl Acad Sci USA 105: 7206–7211. doi:10.1073/pnas.0802593105.

38. Frederick KK, Debelouchina GT, Kayatekin C, Dorminy T, Jacavone AC, et al. (2014) Distinct Prion Strains Are Defined by Amyloid Core Structure and Chaperone Binding Site Dynamics. Chem Biol: 1–11. doi:10.1016/j.chembiol.2013.12.013.

39. Supattapone S (2013) Elucidating the role of cofactors in mammalian prion propagation. Prion 8: 100–104.

40. Li L, Kowal AS (2012) Environmental Regulation of Prions in Yeast. PLoS Pathog 8: e1002973. doi:10.1371/journal.ppat.1002973.g002.

41. Westergard L, True HL (2014) Extracellular environment modulates the formation and propagation of particular amyloid structures. Mol Microbiol. doi:10.1111/mmi.12579.

42. Petkova AT, Ishii Y, Balbach JJ, Antzutkin ON, Leapman RD, et al. (2002) A structural model for Alzheimer's beta -amyloid fibrils based on experimental constraints from solid state NMR. Proc Natl Acad Sci USA 99: 16742–16747. doi:10.1073/pnas.262663499.

43. Sawaya MR, Sambashivan S, Nelson R, Ivanova MI, Sievers SA, et al. (2007) Atomic structures of amyloid cross-beta spines reveal varied steric zippers. Nature 447: 453–457. doi:10.1038/nature05695.

44. Wiltzius JJW, Landau M, Nelson R, Sawaya MR, Apostol MI, et al. (2009) Molecular mechanisms for protein-encoded inheritance. Nat Struct Mol Biol 16: 973–978. doi:10.1038/nsmb.1643.

45. Soto C, Estrada L, Castilla J (2006) Amyloids, prions and the inherent infectious nature of misfolded protein aggregates. Trends Biochem Sci 31: 150–155. doi:10.1016/j.tibs.2006.01.002.

46. Tuite MF, Serio TR (2010) The prion hypothesis: from biological anomaly to basic regulatory mechanism. Nat Rev Mol Cell Biol 11: 823–833. doi:10.1038/nrm3007.

47. Shewmaker F, McGlinchey RP, Wickner RB (2011) Structural Insights into Functional and Pathological Amyloid. J Biol Chem 286: 16533–16540. doi:10.1074/jbc.R111.227108.

48. Patino MM, Liu JJ, Glover JR, Lindquist S (1996) Support for the prion hypothesis for inheritance of a phenotypic trait in yeast. Science 273: 622–626.

49. Paushkin SV, Kushnirov VV, Smirnov VN, Ter-Avanesyan MD (1996) Propagation of the yeast prion-like [psi+] determinant is mediated by oligomerization of the SUP35-encoded polypeptide chain release factor. EMBO J 15: 3127–3134.

50. True HL, Berlin I, Lindquist SL (2004) Epigenetic regulation of translation reveals hidden genetic variation to produce complex traits. Nature 431: 184–187. doi:10.1038/nature02885.

51. Eaglestone SS, Cox BS, Tuite MF (1999) Translation termination efficiency can be regulated in Saccharomyces cerevisiae by environmental stress through a prion-mediated mechanism. EMBO J 18: 1974–1981. doi:10.1093/emboj/18.7.1974.

52. Masel J, Bergman A (2003) The evolution of the evolvability properties of the yeast prion [PSI+]. Evolution 57: 1498–1512.

53. Masel J (2006) Cryptic genetic variation is enriched for potential adaptations. Genetics 172: 1985–1991. doi:10.1534/genetics.105.051649.

54. Giacomelli MG, Hancock AS, Masel J (2007) The conversion of 3' UTRs into coding regions. Mol Biol Evol 24: 457–464. doi:10.1093/molbev/msl172.

55. Masel J, Griswold CK (2009) The strength of selection against the yeast prion [PSI+].

Genetics 181: 1057–1063. doi:10.1534/genetics.108.100297.

56. Lancaster AK, Bardill JP, True HL, Masel J (2010) The spontaneous appearance rate of the yeast prion [PSI+] and its implications for the evolution of the evolvability properties of the [PSI+] system. Genetics 184: 393–400. doi:10.1534/genetics.109.110213.

57. Wickner RB (1994) [URE3] as an altered URE2 protein: evidence for a prion analog in Saccharomyces cerevisiae. Science 264: 566–569.

58. Derkatch IL, Bradley ME, Zhou P, Chernoff YO, Liebman SW (1997) Genetic and environmental factors affecting the de novo appearance of the [PSI+] prion in Saccharomyces cerevisiae. Genetics 147: 507–519.

59. Derkatch IL, Bradley ME, Masse SV, Zadorsky SP, Polozkov GV, et al. (2000) Dependence and independence of [PSI(+)] and [PIN(+)]: a two-prion system in yeast? EMBO J 19: 1942–1952. doi:10.1093/emboj/19.9.1942.

60. Derkatch IL, Bradley ME, Hong JY, Liebman SW (2001) Prions affect the appearance of other prions: the story of [PIN(+)]. Cell 106: 171–182.

61. Osherovich LZ, Weissman JS (2001) Multiple Gln/Asn-rich prion domains confer susceptibility to induction of the yeast [PSI(+)] prion. Cell 106: 183–194.

62. Nakayashiki T, Kurtzman CP, Edskes HK, Wickner RB (2005) Yeast prions [URE3] and [PSI+] are diseases. Proc Natl Acad Sci USA 102: 10575–10580. doi:10.1073/pnas.0504882102.

63. Resende CG, Outeiro TF, Sands L, Lindquist S, Tuite MF (2003) Prion protein gene polymorphisms in Saccharomyces cerevisiae. Mol Microbiol 49: 1005–1017.

64. Sondheimer N, Lindquist S (2000) Rnq1: an epigenetic modifier of protein function in yeast. Mol Cell 5: 163–172.

65. Bruce KL, Chernoff YO (2011) Sequence specificity and fidelity of prion transmission in yeast. Seminars in cell & developmental biology 22: 444–451. doi:10.1016/j.semcdb.2011.03.005.

66. Patel BK, Liebman SW (2007) “Prion-proof” for [PIN+]: infection with in vitro-made amyloid aggregates of Rnq1p-(132-405) induces [PIN+]. J Mol Biol 365: 773–782. doi:10.1016/j.jmb.2006.10.069.

67. Wickner RB, Dyda F, Tycko R (2008) Amyloid of Rnq1p, the basis of the [PIN+] prion, has a parallel in-register beta-sheet structure. Proc Natl Acad Sci USA 105: 2403–2408. doi:10.1073/pnas.0712032105.

68. King C-Y, Diaz-Avalos R (2004) Protein-only transmission of three yeast prion strains. Nature 428: 319–323. doi:10.1038/nature02391.

69. Tanaka M, Chien P, Naber N, Cooke R, Weissman JS (2004) Conformational variations in an infectious protein determine prion strain differences. Nature 428: 323–328. doi:10.1038/nature02392.

70. Schlumpberger M, Prusiner SB, Herskowitz I (2001) Induction of distinct [URE3] yeast prion strains. Mol Cell Biol 21: 7035–7046. doi:10.1128/MCB.21.20.7035-7046.2001.

71. Dobson CM (1999) Protein misfolding, evolution and disease. Trends Biochem Sci 24: 329–332.

72. Zoghbi HY, Orr HT (2000) Glutamine repeats and neurodegeneration. Annu Rev Neurosci 23: 217–247. doi:10.1146/annurev.neuro.23.1.217.

73. Vitrenko YA, Pavon ME, Stone SI, Liebman SW (2007) Propagation of the [PIN+] prion by fragments of Rnq1 fused to GFP. Curr Genet 51: 309–319. doi:10.1007/s00294-007-0127-0.

74. Sondheimer N, Lopez N, Craig EA, Lindquist S (2001) The role of Sis1 in the maintenance of the [RNQ+] prion. EMBO J 20: 2435–2442. doi:10.1093/emboj/20.10.2435.

75. Bardill JP, Dulle JE, Fisher JR, True HL (2009) Requirements of Hsp104p activity and Sis1p binding for propagation of the [RNQ(+)] prion. Prion 3: 151–160.

76. Shibata S, Kurahashi H, Nakamura Y (2009) Localization of prion-destabilizing mutations in the N-terminal non-prion domain of Rnq1 in Saccharomyces cerevisiae. Prion 3: 250–258.

77. Kurahashi H, Pack C-G, Shibata S, Oishi K, Sako Y, et al. (2011) [PSI(+)] aggregate enlargement in rnq1 nonprion domain mutants, leading to a loss of prion in yeast. Genes Cells 16: 576–589. doi:10.1111/j.1365-2443.2011.01511.x.

78. Bardill JP, True HL (2009) Heterologous prion interactions are altered by mutations in the prion protein Rnq1p. J Mol Biol 388: 583–596. doi:10.1016/j.jmb.2009.03.036.

79. DePace AH, Santoso A, Hillner P, Weissman JS (1998) A critical role for amino-terminal glutamine/asparagine repeats in the formation and propagation of a yeast prion. Cell 93: 1241–1252.

80. Osherovich LZ, Cox BS, Tuite MF, Weissman JS (2004) Dissection and design of yeast prions. PLoS Biol 2: E86. doi:10.1371/journal.pbio.0020086.

81. Tank EMH, Harris DA, Desai AA, True HL (2007) Prion protein repeat expansion results in increased aggregation and reveals phenotypic variability. Mol Cell Biol 27: 5445–5455. doi:10.1128/MCB.02127-06.

82. Kalastavadi T, True HL (2008) Prion protein insertional mutations increase aggregation propensity but not fiber stability. BMC Biochem 9: 7. doi:10.1186/1471-2091-9-7.

83. Parham SN, Resende CG, Tuite MF (2001) Oligopeptide repeats in the yeast protein Sup35p stabilize intermolecular prion interactions. EMBO J 20: 2111–2119. doi:10.1093/emboj/20.9.2111.

84. Kadnar ML, Articov G, Derkatch IL (2010) Distinct type of transmission barrier revealed by study of multiple prion determinants of Rnq1. PLoS Genet 6: e1000824. doi:10.1371/journal.pgen.1000824.

85. Morimoto RI (2008) Proteotoxic stress and inducible chaperone networks in neurodegenerative disease and aging. Genes Dev 22: 1427–1438. doi:10.1101/gad.1657108.

86. True HL (2006) The battle of the fold: chaperones take on prions. Trends Genet 22: 110–117. doi:10.1016/j.tig.2005.12.004.

87. Summers DW, Douglas PM, Cyr DM (2009) Prion propagation by Hsp40 molecular chaperones. Prion 3: 59–64.

88. Masison DC, Kirkland PA, Sharma D (2009) Influence of Hsp70s and their regulators on yeast prion propagation. Prion 3: 65–73.

89. Glover JR, Lindquist S (1998) Hsp104, Hsp70, and Hsp40: a novel chaperone system that rescues previously aggregated proteins. Cell 94: 73–82.

90. Tipton KA, Verges KJ, Weissman JS (2008) In vivo monitoring of the prion replication cycle reveals a critical role for Sis1 in delivering substrates to Hsp104. Mol Cell 32: 584–591. doi:10.1016/j.molcel.2008.11.003.

91. Shorter J, Lindquist S (2004) Hsp104 catalyzes formation and elimination of self-replicating Sup35 prion conformers. Science 304: 1793–1797. doi:10.1126/science.1098007.

92. Shorter J, Lindquist S (2006) Destruction or potentiation of different prions catalyzed by similar Hsp104 remodeling activities. Mol Cell 23: 425–438. doi:10.1016/j.molcel.2006.05.042.

93. Inoue Y, Taguchi H, Kishimoto A, Yoshida M (2004) Hsp104 binds to yeast Sup35 prion fiber but needs other factor(s) to sever it. J Biol Chem 279: 52319–52323. doi:10.1074/jbc.M408159200.

94. Chernoff YO, Lindquist SL, Ono B, Inge-Vechtomov SG, Liebman SW (1995) Role of the chaperone protein Hsp104 in propagation of the yeast prion-like factor [psi+]. Science 268: 880–884.

95. Higurashi T, Hines JK, Sahi C, Aron R, Craig EA (2008) Specificity of the J-protein Sis1 in the propagation of 3 yeast prions. Proc Natl Acad Sci USA 105: 16596–16601. doi:10.1073/pnas.0808934105.

96. Moriyama H, Edskes HK, Wickner RB (2000) [URE3] prion propagation in Saccharomyces cerevisiae: requirement for chaperone Hsp104 and curing by overexpressed chaperone Ydj1p. Mol Cell Biol 20: 8916–8922.

97. Kirkland PA, Reidy M, Masison DC (2011) Functions of yeast Hsp40 chaperone Sis1p dispensable for prion propagation but important for prion curing and protection from prion toxicity. Genetics 188: 565–577. doi:10.1534/genetics.111.129460.

98. Kurahashi H, Nakamura Y (2007) Channel mutations in Hsp104 hexamer distinctively affect thermotolerance and prion-specific propagation. Mol Microbiol 63: 1669–1683. doi:10.1111/j.1365-2958.2007.05629.x.

99. Aron R, Higurashi T, Sahi C, Craig EA (2007) J-protein co-chaperone Sis1 required for generation of [RNQ+] seeds necessary for prion propagation. EMBO J 26: 3794–3803. doi:10.1038/sj.emboj.7601811.

100. Lopez N, Aron R, Craig EA (2003) Specificity of class II Hsp40 Sis1 in maintenance of yeast prion [RNQ+]. Mol Biol Cell 14: 1172–1181. doi:10.1091/mbc.E02-09-0593.

101. Summers DW, Douglas PM, Ren H-Y, Cyr DM (2009) The type I Hsp40 Ydj1 utilizes a farnesyl moiety and zinc finger-like region to suppress prion toxicity. J Biol Chem 284: 3628–3639. doi:10.1074/jbc.M807369200.

102. Cheetham ME, Caplan AJ (1998) Structure, function and evolution of DnaJ: conservation and adaptation of chaperone function. Cell Stress Chaperones 3: 28–36.

103. Lu Z, Cyr DM (1998) The conserved carboxyl terminus and zinc finger-like domain of the co-chaperone Ydj1 assist Hsp70 in protein folding. J Biol Chem 273: 5970–5978.

104. Aron R, Lopez N, Walter W, Craig EA, Johnson J (2005) In vivo bipartite interaction between the Hsp40 Sis1 and Hsp70 in Saccharomyces cerevisiae. Genetics 169: 1873–1882. doi:10.1534/genetics.104.037242.

105. Sindi SS, Serio TR (2009) Prion dynamics and the quest for the genetic determinant in protein-only inheritance. Curr Opin Microbiol 12: 623–630. doi:10.1016/j.mib.2009.09.003.

106. Mathur V, Hong JY, Liebman SW (2009) Ssa1 overexpression and [PIN(+)] variants cure [PSI(+)] by dilution of aggregates. J Mol Biol 390: 155–167. doi:10.1016/j.jmb.2009.04.063.

107. Derkatch IL, Uptain SM, Outeiro TF, Krishnan R, Lindquist SL, et al. (2004) Effects of Q/N-rich, polyQ, and non-polyQ amyloids on the de novo formation of the [PSI+] prion in yeast and aggregation of Sup35 in vitro. Proc Natl Acad Sci USA 101: 12934–12939. doi:10.1073/pnas.0404968101.

108. Bagriantsev S, Liebman SW (2004) Specificity of prion assembly in vivo. [PSI+] and [PIN+] form separate structures in yeast. J Biol Chem 279: 51042–51048.

doi:10.1074/jbc.M410611200.

109. Derkatch IL, Liebman SW (2007) Prion-prion interactions. Prion 1: 161–169.

110. Sideri TC, Stojanovski K, Tuite MF, Grant CM (2010) Ribosome-associated peroxiredoxins suppress oxidative stress-induced de novo formation of the [PSI+] prion in yeast. Proc Natl Acad Sci USA 107: 6394–6399. doi:10.1073/pnas.1000347107.

111. Namy O, Galopier A, Martini C, Matsufuji S, Fabret C, et al. (2008) Epigenetic control of polyamines by the prion [PSI+]. Nat Cell Biol 10: 1069–1075. doi:10.1038/ncb1766.

112. Wickner RB, Edskes HK, Shewmaker F, Nakayashiki T (2007) Prions of fungi: inherited structures and biological roles. Nat Rev Microbiol 5: 611–618. doi:10.1038/nrmicro1708.

113. Wickner RB, Edskes HK, Shewmaker F, Nakayashiki T, Engel A, et al. (2007) Yeast prions: evolution of the prion concept. Prion 1: 94–100.

114. Namy O, Duchateau-Nguyen G, Rousset J-P (2002) Translational readthrough of the PDE2 stop codon modulates cAMP levels in Saccharomyces cerevisiae. Mol Microbiol 43: 641–652.

115. Kryndushkin DS, Engel A, Edskes H, Wickner RB (2011) Molecular chaperone Hsp104 can promote yeast prion generation. Genetics 188: 339–348. doi:10.1534/genetics.111.127779.

116. Withee JL, Sen R, Cyert MS (1998) Ion tolerance of Saccharomyces cerevisiae lacking the Ca2+/CaM-dependent phosphatase (calcineurin) is improved by mutations in URE2 or PMA1. Genetics 149: 865–878.

117. Kryndushkin DS, Alexandrov IM, Ter-Avanesyan MD, Kushnirov VV (2003) Yeast [PSI+] prion aggregates are formed by small Sup35 polymers fragmented by Hsp104. J Biol Chem 278: 49636–49643. doi:10.1074/jbc.M307996200.

118. Uptain SM, Sawicki GJ, Caughey B, Lindquist S (2001) Strains of [PSI(+)] are distinguished by their efficiencies of prion-mediated conformational conversion. EMBO J 20: 6236–6245. doi:10.1093/emboj/20.22.6236.

119. Legname G, Nguyen H-OB, Baskakov IV, Cohen FE, DeArmond SJ, et al. (2005) Strain-specified characteristics of mouse synthetic prions. Proc Natl Acad Sci USA 102: 2168–2173. doi:10.1073/pnas.0409079102.

120. Bradley ME, Liebman SW (2003) Destabilizing interactions among [PSI(+)] and [PIN(+)] yeast prion variants. Genetics 165: 1675–1685.

121. Vitrenko YA, Gracheva EO, Richmond JE, Liebman SW (2007) Visualization of aggregation of the Rnq1 prion domain and cross-seeding interactions with Sup35NM. J Biol Chem 282: 1779–1787. doi:10.1074/jbc.M609269200.

122. Salnikova AB, Kryndushkin DS, Smirnov VN, Kushnirov VV, Ter-Avanesyan MD (2005) Nonsense suppression in yeast cells overproducing Sup35 (eRF3) is caused by its non-heritable amyloids. J Biol Chem 280: 8808–8812. doi:10.1074/jbc.M410150200.

123. Schwimmer C, Masison DC (2002) Antagonistic interactions between yeast [PSI(+)] and [URE3] prions and curing of [URE3] by Hsp70 protein chaperone Ssa1p but not by Ssa2p. Mol Cell Biol 22: 3590–3598.

124. Kurahashi H, Ishiwata M, Shibata S, Nakamura Y (2008) A regulatory role of the Rnq1 nonprion domain for prion propagation and polyglutamine aggregates. Mol Cell Biol 28: 3313–3323. doi:10.1128/MCB.01900-07.

125. Kurahashi H, Shibata S, Ishiwata M, Nakamura Y (2009) Selfish prion of Rnq1 mutant in yeast. Genes Cells 14: 659–668. doi:10.1111/j.1365-2443.2009.01297.x.

126. Krobitsch S, Lindquist S (2000) Aggregation of huntingtin in yeast varies with the length of the polyglutamine expansion and the expression of chaperone proteins. Proc Natl Acad Sci USA 97: 1589–1594.

127. Meriin AB, Zhang X, He X, Newnam GP, Chernoff YO, et al. (2002) Huntington toxicity in yeast model depends on polyglutamine aggregation mediated by a prion-like protein Rnq1. J Cell Biol 157: 997–1004. doi:10.1083/jcb.200112104.

128. Gokhale KC, Newnam GP, Sherman MY, Chernoff YO (2005) Modulation of prion-dependent polyglutamine aggregation and toxicity by chaperone proteins in the yeast model. J Biol Chem 280: 22809–22818. doi:10.1074/jbc.M500390200.

129. Muchowski PJ, Schaffar G, Sittler A, Wanker EE, Hayer-Hartl MK, et al. (2000) Hsp70 and hsp40 chaperones can inhibit self-assembly of polyglutamine proteins into amyloid-like fibrils. Proc Natl Acad Sci USA 97: 7841–7846. doi:10.1073/pnas.140202897.

130. Goehler H, Dröge A, Lurz R, Schnoegl S, Chernoff YO, et al. (2010) Pathogenic polyglutamine tracts are potent inducers of spontaneous Sup35 and Rnq1 amyloidogenesis. PLoS ONE 5: e9642. doi:10.1371/journal.pone.0009642.

131. Urakov VN, Vishnevskaya AB, Alexandrov IM, Kushnirov VV, Smirnov VN, et al. (2010) Interdependence of amyloid formation in yeast: implications for polyglutamine disorders and biological functions. Prion 4: 45–52.

132. Duennwald ML, Jagadish S, Giorgini F, Muchowski PJ, Lindquist S (2006) A network of protein interactions determines polyglutamine toxicity. Proc Natl Acad Sci USA 103: 11051–11056. doi:10.1073/pnas.0604548103.

133. Duennwald ML, Jagadish S, Muchowski PJ, Lindquist S (2006) Flanking sequences profoundly alter polyglutamine toxicity in yeast. Proc Natl Acad Sci USA 103: 11045–11050. doi:10.1073/pnas.0604547103.

134. Meriin AB, Zhang X, Miliaras NB, Kazantsev A, Chernoff YO, et al. (2003)

Aggregation of expanded polyglutamine domain in yeast leads to defects in endocytosis. Mol Cell Biol 23: 7554–7565.

135. Meriin AB, Zhang X, Alexandrov IM, Salnikova AB, Ter-Avanesian MD, et al. (2007) Endocytosis machinery is involved in aggregation of proteins with expanded polyglutamine domains. FASEB J 21: 1915–1925. doi:10.1096/fj.06-6878com.

136. Wang Y, Meriin AB, Costello CE, Sherman MY (2007) Characterization of proteins associated with polyglutamine aggregates: a novel approach towards isolation of aggregates from protein conformation disorders. Prion 1: 128–135.

137. Manogaran AL, Hong JY, Hufana J, Tyedmers J, Lindquist S, et al. (2011) Prion formation and polyglutamine aggregation are controlled by two classes of genes. PLoS Genet 7: e1001386. doi:10.1371/journal.pgen.1001386.

138. Derkatch IL, Bradley ME, Liebman SW (1998) Overexpression of the SUP45 gene encoding a Sup35p-binding protein inhibits the induction of the de novo appearance of the [PSI+] prion. Proc Natl Acad Sci USA 95: 2400–2405.

139. Vishveshwara N, Bradley ME, Liebman SW (2009) Sequestration of essential proteins causes prion associated toxicity in yeast. Mol Microbiol 73: 1101–1114. doi:10.1111/j.1365-2958.2009.06836.x.

140. Douglas PM, Summers DW, Ren H-Y, Cyr DM (2009) Reciprocal efficiency of RNQ1 and polyglutamine detoxification in the cytosol and nucleus. Mol Biol Cell 20: 4162–4173. doi:10.1091/mbc.E09-02-0170.

141. Fan C-Y, Ren H-Y, Lee P, Caplan AJ, Cyr DM (2005) The type I Hsp40 zinc finger-like region is required for Hsp70 to capture non-native polypeptides from Ydj1. J Biol Chem 280: 695–702. doi:10.1074/jbc.M410645200.

142. Li J, Qian X, Sha B (2003) The crystal structure of the yeast Hsp40 Ydj1 complexed with its peptide substrate. Structure 11: 1475–1483.

143. Berthelot K, Ta HP, Géan J, Lecomte S, Cullin C (2011) In Vivo and In Vitro Analyses of Toxic Mutants of HET-s: FTIR Antiparallel Signature Correlates with Amyloid Toxicity. J Mol Biol: 1–16. doi:10.1016/j.jmb.2011.07.009.

144. Mitchell-Olds T, Willis JH, Goldstein DB (2007) Which evolutionary processes influence natural genetic variation for phenotypic traits? Nat Rev Genet 8: 845–856. doi:10.1038/nrg2207.

145. Quintana-Murci L, Barreiro LB (2010) The role played by natural selection on Mendelian traits in humans. Annals of the New York Academy of Sciences 1214: 1–17. doi:10.1111/j.1749-6632.2010.05856.x.

146. Kim YE, Hipp MS, Bracher A, Hayer-Hartl M, Ulrich Hartl F (2013) Molecular Chaperone Functions in Protein Folding and Proteostasis. Annu Rev Biochem 82: 323–

355. doi:10.1146/annurev-biochem-060208-092442.

147. Eichner T, Radford SE (2011) A Diversity of Assembly Mechanisms of a Generic Amyloid Fold. Mol Cell 43: 8–18. doi:10.1016/j.molcel.2011.05.012.

148. Kampinga HH, Craig EA (2010) The HSP70 chaperone machinery: J proteins as drivers of functional specificity. Nat Rev Mol Cell Biol 11: 579–592. doi:10.1038/nrm2941.

149. Laufen T, Mayer MP, Beisel C, Klostermeier D, Mogk A, et al. (1999) Mechanism of regulation of hsp70 chaperones by DnaJ cochaperones. Proc Natl Acad Sci USA 96: 5452–5457.

150. Yan W, Craig EA (1999) The glycine-phenylalanine-rich region determines the specificity of the yeast Hsp40 Sis1. Mol Cell Biol 19: 7751–7758.

151. Rüdiger S, Germeroth L, Schneider-Mergener J, Bukau B (1997) Substrate specificity of the DnaK chaperone determined by screening cellulose-bound peptide libraries. EMBO J 16: 1501–1507. doi:10.1093/emboj/16.7.1501.

152. Rüdiger S, Schneider-Mergener J, Bukau B (2001) Its substrate specificity characterizes the DnaJ co-chaperone as a scanning factor for the DnaK chaperone. EMBO J 20: 1042–1050. doi:10.1093/emboj/20.5.1042.

153. Srinivasan SR, Gillies AT, Chang L, Thompson AD, Gestwicki JE (2012) Molecular chaperones DnaK and DnaJ share predicted binding sites on most proteins in the E. coli proteome. Mol Biosyst 8: 2323. doi:10.1039/c2mb25145k.

154. Balch WE, Morimoto RI, Dillin A, Kelly JW (2008) Adapting proteostasis for disease intervention. Science 319: 916–919. doi:10.1126/science.1141448.

155. Taylor RC, Dillin A (2011) Aging as an Event of Proteostasis Collapse. Cold Spring Harbor Perspectives in Biology 3: a004440–a004440. doi:10.1101/cshperspect.a004440.

156. Auluck PK, Chan HYE, Trojanowski JQ, Lee VM-Y, Bonini NM (2002) Chaperone suppression of alpha-synuclein toxicity in a Drosophila model for Parkinson's disease. Science 295: 865–868. doi:10.1126/science.1067389.

157. Kakkar V, Prins LCB, Kampinga HH (2012) DNAJ proteins and protein aggregation diseases. Curr Top Med Chem 12: 2479–2490.

158. Macario AJL, Conway de Macario E (2007) Chaperonopathies by defect, excess, or mistake. Annals of the New York Academy of Sciences 1113: 178–191. doi:10.1196/annals.1391.009.

159. Harms MB, Sommerville RB, Allred P, Bell S, Ma D, et al. (2012) Exome sequencing reveals DNAJB6 mutations in dominantly-inherited myopathy. Ann Neurol 71: 407–416. doi:10.1002/ana.22683.

160. Sarparanta J, Jonson PH, Golzio C, Sandell S, Luque H, et al. (2012) Mutations affecting the cytoplasmic functions of the co-chaperone DNAJB6 cause limb-girdle muscular dystrophy. Nat Genet 44: 450–455. doi:10.1038/ng.1103.

161. Sato T, Hayashi YK, Oya Y, Kondo T, Sugie K, et al. (2013) DNAJB6 myopathy in an Asian cohort and cytoplasmic/nuclear inclusions. Neuromuscular Disorders 23: 269–276. doi:10.1016/j.nmd.2012.12.010.

162. Couthouis J, Raphael AR, Siskind C, Findlay AR, Buenrostro JD, et al. (2014) Exome sequencing identifies a DNAJB6 mutation in a family with dominantly-inherited limb-girdle muscular dystrophy. Neuromuscular Disorders: 1–5. doi:10.1016/j.nmd.2014.01.014.

163. Mitsuhashi S, Kang PB (2012) Update on the Genetics of Limb Girdle Muscular Dystrophy. Seminars in Pediatric Neurology 19: 211–218. doi:10.1016/j.spen.2012.09.008.

164. Watts GDJ, Wymer J, Kovach MJ, Mehta SG, Mumm S, et al. (2004) Inclusion body myopathy associated with Paget disease of bone and frontotemporal dementia is caused by mutant valosin-containing protein. Nat Genet 36: 377–381. doi:10.1038/ng1332.

165. Selcen D, Muntoni F, Burton BK, Pegoraro E, Sewry C, et al. (2009) Mutation in BAG3 causes severe dominant childhood muscular dystrophy. Ann Neurol 65: 83–89. doi:10.1002/ana.21553.

166. Vicart P, Caron A, Guicheney P, Li Z, Prévost MC, et al. (1998) A missense mutation in the alphaB-crystallin chaperone gene causes a desmin-related myopathy. Nat Genet 20: 92–95. doi:10.1038/1765.

167. Miller G (2009) Neurodegeneration. Could they all be prion diseases? Science 326: 1337–1339. doi:10.1126/science.326.5958.1337.

168. Soto C (2012) Transmissible Proteins: Expanding the Prion Heresy. Cell 149: 968–977. doi:10.1016/j.cell.2012.05.007.

169. Pan KM, Baldwin M, Nguyen J, Gasset M, Serban A, et al. (1993) Conversion of alpha-helices into beta-sheets features in the formation of the scrapie prion proteins. Proc Natl Acad Sci USA 90: 10962–10966.

170. Petkova AT, Leapman RD, Guo Z, Yau W-M, Mattson MP, et al. (2005) Self-propagating, molecular-level polymorphism in Alzheimer's beta-amyloid fibrils. Science 307: 262–265. doi:10.1126/science.1105850.

171. Guo JL, Covell DJ, Daniels JP, Iba M, Stieber A, et al. (2013) Distinct α-Synuclein Strains Differentially Promote Tau Inclusions in Neurons. Cell 154: 103–117. doi:10.1016/j.cell.2013.05.057.

172. Safar JG (2012) Molecular pathogenesis of sporadic prion diseases in man. Prion 6:

108–115. doi:10.4161/pri.18666.

173. McGlinchey RP, Kryndushkin D, Wickner RB (2011) Suicidal [PSI+] is a lethal yeast prion. Proc Natl Acad Sci USA 108: 5337–5341. doi:10.1073/pnas.1102762108.

174. Kochneva-Pervukhova NV, Chechenova MB, Valouev IA, Kushnirov VV, Smirnov VN, et al. (2001) [Psi(+)] prion generation in yeast: characterization of the "strain" difference. Yeast 18: 489–497. doi:10.1002/yea.700.

175. Lin J-Y, Liao T-Y, Lee H-C, King C-Y (2011) Inter-Allelic Prion Propagation Reveals Conformational Relationships among a Multitude of [PSI] Strains. PLoS Genet 7: e1002297. doi:10.1371/journal.pgen.1002297.t004.

176. Krishnan R, Lindquist SL (2005) Structural insights into a yeast prion illuminate nucleation and strain diversity. Nature 435: 765–772. doi:10.1038/nature03679.

177. Ter-Avanesyan MD, Kushnirov VV, Dagkesamanskaya AR, Didichenko SA, Chernoff YO, et al. (1993) Deletion analysis of the SUP35 gene of the yeast Saccharomyces cerevisiae reveals two non-overlapping functional regions in the encoded protein. Mol Microbiol 7: 683–692.

178. Ter-Avanesyan MD, Dagkesamanskaya AR, Kushnirov VV, Smirnov VN (1994) The SUP35 omnipotent suppressor gene is involved in the maintenance of the non-Mendelian determinant [psi+] in the yeast Saccharomyces cerevisiae. Genetics 137: 671–676.

179. Alberti S, Halfmann R, King O, Kapila A, Lindquist S (2009) A systematic survey identifies prions and illuminates sequence features of prionogenic proteins. Cell 137: 146–158. doi:10.1016/j.cell.2009.02.044.

180. Bradley ME, Liebman SW (2004) The Sup35 domains required for maintenance of weak, strong or undifferentiated yeast [PSI+] prions. Mol Microbiol 51: 1649–1659.

181. Chang H-Y, Lin J-Y, Lee H-C, Wang H-L, King C-Y (2008) Strain-specific sequences required for yeast [PSI+] prion propagation. Proc Natl Acad Sci USA 105: 13345–13350. doi:10.1073/pnas.0802215105.

182. Legname G, Nguyen H-OB, Peretz D, Cohen FE, DeArmond SJ, et al. (2006) Continuum of prion protein structures enciphers a multitude of prion isolate-specified phenotypes. Proc Natl Acad Sci USA 103: 19105–19110. doi:10.1073/pnas.0608970103.

183. Peretz D, Scott MR, Groth D, Williamson RA, Burton DR, et al. (2001) Strain-specified relative conformational stability of the scrapie prion protein. Protein Sci 10: 854–863. doi:10.1110/ps.39201.

184. Sharma J, Liebman SW (2013) Exploring the basis of [PIN(+)] variant differences in [PSI(+)] induction. J Mol Biol 425: 3046–3059. doi:10.1016/j.jmb.2013.06.006.

185. Bagriantsev SN, Gracheva EO, Richmond JE, Liebman SW (2008) Variant-specific [PSI+] infection is transmitted by Sup35 polymers within [PSI+] aggregates with heterogeneous protein composition. Mol Biol Cell 19: 2433–2443. doi:10.1091/mbc.E08-01-0078.

186. Serio TR, Lindquist SL (2000) Protein-only inheritance in yeast: something to get [PSI+]-ched about. Trends Cell Biol 10: 98–105.

187. Stansfield I, Jones KM, Tuite MF (1995) The end in sight: terminating translation in eukaryotes. Trends Biochem Sci 20: 489–491.

188. Kabani M, Melki R (2011) Yeast prions assembly and propagation: contributions of the prion and non-prion moieties and the nature of assemblies. Prion 5: 277–284. doi:10.4161/pri.5.4.18070.

189. Liebman SW, Bagriantsev SN, Derkatch IL (2006) Biochemical and genetic methods for characterization of [PIN+] prions in yeast. METHODS 39: 23–34. doi:10.1016/j.ymeth.2006.04.010.

190. Maurer-Stroh S, Debulpaep M, Kuemmerer N, López de la Paz M, Martins IC, et al. (2010) Exploring the sequence determinants of amyloid structure using position-specific scoring matrices. Nat Chem Biol 7: 237–242. doi:10.1038/nmeth.1432.

191. Tartaglia GG, Vendruscolo M (2008) The Zyggregator method for predicting protein aggregation propensities. Chem Soc Rev 37: 1395–1401. doi:10.1039/b706784b.

192. Trovato A, Chiti F, Maritan A, Seno F (2006) Insight into the structure of amyloid fibrils from the analysis of globular proteins. PLoS Comput Biol 2: e170. doi:10.1371/journal.pcbi.0020170.

193. Conchillo-Solé O, de Groot NS, Avilés FX, Vendrell J, Daura X, et al. (2007) AGGRESCAN: a server for the prediction and evaluation of "hot spots" of aggregation in polypeptides. BMC Bioinformatics 8: 65. doi:10.1186/1471-2105-8-65.

194. Fernandez-Escamilla A-M, Rousseau F, Schymkowitz J, Serrano L (2004) Prediction of sequence-dependent and mutational effects on the aggregation of peptides and proteins. Nat Biotech 22: 1302–1306. doi:10.1038/nbt1012.

195. Pechmann S, Levy ED, Tartaglia GG, Vendruscolo M (2009) Physicochemical principles that regulate the competition between functional and dysfunctional association of proteins. Proc Natl Acad Sci USA 106: 10159–10164. doi:10.1073/pnas.0812414106.

196. Dosztányi Z, Mészáros B, Simon I (2009) ANCHOR: web server for predicting protein binding regions in disordered proteins. Bioinformatics 25: 2745–2746. doi:10.1093/bioinformatics/btp518.

197. Mészáros B, Simon I, Dosztányi Z (2009) Prediction of protein binding regions in disordered proteins. PLoS Comput Biol 5: e1000376. doi:10.1371/journal.pcbi.1000376.

198. Allen KD, Wegrzyn RD, Chernova TA, Müller S, Newnam GP, et al. (2005) Hsp70 chaperones as modulators of prion life cycle: novel effects of Ssa and Ssb on the Saccharomyces cerevisiae prion [PSI+]. Genetics 169: 1227–1242. doi:10.1534/genetics.104.037168.

199. Ohhashi Y, Ito K, Toyama BH, Weissman JS, Tanaka M (2010) Differences in prion strain conformations result from non-native interactions in a nucleus. Nat Chem Biol 6: 225–230. doi:10.1038/nchembio.306.

200. Liu J-J, Sondheimer N, Lindquist SL (2002) Changes in the middle region of Sup35 profoundly alter the nature of epigenetic inheritance for the yeast prion [PSI+]. Proc Natl Acad Sci USA 99 Suppl 4: 16446–16453. doi:10.1073/pnas.252652099.

201. Maddelein ML, Wickner RB (1999) Two prion-inducing regions of Ure2p are nonoverlapping. Mol Cell Biol 19: 4516–4524.

202. Lakhani VV, Ding F, Dokholyan NV (2010) Polyglutamine induced misfolding of huntingtin exon1 is modulated by the flanking sequences. PLoS Comput Biol 6: e1000772. doi:10.1371/journal.pcbi.1000772.

203. Darnell G, Orgel JPRO, Pahl R, Meredith SC (2007) Flanking polyproline sequences inhibit beta-sheet structure in polyglutamine segments by inducing PPII-like helix structure. J Mol Biol 374: 688–704. doi:10.1016/j.jmb.2007.09.023.

204. Padrick SB, Miranker AD (2001) Islet amyloid polypeptide: identification of long-range contacts and local order on the fibrillogenesis pathway. J Mol Biol 308: 783–794. doi:10.1006/jmbi.2001.4608.

205. Reumers J, Maurer-Stroh S, Schymkowitz J, Rousseau FD (2009) Protein sequences encode safeguards against aggregation. Hum Mutat 30: 431–437. doi:10.1002/humu.20905.

206. Krzewska J, Tanaka M, Burston SG, Melki R (2007) Biochemical and functional analysis of the assembly of full-length Sup35p and its prion-forming domain. J Biol Chem 282: 1679–1686. doi:10.1074/jbc.M608110200.

207. Glover JR, Kowal AS, Schirmer EC, Patino MM, Liu JJ, et al. (1997) Self-seeded fibers formed by Sup35, the protein determinant of [PSI+], a heritable prion-like factor of S. cerevisiae. Cell 89: 811–819.

208. Baxa U, Keller PW, Cheng N, Wall JS, Steven AC (2011) In Sup35p filaments (the [PSI+] prion), the globular C-terminal domains are widely offset from the amyloid fibril backbone. Mol Microbiol 79: 523–532. doi:10.1111/j.1365-2958.2010.07466.x.

209. Ross ED, Minton A, Wickner RB (2005) Prion domains: sequences, structures and interactions. Nat Cell Biol 7: 1039–1044.

210. Toombs JA, Liss NM, Cobble KR, Ben-Musa Z, Ross ED (2011) [PSI+] maintenance is

dependent on the composition, not primary sequence, of the oligopeptide repeat domain. PLoS ONE 6: e21953. doi:10.1371/journal.pone.0021953.

211. Helsen CW, Glover JR (2012) Insight into molecular basis of curing of [PSI+] prion by overexpression of 104-kDa heat shock protein (Hsp104). J Biol Chem 287: 542–556. doi:10.1074/jbc.M111.302869.

212. Borchsenius AS, Müller S, Newnam GP, Inge-Vechtomov SG, Chernoff YO (2006) Prion variant maintained only at high levels of the Hsp104 disaggregase. Curr Genet 49: 21–29. doi:10.1007/s00294-005-0035-0.

213. Borchsenius AS, Wegrzyn RD, Newnam GP, Inge-Vechtomov SG, Chernoff YO (2001) Yeast prion protein derivative defective in aggregate shearing and production of new 'seeds'. EMBO J 20: 6683–6691. doi:10.1093/emboj/20.23.6683.

214. Alexandrov AI, Polyanskaya AB, Serpionov GV, Ter-Avanesyan MD, Kushnirov VV (2012) The Effects of Amino Acid Composition of Glutamine-Rich Domains on Amyloid Formation and Fragmentation. PLoS ONE 7: e46458. doi:10.1371/journal.pone.0046458.t002.

215. Hines JK, Higurashi T, Srinivasan M, Craig EA (2011) Influence of prion variant and yeast strain variation on prion-molecular chaperone requirements. Prion 5: 238–244. doi:10.4161/pri.17818.

216. Hartl FU, Bracher A, Hayer-Hartl M (2011) Molecular chaperones in protein folding and proteostasis. Nature 475: 324–332. doi:10.1038/nature10317.

217. Serio TR, Lindquist SL (1999) [PSI+]: an epigenetic modulator of translation termination efficiency. Annu Rev Cell Dev Biol 15: 661–703. doi:10.1146/annurev.cellbio.15.1.661.

218. Tuite MF, Cox BS (2003) Propagation of yeast prions. Nat Rev Mol Cell Biol 4: 878–890. doi:10.1038/nrm1247.

219. Lum R, Tkach JM, Vierling E, Glover JR (2004) Evidence for an unfolding/threading mechanism for protein disaggregation by Saccharomyces cerevisiae Hsp104. J Biol Chem 279: 29139–29146. doi:10.1074/jbc.M403777200.

220. Tessarz P, Mogk A, Bukau B (2008) Substrate threading through the central pore of the Hsp104 chaperone as a common mechanism for protein disaggregation and prion propagation. Mol Microbiol 68: 87–97. doi:10.1111/j.1365-2958.2008.06135.x.

221. Winkler J, Tyedmers J, Bukau B, Mogk A (2012) Hsp70 targets Hsp100 chaperones to substrates for protein disaggregation and prion fragmentation. J Cell Biol 198: 387–404. doi:10.1083/jcb.201201074.

222. Craig EA, Huang P, Aron R, Andrew A (2006) The diverse roles of J-proteins, the obligate Hsp70 co-chaperone. Rev Physiol Biochem Pharmacol 156: 1–21.

223. Lu Z, Cyr DM (1998) Protein folding activity of Hsp70 is modified differentially by the hsp40 co-chaperones Sis1 and Ydj1. J Biol Chem 273: 27824–27830.

224. Sha B, Lee S, Cyr DM (2000) The crystal structure of the peptide-binding fragment from the yeast Hsp40 protein Sis1. Structure 8: 799–807.

225. Li J, Qian X, Sha B (2009) Heat shock protein 40: structural studies and their functional implications. Protein Pept Lett 16: 606–612.

226. Freeman BC, Myers MP, Schumacher R, Morimoto RI (1995) Identification of a regulatory motif in Hsp70 that affects ATPase activity, substrate binding and interaction with HDJ-1. EMBO J 14: 2281–2292.

227. Qian X, Hou W, Zhengang L, Sha B (2002) Direct interactions between molecular chaperones heat-shock protein (Hsp) 70 and Hsp40: yeast Hsp70 Ssa1 binds the extreme C-terminal region of yeast Hsp40 Sis1. Biochem J 361: 27–34.

228. Li J, Wu Y, Qian X, Sha B (2006) Crystal structure of yeast Sis1 peptide-binding fragment and Hsp70 Ssa1 C-terminal complex. Biochem J 398: 353–360. doi:10.1042/BJ20060618.

229. Fan Q, Park K-W, Du Z, Morano KA, Li L (2007) The role of Sse1 in the de novo formation and variant determination of the [PSI+] prion. Genetics 177: 1583–1593. doi:10.1534/genetics.107.077982.

230. Jung G, Jones G, Wegrzyn RD, Masison DC (2000) A role for cytosolic hsp70 in yeast [PSI(+)] prion propagation and [PSI(+)] as a cellular stress. Genetics 156: 559–570.

231. Needham PG, Masison DC (2008) Prion-impairing mutations in Hsp70 chaperone Ssa1: effects on ATPase and chaperone activities. Arch Biochem Biophys 478: 167–174. doi:10.1016/j.abb.2008.07.023.

232. Sharma D, Masison DC (2008) Functionally redundant isoforms of a yeast Hsp70 chaperone subfamily have different antiprion effects. Genetics 179: 1301–1311. doi:10.1534/genetics.108.089458.

233. Hines JK, Li X, Du Z, Higurashi T, Li L, et al. (2011) [SWI], the prion formed by the chromatin remodeling factor Swi1, is highly sensitive to alterations in Hsp70 chaperone system activity. PLoS Genet 7: e1001309. doi:10.1371/journal.pgen.1001309.

234. Jones GW, Masison DC (2003) Saccharomyces cerevisiae Hsp70 mutations affect [PSI+] prion propagation and cell growth differently and implicate Hsp40 and tetratricopeptide repeat cochaperones in impairment of [PSI+]. Genetics 163: 495–506.

235. Du Z, Park K-W, Yu H, Fan Q, Li L (2008) Newly identified prion linked to the chromatin-remodeling factor Swi1 in Saccharomyces cerevisiae. Nat Genet 40: 460–465. doi:10.1038/ng.112.

236. Derdowski A, Sindi SS, Klaips CL, DiSalvo S, Serio TR (2010) A size threshold limits prion transmission and establishes phenotypic diversity. Science 330: 680–683. doi:10.1126/science.1197785.

237. Lee S, Sielaff B, Lee J, Tsai FTF (2010) CryoEM structure of Hsp104 and its mechanistic implication for protein disaggregation. Proc Natl Acad Sci USA 107: 8135–8140. doi:10.1073/pnas.1003572107.

238. Seyffer F, Kummer E, Oguchi Y, Winkler J, Kumar M, et al. (2012) Hsp70 proteins bind Hsp100 regulatory M domains to activate AAA+ disaggregase at aggregate surfaces. Nat Struct Mol Biol 19: 1347–1355. doi:10.1038/nsmb.2442.

239. Sielaff B, Tsai FTF (2010) The M-Domain Controls Hsp104 Protein Remodeling Activity in an Hsp70/Hsp40-Dependent Manner. J Mol Biol 402: 30–37. doi:10.1016/j.jmb.2010.07.030.

240. Miot M, Reidy M, Doyle SM, Hoskins JR, Johnston DM, et al. (2011) Species-specific collaboration of heat shock proteins (Hsp) 70 and 100 in thermotolerance and protein disaggregation. Proc Natl Acad Sci USA 108: 6915–6920. doi:10.1073/pnas.1102828108.

241. Reidy M, Miot M, Masison DC (2012) Prokaryotic Chaperones Support Yeast Prions and Thermotolerance and Define Disaggregation Machinery Interactions. Genetics 192: 185–193. doi:10.1534/genetics.112.142307.

242. Dulle JE, Stein KC, True HL (2014) Regulation of the Hsp104 middle domain activity is critical for yeast prion propagation. PLoS ONE 9: e87521. doi:10.1371/journal.pone.0087521.

243. Hines JK, Craig EA (2011) The sensitive [SWI (+)] prion: New perspectives on yeast prion diversity. Prion 5.

244. Perales-Calvo J, Muga A, Moro F (2010) Role of DnaJ G/F-rich domain in conformational recognition and binding of protein substrates. J Biol Chem 285: 34231–34239. doi:10.1074/jbc.M110.144642.

245. Hu J, Wu Y, Li J, Qian X, Fu Z, et al. (2008) The crystal structure of the putative peptide-binding fragment from the human Hsp40 protein Hdj1. BMC Struct Biol 8: 3. doi:10.1186/1472-6807-8-3.

246. Yang Z, Hong JY, Derkatch IL, Liebman SW (2013) Heterologous Gln/Asn-Rich Proteins Impede the Propagation of Yeast Prions by Altering Chaperone Availability. PLoS Genet 9: e1003236. doi:10.1371/journal.pgen.1003236.s007.

247. Tyedmers J, Mogk A, Bukau B (2010) Cellular strategies for controlling protein aggregation. Nat Rev Mol Cell Biol 11: 777–788. doi:10.1038/nrm2993.

248. Shaner L, Sousa R, Morano KA (2006) Characterization of Hsp70 binding and

nucleotide exchange by the yeast Hsp110 chaperone Sse1. Biochemistry 45: 15075–15084. doi:10.1021/bi061279k.

249. Udan M, Baloh RH (2011) Implications of the prion-related Q/N domains in TDP-43 and FUS. Prion 5: 1–5.

250. Udan-Johns M, Bengoechea R, Bell S, Shao J, Diamond MI, et al. (2013) Prion-like nuclear aggregation of TDP-43 during heat shock is regulated by HSP40/70 chaperones. Hum Mol Genet. doi:10.1093/hmg/ddt408.

251. Kikis EA, Gidalevitz T, Morimoto RI (2010) Protein homeostasis in models of aging and age-related conformational disease. Adv Exp Med Biol 694: 138–159.

252. Tenreiro S, Munder MC, Alberti S, Outeiro TF (2013) Harnessing the power of yeast to unravel the molecular basis of neurodegeneration. J Neurochem 127: 438–452. doi:10.1111/jnc.12271.

253. Pereira C, Coutinho I, Soares J, Bessa C, Leão M, et al. (2012) New insights into cancer-related proteins provided by the yeast model. FEBS J 279: 697–712. doi:10.1111/j.1742-4658.2012.08477.x.

254. Fuentealba RA, Udan M, Bell S, Wegorzewska I, Shao J, et al. (2010) Interaction with polyglutamine aggregates reveals a Q/N-rich domain in TDP-43. J Biol Chem 285: 26304–26314. doi:10.1074/jbc.M110.125039.

255. Durrenberger PF, Filiou MD, Moran LB, Michael GJ, Novoselov S, et al. (2009) DnaJB6 is present in the core of Lewy bodies and is highly up-regulated in parkinsonian astrocytes. J Neurosci Res 87: 238–245. doi:10.1002/jnr.21819.

256. Hageman J, Rujano MA, van Waarde MAWH, Kakkar V, Dirks RP, et al. (2010) A DNAJB Chaperone Subfamily with HDAC-Dependent Activities Suppresses Toxic Protein Aggregation. Mol Cell 37: 355–369. doi:10.1016/j.molcel.2010.01.001.

257. Watson ED, Geary-Joo C, Hughes M, Cross JC (2007) The Mrj co-chaperone mediates keratin turnover and prevents the formation of toxic inclusion bodies in trophoblast cells of the placenta. Development 134: 1809–1817. doi:10.1242/dev.02843.

258. Jahn TR, Radford SE (2008) Folding versus aggregation: Polypeptide conformations on competing pathways. Arch Biochem Biophys 469: 100–117. doi:10.1016/j.abb.2007.05.015.

259. Hageman J, Kampinga HH (2009) Computational analysis of the human HSPH/HSPA/DNAJ family and cloning of a human HSPH/HSPA/DNAJ expression library. Cell Stress Chaperones 14: 1–21. doi:10.1007/s12192-008-0060-2.

260. Suarez-Cedeno G, Winder T, Milone M (2013) DNAJB6 Myopathy: A vacuolar myopathy with childhood onset. Muscle Nerve. doi:10.1002/mus.24106.

261. Ju J-S, Fuentealba RA, Miller SE, Jackson E, Piwnica-Worms D, et al. (2009) Valosin-containing protein (VCP) is required for autophagy and is disrupted in VCP disease. J Cell Biol 187: 875–888. doi:10.1083/jcb.200908115.

262. Walker AK, Soo KY, Sundaramoorthy V, Parakh S, Ma Y, et al. (2013) ALS-associated TDP-43 induces endoplasmic reticulum stress, which drives cytoplasmic TDP-43 accumulation and stress granule formation. PLoS ONE 8: e81170. doi:10.1371/journal.pone.0081170.

263. Jiang J, Maes EG, Taylor AB, Wang L, Hinck AP, et al. (2007) Structural basis of J cochaperone binding and regulation of Hsp70. Mol Cell 28: 422–433. doi:10.1016/j.molcel.2007.08.022.

264. Wu Y, Li J, Jin Z, Fu Z, Sha B (2005) The crystal structure of the C-terminal fragment of yeast Hsp40 Ydj1 reveals novel dimerization motif for Hsp40. J Mol Biol 346: 1005–1011. doi:10.1016/j.jmb.2004.12.040.

265. Izawa I, Nishizawa M, Ohtakara K, Ohtsuka K, Inada H, et al. (2000) Identification of Mrj, a DnaJ/Hsp40 family protein, as a keratin 8/18 filament regulatory protein. J Biol Chem 275: 34521–34527. doi:10.1074/jbc.M003492200.

266. Chuang J-Z, Zhou H, Zhu M, Li S-H, Li X-J, et al. (2002) Characterization of a brain-enriched chaperone, MRJ, that inhibits Huntingtin aggregation and toxicity independently. J Biol Chem 277: 19831–19838. doi:10.1074/jbc.M109613200.

267. Fayazi Z, Ghosh S, Marion S, Bao X, Shero M, et al. (2006) A Drosophila ortholog of the human MRJ modulates polyglutamine toxicity and aggregation. Neurobiol Dis 24: 226–244. doi:10.1016/j.nbd.2006.06.015.

268. Mitra A, Menezes ME, Shevde LA, Samant RS (2010) DNAJB6 induces degradation of beta-catenin and causes partial reversal of mesenchymal phenotype. J Biol Chem 285: 24686–24694. doi:10.1074/jbc.M109.094847.

269. Cajo GC, Horne BE, Kelley WL, Schwager F, Georgopoulos C, et al. (2006) The role of the DIF motif of the DnaJ (Hsp40) co-chaperone in the regulation of the DnaK (Hsp70) chaperone cycle. J Biol Chem 281: 12436–12444. doi:10.1074/jbc.M511192200.

270. Krzewska J, Langer T, Liberek K (2001) Mitochondrial Hsp78, a member of the Clp/Hsp100 family in Saccharomyces cerevisiae, cooperates with Hsp70 in protein refolding. FEBS Lett 489: 92–96.

271. Park S-H, Kukushkin Y, Gupta R, Chen T, Konagai A, et al. (2013) PolyQ Proteins Interfere with Nuclear Degradation of Cytosolic Proteins by Sequestering the Sis1p Chaperone. Cell: 1–12. doi:10.1016/j.cell.2013.06.003.

272. Summers DW, Wolfe KJ, Ren H-Y, Cyr DM (2013) The Type II Hsp40 Sis1 Cooperates with Hsp70 and the E3 Ligase Ubr1 to Promote Degradation of Terminally Misfolded Cytosolic Protein. PLoS ONE 8: e52099. doi:10.1371/journal.pone.0052099.s004.

273. Verghese J, Abrams J, Wang Y, Morano KA (2012) Biology of the Heat Shock Response and Protein Chaperones: Budding Yeast (Saccharomyces cerevisiae) as a Model System. Microbiology and Molecular Biology Reviews 76: 115–158. doi:10.1128/MMBR.05018-11.

274. Wang Y, Gibney PA, West JD, Morano KA (2012) The yeast Hsp70 Ssa1 is a sensor for activation of the heat shock response by thiol-reactive compounds. Mol Biol Cell 23: 3290–3298. doi:10.1091/mbc.E12-06-0447.

275. Gillis J, Schipper-Krom S, Juenemann K, Gruber A, Coolen S, et al. (2013) The DNAJB6 and DNAJB8 Protein Chaperones Prevent Intracellular Aggregation of Polyglutamine Peptides. J Biol Chem 288: 17225–17237. doi:10.1074/jbc.M112.421685.

276. Månsson C, Kakkar V, Monsellier E, Sourigues Y, Härmark J, et al. (2013) DNAJB6 is a peptide-binding chaperone which can suppress amyloid fibrillation of polyglutamine peptides at substoichiometric molar ratios. Cell Stress Chaperones. doi:10.1007/s12192-013-0448-5.

277. Johnson JL, Craig EA (2001) An essential role for the substrate-binding region of Hsp40s in Saccharomyces cerevisiae. J Cell Biol 152: 851–856.

278. Davies KE, Nowak KJ (2006) Molecular mechanisms of muscular dystrophies: old and new players. Nat Rev Mol Cell Biol 7: 762–773. doi:10.1038/nrm2024.

279. Kushnirov VV (2000) Rapid and reliable protein extraction from yeast. Yeast 16: 857–860. doi:10.1002/1097-0061(20000630)16:9<857::AID-YEA561>3.0.CO;2-B.

280. Lin CA, Ellis SR, True HL (2010) The Sua5 protein is essential for normal translational regulation in yeast. Mol Cell Biol 30: 354–363. doi:10.1128/MCB.00754-09.

281. Willis MS, Schisler JC, Portbury AL, Patterson C (2009) Build it up-Tear it down: protein quality control in the cardiac sarcomere. Cardiovasc Res 81: 439–448. doi:10.1093/cvr/cvn289.

282. Telling GC (2013) The importance of prions. PLoS Pathog 9: e1003090. doi:10.1371/journal.ppat.1003090.

283. Liao L, Cheng D, Wang J, Duong DM, Losik TG, et al. (2004) Proteomic characterization of postmortem amyloid plaques isolated by laser capture microdissection. J Biol Chem 279: 37061–37068. doi:10.1074/jbc.M403672200.

284. Manogaran AL, Fajardo VM, Reid RJD, Rothstein R, Liebman SW (2010) Most, but not all, yeast strains in the deletion library contain the [PIN(+)] prion. Yeast 27: 159–166. doi:10.1002/yea.1740.

285. Halfmann R, Jarosz DF, Jones SK, Chang A, Lancaster AK, et al. (2012) Prions are a common mechanism for phenotypic inheritance in wild yeasts. Nature 482: 363–368.

doi:10.1038/nature10875.

286. Kelly AC, Shewmaker FP, Kryndushkin D, Wickner RB (2012) Sex, prions, and plasmids in yeast. Proc Natl Acad Sci USA 109: E2683–E2690. doi:10.1073/pnas.1213449109.

287. Muralidharan V, Oksman A, Pal P, Lindquist S, Goldberg DE (2012) Plasmodium falciparum heat shock protein 110 stabilizes the asparagine repeat-rich parasite proteome during malarial fevers. Nature communications 3: 1310. doi:10.1038/ncomms2306.

288. Wisen S, Gestwicki JE (2008) Identification of small molecules that modify the protein folding activity of heat shock protein 70. Analytical Biochemistry 374: 371–377. doi:10.1016/j.ab.2007.12.009.

289. Plotkin JB, Kudla G (2010) Synonymous but not the same: the causes and consequences of codon bias. Nat Rev Genet 12: 32–42. doi:10.1038/nrg2899.

290. Chernova TA, Romanyuk AV, Karpova TS, Shanks JR, Ali M, et al. (2011) Prion Induction by the Short-Lived, Stress-Induced Protein Lsb2 Is Regulated by Ubiquitination and Association with the Actin Cytoskeleton. Mol Cell 43: 242–252. doi:10.1016/j.molcel.2011.07.001.

291. van Ham TJ, Holmberg MA, van der Goot AT, Teuling E, García-Arencibia M, et al. (2010) Identification of MOAG-4/SERF as a Regulator of Age-Related Proteotoxicity. Cell 142: 601–612. doi:10.1016/j.cell.2010.07.020.

292. Falsone SF, Meyer NH, Schrank E, Leitinger G, Pham CLL, et al. (2012) SERF protein is a direct modifier of amyloid fiber assembly. CellReports 2: 358–371. doi:10.1016/j.celrep.2012.06.012.

293. Kaganovich D, Kopito R, Frydman J (2008) Misfolded proteins partition between two distinct quality control compartments. Nature 454: 1088–1095. doi:10.1038/nature07195.

294. Hu K-N, McGlinchey RP, Wickner RB, Tycko R (2011) Segmental Polymorphism in a Functional Amyloid. Biophys J 101: 2242–2250. doi:10.1016/j.bpj.2011.09.051.

Appendix A: Spontaneous Variants of the [*RNQ*+] Prion in Yeast Demonstrate the Extensive Conformational Diversity Possible with Prion Proteins

Vincent J. Huang, Kevin C. Stein, and Heather L. True

This appendix is published in *PLOS ONE* 8, e79582 (2013).

OPEN ACCESS Freely available online

PLOS ONE

Spontaneous Variants of the [*RNQ*+] Prion in Yeast Demonstrate the Extensive Conformational Diversity Possible with Prion Proteins

Vincent J. Huang, Kevin C. Stein, Heather L. True*

Department of Cell Biology and Physiology, Washington University School of Medicine, Saint Louis, Missouri, United States of America

Abstract

Prion strains (or variants) are structurally distinct amyloid conformations arising from a single polypeptide sequence. The existence of prion strains has been well documented in mammalian prion diseases. In many cases, prion strains manifest as variation in disease progression and pathology, and in some cases, these prion strains also show distinct biochemical properties. Yet, the underlying basis of prion propagation and the extent of conformational possibilities available to amyloidogenic proteins remain largely undefined. Prion proteins in yeast that are also capable of maintaining multiple self-propagating structures have provided much insight into prion biology. Here, we explore the vast structural diversity of the yeast prion [*RNQ*+] in *Saccharomyces cerevisiae*. We screened for the formation of [*RNQ*+] *in vivo*, allowing us to calculate the rate of spontaneous formation as ~2.96×10^{-6}, and successfully isolate several different [*RNQ*+] variants. Through a comprehensive set of biochemical and biological analyses, we show that these prion variants are indeed novel. No individual property or set of properties, including aggregate stability and size, was sufficient to explain the physical basis and range of prion variants and their resulting cellular phenotypes. Furthermore, all of the [*RNQ*+] variants that we isolated were able to facilitate the *de novo* formation of the yeast prion [*PSI*+], an epigenetic determinant of translation termination. This supports the hypothesis that [*RNQ*+] acts as a functional amyloid in regulating the formation of [*PSI*+] to produce phenotypic diversity within a yeast population and promote adaptation. Collectively, this work shows the broad spectrum of available amyloid conformations, and thereby expands the foundation for studying the complex factors that interact to regulate the propagation of distinct aggregate structures.

Citation: Huang VJ, Stein KC, True HL (2013) Spontaneous Variants of the [*RNQ*+] Prion in Yeast Demonstrate the Extensive Conformational Diversity Possible with Prion Proteins . PLoS ONE 8(10): e79582. doi:10.1371/journal.pone.0079582

Editor: Jiyan Ma, Ohio State University, United States of America

Received August 14, 2013; **Accepted** October 2, 2013; **Published** October 25, 2013

Funding: This work was supported by National Institutes of Health grants F31AG040899 (KCS) and GM072778 (HLT). The funders had no role in study design, data collection and analysis, decision to publish, or preparation of the manuscript.

Competing interests: The authors have declared that no competing interests exist.

* E-mail: heather.true@wustl.edu

Introduction

Protein misfolding disorders refer broadly to a class of human diseases associated with the failure of a protein or peptide to adopt its native, functional conformation [1]. Such misfolding can lead to the formation of fibrillar aggregates called amyloid. Amyloid fibers typically form as a β sheet-rich structure in a self-replicating process [2]. These highly ordered arrangements of β sheets are formed from non-covalent interactions of neighboring polypeptides in which the β strands run perpendicular to the fibril axis [1,3]. This fundamental architecture is shared among a variety of proteins associated with unrelated protein conformational disorders, including Alzheimer's disease and Type II diabetes [4]. Interestingly, significant conformational variation can exist while still maintaining this generic amyloid structure [5]. Such amyloid polymorphism has been most studied in the context of prion strains, but recent data suggest that it is a common feature of many amyloidogenic proteins [6,7,8].

Prion diseases, also called transmissible spongiform encephalopathies (TSEs), represent a subset of protein misfolding disorders that are invariably fatal [9]. These diseases include bovine spongiform encephalopathy (BSE) in cattle and Creutzfeldt-Jakob disease (CJD) in humans. TSEs develop when the host-encoded prion protein, PrP^{C}, assumes the abnormal β sheet-rich PrP^{Sc} conformation [10]. This infectious structure self-propagates by sequestering native PrP^{C} and templating further conversion to PrP^{Sc} [11,12].

Initial transmission experiments with PrP^{Sc} encountered what is now known as the "species barrier" [13]. This refers to the observation that transmission of PrP^{Sc} between two different species is typically far less efficient than transmission within the same species [14]. This barrier may be partially due to changes in amino acid sequence, but can also be due to changes in the

self-propagating structure of the protein itself. Indeed, even within a single species, pathological variation in TSEs and different biochemical signatures of PrP^{Sc} have been observed, leading to the isolation of distinct PrP^{Sc} types [15,16]. These different types of PrP^{Sc} are called prion strains, and represent amyloid conformations of PrP that are structurally unique. In many cases, different prion strains show differences in biochemical properties, such as protease resistance or denaturant sensitivity, which correlate with variation in pathology and the time course of disease [17,18,19,20,21,22]. However, in other cases, prion strains have been isolated that vary in pathology, yet remain biochemically indistinguishable, according to the levels of sensitivity available with current assays [23]. Moreover, while genetic polymorphisms in PrP bias the formation of particular conformations of PrP^{Sc}, a single primary sequence can propagate a multitude of distinct prion strains [14]. Indeed, it has been estimated that the range of heterogeneity seen in samples from patients with sporadic CJD represents over 30 distinct prion strains [24,25]. Clearly, the structural limits of amyloid polymorphism of prion strains are quite large.

Interestingly, functionally distinct prion proteins exist in fungi such as the yeast *Saccharomyces cerevisiae* [26,27]. Yeast prion proteins share many of the same misfolding and aggregation characteristics as the proteins associated with human protein conformational disorders. As such, yeast has provided a tractable model system to investigate many facets of protein aggregation and prion biology, including that of prion strain diversity. As in mammals, prion strains in yeast (termed prion variants) are conformationally distinct, self-propagating amyloid structures. This formation of amyloid in yeast leads to changes in cellular phenotypes, which typically resemble a loss-of-function phenotype of the prion protein [28,29,30,31]. One of the most well-studied prion proteins in *S. cerevisiae* is the translation termination factor Sup35. Sup35 is the eRF3 that normally exists in a complex that functions to recognize stop codons in mRNA and facilitate the release of polypeptide chains from ribosomes [32,33]. Conversion of Sup35 into its prion form, [*PSI*+], establishes a loss-of-function phenotype that is dominant and inherited in a non-Mendelian fashion [31]. In [*PSI*+] cells, much of the Sup35 is sequestered into prion aggregates, thereby impairing translation termination and causing readthrough of stop codons (also known as nonsense suppression) [34,35].

[*PSI*+] variants have been broadly classified into categories based on the degree of nonsense suppression [36]. Two well-characterized variants are strong [*PSI*+] and weak [*PSI*+]. Cells propagating the strong [*PSI*+] variant exhibit a greater amount of nonsense suppression as compared to cells propagating the weak [*PSI*+] variant [36]. Studies of strong and weak [*PSI*+] led to a model that proposed an explanation for how differences in the biochemical properties of these [*PSI*+] variants correlate with differences in biological phenotypes [5,37,38,39,40,41]. This model posits that decreased fiber stability results in increased fragmentation, thereby giving rise to a greater number of prion seeds, and thus more fibril "free ends" that can recruit and sequester natively-folded Sup35 [39]. Ultimately, the more “free ends” available are hypothesized to correlate to an increased rate of fiber growth that, in the case of the [*PSI*+] prion, modulates the strength of the nonsense suppression phenotype as the efficiency of translation termination is linked to the size of the soluble, active pool of Sup35 [41]. Interestingly, these trends have been recapitulated with some PrP^{Sc} strains, as lower aggregate stability correlated with a shorter incubation period and earlier onset of disease [42]. However, this correlation between aggregate stability and fiber growth does not explain differences in all PrP^{Sc} strains [21], or even in prion variants of another yeast prion, [*RNQ*+] [43]. Indeed, even with the [*PSI*+] prion, there may be multiple ways to acquire phenotypically similar prion variants [39,44,45]. Such differences highlight the remarkable conformational diversity of amyloid and the fact that there may be several ways to generate amyloid variant structures from a single polypeptide sequence.

The [*RNQ*+] prion, comprised of the Rnq1 protein, is also called [*PIN*+] for [*PSI*+]-inducible, as it is required for the *de novo* formation of all [*PSI*+] variants *in vivo* [46,47,48,49,50]. It has been hypothesized that Rnq1 aggregates facilitate the formation of [*PSI*+] by interacting with soluble Sup35 and acting as an imperfect template to cross-seed the formation of [*PSI*+] [46]. Interestingly, a set of [*RNQ*+] variants was isolated that differ in their relative ability to influence the formation of [*PSI*+] [51]. Cells harboring some [*RNQ*+] variants afforded low levels of [*PSI*+] formation, while [*PSI*+] formed much more readily in cells propagating other [*RNQ*+] variants. Such cross-seeding between heterologous proteins may in fact be a common feature among protein conformational disorders [52]. Recently, variants of α-synuclein, the protein that misfolds and aggregates in Parkinson’s disease, have been reported to differentially influence the formation of tau inclusions [53]. However, what properties allow some amyloid structures to promote heterologous cross-seeding more efficiently than others remains unanswered.

Additional biochemical characterization of the [*RNQ*+] variants suggested that the variation in [*PSI*+] formation likely resulted from underlying structural differences between [*RNQ*+] variants and subsequent changes in the interaction with Sup35 [54,55,56]. However, as Rnq1 has no known function in its monomeric state, identification of spontaneously formed [*RNQ*+] cells has been cumbersome. As such, most of the [*RNQ*+] variants investigated to date were isolated by screening for [*PIN*+] cells (which turned out to be [*RNQ*+]) that had formed the [*PSI*+] prion [51]. Therefore, the conformational diversity observed in the set of previously characterized spontaneous [*RNQ*+] variants remains limited to aggregate structures of Rnq1 that are capable of inducing [*PSI*+].

Here, we explore the degree of structural variation that is possible with the [*RNQ*+] prion when not linked to the ability to induce [*PSI*+]. We isolated a novel set of spontaneously formed [*RNQ*+] variants using a chimeric [*RNQ*+] reporter protein (RRP) that allowed us to phenotypically monitor the [*RNQ*+] status of a cell. The large set of [*RNQ*+] variants that we isolated exhibited a wide range of phenotypes, differing in terms of their [*RRP*+] phenotype, mitotic stability, aggregate size and stability, distribution pattern of aggregates *in vivo*, and in the ability to induce [*PSI*+]. We show that all of the [*RNQ*+]

variants we obtained and analyzed in this study are distinct from those originally isolated [51]. These findings demonstrate the tremendous amount of conformational diversity that can be generated from a single amyloidogenic protein. By expanding the number of existing [*RNQ*+] variants, we are poised to better understand what factors dictate the ability of a given prion variant to form, propagate, and cause a particular phenotype. This will provide insight into the structural basis of prion strains and may help elucidate the mechanisms underlying pathological variation in protein misfolding diseases and the species transmission barrier of prion diseases.

Materials and Methods

Yeast Strains, Plasmids, and Media

All *S. cerevisiae* strains used in this study were derivatives of 74-D694 (*ade1-14 ura3-52 leu2-3,112 trp1-289 his3-Δ200*). Yeast harboring the s.d. low, s.d. medium, s.d. high, s.d. very high, or m.d. high [*RNQ*+] variants were kind gifts from Dr. Susan Liebman [51,54]. Construction of the yeast strains expressing RRP ([*RNQ*+] reporter protein) used to phenotypically monitor the [*RNQ*+] prion were previously described [57]. Briefly, by the pop-in/pop-out method, *SUP35* was replaced with the RRP gene encoding a fusion protein consisting of the prion-forming domain of Rnq1 and the M and C domains of Sup35. [*psi*-] [*RNQ*+] strains propagating the novel [*RNQ*+] variants described in this study were created by mating the [*RNQ*+] RRP strains to a wild-type 74-D694 [*psi*-] [*rnq*-] strain, and sporulating to obtain haploids containing *SUP35* instead of *RRP*. The presence of *SUP35* and the absence of *RRP* were confirmed by colony PCR and western blot.

pEMBL-*SUP35* was created through a similar process as a previously described pEMBL-*SUP2* plasmid [58]. The *SUP35* promoter was first amplified using oligonucleotides 5'-CGCCTCGAGGACGACGCGTCACAGTG and 5'-CCCGGATCCTGTTGCTAGTGGGCAGATATAG, digested with XhoI/BamHI, and ligated into pEMBL-yex4 (2μ, *URA3*). The *SUP35* open reading frame and terminator were then amplified using oligonucleotides 5'-CGCGGATCCACTAGTATGTCGGATTCAAACCAAGG and 5'-GGGGAGCTCGTGATTGAAGGAGTTGAAACCTTGC, digested with BamHI/XbaI, and ligated, thereby disrupting the GAL-CYC1 promoter of pEMBL-yex4.

Yeast were grown at 30°C in YEPD (complete media containing 2% dextrose, 2% peptone, 1% yeast extract) or synthetic dextrose (SD) media (2% dextrose, 0.67% yeast nitrogen base without amino acids) lacking the indicated nutrients to select for transformed plasmids, [*PSI*+] cells, or [*RNQ*+] RRP cells. As indicated, ¼YEPD plates containing 0.25% yeast extract were used to better visualize colony color phenotypes. Transient growth on YEPD containing 3mM guanidine hydrochloride (GdnHCl) was used to check curability of the [*PRION*+] status, as GdnHCl inhibits the chaperone Hsp104 that is required for prion propagation [59,60,61].

Prion Color Assay

The yeast strain 74-D694 harbors the *ade1-14* allele having a premature nonsense mutation that can be used to easily monitor the [*PSI*+] status of cells [62]. Soluble Sup35 in [*psi*-] cells functions to faithfully terminate translation at the premature stop codon. As such, these cells are unable to complete the adenine biosynthetic pathway, cannot grow on medium lacking adenine, and appear red when grown on a rich medium, such as YEPD, due to the accumulation of a metabolic intermediate in the pathway. Conversely, the aggregation of Sup35 in [*PSI*+] cells results in readthrough of the nonsense mutation in *ade1-14*, thereby allowing cells to grow on medium lacking adenine. The extent of nonsense suppression can vary depending on the prion variant that propagates and the associated degree of Sup35 sequestration. When Sup35 is efficiently sequestered in strong [*PSI*+] cells, colonies are white and grow robustly on SD-ade. In contrast, weak [*PSI*+] cells do not sequester Sup35 as efficiently and are pink in color on YEPD and grow less well on SD-ade. As described previously, RRP can functionally replace Sup35. Analogous to Sup35, RRP co-aggregates with Rnq1 in [*RNQ*+] cells, but remains soluble and is functional in translation termination in [*rnq*-] cells [57]. The RRP construct in 74-D694 allows [*RNQ*+] variants to be distinguished phenotypically in the same manner as [*PSI*+] variants. Before evaluating color phenotypes, YEPD plates were moved from 30°C to 4°C for at least one day to allow the colony color to develop.

Spontaneous [RNQ+] Formation

The spontaneous formation of [*RNQ*+] was quantified using a [*rnq*-] strain expressing RRP and following previously described methods with some modifications [57,63]. This strain was transformed with pRS415-*ura3-197*, a kind gift from Dr. Yoshikazu Nakamura, that carries an allele of *URA3* with a nonsense mutation (UGA) at W197, which is suppressed in [*PSI*+] and [*RNQ*+] RRP cells [64]. Eight single transformants were independently grown in SD-leu to an OD_{600} of ~1.6. 150μl of each culture was plated onto SD-ade-ura medium to select for colonies that could suppress both the *ade1-14* and *ura3-197* alleles. These plates were incubated at 30°C overnight, moved to 4°C for two weeks (as cold has been shown to enhance *de novo* prion formation [46]), and then incubated at 30°C for another two weeks. All colonies that had acquired the white or pink phenotype indicative of *ade1-14* and *ura3-197* suppression were counted and spotted onto YEPD, YEPD containing 3mM GdnHCl, and SD-ade. Colonies were scored as true [*RNQ*+] if growth on YEPD+3mM GdnHCl resulted in a permanent color change from white or pink to red, thereby demonstrating curability of the [*RRP*+] phenotype.

The total number of cells plated on the SD-ade-ura medium for each independent culture was determined by plating 200μl of a 1:10,000 dilution of the overnight culture onto SD-leu, which selected for the presence of pRS415-*ura3-197*. The total number of cells plated on SD-ade-ura for each culture was calculated by multiplying the number of colonies counted on SD-leu by a dilution factor of 52,500, calculated as follows: (# of colonies on SD-leu/200μl) * 10,000 * 150μl * 7 SD-ade-ura plates.

Mitotic Stability of [RNQ+]

The mitotic stability of [*RNQ*+] was determined as previously described [43]. Independent colonies of each [*RNQ*+] variant expressing RRP were grown overnight in YEPD to an OD_{600} of ~2.5. 250µl of a 1:10,000 dilution of each culture was plated onto 13cm diameter YEPD plates. Mitotic loss of the [*RNQ*+] prion was scored as any red colony or any colony exhibiting red sectoring. Over 1,500 colonies were counted for each [*RNQ*+] variant. The percentage of mitotic loss was calculated by dividing the number of red and red sectoring cells by the total number of cells. [*RNQ*+] variants were characterized as mitotically stable if the percentage of prion loss was less than 0.5%. Additionally, cells were grown in YEPD medium overnight and normalized by OD_{600}, followed by spotting 5-fold serial dilutions of cells onto ¼YEPD, YEPD+3mM GdnHCl, and SD-ade plates. Plates were incubated at 30°C for 3 days for the rich media and 7 days for SD-ade.

Thermal Stability Assay

To analyze the stability of Rnq1 aggregates, cells were washed and lysed with 425-600µm acid-washed glass beads (Sigma-Aldrich) by vortexing in buffer containing 100mM Tris-HCl pH 7.5, 200mM NaCl, 1mM ethylenediaminetetraacetic acid (EDTA), 5% glycerol, 0.5mM dithiothreitol (DTT), 50mM N-ethylmaleimide (NEM), 3mM phenylmethylsulfonyl fluoride (PMSF), and Roche complete mini protease inhibitor cocktail for 3 min at high speed at 4°C twice with a 5 min incubation on ice in between. After adding an equal volume of RIPA buffer (50mM Tris-HCl pH 7.0, 200mM NaCl, 1% Triton X-100, 0.5% sodium deoxycholate, 0.1% SDS) following lysis, cell debris was removed by centrifugation at 3,300g for 15 seconds. Pre-cleared lysates were incubated in sample buffer (50mM Tris-HCl pH 6.8, 10% glycerol, 2% SDS, 100mM DTT) and treated for 5 minutes across a temperature gradient ranging between 45-95°C, and also at 25°C and 100°C. Samples were analyzed by SDS-PAGE. When subjected to higher temperatures, Rnq1 aggregates are solubilized and able to enter the SDS-PAGE gel. Protein separated by SDS-PAGE was then transferred to PVDF membrane for western blotting with an anti-Rnq1 antibody. ImageJ was used to quantify the resulting bands. All readings were normalized to the 100°C band, and the results were plotted using Origin 8.1 software.

Semi-Denaturing Detergent Agarose Gel Electrophoresis

SDD-AGE was performed as previously described with slight modifications [57]. Yeast cells were lysed by vortexing with glass beads as described above in buffer containing 25mM Tris-HCl pH 7.5, 100mM NaCl, 1mM EDTA, Roche complete mini protease inhibitor, 0.5mM DTT, 3mM PMSF, 5µg/mL pepstatin, and 40mM NEM. Cell debris was cleared by centrifugation at 3,300g for 30 sec. Lysates were incubated with sample buffer (60mM Tris-HCl pH 6.8, 5% glycerol, 2% SDS) for 7 minutes at room temperature and 40µg of protein was separated on a 1.5% Tris-glycine agarose gel. Protein was transferred to PVDF membrane overnight and analyzed by western blot using an anti-Rnq1 antibody.

[*PSI*+] Induction

The *de novo* formation of [*PSI*+] was monitored as previously described [43,57]. Yeast propagating different [*RNQ*+] prion variants were transformed with pEMBL-*SUP35*. At least three independent overnight cultures were started for each prion variant in SD-ura and grown to an OD_{600} of 0.6-1.5. Each culture was diluted roughly 1:8,000 in water before plating 250µl onto 13cm diameter ¼YEPD plates and incubated at 30°C for 5 days, followed by overnight incubation at 4°C for color development. [*PSI*+] colonies were scored as any white/pink colonies or colonies having white/pink sectoring. More than 1,200 colonies were scored for each [*RNQ*+] variant. Previous studies have reported that only ~12% of the white/pink sectoring colonies are the result of nonheritable amyloids that cause Sup35 over-expression-dependent nonsense suppression, while the rest contain *bona fide* [PSI+] [57,65]. As an alternative means of assessing [*PSI*+] induction, overnight cultures were normalized by OD_{600} and spotted in 5-fold serial dilutions onto ¼YEPD, YEPD+3mM GdnHCl, and SD-ade. Plates were incubated at 30°C for 3 days for the rich media and 9 days for SD-ade.

To characterize the [*PSI*+] variants that formed, ~300 individual [*PSI*+] colonies of each [*RNQ*+] variant were spotted onto ¼YEPD, YEPD+3mM GdnHCl, and SD-ade. Plates were incubated at 30°C for 3 days for the rich media and 6 days for SD-ade. Based primarily on growth on SD-ade, [*PSI*+] variants that were confirmed curable after transient growth on YEPD +3mM GdnHCl were classified as one of the following: very weak (≤3 colonies in the spot), weak (growth covering up to 50% of the spot), medium (growth covering 50-90% of the spot), or strong (dense growth covering >90% of the spot in addition to white colonies present on ¼YEPD).

Microscopy

When expressed in [*RNQ*+] cells, Rnq1-GFP decorates Rnq1 aggregates to form fluorescent foci in prion variant-specific patterns, while remaining diffuse in [*rnq*-] cells [48,55]. Cells were transformed with the copper inducible pRS316*CUP1-RNQ1*(*153-405*)-*GFP*, a kind gift from Dr. Susan Lindquist, as used in previous studies [48,55]. Overnight cultures were grown to an OD_{600} of ~1.0 in SD-ura before backdiluting to an OD_{600} of 0.2 in SD-ura containing 50µM $CuSO_4$ for ~2.5 hours prior to imaging. Samples were prepared on agar pads (3% wt/vol in liquid SD-ura) and plated directly onto VWR 3in x 1in, 1mm thick microscope slides. Fisherbrand No.#1.5 microscope coverslips were secured with nail polish. Images were collected using a Zeiss Axiovert 200 Inverted Microscope equipped with a Zeiss 100x/1.4 NA oil objective. Slidebook 5.0 (Intelligent Imaging Innovations) was used to analyze captured images and deconvolve (no neighbors algorithm) GFP Z-stacks.

Results

Rate of spontaneous [*RNQ*+] formation

In analyzing the conformational diversity of the [*RNQ*+] prion, we first wanted to quantify the rate of spontaneous [*RNQ*+] formation and compare it to what was previously described for

Table 1. Rate of spontaneous [*RNQ*+] formation.

Replicate	# [*RRP*+] Colonies	Colonies on SD-leu	Total Colonies Plated on SD-ade-ura (x10^6)	Rate of Spontaneous [*RNQ*+] Formation (x10^{-6})
1	54	136	7.14	7.56
2	33	265	13.91	2.37
3	34	355	18.64	1.82
4	41	350	18.38	2.23
5	34	164	8.61	3.95
6	33	202	10.61	3.11
7	26	212	11.13	2.34
8	33	168	8.82	3.74
Total	288	1852	97.23	2.96

Eight independent overnight cultures of [*rnq*-] cells (*ura3-197*, *ade1-14*) expressing RRP were plated onto SD-ade-ura to select for nonsense suppressors, and to SD-leu to calculate the total number of colonies plated. [*RNQ*+] colonies were identified by curability after transient growth on YEPD+3mM GdnHCl.

doi: 10.1371/journal.pone.0079582.t001

[*PSI*+] and other yeast prions. As the [*RNQ*+] prion has no easily observable phenotype other than its essential role in [*PSI*+] induction, we used a chimeric protein called RRP ([*RNQ*+] reporter protein), which we created previously to monitor the [*RNQ*+] status of cells [57]. RRP consists of the prion-forming domain (PFD) of Rnq1 (amino acids 153-405) fused to the M and C domains of Sup35 (amino acids 124-685), such that the fusion retains functionality in translation termination. In its soluble form, RRP acts as the functional equivalent to Sup35 by faithfully recognizing stop codons to terminate translation. However, in [*RNQ*+] cells, RRP and Rnq1 co-aggregate to cause global [*PSI*+]-like nonsense suppression.

To screen for the spontaneous formation of [*RNQ*+], we used a 74-D694 [*rnq*-] strain with the endogenous *SUP35* gene replaced by *RRP*. This strain harbored the [*PSI*+] and [*RRP*+] suppressible *ade1-14* and *ura3-197* alleles. As such, to monitor conversion to [*RNQ*+], we plated overnight cultures onto SD-ade-ura medium to select for cells that could suppress the premature stop codons in both alleles in a [*RRP*+]-dependent manner. Cells were scored as [*RNQ*+] if phenotypic curability was demonstrated after growth on medium containing guanidine hydrochloride (YEPD+3mM GdnHCl), which inhibits the chaperone Hsp104 required to propagate yeast prions [59,60,61]. Sedimentation assays were used to confirm the [*RNQ*+] status of a subset of these colonies by the presence of Rnq1 in the insoluble fraction (data not shown). Of the ~9.7x10^7 cells plated on SD-ade-ura and >2,600 colonies spotted, 288 [*RNQ*+] colonies were identified (Table 1). This gave a rate of ~2.96x10^{-6} for the spontaneous formation of [*RNQ*+], which is slightly higher than the rate of [*PSI*+] formation previously reported [63].

Spontaneous [*RNQ*+] formation yields mixed population of [*RNQ*+] variants

Interestingly, the spontaneously formed [*RNQ*+] colonies showed differences in growth on SD-ade, indicative of varying levels of nonsense suppression (data not shown). As the degree of nonsense suppression is a measure of distinct prion variants of [*PSI*+] [36] and [*RNQ*+] using RRP [43], this suggested that multiple [*RNQ*+] variants had formed spontaneously in our screen.

We wanted to isolate a subset of conformationally distinct [*RNQ*+] variants in order to perform a more extensive analysis on what types of aggregate structures were formed. Previous studies have shown that one property that can differ with variants of [*PSI*+] and [*RNQ*+] is the frequency of loss during mitotic division [36,43]. Therefore, to examine mitotic stability, overnight cultures of yeast harboring a large subset of our spontaneous [*RNQ*+] variants expressing RRP were plated onto YEPD. This produced a wide range of colorimetric phenotypes that were initially categorized as either stable or unstable. Stable [*RNQ*+] variants exhibited colonies that had a homogenous [*RRP*+] phenotype of one colony color (Figure 1A). Unstable [*RNQ*+] variants, on the other hand, displayed heterogeneous [*RRP*+] phenotypes, often within a single colony (Figure 1B). Some of these unstable [*RNQ*+] variants displayed a high frequency of mitotic loss, as indicated by the presence of red sectors or colonies that were entirely red. Other unstable [*RNQ*+] variants showed a mix of non-red colonies, including colonies that exhibited sectors of various shades of pink, and appeared similar to previously reported yeast strains harboring “undifferentiated” and “unspecified” variants of [PSI+] [66,67].

Four [*RNQ*+] variants were selected that had a stable colony color phenotype with little mitotic loss (<0.25%). These mitotically stable variants differed in the degree of [*RRP*+]-mediated nonsense suppression, and are referred to hereafter as strong [*RNQ*+] (white colonies), medium [*RNQ*+] (light pink), weak [*RNQ*+] (medium pink), and very weak [*RNQ*+] (dark pink). This classification helps distinguish our [*RNQ*+] variants from the [*RNQ*+] variants previously described, in which the nomenclature corresponded to different levels of [*PSI*+] induction and the pattern of Rnq1-GFP fluorescence [51,55]. To compare these two sets of [*RNQ*+] variants phenotypically, we spotted serial dilutions of normalized cells onto ¼YEPD and SD-ade plates (Figure 1C). Relative growth on SD-ade showed that very weak [*RNQ*+], weak [*RNQ*+], and medium [*RNQ*+] displayed intermediate growth between that of s.d. medium [*RNQ*+] and m.d. high [*RNQ*+], whereas strong [*RNQ*+] had more robust [*RRP*+]-mediated nonsense suppression and growth that was comparable to that of m.d. high [*RNQ*+].

Seven mitotically unstable [*RNQ*+] variants were also chosen for further analysis. C3 and G6 exhibited high frequencies of mitotic loss, while A5, B1, D3, E1, and G4 displayed a heterogeneous mixture of non-red sectoring [*RRP*+] phenotypes. For instance, many E1 colonies were dark pink with light pink sectors, while many B1 colonies were white with light pink sectors. These phenotypes can be contrasted with true mitotic loss, which is represented by sectoring to red. Interestingly, upon subsequent restreaking, the sectoring

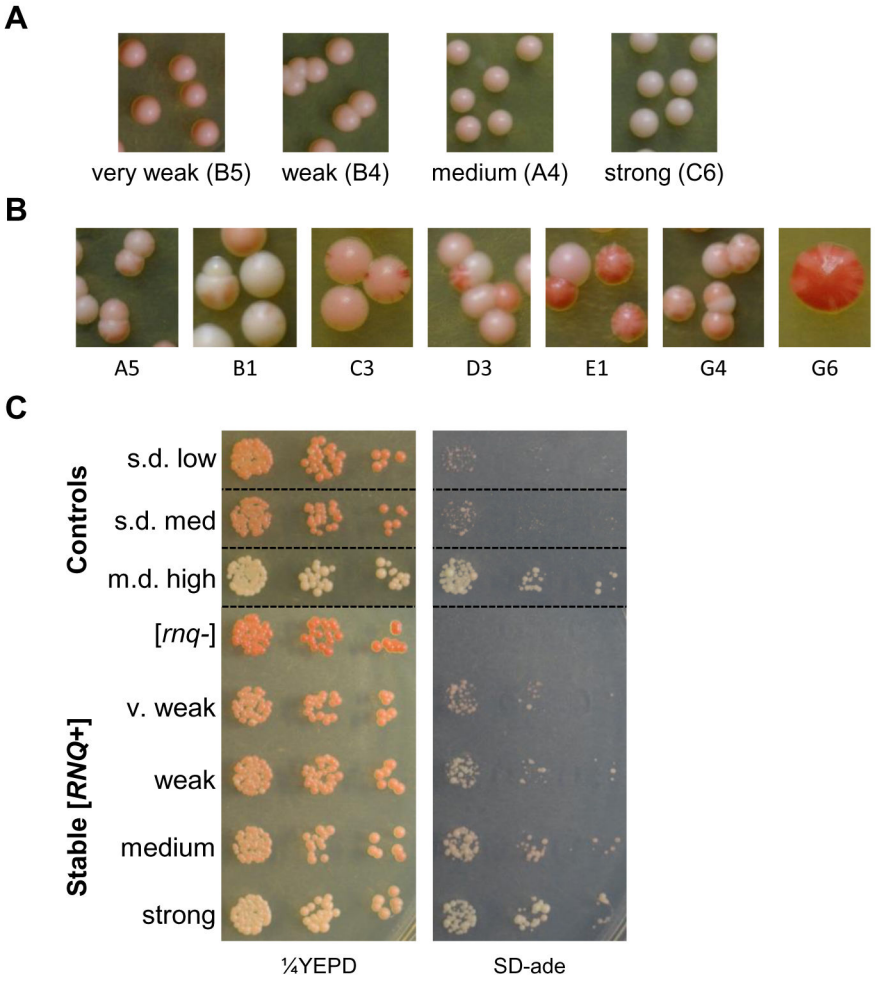

Figure 1. Spontaneous [*RNQ*+] formation produces multiple variants with unique [*RRP*+] phenotypes. Cultures of cells expressing RRP and harboring a spontaneous [*RNQ*+] variant were plated onto YEPD and scored for color and sectoring phenotypes. [*RNQ*+] variants were characterized as (A) stable or (B) unstable. Representative pictures are shown for each variant. (C) Normalized numbers of cells expressing RRP and harboring the indicated [*RNQ*+] variant were plated in 5-fold serial dilutions onto ¼YEPD and SD-ade media. Dotted lines denote where spots from the same plate have been cropped for clarity.

doi: 10.1371/journal.pone.0079582.g001

phenotypes of A5 and C3 stabilized into homogenous populations of colonies (data not shown).

[*RRP*+] phenotype does not correlate with [*PSI*+] induction

As the original [*RNQ*+] variants were classified by their ability to template the formation of [*PSI*+], we wanted to determine the efficiency with which our spontaneously formed [*RNQ*+] variants facilitated conversion to [*PSI*+]. We began by generating [*psi*-] [*RNQ*+] strains with each of our [*RNQ*+] variants. We obtained haploids expressing *SUP35* in place of *RRP* by mating the RRP-expressing strains to [*psi*-] [*rnq*-] cells to obtain diploids, followed by random sporulation or tetrad dissection and selecting haploids of the appropriate genotype. Interestingly, we noticed that there were two distinct populations of [*RNQ*+] RRP B1 colonies with contrasting [*RRP*+] phenotypes, one white with extensive light pink sectors (B1 P/W) and the other predominately white with very minor pink sectoring (B1 W). We proceeded with the independent mating of cells having each of these phenotypes to determine whether differences in [*RRP*+] phenotypes of clones from the same population would be reflected in [*PSI*+] induction efficiency. Both the diploids and haploids we obtained following sporulation were red in colony color, as these [*psi*-] [*RNQ*+] cells now had soluble wild-type Sup35 to function in faithful translation termination.

In order to assess how well each [*RNQ*+] variant could facilitate [*PSI*+] induction, we transformed the progeny we generated with a plasmid over-expressing Sup35. After overnight growth in selection medium to maintain expression of

the transformed plasmid, cells were plated onto ¼YEPD plates. Any pink/white colonies or colonies with pink/white sectoring were scored as [*PSI*+], and the rate of [*PSI*+] formation was calculated as the number of those colonies divided by the total number of cells plated (Figure 2A). For comparison, we also confirmed the rates of [*PSI*+] formation for the previously published [*RNQ*+] variants, along with [*rnq*-] cells.

Confirming our previous results [43], the efficiency of [*PSI*+] induction for the previously described s.d. low, s.d. medium, and m.d. high [*RNQ*+] variants positively correlated with their [*RRP*+] phenotypes. Higher [*PSI*+] induction corresponded to a stronger [*RRP*+] phenotype. However, as we previously observed with [*RNQ*+] variants formed from transforming *in vitro* fibers [43], this trend did not hold for our set of stable [*RNQ*+] variants. Strong [*RNQ*+] and very weak [*RNQ*+] induced [*PSI*+] at fairly similar frequencies (45% and 54% respectively), while medium [*RNQ*+] and weak [*RNQ*+] exhibited lower rates of [*PSI*+] induction comparable to that of s.d. low [*RNQ*+]. Interestingly, many of our unstable [*RNQ*+] variants induced the formation of [*PSI*+] at higher rates relative to our stable [*RNQ*+] variants. Six of the eight unstable [*RNQ*+] variants induced [*PSI*+] very efficiently, at rates between 50-70%, while D3 and G6 facilitated [*PSI*+] induction at slightly lower rates of ~40%.

Knowing that different [*RNQ*+] variants can promote the formation of [*PSI*+] to different extents, we were interested in determining whether the distinct amyloid structures of our [*RNQ*+] variants would bias the formation of particular [*PSI*+] variants, as reported in studies with other [*RNQ*+] variants [55,56]. To quantitatively evaluate the [*PSI*+] variant profile that corresponded to each of our [*RNQ*+] variants, we spotted newly induced [*PSI*+] colonies onto a set of ¼YEPD, YEPD +3mM GdnHCl, and SD-ade plates. Growth on SD-ade after six days of incubation at 30°C was used as the primary determinant in scoring the strength of each [*PSI*+] variant as very weak, weak, medium, or strong (Figure 2B-C). All 12 [*RNQ*+] variants appeared capable of inducing multiple variants of [*PSI*+], but the vast majority of the [*PSI*+] variants were categorized as very weak [*PSI*+] or weak [*PSI*+]. Indeed, A5 induced no strong variants of [*PSI*+]. In contrast, strong [*RNQ*+], very weak [*RNQ*+], and B1 P/W induced noticeably stronger [*PSI*+] variants than the other [*RNQ*+] variants in the subset. Interestingly, while B1 P/W and B1 W supported similar rates of [*PSI*+] formation, B1 P/W induced markedly stronger variants of [*PSI*+] than B1 W. Finally, as with the rate of [*PSI*+] induction, no correlation appeared to exist between the [*RRP*+]-mediated nonsense suppression phenotype of the four stable [*RNQ*+] variants and their corresponding induced [*PSI*+] variant profile.

To further investigate the extent to which our spontaneously formed [*RNQ*+] variants can induce conversion to [*PSI*+], we generated 28 more [*psi*-] [*RNQ*+] haploids expressing *SUP35* in place of *RRP* as described above. These yeast strains propagated other [*RNQ*+] variants that had spontaneously formed in our initial screen. To monitor [*PSI*+] induction capacity, we over-expressed Sup35 as above and spotted normalized numbers of cells onto ¼YEPD and SD-ade plates (Figure 2D). As the overall growth of [*PSI*+] colonies on SD-ade is presumably influenced by both the rate of [*PSI*+] induction and the strength of the [*PSI*+] variant induced, we used this as a qualitative measure of [*PSI*+] induction efficiency by comparing the growth on SD-ade to that of the five previously published [*RNQ*+] variants and a [*rnq*-] control strain. Surprisingly, even though we screened for [*RNQ*+] formation independent of the ability to form [*PSI*+], all 28 spontaneously formed [*RNQ*+] variants were able to induce [*PSI*+] to some degree. By comparing our [*RNQ*+] variants to those previously published, we further scored the [*PSI*+] induction capacity of our [*RNQ*+] variants as low, medium, high, or very high (Figure 2E). Interestingly, an overwhelming majority of our [*RNQ*+] variants (22 out of 28) were categorized as inducing [*PSI*+] at low or medium levels. We identified E5 as an outlier in the data set in displaying robust growth on SD-ade, even greater than that of s.d. very high [*RNQ*+].

Rnq1-GFP aggregation patterns of [*RNQ*+] variants

In addition to [*PSI*+] induction levels, fluorescence microscopy was also utilized to identify the original [*RNQ*+] variants as potentially distinct structures [55]. With expression of an inducible Rnq1(153-405)-GFP fusion construct [48,55], [*rnq*-] cells were shown to display diffuse fluorescence. In [*RNQ*+] cells, however, the fluorescent signal was localized in discrete, cytosolic foci. Two distinct GFP aggregation patterns emerged among the [*RNQ*+] variants: single-dot (s.d.), in which cells had one focus of GFP fluorescence, or multiple-dot (m.d.) where cells had multiple foci. As such, we set out to examine the Rnq1(153-405)-GFP fluorescence characteristics of 12 of the [*RNQ*+] variants that we had isolated.

Previous studies have reported that, in their respective yeast strains, both the s.d. and m.d. Rnq1-GFP fluorescence patterns form with great efficiency, appearing in >75% of s.d [*RNQ*+] cells or >50% of m.d. [*RNQ*+] cells, respectively [55,68]. We recapitulated these findings for s.d. low [*RNQ*+], but also found that m.d. high [*RNQ*+] displayed a third Rnq1-GFP pattern as the dominant population (Figure 3A). This pattern was characterized by many petite foci (p.f.) that were much smaller and fainter in intensity than those observed with the s.d. and m.d. patterns.

When analyzing the Rnq1-GFP aggregation patterns of our stable and unstable [*RNQ*+] variants, we found that these variants often did not fall into a strict bimodal classification of s.d. or m.d. (Figure 3B-C). Instead, we observed a gradient of patterns, which varied in the relative proportions of s.d., m.d., and p.f. cells (Table 2). Placed at one end of the spectrum, s.d. low [*RNQ*+] and our medium [*RNQ*+] had ~85-95% of foci-containing cells having the s.d. pattern. Although the majority of very weak [*RNQ*+], A5, and C3 cells similarly had the s.d. pattern, these variants also had an appreciable number of cells (~15-25%) that harbored the m.d. fluorescence pattern. In contrast, at the other end of the spectrum, the Rnq1-GFP aggregate pattern of m.d. high [*RNQ*+] consisted of both p.f. and m.d. patterns in >90% of cells. While strong [*RNQ*+] cells also predominately displayed the p.f. pattern, the m.d. pattern was not observed. Interestingly, several of our [*RNQ*+] variants showed intermediate phenotypes on this spectrum. For instance, weak [*RNQ*+] and B1 W showed all three patterns with no dominant population easily recognizable, thereby

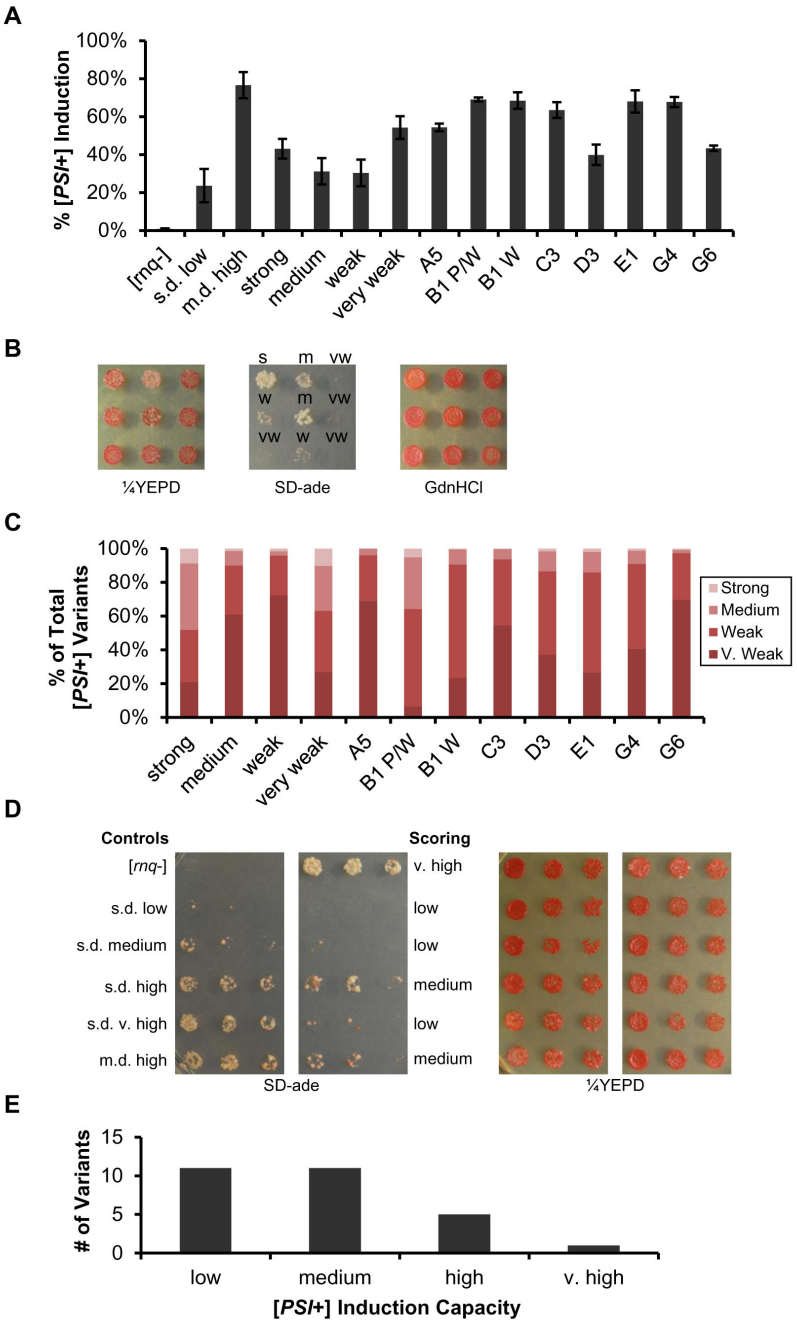

Figure 2. The [*PSI*+] induction rate and [*PSI*+] variant distribution is variable. (A) The induction of [*PSI*+] by over-expressing Sup35 in our 12 [*RNQ*+] variants was analyzed quantitatively by counting the number of [*PSI*+] colonies that formed on ¼YEPD plates from at least three independent experiments. Error bars represent standard error. Nonsense suppression by nonheritable amyloid due to the over-expression of Sup35 has been previously shown to only account for a small percentage of white/pink sectoring colonies (B) Example of scoring the newly induced [*PSI*+] variants as very weak (vw), weak (w), medium (m), or strong (s) by spotting [*PSI*+] colonies onto ¼YEPD, YEPD+3mM GdnHCl, and SD-ade media. (C) Counts of [*PSI*+] variants were plotted as a fraction of total [*PSI*+] colonies scored. (D) Example plate of scoring the ability of spontaneous [*RNQ*+] variants to induce [*PSI*+] upon Sup35 over-expression. [*PSI*+] induction efficiency was scored into one of four classifications by assessing colony growth on SD-ade relative to that of five previously described [*RNQ*+] variants: low (ranges from no growth to less growth than s.d. medium), medium (growth equivalent to s.d. medium to less than s.d. high), high (growth equivalent to s.d. high to less than s.d. very high), and very high (growth equivalent to s.d. very high or greater). (E) The types of [*RNQ*+] variants that spontaneously formed categorized based on the levels of [*PSI*+] induction.

doi: 10.1371/journal.pone.0079582.g002

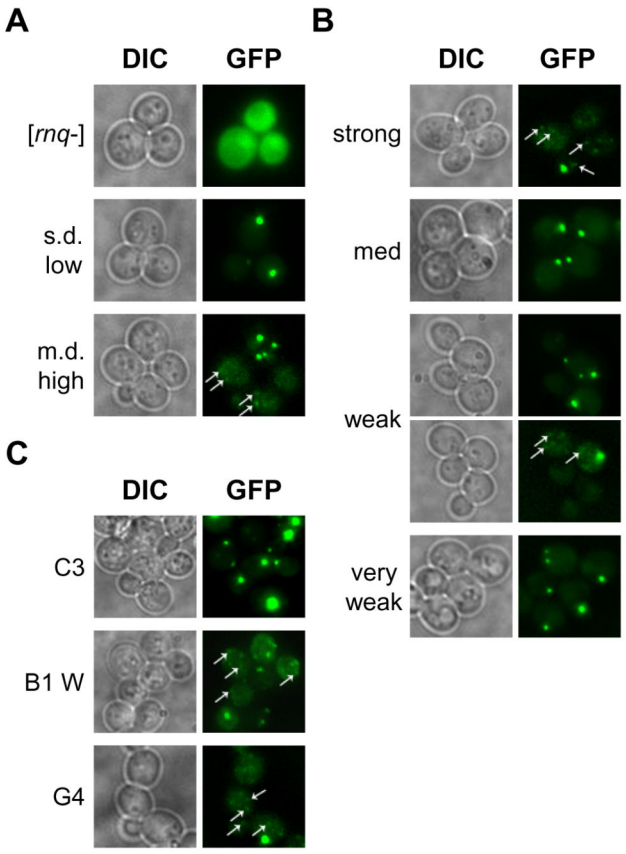

Figure 3. Spontaneously formed [*RNQ*+] variants show diversity in Rnq1-GFP aggregation patterns. Cells were transformed with a plasmid expressing Rnq1(153-405)-GFP under the *CUP1* promoter. Prior to imaging, transformants were transferred to induction medium containing 50μM $CuSO_4$ and grown for ~2.5 hours. A variety of fluorescence patterns were observed, including: a single focus, large multiple foci, and numerous petite foci. Arrows identify petite foci that are fainter and smaller. Representative images in differential interference contrast mode (DIC) and under a GFP-emitted light filter (GFP) are shown for (A) previously published [*RNQ*+] variants and [*rnq*-], (B) all of the stable [*RNQ*+] variants, and (C) a subset of the unstable [*RNQ*+] variants.

doi: 10.1371/journal.pone.0079582.g003

highlighting the extent of conformational diversity present in our spontaneous [*RNQ*+] variants.

Spontaneous [*RNQ*+] variants propagate thermally stable amyloid structures

In vitro studies of Sup35 suggested that strong [*PSI*+] arises from amyloid fibers that have a relatively shorter protected core as compared to Sup35 aggregates of weak [*PSI*+] [40]. This difference in amyloid core length was found to positively correlate with fiber stability: the longer core of weak [*PSI*+] resulted in greater stability than strong [*PSI*+] [39]. Similarly, we found previously that more stable amyloid fibers of Rnq1-PFD produced weaker prion variants of [*RNQ*+], while less stable fibers propagated stronger [*RNQ*+] variants [43]. The resultant differences in phenotype with different [*PSI*+] and [*RNQ*+] variants were initially attributed to the ability of fibers to produce more free ends that are required for sequestering and converting monomeric protein [40]. Thus, less stable fibers produce more active "seeds" that convert soluble protein to the prion conformer faster, resulting in stronger biological phenotypes.

Table 2. Rnq1-GFP fluorescence patterns show diversity among [*RNQ*+] variants.

[*RNQ*+] Variant	Rnq1-GFP Characterization
[*rnq*-]	Diffuse fluorescence
s.d. low	One large focus (s.d.)
m.d. high	Multiple large foci (m.d.) and numerous petite foci (p.f.)
strong	Majority p.f.
medium	Majority s.d.
weak	Diversity: p.f., s.d., and m.d. present
very weak	Majority s.d., also m.d. present
A5	Majority s.d., also m.d. present
B1 P/W	Roughly 50% p.f., 50% s.d.
B1 W	Diversity: p.f., s.d., and m.d. present
C3	Majority s.d., also m.d. present
D3	Roughly 50% p.f., 50% s.d.
E1	Majority p.f., low percentage of s.d.
G4	Majority p.f., low percentage of s.d.
G6	Majority p.f., low percentage of s.d.

[*RNQ*+] variants expressing Rnq1(153-405)-GFP were characterized by the relative number of GFP aggregate-containing cells with single-dot (s.d.), multiple-dot (m.d.), or petite-foci (p.f.) fluorescence patterns. For each [*RNQ*+] variant, Z-stacks of at least 150 cells were analyzed.

doi: 10.1371/journal.pone.0079582.t002

We were interested in determining whether the stability of our stable and unstable [*RNQ*+] variants would show a similar relationship with either their [*RRP*+] phenotype or efficiency in [*PSI*+] induction. Using thermal denaturation as an indicator of stability, we subjected cell lysates of our [*RNQ*+] variants to a temperature gradient and analyzed the samples by SDS-PAGE and western blot to determine the temperature at which 50% of the Rnq1 protein was liberated from the aggregates. Aggregates of all 12 [*RNQ*+] variants were shown to be very thermal stable with melting temperatures (T_m) ranging from 80-95°C (Figure 4A-B). Rnq1 aggregates from medium [*RNQ*+] cells displayed the greatest sensitivity to temperature, with a T_m ~80°C, contrasting sharply with strong [*RNQ*+], in which Rnq1 aggregates remained largely intact at 90°C. While aggregates of s.d. low [*RNQ*+] showed a stability similar to our [*RNQ*+] variants, m.d. high [*RNQ*+] remained a striking outlier of all known [*RNQ*+] variants in exhibiting a T_m below 60°C, as demonstrated previously [54].

SDD-AGE reveals variant-specific differences in aggregate size distribution

Previous studies with the [*PSI*+] and [*RNQ*+] prions have shown that the SDS-resistant, higher molecular weight protein

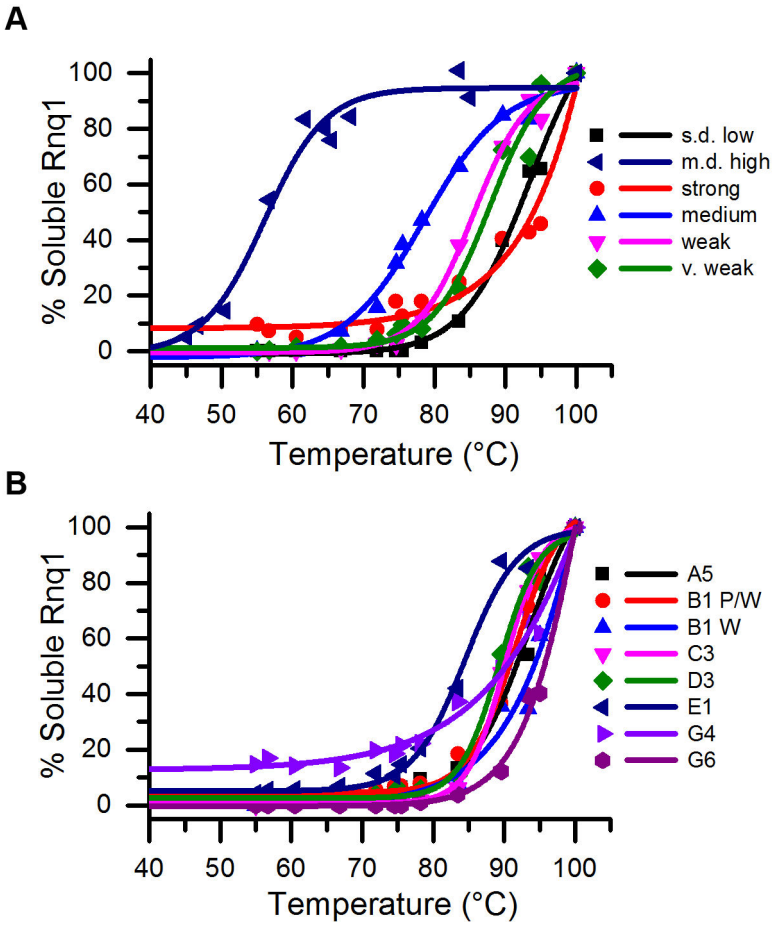

Figure 4. Aggregates of spontaneous [*RNQ*+] variants show similar thermal stability. Cell lysates were incubated for five minutes at different temperatures, run on an SDS-PAGE, and analyzed by western blot using an anti-Rnq1 antibody. The amount of soluble Rnq1 of both the (A) stable [*RNQ*+] variants and (B) unstable [*RNQ*+] variants was quantified with ImageJ and graphed as a percentage of soluble Rnq1 at 100°C. One representative experiment is shown, but in all cases, data were highly reproducible.

doi: 10.1371/journal.pone.0079582.g004

aggregates can be resolved from the monomeric species and visualized using semi-denaturing detergent agarose gel electrophoresis (SDD-AGE) and western blot [37,54]. Furthermore, distinct prion variants can show different sizes of aggregates by SDD-AGE. For instance, many weak [*PSI*+] cell lysates harbor noticeably larger Sup35 aggregates than strong [PSI+] [37,39]. Slight differences also exist between some of the previously characterized [*RNQ*+] variants [54]. Therefore, we asked whether SDD-AGE analysis of our 12 stable and unstable [*RNQ*+] variants would reveal any additional differences in structural properties of the Rnq1 aggregates.

Indeed, with cell lysates harboring each of our [*RNQ*+] variants, we found reproducible differences in aggregate distribution between many of the [*RNQ*+] variants of our subset (Figure 5). The higher molecular weight species of strong [*RNQ*+], medium [*RNQ*+], weak [*RNQ*+], B1 W, and G6 consistently migrated with a similar size as that of the previously published s.d. [*RNQ*+] variants (Figure 5 and data not shown). Other [*RNQ*+] variants, however, including very weak [*RNQ*+], C3, D3, and G4 contained a species that migrated slightly faster. A5 exhibited minor differences in aggregate distribution across multiple trials. Interestingly, B1 P/W and B1 W displayed modest, but reproducible differences as Rnq1 aggregates of B1 W were slightly larger than those found in B1 P/W lysates, despite having formed initially in the same colony. In striking contrast, E1 was the most unique and showed the bulk of the aggregated Rnq1 propagating in larger structures as compared to the other variants. Moreover, the aggregates of medium [*RNQ*+] consistently appeared much fainter in intensity, a property also observed with m.d. high [*RNQ*+] (data not shown).

Discussion

In this study, we describe the isolation and characterization of several novel [*RNQ*+] variants that formed spontaneously *in vivo*. In the process of isolating these variants, we were able to estimate the rate of spontaneous [*RNQ*+] formation to be

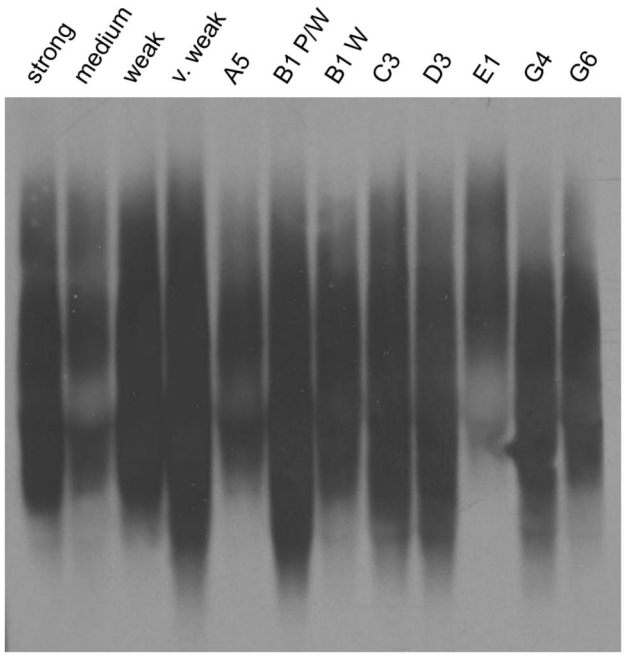

Figure 5. SDS-resistant aggregates of spontaneously formed [*RNQ*+] display modest, variant-specific differences in aggregate distribution. Aggregate distribution of [*RNQ*+] variants was analyzed using SDD-AGE by loading normalized amounts of protein from cell lysates onto an agarose gel containing SDS. Rnq1 was visualized by western blot using an anti-Rnq1 antibody.

doi: 10.1371/journal.pone.0079582.g005

~2.96×10^{-6}. It was previously reported that the spontaneous rate of [*PSI*+] formation in [*psi*-] [*RNQ*+] yeast cells was 5.8×10^{-7} [63]. Hence, even when a high [*RNQ*+] variant is available to facilitate the formation of [*PSI*+], the *de novo* formation of [*RNQ*+] under our growth conditions occurs about 5 times more frequently. This places Rnq1 alongside other yeast prion proteins that all have a higher rate of formation than [*PSI*+], and are thought to have a functional role in the cell [69]. Moreover, while the ability to induce [*PSI*+] was not a requirement for isolation, every [*RNQ*+] variant analyzed in this study was shown to facilitate [*PSI*+] formation to some degree. These data suggest that the [*RNQ*+] prion, rather than simply acting as a promiscuous amyloid, might actually function to induce the formation of [*PSI*+] [70]. Although use of the RRP chimera remains the only way to easily measure the rate of [*RNQ*+] formation, one caveat here is that an extra copy of the Rnq1-PFD as part of RRP may contribute to a higher rate of spontaneous [*RNQ*+] formation.

In addition to being able to phenotypically monitor the formation of [*RNQ*+] with the use of RRP, the chimera also allowed us to identify distinct structures of aggregated Rnq1. After extensively characterizing the cellular and biochemical properties of 12 of the [*RNQ*+] variants that formed, we found that these different structures are indeed novel. While it is clear that no single property can fully differentiate between structural isomers of [*RNQ*+], when the properties we analyzed are considered collectively, each of our [*RNQ*+] variants displays a unique set of characteristics that distinguishes it from the others, as well as from the previously described [*RNQ*+] variants.

Four of the [*RNQ*+] variants we isolated and characterized were mitotically stable, but differed in their [*RRP*+] phenotype. In contrast to [*PSI*+] variants and [*RNQ*+] variants formed from *in vitro* fibers that were previously reported [39,43], the degree of nonsense suppression of each of the stable [*RNQ*+] variants described in this study did not correlate to differences in stability or any of the other properties we examined.

Among the eight unstable [*RNQ*+] variants within our set, many displayed some degree of prion loss through mitotic division. While previous studies have documented a transient stage of mitotic instability in cells harboring newly induced [*PSI*+] and [RNQ+] [50,55], several of our [*RNQ*+] isolates were able to maintain their sectoring to red phenotypes through both restreaking and storage (data not shown). Strikingly, some of our unstable [*RNQ*+] variants exhibited more complex colony color phenotypes, such as A5, B1, D3, E1, and G6, in which colonies displayed sectors of various shades of pink. These findings suggest that multiple [*RNQ*+] variant types may have formed within the clonal population arising from a single cell. The B1 [*RNQ*+] variant epitomizes this observation, as our initial streak of cells harboring this prion variant produced white colonies with varying amounts of light pink sectoring, solid light pink colonies, and solid white colonies. Evidence of a single yeast strain harboring multiple prion conformations has also been observed with [*PSI*+]. Recently, clones isolated from a single [*PSI*+] colony exhibited a range of transmission profiles across an intra-species barrier, leading authors to propose that an ensemble, or cloud, of [*PSI*+] variants had been propagating in the parent cell [71]. Similarly, others have described an "unspecified" [*PSI*+] phenotype that was characterized by white colonies that sectored to pink, which gave rise to progeny carrying weak [*PSI*+], strong [*PSI*+], or unspecified [*PSI*+] [67]. In contrast to the "cloud" hypothesis, these authors consider an alternative possibility in which a single [*PSI*+] structure responsible for the unspecified [*PSI*+] phenotype is able to undergo a conformational maturation process into more than one distinct [*PSI*+] variant. Similarly, fibers of α-synuclein that were formed *in vitro* were recently shown to undergo a maturation process and form distinct aggregate conformations over time [53]. Both the "cloud" and "maturation" models may be applicable to our unstable [*RNQ*+] variants. Presumably, a host of factors, which also include competition between prion variants [51] and strain mutation [72], may play a role in dictating how prions propagate and which variants ultimately emerge phenotypically.

The original set of [*RNQ*+] variants (referred to as [*PIN*+] variants) was obtained by over-expressing Sup35 in [*psi*-] [*rnq*-] cells and selecting for cells that converted to [*PSI*+] [51]. As *de novo* formation of [*PSI*+] requires [*RNQ*+] (which is the prion responsible for [*PIN*+]), [*RNQ*+] contemporaneously formed in these cells. In contrast, our [*RNQ*+] variants were isolated in a different manner using [*RRP*+]-mediated nonsense suppression, allowing us to obtain [*RNQ*+] variants with no connection to [*PSI*+] formation. Surprisingly, we found that all

40 of the spontaneous [*RNQ*+] variants induced [*PSI*+] at some level, albeit many facilitated [*PSI*+] formation at low to medium levels. These findings highlight the intrinsic relationship between [*RNQ*+] and [*PSI*+], and support the possibility that [*RNQ*+] functions primarily as a regulatory element in initiating the formation of [*PSI*+] [70].

Many groups have speculated on the role of [*PSI*+] in nature, either as a harmful pathogenic state [73] or as a beneficial mechanism of generating heritable phenotypic diversity in response to stressful or shifting environmental conditions [74,75,76,77]. In the latter case, it is hypothesized that [*PSI*+]-mediated nonsense suppression allows translation of coding sequences downstream of stop codons, thereby creating novel gene products that may facilitate the evolution of new traits [76,78]. While reduced fidelity in translation termination could be deleterious, cells forming particular [*PSI*+] variants may in fact produce heritable, advantageous phenotypes that allow survival of the population without requiring immediate genetic change. Indeed, when cells were subjected to a range of environmental stresses, a correlation was found between the severity of stress and the frequency of [*PSI*+] formation, suggesting that cells may induce [*PSI*+] when a rapid adaptive response is needed [75]. With the discovery of [*PIN*+] as an essential factor for *de novo* [*PSI*+] formation, a two-prion system of epigenetic translation regulation was proposed [50]. The findings that we present here highlight the extent of conformational diversity that exists for the [*RNQ*+] prion. Such structural variation of [*RNQ*+] may contribute to differentially modulating the switch into a [*PSI*+] state, and influence the expansive phenotypic diversity observed with [*PSI*+]-dependent traits [76].

By isolating a number of novel [*RNQ*+] variants and adding to those previously described, we show the widespread variability in structures that the Rnq1 protein can assume. A high number of conformational possibilities have also been shown for [PSI+] [71,73], making the classification into strong and weak [*PSI*+] variants overly simplistic. We speculate that such diversity is not limited to these prion proteins, but may exist with many amyloidogenic proteins. Indeed, it was recently suggested that PrP may form over 30 distinct prion strains in humans [24]. Therefore, studying the numerous structural variants of [*RNQ*+] may help elucidate what biochemical properties or cellular factors contribute to the prion variant that propagates and how it manifests phenotypically.

Acknowledgements

We thank members of the True Lab for helpful discussions and critical comments on the manuscript. We are grateful to R. Stewart and R. Wilkinson for assistance with microscopy. We also thank S. Liebman, Y. Nakamura, and S. Lindquist for reagents.

Author Contributions

Conceived and designed the experiments: VJH KCS HLT. Performed the experiments: VJH KCS. Analyzed the data: VJH KCS HLT. Wrote the manuscript: VJH KCS HLT.

References

1. Chiti F, Dobson CM (2006) Protein misfolding, functional amyloid, and human disease. Annu Rev Biochem 75: 333-366. doi:10.1146/annurev.biochem.75.101304.123901. PubMed: 16756495.
2. Chien P, Weissman JS, DePace AH (2004) Emerging principles of conformation-based prion inheritance. Annu Rev Biochem 73: 617-656. doi:10.1146/annurev.biochem.72.121801.161837. PubMed: 15189155.
3. Sunde M, Blake C (1997) The structure of amyloid fibrils by electron microscopy and X-ray diffraction. Adv Protein Chem 50: 123-159. doi:10.1016/S0065-3233(08)60320-4. PubMed: 9338080.
4. Selkoe DJ (2003) Folding proteins in fatal ways. Nature 426: 900-904. doi:10.1038/nature02264. PubMed: 14685251.
5. Toyama BH, Weissman JS (2011) Amyloid structure: conformational diversity and consequences. Annu Rev Biochem 80: 557-585. doi:10.1146/annurev-biochem-090908-120656. PubMed: 21456964.
6. Wiltzius JJ, Landau M, Nelson R, Sawaya MR, Apostol MI et al. (2009) Molecular mechanisms for protein-encoded inheritance. Nat Struct Mol Biol 16: 973-978. doi:10.1038/nsmb.1643. PubMed: 19684598.
7. Sawaya MR, Sambashivan S, Nelson R, Ivanova MI, Sievers SA et al. (2007) Atomic structures of amyloid cross-beta spines reveal varied steric zippers. Nature 447: 453-457. doi:10.1038/nature05695. PubMed: 17468747.
8. Colletier JP, Laganowsky A, Landau M, Zhao M, Soriaga AB et al. (2011) Molecular basis for amyloid-beta polymorphism. Proc Natl Acad Sci U S A 108: 16938-16943. doi:10.1073/pnas.1112600108. PubMed: 21949245.
9. Prusiner SB (1998) Prions. Proc Natl Acad Sci U S A 95: 13363-13383. doi:10.1073/pnas.95.23.13363. PubMed: 9811807.
10. Prusiner SB (1982) Novel proteinaceous infectious particles cause scrapie. Science 216: 136-144. doi:10.1126/science.6801762. PubMed: 6801762.
11. Prusiner SB, Scott M, Foster D, Pan KM, Groth D et al. (1990) Transgenetic studies implicate interactions between homologous PrP isoforms in scrapie prion replication. Cell 63: 673-686. doi:10.1016/0092-8674(90)90134-Z. PubMed: 1977523.
12. Weissmann C (1991) A 'unified theory' of prion propagation. Nature 352: 679-683. doi:10.1038/352679a0. PubMed: 1876183.
13. Bruce M, Chree A, McConnell I, Foster J, Pearson G et al. (1994) Transmission of bovine spongiform encephalopathy and scrapie to mice: strain variation and the species barrier. Philos Trans R Soc Lond B Biol Sci 343: 405-411. doi:10.1098/rstb.1994.0036. PubMed: 7913758.
14. Collinge J, Clarke AR (2007) A general model of prion strains and their pathogenicity. Science 318: 930-936. doi:10.1126/science.1138718. PubMed: 17991853.
15. Fraser H, Dickinson AG (1973) Scrapie in mice. Agent-strain differences in the distribution and intensity of grey matter vacuolation. J Comp Pathol 83: 29-40. doi:10.1016/0021-9975(73)90024-8. PubMed: 4199908.
16. Bruce ME (2003) TSE strain variation. Br Med Bull 66: 99-108. doi:10.1093/bmb/66.1.99. PubMed: 14522852.
17. Caughey B, Raymond GJ, Bessen RA (1998) Strain-dependent differences in beta-sheet conformations of abnormal prion protein. J Biol Chem 273: 32230-32235. doi:10.1074/jbc.273.48.32230. PubMed: 9822701.
18. Safar J, Wille H, Itri V, Groth D, Serban H et al. (1998) Eight prion strains have PrP(Sc) molecules with different conformations. Nat Med 4: 1157-1165. doi:10.1038/2654. PubMed: 9771749.
19. Kuczius T, Groschup MH (1999) Differences in proteinase K resistance and neuronal deposition of abnormal prion proteins characterize bovine spongiform encephalopathy (BSE) and scrapie strains. Mol Med 5: 406-418. PubMed: 10415165.
20. Wadsworth JD, Hill AF, Joiner S, Jackson GS, Clarke AR et al. (1999) Strain-specific prion-protein conformation determined by metal ions. Nat Cell Biol 1: 55-59. doi:10.1038/9030. PubMed: 10559865.
21. Peretz D, Scott MR, Groth D, Williamson RA, Burton DR et al. (2001) Strain-specified relative conformational stability of the scrapie prion protein. Protein Sci 10: 854-863. doi:10.1110/ps.39201. PubMed: 11274476.
22. Safar J, Cohen FE, Prusiner SB (2000) Quantitative traits of prion strains are enciphered in the conformation of the prion protein. Arch Virol Suppl: 227-235. PubMed: 11214926.

23. Angers RC, Kang HE, Napier D, Browning S, Seward T et al. (2010) Prion strain mutation determined by prion protein conformational compatibility and primary structure. Science 328: 1154-1158. doi: 10.1126/science.1187107. PubMed: 20466881.
24. Safar JG (2012) Molecular pathogenesis of sporadic prion diseases in man. Prion 6: 108-115. doi:10.4161/pri.18666. PubMed: 22421210.
25. Kim C, Haldiman T, Cohen Y, Chen W, Blevins J et al. (2011) Protease-sensitive conformers in broad spectrum of distinct PrPSc structures in sporadic Creutzfeldt-Jakob disease are indicator of progression rate. PLOS Pathog 7: e1002242. PubMed: 21931554.
26. Benkemoun L, Saupe SJ (2006) Prion proteins as genetic material in fungi. Fungal Genet Biol 43: 789-803. doi:10.1016/j.fgb.2006.06.006. PubMed: 16901730.
27. Liebman SW, Chernoff YO (2012) Prions in yeast. Genetics 191: 1041-1072. doi:10.1534/genetics.111.137760. PubMed: 22879407.
28. Patel BK, Gavin-Smyth J, Liebman SW (2009) The yeast global transcriptional co-repressor protein Cyc8 can propagate as a prion. Nat Cell Biol 11: 344-349. doi:10.1038/ncb1843. PubMed: 19219034.
29. Du Z, Park KW, Yu H, Fan Q, Li L (2008) Newly identified prion linked to the chromatin-remodeling factor Swi1 in Saccharomyces cerevisiae. Nat Genet 40: 460-465. doi:10.1038/ng.112. PubMed: 18362884.
30. Wickner RB (1994) [URE3] as an altered URE2 protein: evidence for a prion analog in Saccharomyces cerevisiae. Science 264: 566-569. doi: 10.1126/science.7909170. PubMed: 7909170.
31. Ter-Avanesyan MD, Dagkesamanskaya AR, Kushnirov VV, Smirnov VN (1994) The SUP35 omnipotent suppressor gene is involved in the maintenance of the non-Mendelian determinant [psi+] in the yeast Saccharomyces cerevisiae. Genetics 137: 671-676. PubMed: 8088512.
32. Frolova L, Le Goff X, Rasmussen HH, Cheperegin S, Drugeon G et al. (1994) A highly conserved eukaryotic protein family possessing properties of polypeptide chain release factor. Nature 372: 701-703. doi:10.1038/372701a0. PubMed: 7990965.
33. Stansfield I, Jones KM, Kushnirov VV, Dagkesamanskaya AR, Poznyakovski AI et al. (1995) The products of the SUP45 (eRF1) and SUP35 genes interact to mediate translation termination in Saccharomyces cerevisiae. EMBO J 14: 4365-4373. PubMed: 7556078.
34. Patino MM, Liu JJ, Glover JR, Lindquist S (1996) Support for the prion hypothesis for inheritance of a phenotypic trait in yeast. Science 273: 622-626. doi:10.1126/science.273.5275.622. PubMed: 8662547.
35. Paushkin SV, Kushnirov VV, Smirnov VN, Ter-Avanesyan MD (1996) Propagation of the yeast prion-like [psi+] determinant is mediated by oligomerization of the SUP35-encoded polypeptide chain release factor. EMBO J 15: 3127-3134. PubMed: 8670813.
36. Derkatch IL, Chernoff YO, Kushnirov VV, Inge-Vechtomov SG, Liebman SW (1996) Genesis and variability of [PSI] prion factors in Saccharomyces cerevisiae. Genetics 144: 1375-1386. PubMed: 8978027.
37. Kryndushkin DS, Alexandrov IM, Ter-Avanesyan MD, Kushnirov VV (2003) Yeast [PSI+] prion aggregates are formed by small Sup35 polymers fragmented by Hsp104. J Biol Chem 278: 49636-49643. doi: 10.1074/jbc.M307996200. PubMed: 14507919.
38. Tanaka M, Chien P, Naber N, Cooke R, Weissman JS (2004) Conformational variations in an infectious protein determine prion strain differences. Nature 428: 323-328. doi:10.1038/nature02392. PubMed: 15029196.
39. Tanaka M, Collins SR, Toyama BH, Weissman JS (2006) The physical basis of how prion conformations determine strain phenotypes. Nature 442: 585-589. doi:10.1038/nature04922. PubMed: 16810177.
40. Toyama BH, Kelly MJ, Gross JD, Weissman JS (2007) The structural basis of yeast prion strain variants. Nature 449: 233-237. doi:10.1038/nature06108. PubMed: 17767153.
41. Uptain SM, Sawicki GJ, Caughey B, Lindquist S (2001) Strains of [PSI(+)] are distinguished by their efficiencies of prion-mediated conformational conversion. EMBO J 20: 6236-6245. doi:10.1093/emboj/20.22.6236. PubMed: 11707395.
42. Ayers JI, Schutt CR, Shikiya RA, Aguzzi A, Kincaid AE et al. (2011) The strain-encoded relationship between PrP replication, stability and processing in neurons is predictive of the incubation period of disease. PLOS Pathog 7: e1001317. PubMed: 21437239.
43. Kalastavadi T, True HL (2010) Analysis of the [RNQ+] prion reveals stability of amyloid fibers as the key determinant of yeast prion variant propagation. J Biol Chem 285: 20748-20755. doi:10.1074/jbc.M110.115303. PubMed: 20442412.
44. Krishnan R, Lindquist SL (2005) Structural insights into a yeast prion illuminate nucleation and strain diversity. Nature 435: 765-772. doi: 10.1038/nature03679. PubMed: 15944694.
45. Foo CK, Ohhashi Y, Kelly MJ, Tanaka M, Weissman JS (2011) Radically different amyloid conformations dictate the seeding specificity of a chimeric Sup35 prion. J Mol Biol 408: 1-8. doi:10.1016/j.jmb.2011.02.025. PubMed: 21333653.
46. Derkatch IL, Bradley ME, Hong JY, Liebman SW (2001) Prions affect the appearance of other prions: the story of [PIN(+)]. Cell 106: 171-182. doi:10.1016/S0092-8674(01)00427-5. PubMed: 11511345.
47. Osherovich LZ, Weissman JS (2001) Multiple Gln/Asn-rich prion domains confer susceptibility to induction of the yeast [PSI(+)] prion. Cell 106: 183-194. doi:10.1016/S0092-8674(01)00440-8. PubMed: 11511346.
48. Sondheimer N, Lindquist S (2000) Rnq1: an epigenetic modifier of protein function in yeast. Mol Cell 5: 163-172. doi:10.1016/S1097-2765(00)80412-8. PubMed: 10678178.
49. Derkatch IL, Bradley ME, Zhou P, Chernoff YO, Liebman SW (1997) Genetic and environmental factors affecting the de novo appearance of the [PSI+] prion in Saccharomyces cerevisiae. Genetics 147: 507-519. PubMed: 9335589.
50. Derkatch IL, Bradley ME, Masse SV, Zadorsky SP, Polozkov GV et al. (2000) Dependence and independence of [PSI(+)] and [PIN(+)]: a two-prion system in yeast? EMBO J 19: 1942-1952. doi:10.1093/emboj/19.9.1942. PubMed: 10790361.
51. Bradley ME, Edskes HK, Hong JY, Wickner RB, Liebman SW (2002) Interactions among prions and prion "strains" in yeast. Proc Natl Acad Sci U S A 99 Suppl 4: 16392-16399. doi:10.1073/pnas.152330699. PubMed: 12149514.
52. Morales R, Green KM, Soto C (2009) Cross currents in protein misfolding disorders: interactions and therapy. CNS Neurol Disord Drug Targets 8: 363-371. doi:10.2174/187152709789541998. PubMed: 19702573.
53. Guo JL, Covell DJ, Daniels JP, Iba M, Stieber A et al. (2013) Distinct α-synuclein strains differentially promote tau inclusions in neurons. Cell 154: 103-117. doi:10.1016/j.cell.2013.05.057. PubMed: 23827677.
54. Bagriantsev S, Liebman SW (2004) Specificity of prion assembly in vivo. [PSI+] and [PIN+] form separate structures in yeast. J Biol Chem 279: 51042-51048. doi:10.1074/jbc.M410611200. PubMed: 15465809.
55. Bradley ME, Liebman SW (2003) Destabilizing interactions among [PSI(+)] and [PIN(+)] yeast prion variants. Genetics 165: 1675-1685. PubMed: 14704158.
56. Sharma J, Liebman SW (2013) Exploring the Basis of [PIN(+)] Variant Differences in [PSI(+)] Induction. J Mol Biol 425: 3046-3059. doi: 10.1016/j.jmb.2013.06.006. PubMed: 23770111.
57. Bardill JP, True HL (2009) Heterologous prion interactions are altered by mutations in the prion protein Rnq1p. J Mol Biol 388: 583-596. doi: 10.1016/j.jmb.2009.03.036. PubMed: 19324054.
58. Ter-Avanesyan MD, Kushnirov VV, Dagkesamanskaya AR, Didichenko SA, Chernoff YO et al. (1993) Deletion analysis of the SUP35 gene of the yeast Saccharomyces cerevisiae reveals two non-overlapping functional regions in the encoded protein. Mol Microbiol 7: 683-692. doi: 10.1111/j.1365-2958.1993.tb01159.x. PubMed: 8469113.
59. Tuite MF, Mundy CR, Cox BS (1981) Agents that cause a high frequency of genetic change from [psi+] to [psi-] in Saccharomyces cerevisiae. Genetics 98: 691-711. PubMed: 7037537.
60. Jung G, Masison DC (2001) Guanidine hydrochloride inhibits Hsp104 activity in vivo: a possible explanation for its effect in curing yeast prions. Curr Microbiol 43: 7-10. doi:10.1007/s002840010251. PubMed: 11375656.
61. Ferreira PC, Ness F, Edwards SR, Cox BS, Tuite MF (2001) The elimination of the yeast [PSI+] prion by guanidine hydrochloride is the result of Hsp104 inactivation. Mol Microbiol 40: 1357-1369. doi: 10.1046/j.1365-2958.2001.02478.x. PubMed: 11442834.
62. Chernoff YO, Lindquist SL, Ono B, Inge-Vechtomov SG, Liebman SW (1995) Role of the chaperone protein Hsp104 in propagation of the yeast prion-like factor [psi+]. Science 268: 880-884. doi:10.1126/science.7754373. PubMed: 7754373.
63. Lancaster AK, Bardill JP, True HL, Masel J (2010) The spontaneous appearance rate of the yeast prion [PSI+] and its implications for the evolution of the evolvability properties of the [PSI+] system. Genetics 184: 393-400. doi:10.1534/genetics.109.110213. PubMed: 19917766.
64. Kurahashi H, Nakamura Y (2007) Channel mutations in Hsp104 hexamer distinctively affect thermotolerance and prion-specific propagation. Mol Microbiol 63: 1669-1683. doi:10.1111/j.1365-2958.2007.05629.x. PubMed: 17367387.
65. Salnikova AB, Kryndushkin DS, Smirnov VN, Kushnirov VV, Ter-Avanesyan MD (2005) Nonsense suppression in yeast cells overproducing Sup35 (eRF3) is caused by its non-heritable amyloids. J Biol Chem 280: 8808-8812. PubMed: 15618222.
66. Bradley ME, Liebman SW (2004) The Sup35 domains required for maintenance of weak, strong or undifferentiated yeast [PSI+] prions. Mol Microbiol 51: 1649-1659. doi:10.1111/j.1365-2958.2003.03955.x. PubMed: 15009892.

67. Sharma J, Liebman SW (2012) [PSI(+)] prion variant establishment in yeast. Mol Microbiol 86: 866-881. doi:10.1111/mmi.12024. PubMed: 22998111.
68. Lancaster DL, Dobson CM, Rachubinski RA (2013) Chaperone proteins select and maintain [PIN+] prion conformations in Saccharomyces cerevisiae. J Biol Chem 288: 1266-1276. doi:10.1074/jbc.M112.377564. PubMed: 23148221.
69. Hines JK, Craig EA (2011) The sensitive [SWI (+)] prion: new perspectives on yeast prion diversity. Prion 5: 164-168. doi:10.4161/pri.5.3.16895. PubMed: 21811098.
70. Stein KC, True HL (2011) The [RNQ+] prion: A model of both functional and pathological amyloid. Prion 5: 291-298. doi:10.4161/pri.18213. PubMed: 22052347.
71. Bateman DA, Wickner RB (2013) The [PSI+] prion exists as a dynamic cloud of variants. PLOS Genet 9: e1003257.
72. Li J, Browning S, Mahal SP, Oelschlegel AM, Weissmann C (2010) Darwinian evolution of prions in cell culture. Science 327: 869-872. doi:10.1126/science.1183218. PubMed: 20044542.
73. McGlinchey RP, Kryndushkin D, Wickner RB (2011) Suicidal [PSI+] is a lethal yeast prion. Proc Natl Acad Sci U S A 108: 5337-5341. doi:10.1073/pnas.1102762108. PubMed: 21402947.
74. Halfmann R, Jarosz DF, Jones SK, Chang A, Lancaster AK et al. (2012) Prions are a common mechanism for phenotypic inheritance in wild yeasts. Nature 482: 363-368. doi:10.1038/nature10875. PubMed: 22337056.
75. Tyedmers J, Madariaga ML, Lindquist S (2008) Prion switching in response to environmental stress. PLOS Biol 6: e294. doi:10.1371/journal.pbio.0060294. PubMed: 19067491.
76. True HL, Lindquist SL (2000) A yeast prion provides a mechanism for genetic variation and phenotypic diversity. Nature 407: 477-483. doi:10.1038/35035005. PubMed: 11028992.
77. Eaglestone SS, Cox BS, Tuite MF (1999) Translation termination efficiency can be regulated in Saccharomyces cerevisiae by environmental stress through a prion-mediated mechanism. EMBO J 18: 1974-1981. doi:10.1093/emboj/18.7.1974. PubMed: 10202160.
78. True HL, Berlin I, Lindquist SL (2004) Epigenetic regulation of translation reveals hidden genetic variation to produce complex traits. Nature 431: 184-187. doi:10.1038/nature02885. PubMed: 15311209.